GEOLOGY OF THE SOUTH RAMP - STATION 55+00 TO 78+77, EXPLORATORY STUDIES FACILITY, YUCCA MOUNTAIN PROJECT, YUCCA MOUNTAIN, NEVADA

by G.L.W. Eatman, W.L. Singleton, T.C. Moyer, D.L. Barr, A.L. Albin, R.C. Lung, and S.C. Beason

---

Bureau of Reclamation and U.S. Geological Survey

Prepared in cooperation with the
NEVADA FIELD OFFICE,
U.S. DEPARTMENT OF ENERGY,
under Interagency Agreement DE-AI08-92NV10874

Denver, Colorado
1997

TABLE OF CONTENTS

FIGURES

TABLES

DRAWINGS

PHOTOS

PLATES

PREFACE

This report is being submitted to the U.S. Department of Energy to fulfill Level 3 Milestone SPG42CM3: Report on the Geology, South Ramp Station 55+00 to South Portal. The Planning and Scheduling Account Number is 1.2.3.2.2.1.2 for the Summary Account titled: Geologic Mapping of the Exploratory Studies Facility. It is the summarization of the U.S. Bureau of Reclamation's mapping of the stratigraphy and structure of the South Ramp from Stations 55+00 to the South Portal. Included in the report are statistical analyses of fractures and the geotechnical characterization which presents rock mass quality ratings and rock mass mechanical properties.

Preface Table 1 is the PACS description/completion criteria of Milestone SPG42CM3 in outline form. The table is provided as a guide for DOE reviewers in verifying completion of the milestone. Documentation attached to this preface as part of the milestone requirements include copies of Technical Data Information Forms identifying acquired and developed data generated for this report (Attachment 1) and copies of the transmittal letters to the GENISES Administrator describing the data submitted for entry into the Technical Data Base (Attachment 2).

All the data used in the development of this report were collected and the report was prepared in accordance with approved quality assurance procedures which implement requirements of the Quality Assurance Requirements Descriptions. Therefore, the developed data from this report and all data used have a Q status.

PREFACE TABLE 1 - Description/completion criteria location summary for U.S. Department of Energy Level 3 Milestone: SPG42CM3 - Geology of the South Ramp, Station 55+00 to 78+77, Exploratory Studies Facility, Yucca Mountain Project, Yucca Mountain, Nevada

CRITERIA	LOCATION/COMPLETION INFORMATION
TECHNICAL REQUIREMENTS	
1. This report will integrate all mapping and other data, including, as appropriate, data from the north/south main drift report, to present a complete description of the geology of the north/south main drift of the ESF.	The report integrates all mapping and data obtained from Stations 55+00 through 78+77 of the South Ramp. Data obtained from the North/South Main Drift is referenced as appropriate within the report.
2. Maps included with the report will cover from station 55+00 to the south portal, and be presented at a scale of 1:125.	All Full Periphery Geotechnical Maps (FPGM) covering Stations 55+00 to the South Portal are presented at a scale of 1:125. These maps have been submitted separately to the DOE Technical Data Base and the RPC as part of the data packages identified by the ATDT Data Tracking Numbers listed below. FPGMs for Stations 55+00 to 65+00 were previously submitted 2/28/97 to the DOE in fulfillment of Level 3 Milestone SPG42BM3. Copies of FPGMs for Stations 65+00 to 78+77 are provided with this report. See Attachments 1 and 2 of the Preface for copies of the TDIFs and GENISES transmittal letters pertinent to this milestone.

DTN	STATION #
GS970808314224.009	(65+00 - 70+00)
GS970808314224.011	(70+00 - 75+00)
GS970808314224.013	(75+00 - 78+77)

PREFACE TABLE 1 (Continued) - Description/completion criteria location summary for U.S. Department of Energy Level 3 Milestone: SPG42CM3 - Geology of the South Ramp, Station 55+00 to 78+77, Exploratory Studies Facility, Yucca Mountain Project, Yucca Mountain, Nevada

CRITERIA	LOCATION/COMPLETION INFORMATION
3. These full-periphery geotechnical maps will show: A. Mapped geologic units and subunits, fractures, faults, and other important structural features (as appropriate), B. The location of all samples collected by the mapping group (or collected by the PIs and/or the ESF Technical Coordination Office), and C. As-constructed installed ground support and type.	The full periphery geotechnical maps incorporate Items A, B, and C of this criteria.

PREFACE TABLE 1 (Continued) - Description/completion criteria location summary for U.S. Department of Energy Level 3 Milestone: SPG42CM3 - Geology of the South Ramp, Station 55+00 to 78+77, Exploratory Studies Facility, Yucca Mountain Project, Yucca Mountain, Nevada

CRITERIA	LOCATION/COMPLETION INFORMATION
4. The deliverable will supply fracture analysis for the south ramp in the form of tabulated data sets, stereo plots, and statistical treatment of fracture information (by stratigraphic unit, or some selected interval along the course of tunnel excavation).	Within the report the sections on "Structure" and "Statistical Analysis" supply the statistical treatment of the fracture analysis. Additional fracture analyses are provided by the stereonets graphically presented on the FPGMs identified above in Item 3. Detailed Line Surveys (DLS) present tabulated fracture data. DLS data for Stations 55+00 to 65+00 were previously submitted 2/28/97 to the DOE in fulfillment of Level 3 Milestone SPG42BM3 Copies of DLSs for Stations 65+00 to 78+77 are provided with this report. The DLSs for Stations 65+00 to 78+77 have been submitted separately to the DOE Technical Data Base and to the RPC as part of the data packages identified by ATDT DTNs below. See Attachments 1 and 2 of the Preface for copies of the TDIFs and GENISES transmittal letters pertinent to this milestone. **DTN** **STATION #** GS970808314224.008 (65+00 - 70+00) GS970808314224.010 (70+00 - 75+00) GS970808314224.012 (75+00 - 78+77)
5. A cross section comparing the predicted geology of the south ramp and as-determined structural and stratigraphic interpretations will be presented.	See Drawing OA-46-301 provided in a pocket at the back of the report. This drawing has been submitted to the DOE Technical Data Base as part of this report and is identified by DTN GS970808314224.016. See Attachments 1 and 2 of the Preface for copies of the TDIF and the GENISES transmittal letter for.

PREFACE TABLE 1 (Continued) - Description/completion criteria location summary for U.S. Department of Energy Level 3 Milestone: SPG42CM3 - Geology of the South Ramp, Station 55+00 to 78+77, Exploratory Studies Facility, Yucca Mountain Project, Yucca Mountain, Nevada

CRITERIA	LOCATION/COMPLETION INFORMATION
6. Predicted and actual stratigraphic, structural and other key features will be discussed in the report.	See Drawing OA-46-301 and the information provided in the section titled "Comparative Cross Section" within the "Structure" section of the report.
7. Important sampling and testing activities will be identified and discussed, as appropriate.	Funding for the USBR's systematic sampling program in the ESF was terminated in September 1995, prior to excavation of the Main Drift. Location of samples collected by LANL in the South Ramp are identified on the FPGMs (see Item 3). See also Appendix II - "Sample Locations and Descriptions," of this report.
8. Results of the detailed line survey and appropriate graphical and tabular presentation of data will be included in the report.	See the "Structure" section of the report and Drawings OA-46-306, OA-46-307, and OA-46-308 in the pockets in the back of the report.
9. A summary of photographic work conducted in support of the mapping exercise will be provided as part of the report.	See Appendix VI - "Photos and Plates" for photographs with captions.
10. The stereophotography will be identified within the report (photo numbers, current archive location) for future reference.	See Appendix II - "Photogrammetric Negative Numbers and Camera Locations."
11. The report will briefly describe any unusual features observed in the mapping, detailed line survey, photogrammetry, or sampling exercises.	See "Additional Features" section.

PREFACE TABLE 1 (Continued) - Description/completion criteria location summary for U.S. Department of Energy Level 3 Milestone: SPG42CM3 - Geology of the South Ramp, Station 55+00 to 78+77, Exploratory Studies Facility, Yucca Mountain Project, Yucca Mountain, Nevada

CRITERIA	LOCATION/COMPLETION INFORMATION
12. Results of the RQD and Q&RMR analyses will also be provided and integrated into map or other graphical presentations of related data.	The results are provided on FPGMs (see Item 3) and within the "Geotechnical Characterization" section of the report.
13. The following will be included in the report: A. Alcove maps (for additional constructed portions of Alcove 5, the thermal test facility, and Alcove 6, the north Ghost dance Alcove), B. A summary of detailed line survey data, C. Stereo photographic information, D. Tabulations and assessment of structural data from alcove mapping investigations, and E. Statistical treatment of alcove fracture data.	The remaining portions of Alcove 5 were submitted June 30, 1997 to the DOE Technical Data Base and the RPC as fulfillment of Level 4 Milestone SPG42FM4. Identification numbers are listed below. Alcove 6 data have been submitted separately to the DOE Technical Data Base and RPC in fulfillment of this milestone and are identified below. Copies of DLSs and FPGMs for Alcove 6 are provided with this report. See Attachments 1 and 2 of the Preface for copies of Alcove 5 and Alcove 6 TDIFs and GENISES transmittal letters. **ALCOVE 5 DTNs:** GS970608314224.006 (DLS) GS970608314224.007 (FPGM) **ALCOVE 6 DTNs:** GS970808314224.014 (DLS) GS970808314224.015 (FPGM) Items C, D, and E of this criteria are summarized in the "Alcoves" part of the section, "Additional Features."

PREFACE TABLE 1 (Continued) - Description/completion criteria location summary for U.S. Department of Energy Level 3 Milestone: SPG42CM3 - Geology of the South Ramp, Station 55+00 to 78+77, Exploratory Studies Facility, Yucca Mountain Project, Yucca Mountain, Nevada

CRITERIA	LOCATION/COMPLETION INFORMATION
REGULATORY REQUIREMENTS:	
1. This deliverable shall be prepared in accordance with OCRWM approved quality assurance procedures implementing requirements of the Quality Assurance Requirements Description.	See the Preface.
2. The product shall be developed on the basis of the best technical data, including both Q and non-Q data. The Q status of the data used and cited in the report shall be appropriately noted.	See the Preface.
3. **OPTIONAL:** Stratigraphy used shall be consistent with the Reference Information Base section 1.12(a): Stratigraphy-Geologic Lithologic Stratigraphy.	Stratigraphy used is in compliance with the RIB section 1.12(a).
4. Within the report's Reference Section, references to data used in the report shall include record Accession Numbers or Data Tracking Numbers when available.	Data used for development of this report are identified by DTN in Appendix V - "Data Tracking Numbers for Review Packages." Reports or publications identified in the Reference section were not used as data sources but for corroborative or informational purposes only.

PREFACE TABLE 1 (Continued) - Description/completion criteria location summary for U.S. Department of Energy Level 3 Milestone: SPG42CM3 - Geology of the South Ramp, Station 55+00 to 78+77, Exploratory Studies Facility, Yucca Mountain Project, Yucca Mountain, Nevada

CRITERIA	LOCATION/COMPLETION INFORMATION
5. Technical data contained within the deliverable and not already incorporated in the Geographic nodal Information Study and Evaluation System (GENISES) shall be submitted for incorporation into the GENISES in accordance with YAP-SIII.3Q.	The developed data generated from this report are identified in the ATDT system under TDIF DTN GS970808314224.016. See Attachments 1 and 2 of the Preface for copies of the TDIF and the GENISES transmittal letter.
6. Verification of technical data submittal compliance shall be demonstrated by including as part of the deliverable: 1. A copy of the Technical Data Information Form generated identifying the data in the Automated Technical Data Tracking system, and 2. A copy of the transmittal letter attached to the technical data transmittal to the GENISES Administrator.	See Attachments 1 and 2 of the Preface.
7. This deliverable shall be processed in accordance with YAP-5.1Q.	See YAR accompanying this milestone deliverable.

ABSTRACT

The Exploratory Studies Facility (ESF), under construction at Yucca Mountain, is being studied to determine its suitability as a permanent high-level nuclear waste repository. This report presents a summary of data collected by U.S. Bureau of Reclamation (USBR) personnel on behalf of the U.S. Geological Survey (USGS). This report focuses on the South Ramp, and includes that portion of the tunnel from Sta. 55+00 to 59+35.47 (a part of the Main Drift) and the curved section from Sta. 59+35.47 to 64+25.21. The true South Ramp portion of the tunnel is from Sta. 64+25.21 to the end of the tunnel at Sta. 78+77. Alcoves 5, 6, and 7, which are located off the Main Drift, are also addressed.

The pre-construction cross section and the as-built cross section are generally similar, but discrepancies occur at Sta. 71+00 to 72+00 and 78+00. On the pre-construction section a down dropped block or graben is shown at around Sta. 72+00. The as-built section shows only the fault at Sta. 71+30 with the graben pinching out above the tunnel alignment. At Sta. 78+00, surface mapping indicated a low angle reverse fault based on the geometry of the surface trace. This fault is shown as a high angle reverse fault on the as-built section, therefore this structure must be steepening with depth. In general, conditions are as predicted.

From Sta. 55+00 to 78+77 there are 716 features described in the Detailed Line Survey (DLS) and Full Periphery Geologic Maps (FPGM) as faults and shears. Of these features, 710 have an offset of less than 4.0 m. The distribution of these features along this portion of the ESF is variable with the highest concentration of faults and shears around Sta. 70+00. Azimuths also range from 0° to 360° with the highest concentration around 140°. Three of the six faults with over 4.0 m of offset are noteworthy. The Dune Wash fault at Sta. 67+87.25 has about 52 m of down-to- the-west offset. The Ghost Dance fault at Sta. 57+30 has about 1.2 m offset down-to-the-west. The fault at Sta. 70+58 has about 50 m offset down to the west.

This portion of the ESF is characterized by frequent changes in lithology due to faulting. Some

of the lithologic units are repeated two or three times. Stereonet analysis contours identified fracture sets similar to the fracture sets found in the Main Drift, but with a general clockwise rotation. Visual analysis of stereonet contour plots identified a set of fractures with azimuths ranging from 185° to 220° in portions of the South Ramp which is not found in the Main Drift.

A sampling bias for DLS fractures with strike azimuths parallel or subparallel to the tunnel is evident through the curved section of the tunnel on a plot showing the relationship of the tunnel bearing to a strike azimuth vs. station scatter plot of fractures. The sampling bias is also evident from an examination of the stereonet plots of the 100 meter FPGM's.

Three primary fracture sets were identified in most of the South Ramp Topopah Spring Tuff fracture data using cluster analysis. These are similar to sets identified in the Main Drift fracture data, and consist of northwest and northeast trending sets, and a low-angle set of fractures. These sets differ from peak fracture orientations observed in the North Ramp. South Ramp Tiva Canyon Tuff fracture characteristics differ from those of the Topopah Spring Tuff.

Geotechnical characterization of the South Ramp includes rock mass quality descriptions and comparisons of the theoretical ground support requirements and the installed ground support. Rock mass descriptions are based on two empirical classification systems; rock quality (Q system) and rock mass rating (RMR). Rock quality ratings are reported for three thermal-mechanical units. The theoretical ground support requirement is based on field rock mass data (this report) and the Exploratory Studies Facility design documents.

Additional features of interest, including damp zones noted at the time of excavation, and a feature at Sta. 74+36 observed to be "exhaling" significant amounts of air are discussed in detail.

INTRODUCTION

Yucca Mountain is a site under consideration for a high-level, long-term underground nuclear-waste repository. Located 100 miles northwest of Las Vegas in southwestern Nevada (Fig.1), Yucca Mountain lies on the western edge of the Nevada Test Site (NTS). The United States Geological Survey (USGS)/United States Bureau of Reclamation (USBR), under direction of the Department of Energy (DOE), has undertaken this study as part of a larger investigation to characterize the geology of Yucca Mountain in order to evaluate its suitability as a repository site.

As part of its ongoing investigations, DOE is constructing the Exploratory Studies Facility (ESF). The ESF consists of a series of underground excavations designed to investigate the subsurface geology and hydrology of Yucca Mountain (Fig. 2). The initial feature of the ESF was the North Ramp, a 7.62 m diameter tunnel approximately 2,800 m long with a bearing of 299° and a decline of 2.1 percent. The North Ramp provides access to the Main Drift, a north-south access excavation 3,154 m long, oriented down the eastern edge of the potential repository block. The South Ramp, which provides a southern access to the repository horizon, is approximately 1,800 m long. The South Ramp was completed April 25, 1997 (see Photo 11). A second phase of the ESF may include excavations to and through the Calico Hills Formation at a level below the proposed repository. Configuration of these deeper excavations is in the planning phase.

The North Ramp portal of the ESF is at Exile Hill within Midway Valley. The starter tunnel opening is a 60-m-long, 10-m-high, horseshoe-shaped tunnel excavated by drill/blast methods. The starter tunnel excavation served as a launch chamber for the tunnel-boring machine (TBM) excavating the North Ramp. The TBM is a fully-shielded machine manufactured by Construction Tunneling Services of Kent, Washington. The TBM trailing gear has been constructed with a special 45-m-long section that provides geologists with relatively unobstructed views of the tunnel walls. The trailing gear is also equipped with a moveable gantry which travels independently of the TBM, permitting access to the tunnel periphery.

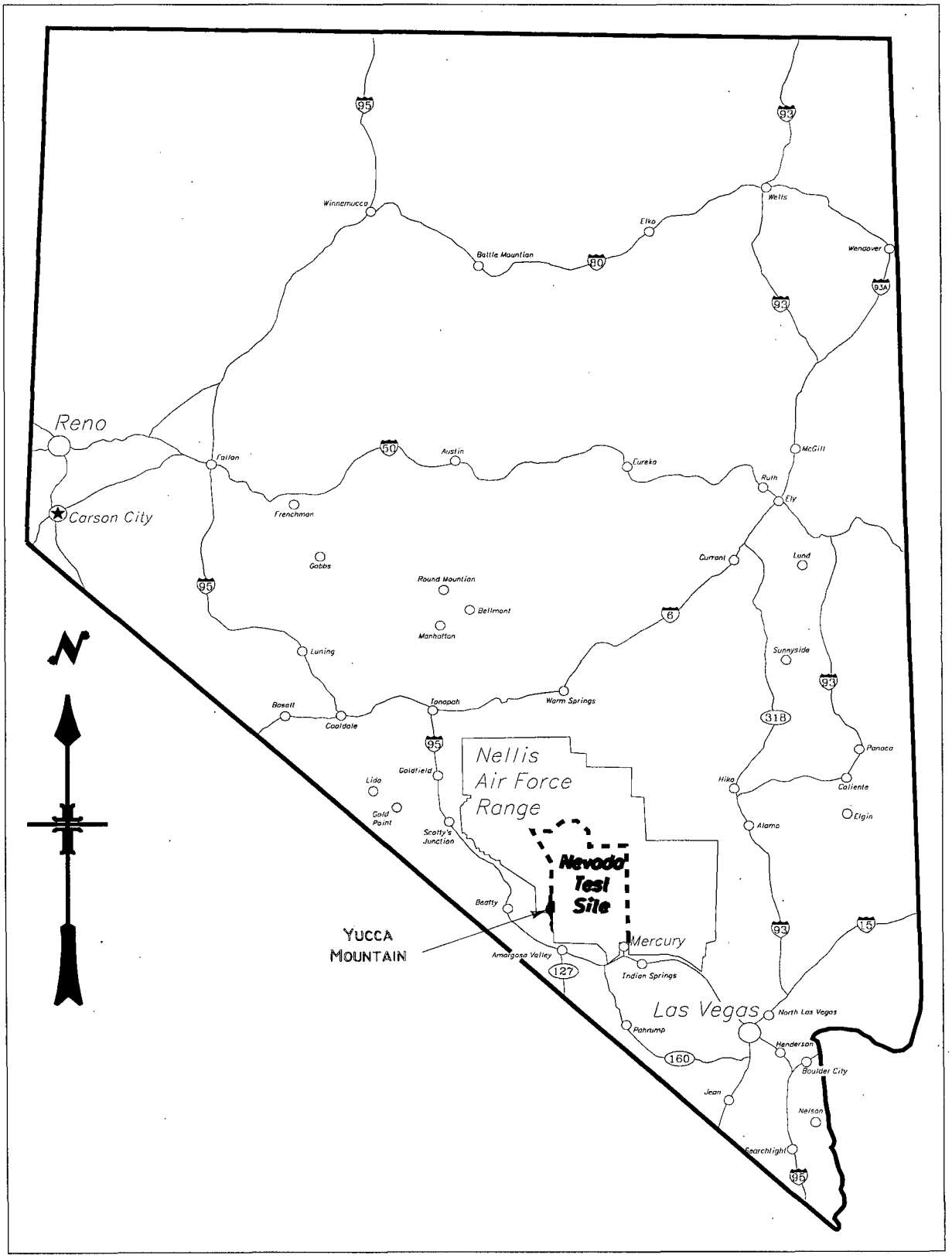

Figure 1. Location map of Yucca Mountain with respect to the state of Nevada (not to scale).

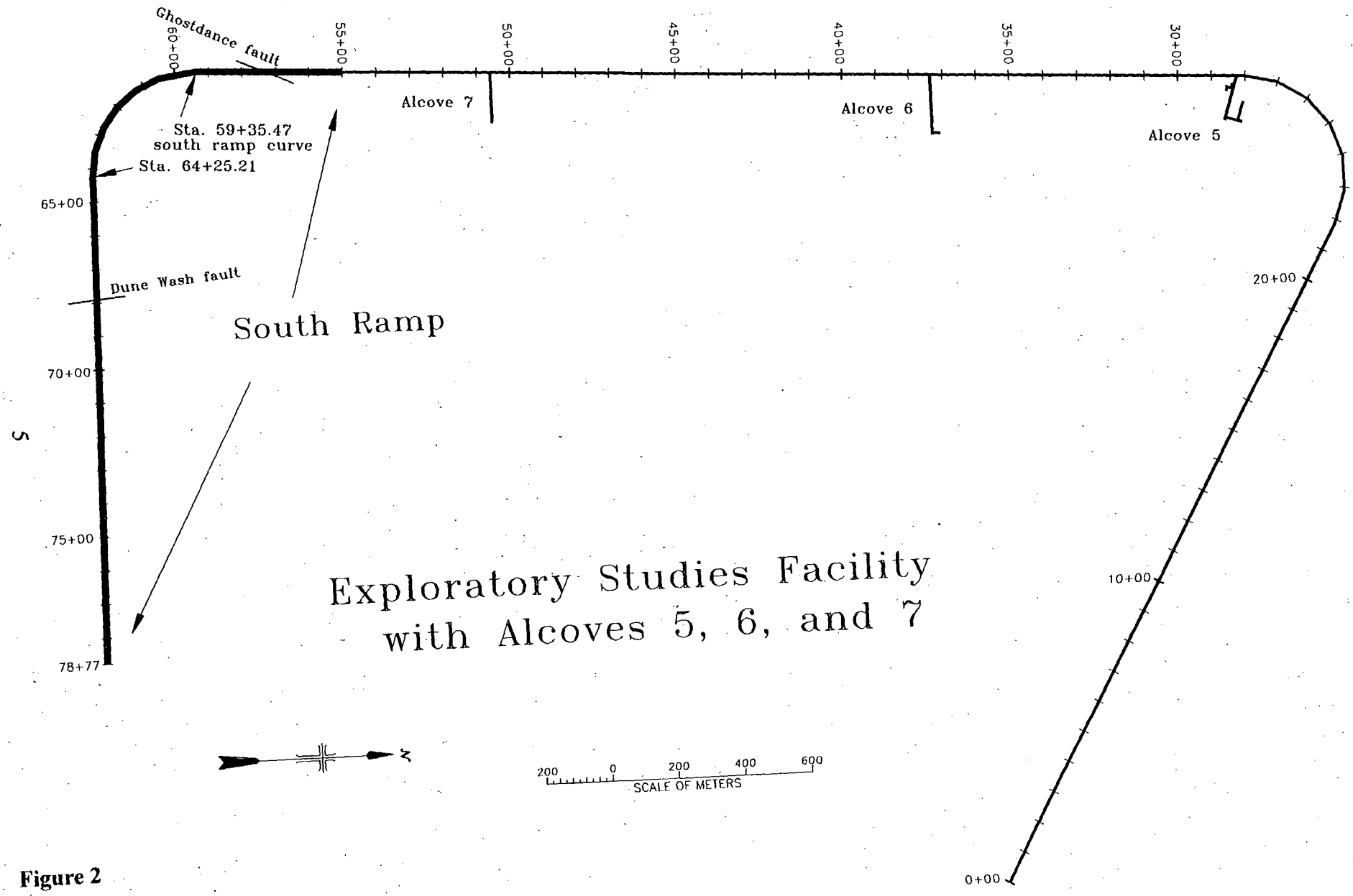
Ghostdance fault
60+00
55+00
50+00
45+00
40+00
35+00
30+00
Alcove 7
Alcove 6
Alcove 5
Sta. 59+35.47
south ramp curve
Sta. 64+25.21
65+00
Dune Wash fault
South Ramp
70+00
75+00
78+77
20+00
10+00
0+00
Exploratory Studies Facility
with Alcoves 5, 6, and 7
N
200 0 200 400 600
SCALE OF METERS

Figure 2

Objectives

This report is a summary of the data collected by USBR personnel on behalf of the USGS from Sta. 55+00 to 78+77 of the ESF South Ramp, as well as Alcoves 5, 6, and 7. The report includes descriptions of lithostratigraphic units, fracture statistics and cluster analysis, an analysis of rock mass quality, and a discussion of special features observed along the South Ramp. One goal of this project is to gain a clearer understanding of the fracture patterns and rock characteristics in the South Ramp area. Because fractures provide potential pathways through which water and gases can access stored waste and transport radionuclides into the surrounding environment, fracture data are analyzed to determine whether fractures can be grouped into sets with common features that relate to rock type or regional tectonic history. These relationships will help other investigators formulate more rigorous models of fluid movement and tectonism in the Yucca Mountain region.

Regional Geology

Yucca Mountain lies in southern Nevada, in the Great Basin, which is part of the Basin and Range structural/physiographic province. In the Yucca Mountain area, pre-Tertiary rocks consisting of a thick sequence of Proterozoic and Paleozoic sedimentary rocks underlie approximately 1000 to 3000 m of Miocene volcanic rock (Gibson and others, 1990).

The Miocene volcanic sequence exposed at Yucca Mountain includes units of the Paintbrush and Timber Mountain Groups (Sawyer and others, 1994). The Paintbrush Group consists of pyroclastic rock and lavas originating from the Claim Canyon caldera, approximately 6 km north of the study area, from 12.8 to 12.7 Ma old (Byers and others, 1976; Sawyer and others, 1994). The Paintbrush Group includes a homoclinal sequence consisting of four formations of pyroclastic-flow and pyroclastic-fall deposits with interbedded lavas which dip 5-10° to the east (Byers and others, 1976; Christiansen and others, 1977; Broxton and others, 1993). Two of these formations, the Topopah Spring and Tiva Canyon Tuffs, are voluminous, densely welded,

compositionally zoned pyroclastic outflow sheets that grade upward from rhyolite composition to quartz latite composition (Lipman and others, 1966; Byers and others, 1976; Schuraytz and others, 1989).

Yucca Mountain is bounded on three sides by alluvium-filled structural valleys consisting mostly of alluvial fan deposits (fluvial and colluvial sediments) and some thin eolian deposits. Yucca Mountain is bounded on the north by the Claim Canyon and Timber Mountain Calderas. The Yucca Mountain area is cut by north-south-striking normal faults which separate the Tertiary volcanics into blocks one to four km wide (Scott, 1990). The proposed repository block is bounded by the Solitario Canyon fault to the west and the Bow Ridge fault to the east. Both faults dip steeply toward the west (Scott and Bonk, 1984; Day and others, written comm., 1996), and have hundreds of meters of displacement.

Site Characterization Techniques

Geologic site-characterization activities performed at the ESF by the USBR for the USGS include the following techniques taken from a technical procedure entitled *Underground Geologic Mapping* (U.S. Bureau of Reclamation and U.S. Geological Survey, 1997).

Full-Periphery Geologic Mapping

Geologic mapping in the ESF records lithostratigraphic and structural features at a scale of 1:125 (refer to Drawings OA-46-257 through -282, and OA-46-293 through -294). These drawings are developed in the full-periphery style in which the tunnel walls, are "unrolled" to produce a flat map of the tunnel periphery. Structural discontinuities with trace lengths longer than 1 m and lithostratigraphic contacts were recorded on field sheets. Traces of lithostratigraphic and structural features were then digitized using AutoCAD. The maps were field checked for accuracy, consistency and completeness. The full-periphery geologic maps are located in the Records Processing Center with their associated data tracking numbers listed in

Appendix V.

Detailed Line Surveys

Detailed line surveys (DLS) were conducted along the right wall, normally 0.9 m below the springline. A metric measuring tape was affixed to the wall and discontinuities that intersect the wall within 30 cm of the tape were documented. Minimum trace length for the DLS was 1 m. Data on the shorter fractures, 30 cm to 1 m, was collected in 50 m intervals every 500 m, (between Sta. 55+00 and 55+50, 60+00 and 60+50, 65+00 and 65+50, 70+00 and 70+50, 75+00 and 75+50). Over 3200 fractures, cooling joints, vapor-phase partings, faults and shears were recorded by DLS in the South Ramp. Discontinuities were 77 percent fractures, 1 percent cooling joints, 8 percent vapor-phase partings, and 14 percent faults and shears. The DLS data are located in the Records Processing Center: their data tracking numbers are listed in Appendix V. The following characteristics were recorded in the DLS.

Station - A discontinuity is located on the DLS tape to the nearest 0.01 m giving each discontinuity a unique identifier.

Orientation - The orientation of a geologic feature is determined using a goniometer for strike azimuth and a Brunton compass for dip values. Orientations were recorded using the right-hand rule where the direction of the dip is 90° to the right (clockwise) of strike.

Type - Discontinuities include lithologic contacts, fractures, cooling joints, vapor-phase partings, faults, and shears. Vapor-phase partings are discontinuities that consist of roughly linear accumulations of vapor-phase minerals and are parallel to subparallel to lithostratigraphic layering. Fractures are those discontinuities that have no visible offset. Cooling joints are a class of fracture that presumably formed as a result of stresses in the cooling volcanic sheet. Shears are those

discontinuities having less than 0.1 m offset, or when offset is indeterminate. Faults are those discontinuities with greater than 0.1 m offset.

Trace length - Trace length is the length of the discontinuity on the tunnel wall. The trace length is two measurements, from the DLS tape to the discontinuity's upper end, and from the tape to its lower end. These two measurements allow the discontinuity to be accurately located relative to the DLS tape and other discontinuities.

Height, Width - The height and width are measured on an imaginary extension of the discontinuity plane. A horizontal line extending on strike from the highest point on the plane defines the upper boundary of the plane. A line parallel to the dip of the discontinuity extending from the point of its greatest lateral extent defines the lateral boundary of the plane. The height and widths are the maximum dimensions of that plane, width being measured parallel to strike and height being measured parallel to dip.

Terminations - The number of visible ends (terminations) are counted. The type of termination is also recorded. If the discontinuity extends out of view, such as continuing under the concrete invert sections, or obscured by the tunnels steel support, it is recorded as such. The visible ends are recorded as ending in rock or ending in another discontinuity. The acute angle at which one discontinuity terminates into another is specified as intersecting either at less than or greater than 45°.

Aperture - The minimum and maximum open, unfilled space between a discontinuity's surfaces is recorded as the aperture.

Roughness - The roughness scale is based on the scale used by the USBR (U.S. Bureau of

Reclamation, 1988). Roughness (R) characterizes the small-scale asperities of the fracture surface on a scale from 1 to 6. R1 designates a stepped surface with near-normal steps and ridges. R6 designates a very smooth, shiny, and polished surface.

Infilling type and thickness - Mineral coatings and infillings are described by their appearance, color, hardness, reaction to dilute hydrochloric acid, and fluorescence in UV light.

Description of Lithostratigraphic Units

Lithologic descriptions include compositional data, rock color and texture, welding features, secondary crystallization and alteration, depositional features, and stratigraphic relationships. The percentages of pumice clasts, matrix phenocrysts, lithic fragments, and lithophysae are visual estimates determined using charts produced by the American Geological Institute (Compton, 1962). The matrix percentages were subsequently computed by subtraction of the other rock components from 100 percent. Colors were determined on dry surfaces under tunnel lighting conditions using a standard Munsell rock-color chart (Geological Society of America, 1991). Unless otherwise noted, all stratigraphic stationing is given at springline on the right wall of the tunnel and are metric (Sta. 65+15 refers to 6515 m from the North Portal). Unit contacts were identified and recorded as the tunnel walls were geologically mapped in 1996 and 1997, however, detailed rock descriptions were not developed until the late spring and early summer of 1997. By this time the tunnel walls, especially below springline, had accumulated a significant amount of dust that locally obscured fine details of the units. Descriptions from approximately Sta. 74+05 to 78+77 were developed without benefit of tunnel lights.

Stereophotographic Coverage

Excavated tunnel walls were photographed from the mapping gantry on the trailing gear of the TBM. The photographs were taken with 60 percent longitudinal overlap and 20 percent circumferential overlap. The photographs provide full stereo photographic documentation of the tunnel walls and provide for future photogrammetric analysis if desired. The photographs are maintained and archived by the Management and Operations Contractor in Las Vegas, Nevada.

Rock Sampling

Funding for the USBR's systematic sampling program in the ESF was terminated in September, 1995, prior to the excavation of the Main Drift. Los Alamos National Laboratories (LANL) has since collected samples at the request of the individual Principal Investigators. The sample locations are shown on the FPGMs and are listed in tabular form in Appendix III.

LITHOSTRATIGRAPHY

The lithostratigraphy of the ESF South Ramp is described using the nomenclature and unit divisions of Sawyer and others (1994) and Buesch and others (1996) (Fig. 3). Although the subdivisions of the crystal-rich vitric zone of the Topopah Spring Tuff that are based on welding (Buesch and others, 1996) are used, the pyroclastic-flow deposit is distinguished from the overlying pumice-fall deposit. These deposits are described separately in subsequent sections. Lithostratigraphic units discussed in this report begin with the Tiva Canyon crystal-poor upper lithophysal zone (Tpcpul), and continue down through to the Topopah Spring crystal-poor lower lithophysal zone (Tptpll), as illustrated on Fig. 3. The locations of the lithostratigraphic contacts identified in the South Ramp are summarized in Table 1.

The exposures in the South Ramp clarify and confirm many lithostratigraphic relationships that were previously inferred from studies of drill core, downhole video, and hydrologic properties or observed in the North Ramp tunnel walls (Barr and others, 1996). The variable and localized character of fumarolic alteration at the top of the Topopah Spring Tuff pyroclastic-flow deposit (Moyer and others, 1996) is clearly exhibited in three South Ramp locales. Also, the expected stratigraphic thinning of the PTn hydrogeologic unit described by Moyer and others (1996) is observed in South Ramp exposures.

Tiva Canyon Tuff

The South Ramp penetrates pyroclastic-flow units of the Tiva Canyon Tuff from the central portion of the crystal-poor upper lithophysal zone to the base of the deposit. Partial sections exposed in fault-bounded blocks occur from Sta. 66+98 to 67+62, Sta. 67+62 to 67+88, and Sta. 74+90.6 to 74+94.7. The South Portal box cut exposed units from the central portion of the crystal-poor upper lithophysal zone to the lower portion of the mixed pumice subzone of the crystal-rich nonlithophysal zone. The stratigraphy of the South Portal units will be discussed in a separate report. This section provides summary rock unit and contact descriptions for the zones

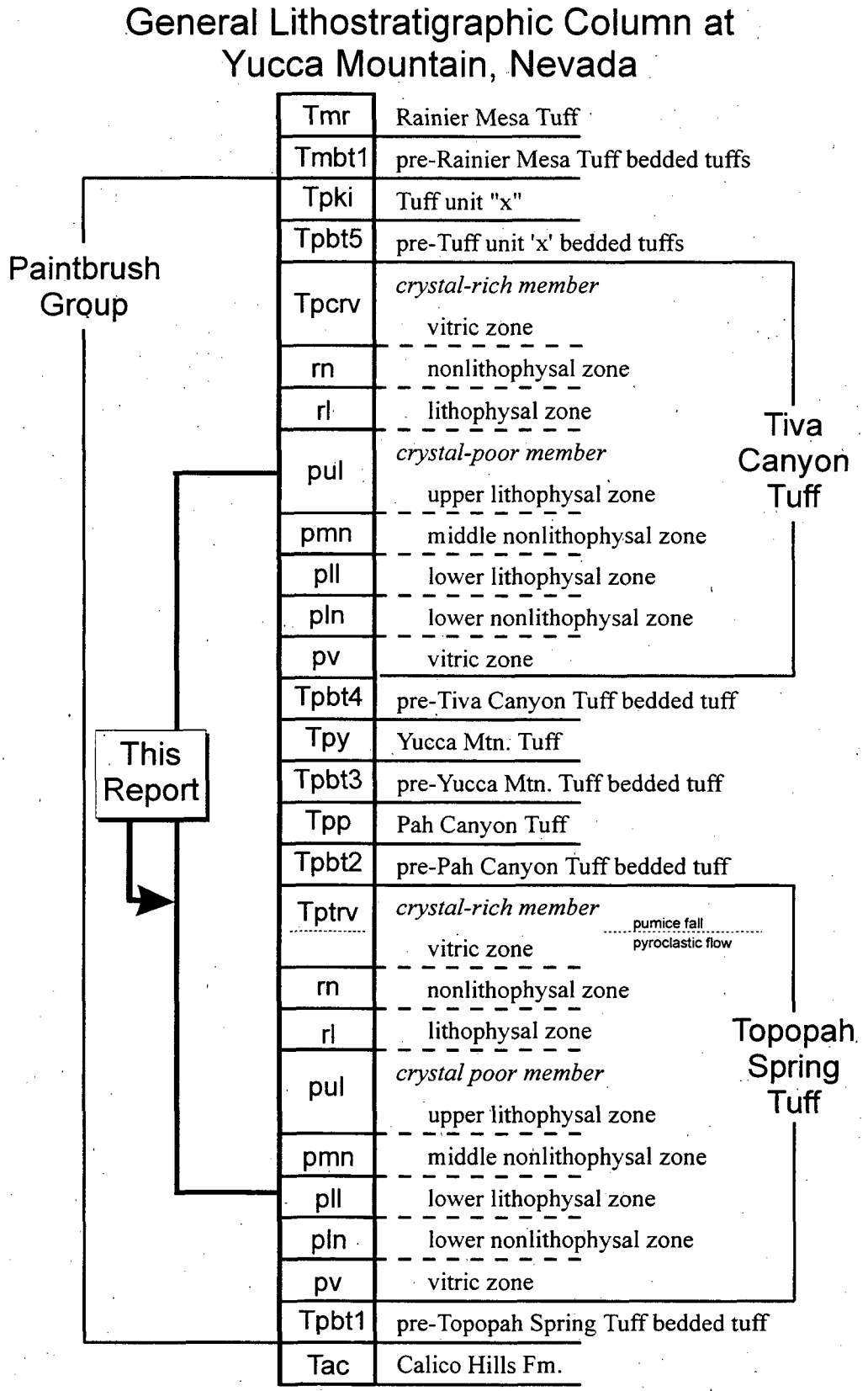

Figure 3. Lithostratigraphic column of the Paintbrush Group at Yucca Mountain showing the stratigraphic interval described in this report.

Table 1. Lithostratigraphic Contacts from Sta. 55+00 to 78+77

Unit*	Stationing**	Comments
Tptpmn	55+00 to 57+29	Ghost Dance Fault at 57+29.
Tptpll	57+29 to 58+78	
Tptpmn	58+78 to 63+08	Tsw2/TSw1 contact at 63+08.
Tptpul	63+08 to 64+55	
Tptrl	64+55 to 65+07	Crystal transition subzone (Tptrl1) from 64+55 to 64+93.
Tptrn	65+07 to 65+25	Faulted contact at 65+25.
Tptrl	62+25 to 65+27	
Tptrn	65+27 to 66+34	
Tptrv1	66+34 to 66+37.5	TSw1/PTn contact at 66+37.5; Tpt flow/fall contact at 66+37.5.
Tptrv2	66+37.5 to 66+38.5	Unit locally is absent.
Tptrv3	66+38.5 to 66+49	Ash layer 1 of Buesch and others (top of Tpt) at 66+49.
Tpbt2	66+49 to 66+80.5	Faulting repeats part of section.
Tpbt3	66+80.5 to 66+94	Pah Canyon Tuff is absent.
Tpbt4	66+94 to 66+98	Yucca Mountain Tuff is absent.
Tpcpv	66+98 to 67+25	Nonwelded to moderately welded break at 67+18.
Tpcpln	67+25 to 67+62	Moderately to densely welded break (PTn/TCw contact) at 67+28.5; faulted contact at 67+62 (TCw/PTn contact).
Tpcpv	67+62 to 67+70	Interval is moderately welded; section is incomplete.
Tpcpln	67+70 to 67+88	Moderately to densely welded break (PTn/TCw contact) at 67+78.
Fault Zone	67+88 to 67+91	Dune Wash fault zone contains tilted block with Tptrv1, incomplete Tptrv3, incomplete Tpbt2, and incomplete Tpbt3.
Tptpul	67+91 to 68+47	Incomplete section.
Tptrl	68+47 to 68+85	Crystal transition subzone (Tptrl1) from 68+47 to 68+65.5.
Tptrn	68+85 to 69+90.5	
Tptrv1	69+90.5 to 69+96	TSw1/PTn contact at 69+96; Tpt flow/fall contact at 69+96; top of flow locally moderately welded.
Tptrv3	69+96 to 70+07	Tptrv2 absent; ash layer 1 of Buesch and others (top of Tpt) at 70+07.
Tpbt2	70+07 to 70+58	Faulting repeats part of section; faulted contact at 70+58 (PTn/TSw2 contact).

Tptpmn	70+58 to 71+68	TSw2/TSw1 contact at 71+68.
Tptpul	71+68 to 73+02	
Tptrl	73+02 to 73+41	Crystal transition subzone (Tptrl1) from 73+02 to 73+27.5.
Tptrn	73+41 to 74+40	
Tptrv2	74+40 to 74+41	Subunit is devitrified; Tptrv1 is absent; Tpt flow/fall contact at 74+41; TSw1/PTn contact at 74+40.
Tptrv3	74+41 to 74+50.5	Ash layer 1 of Buesch and others (top of Tpt) at 74+50.5.
Tpbt2	74+50.5 to 74+77	
Tpp	74+77 to 74+81.3	Possibly reworked.
Tpbt3	74+81.3 to 74+87.5	
Tpbt4	74+87.5 to 74+90.6	Yucca Mountain Tuff is absent.
Tpcpv	74+90.6 to 74+94.7	Nonwelded; faulted contact at 74+94.7.
Tpbt4	74+94.7 to 74+96.4	
Tpcpv	74+96.4 to 75+14.6	Nonwelded to moderately welded break at 75+04.5.
Tpcpln	75+14.6 to 76+03	Moderately to densely welded break (PTn/TCw contact) at 75+16.
Tpcpmn	76+03 to 78+40	Tpcpll is absent.
Tpcpul	78+40 to 78+77	South portal at 78+77.

* Unit designations after Buesch and others, 1996.
** Measured along springline, right rib.

traversed by the South Ramp, outlines the stratigraphic and depositional features observed in the tunnel walls, and describes general features of welding, secondary crystallization, and alteration.

Rock Unit and Contact Descriptions

Crystal-Poor Member

Upper Lithophysal Zone (Tpcpul)

The crystal-poor upper lithophysal zone is a densely welded, devitrified and vapor-phase altered pyroclastic-flow deposit that is composed of 71 to 92 percent matrix, 2 to 3 percent phenocrysts, less than 1 percent lithic fragments, 3 to 5 percent pumice, and 3 to 20 percent lithophysae. Devitrified matrix grades upward from pale red-purple (5RP6/1, 5RP7/1) to pale red (5R6/2) and contains submillimeter blebs of very light gray to white (N8 to N9) vapor-phase material peppered throughout. Spots of light to very light gray (N7, N8), vapor-phase alteration form from 5 to 10 percent to 40 to 50 percent of the matrix. Vapor-phase spots typically have subspherical shapes and diameters of 5 to 20 mm and may have a central streak of white (N9) vapor-phase minerals or a small, gash-like central cavity. Phenocrysts are predominantly feldspar with traces of biotite. Subangular to subrounded lithic clasts of light gray (N7), devitrified volcanic rock have diameters generally smaller than 10 mm. Pumice clasts, which are difficult to discern throughout the zone, are mostly smaller than 40 mm, light to very light gray (N7, N8), and altered to fine-grained vapor-phase minerals.

From Sta. 78+40 to 78+51, subspherical to ellipsoidal lithophysae compose 7 to 15 percent of the rock mass, and range from 40 x 50 mm to 300 x 300 mm. From Sta. 78+51 to 78+64, ellipsoidal to lenticular lithophysae compose 1 to 20 percent of the rock. Lithophysae form 15 to 20 percent of the rock through most of this interval, except in the upper few meters, where pods or pockets of rock with 1 to 3 percent lithophysae are present. Cavities in this interval typically are from 100 x 250 mm to 300 x 340 mm in size, but they range from 15 x 25 mm to 500 x 1000 mm,

with larger cavities aligned along vapor-phase partings. From Sta. 78+64 to 78+77, subspherical to ellipsoidal lithophysae compose from 3 to 20 percent of the rock. Cavities vary from 15 x 25 mm to 400 x 600 mm, with most smaller than 250 x 350 mm. The lower 2 to 3 stratigraphic meters of the interval have 3 to 10 percent lithophysae that are smaller than 110 x 130 mm. Lithophysal cavities have from 5 to 30 mm of vapor-phase silica and minor hematite coating platy interior rock fragments or lining the cavity walls. Large cavities have overgrowths of tabular calcite atop the vapor-phase minerals.

The lower zone contact is sharp and planar to slightly undulatory. The contact is marked by a downward decrease in lithophysae from 5 to 7 percent above to less than 1 percent below.

Middle Nonlithophysal Zone (Tpcpmn)

This densely welded, devitrified zone is composed of 84 to 93 percent matrix, 2 to 3 percent phenocrysts, less than 1 percent lithic fragments, 5 to 12 percent pumice and less than 1 percent lithophysae. Matrix grades upward from a mottled mix of pale brown and light brown (5YR6/2 and 5YR6/4) to pale brown (5YR5/1) to a mottled mix of grayish red and grayish orange-pink or grayish pink (5R4/1, 5R4/2 and 5YR7/2, 5R8/2) to pale red (5R6/2, 10R6/2) to a mottled mix of pale red-purple and light gray (5RP6/1, N7). Shard texture is partially preserved in the lower part of the zone (Sta. 76+03 to 76+20), but is destroyed at higher stratigraphic levels. Vapor-phase alteration occurs as submillimeter blebs of grayish pink material that locally compose a few percent of the matrix. Ellipsoidal spots of vapor-phase alteration, which have diameters of 15 to 25 mm, form 1 to 7 percent of the matrix from Sta. 76+60 to 76+73. Phenocrysts are predominantly feldspar with traces of biotite. Subangular to subrounded lithic clasts of light gray (N7), devitrified volcanic rock generally have diameters smaller than 10 mm. Pumice clasts are typically 5 to 35 mm (long axis), but occur to 100 mm, and are notably larger (40 to 120 mm) in a swarm that occurs at Sta. 76+39. The clasts are elongated, with shape ratios of 3:1 to 8:1. Pumice clasts in the lower part of the zone (Sta. 76+03 to 77+76) are a mix of grayish red (5R4/1, 5R4/2), devitrified material and grayish orange-pink and grayish pink (5YR7/2, 5R8/2)

vapor-phase material. Pumice clasts are replaced by sugary vapor-phase material from Sta. 77+76 to 78+40; these clasts are shades of grayish pink, light gray, or very light gray (5R8/2, N7, N8). Lithophysae form less than 1 percent of the rock from Sta. 76+60 to 76+73 and Sta. 77+87 to 78+09, but are absent elsewhere. The lithophysae vary from gash-like features in the centers of vapor-phase spots to ellipsoidal or lenticular cavities 20 to 280 mm long.

Vapor-phase partings form continuous features with vertical spacings of 25 to 60 cm from Sta. 76+03 to 76+27 and 76+60 to 77+76. Elsewhere, vapor-phase partings cannot be traced from invert to crown and occur with stringers of vapor-phase material 10 to 40 cm long. The middle nonlithophysal zone rock generally breaks in a conchoidal manner, except in lithophysae-bearing intervals, where fracture is irregular and in the basal few meters (Sta. 76+03 to 76+27), where fracture is quasi-conchoidal to irregular.

The lower contact of this zone is indistinct, but is marked by numerous closely spaced vapor-phase partings above the contact.

Lower Lithophysal Zone (Tpcpll)

The lower lithophysal zone (Tpcpll) (Fig. 3) is not encountered in the South Ramp (Table 1).

Lower Nonlithophysal Zone (Tpcpln)

The crystal-poor lower nonlithophysal zone is a moderately to densely welded, devitrified pyroclastic-flow deposit composed of at least 3 poorly sorted, matrix-supported flow units. The zone, which grades upward from moderately welded (Sta. 67+25 to 67+29 and Sta. 75+14.6 to 75+16) to densely welded (Sta. 67+29 to 67+62 and Sta. 75+16 to 76+03), is composed of 69 to 92 percent matrix, 2 to 3 percent phenocrysts, 1 to 3 percent lithic fragments, and 5 to 25 percent pumice (locally 25 to 70 percent in swarms). Where moderately welded, the rock is grayish orange-pink (5YR7/2; 5YR7/1), with a moderately deformed matrix that contains a small amount

of intershard porosity and visible shard texture. Where densely welded, the rock occurs in shades of pale red (5R6/2, 10R6/2) to pale brown (5YR6/2, 5YR5/2) and may appear as mottled mixes of these colors and moderate brown (5YR6/4) or grayish orange-pink (5YR7/2). Densely welded matrix is strongly deformed and lacks intershard porosity. Shard texture is preserved in the lower part of the unit (for example, Sta. 75+14.6 to 75+60), but partially to completely destroyed at higher stratigraphic levels. Phenocrysts are predominantly feldspar with traces of biotite. Subangular to subrounded lithic clasts, predominantly of moderate red (10R4/4), grayish red (5R4/1, 5R4/2), and light gray (N7) devitrified volcanic rock, but with traces of light gray (N7) and grayish black (N2) glassy volcanic rock, are generally smaller than 10 mm in diameter (up to 15 mm). Pumice clasts in the exposure from Sta. 67+25 to 67+62 are grayish black (N2) and vitric in the basal meter of the zone, but are moderate reddish orange to moderate orange-pink (10R6/6 to 10R7/4) and argillically altered elsewhere. Spherulites occur within and along the margins of argillically altered pumice clasts from Sta. 67+46 to 67+62. Pumice clasts in the exposure from Sta. 75+14.6 to 75+70 are a mix of moderate reddish orange, argillically altered clasts and medium gray to grayish red (N5 to 5R4/1), devitrified clasts. Argillically altered clasts predominate in the lower part of the interval, but decrease in abundance upward as spherulites forming along the clast margins progressively consume the clast interiors. From Sta. 75+70 to 76+03, pumice clasts are primarily grayish red (5R4/2, 10R4/2) and granophyrically or spherulitically devitrified. Pumice clasts typically are 5 to 80 mm (long axis), with shape ratios of 2:1 to 6:1 in the lower part of the zone and 4:1 to 10:1 in the upper part of the zone.

Flow unit boundaries are marked by two pumice swarms. The lower swarm (Sta. 67+46 and 75+69.5) is 10 to 40 cm thick and lenticular, with 30 to 180 mm (long axis) pumice clasts and shape ratios of 3:1 to 10:1. Pumice content within the lower swarm varies from 40 to 70 percent at Sta. 67+46 to 25 to 30 percent at Sta. 75+69.5. The upper swarm (Sta. 67+59 and 75+75.7) is 20 to 60 cm thick and planar to wedge-shaped, with 30 to 180 mm (long axis) pumice clasts and shape ratios of 3:1 to 8:1 (Photo 1). Pumice composes from 25 to 50 percent of the upper swarm and is reverse graded in some exposures. A faintly laminated, crystal-rich (20 to 25 percent) surge horizon that is 2.0 to 2.5 cm thick, occurs between the two pumice swarms at Sta. 75+73.

The crystal-poor lower nonlithophysal zone contains numerous smooth, high-angle, curviplanar fractures, some of which have apertures of 5 to 15 cm and are infilled with crushed, broken, or pulverized wall rock. The rock comprising this zone has a quasi-conchoidal fracture.

The lower contact of the zone is generally planar and grades (from devitrified to vitric) over 10 to 20 cm. The contact is marked by the abrupt downward change from devitrified to vitric or argillically altered rock.

Vitric Zone (Tpcpv)

The crystal-poor vitric zone is a nonwelded to moderately welded, vitric to slightly altered pyroclastic-flow deposit composed of two poorly sorted, matrix-supported flow units. The zone, which grades upward from non- to partly welded (Sta. 66+98 to 67+18 and Sta. 74+94.7 to 75+04.5) to moderately welded (Sta. 67+18 to 67+25 and Sta. 75+04.5 to 76+14.6), is composed of 57 to 94 percent matrix, 2 to 3 percent phenocrysts, 1 to 5 percent lithic fragments, and 3 to 35 percent pumice. The flow units are separated by a comparatively coarse-grained, laminated surge horizon 11 to 15 cm thick that occurs at Sta. 67+19 and 75+00.2. Where vitric, the zone is moderate yellowish brown (10YR6/4 grading upward to 10YR5/4), but locally is moderate orange-pink (5YR7/4) where argillically altered (for example, Sta. 67+18 to 67+20). The matrix is ash-rich and contains abundant dark yellowish orange (10YR6/6) and black (N1) cuspate to bubble-textured glass shards. The matrix, which is nondeformed and friable in the basal nonwelded interval, grades stratigraphically upward to slightly to moderately deformed and indurated as the degree of welding increases. Phenocrysts are predominantly feldspar with traces of biotite. Angular to subrounded lithic clasts of devitrified volcanic rock in shades of moderate red (10R4/4) and grayish red (5R4/1, 5R4/2) and glassy volcanic rock in shades of light gray (N7) and grayish black (N2) are generally smaller than 5 mm in diameter (up to 20 mm) and vary from 1 to 3 percent in the lower flow unit to 3 to 5 percent in the upper flow unit. Grayish pink (5R8/2) to pinkish gray (5YR8/1) pumice clasts, which are finely vesicular and vitric to slightly altered, typically are smaller than 25 mm and grade upward from nondeformed and randomly

oriented to moderately well aligned and deformed with shape ratios of 2:1 or 4:1. Pumice content varies vertically and laterally within each flow unit. At Sta. 66+98 to 67+19, the pumice abundance in the lower flow unit decreases from 10 to 15 percent near the base of the unit to 7 to 10 percent near the top of the unit. In contrast, pumice content in the lower flow unit at Sta. 74+96.4 to 75+00.2 increases upward from 3 to 5 percent to 10 to 15 percent; the basal 25 cm contains 25 to 35 percent pumice. Pumice clasts comprise 3 to 5 percent of the upper flow unit at Sta. 67+19 to 67+25. However, at Sta. 75+00.2 to 75+14.6, the pumice content in the upper flow unit decreases upward from 10 to 15 percent to 7 to 10 percent.

The pyroclastic-surge deposit is planar laminated, moderately well sorted, clast-supported and composed of 0 to 10 percent matrix ash, 15 to 25 percent crystals, 15 to 25 percent lithic fragments, and 50 to 60 percent pumice. The types of crystals, lithic fragments, and pumice clasts are similar to those found in the enclosing pyroclastic-flow deposits. Lithic fragments are mostly smaller than 7 mm, but range to 12 mm; pumice clasts are typically smaller than 5 mm but range to 25 mm.

The basal 1 to 3 cm of the Tiva Canyon Tuff is a coarse, clast-supported lag deposit that slowly pinches and swells. The lag is composed of dark yellowish orange (5YR6/6) and black (N1), cuspate to blocky glass shards, 5 to 7 percent feldspar crystals, 3 to 5 percent lithic clasts, and 20 to 25 percent pumice. Lithic clasts of grayish red to moderate red (5R4/1 to 5R4/4), devitrified volcanic rock typically are smaller than 5 mm. Grayish pink (5R8/2), vitric to slightly altered pumice clasts vary from 1 to 15 mm in diameter.

The lower contact of the crystal-poor vitric zone of the Tiva Canyon Tuff is sharp, depositional and planar to gently waviform (Photo 2). The contact is marked by the downward change from matrix-supported pyroclastic-flow material above to clast-supported, slightly altered pumice fall material below. The contact appears as a sharp break in color from moderate yellowish brown (10YR6/4) above to moderate reddish orange (10R6/6) below.

Stratigraphic and Depositional Features

The Tiva Canyon Tuff is composed of multiple pyroclastic-flow units. Several flow-unit boundaries are apparent in the lower part of the formation, but primary depositional features are locally obscured by welding and recrystallization at higher stratigraphic levels.

A swarm of comparatively coarse pumice clasts that occurs within the crystal-poor middle nonlithophysal zone marks a possible flow boundary at Sta. 76+39 (see Fisher and Schmincke, 1984). The swarm, which has an approximate thickness of 0.2 to 0.3 m, contains clasts that range in size from 4 to 12 cm (long axis).

Three flow-unit boundaries are recognized locally within the crystal-poor lower nonlithophysal zone. Two occur as laterally continuous swarms of coarse pumice clasts, approximately 0.1 to 0.6 m thick, at the tops of flow units. Within the swarms, pumice clasts compose up to 70 percent of the rock, have diameters of up to 18 cm (long axis), and locally are reverse graded. The swarms are visible in two exposures in the South Ramp (Sta. 67+46 and 67+59; Sta. 75+69.5 and 75+75.7). The swarms are stratigraphically separated by 3.1 and 2.5 m, respectively (Photo 1). A third flow boundary is defined by a thin, crystal-rich surge horizon that occurs between the two pumice swarms at Sta. 75+73 (1.2 m stratigraphically above the lower pumice swarm).

The crystal-poor vitric zone comprises two flow units that are separated by a laterally continuous, laminated surge deposit. The surge deposit, which varies in thickness from 0.11 to 0.15 cm, is exposed at Sta. 67+19 and 75+00.2. The crystal- and lithic-rich character of the deposit suggests that it is a ground surge layer associated with the overlying flow unit (see Fisher and Schmincke, 1984). This flow boundary (surge deposit) occurs approximately 5 m stratigraphically above the base of the Tiva Canyon Tuff at Sta. 67+19 and 2.3 m stratigraphically above the base of the formation at Sta. 75+00.2. The boundary separates two pyroclastic-flow deposits that can be distinguished from each other by their abundances of lithic fragments.

The base of the Tiva Canyon Tuff is marked by a coarse ground layer that varies in thickness from 1 to 3 cm. The ground layer, which contains abundant cuspate to blocky glass shards, is clast-supported and has more crystals and lithic fragments than the overlying pyroclastic-flow deposit.

Features of Welding, Secondary Crystallization, and Alteration

The degree of welding of the Tiva Canyon Tuff increases stratigraphically upward from the base of the deposit to the lower part of the crystal-poor lower lithophysal zone (where the deposit becomes densely welded at Sta. 75+16). Increased welding results in the progressive loss of matrix porosity, increases in matrix deformation, increases in the degree of induration, progressive elongation and alignment of pumice clasts, and changes in fracture character. Bubble-textured vitric shards are non- to slightly deformed in the basal 2.5 to 3 m of the deposit. In this nonwelded interval, the rock contains randomly oriented, undeformed pumice fragments and fractures around shard boundaries. In contrast, the moderately welded interval, which is 3 to 4 m thick, contains notably less porous matrix composed of deformed bubble-textured vitric or devitrified shards. Moderately welded rock contains crudely aligned and slightly elongated pumice clasts and fractures across shard boundaries. Densely welded rock lacks matrix porosity, is strongly deformed and indurated, and contains elongated and aligned pumice fragments that lack primary porosity. From the lower part of the crystal-poor lower lithophysal zone to the crystal-poor upper lithophysal zone the rock remains comparatively constant as densely welded.

Vapor-phase minerals are present as euhedral crystals that line the interiors of lithophysal cavities in the crystal-poor upper lithophysal and middle nonlithophysal zones (the interval from Sta. 76+60 to 76+73). Fine-grained vapor-phase minerals replace pumice clasts in the upper part of the crystal-poor middle nonlithophysal zone and throughout the upper lithophysal zone (Sta. 77+76 to 78+77). In addition, vapor-phase alteration of the rock matrix generally occurs as discrete spots in the crystal-poor upper lithophysal zone and as partings and stringers in the

crystal-poor middle and lower nonlithophysal zones.

Pumice clasts and the rock matrix are devitrified in units stratigraphically above the crystal-poor vitric zone. Exceptions include a thin interval of vitric pumice fiamme observed in the basal meter of the crystal-poor lower nonlithophysal zone at Sta. 67+25 and the lower and central portions of the lower nonlithophysal zone, which host argillically altered pumice clasts. Devitrification predominantly takes the form of granophyric replacement, although pumice clasts in the upper part of the crystal-poor lower nonlithophysal zone are spherulitically devitrified. Devitrification obliterates shard textures in units that lie stratigraphically above the lower nonlithophysal zone.

Argillic alteration affects two portions of the Tiva Canyon Tuff. Pumice clasts in the crystal-poor lower nonlithophysal zone are variably replaced by clay minerals from Sta. 67+26 to 67+62 and Sta. 75+14.6 to 75+70. Weak argillic alteration affects portions of the crystal-poor vitric zone at Sta. 67+16 and 75+05. In both exposures, the alteration occurs near the transition from partially welded to moderately welded rock and imparts a moderate orange-pink coloration for a stratigraphic interval of 1 to 2 m. Argillically altered tuff also occurs along planar fractures in the partly welded portion of the crystal-poor vitric zone (Sta. 67+16).

Pre-Tiva Canyon Tuff Bedded Tuff

The pre-Tiva Canyon Tuff bedded tuff (Tpbt4) deposits are exposed along the South Ramp tunnel walls from approximately Sta. 66+94 to 66+98 and Sta. 74+87.5 to 74+90 (Table 1). The unit is described below and shown in Photo 2.

Rock Unit and Contact Descriptions

The pre-Tiva Canyon Tuff bedded tuff is a nonwelded, moderate- to well-sorted pumiceous deposit. The tuff is composed of 86 to 98 percent pumice, 1 to 2 percent crystals, 1 to 7 percent

lithic fragments, and less than 5 percent matrix, except in the upper 0.2 to 0.5 m, where matrix material increases to 30 to 40 percent and pumice content is correspondingly less. Matrix material is typically light brown to moderate reddish orange (5YR6/6 to 10R6/6) in the upper part of the deposit, but occurs as a thin, grayish orange-pink (5YR7/2) coating on grains in the lower part of the deposit. The downward decrease in the amount of matrix imparts an abrupt change in rock color from moderate reddish orange (10R6/6) above to grayish pink (5R8/2) or very light gray (N8) below (Photo 2). Pumice clasts are white (N9) and vitric, with diameters that range from 1 to 3 mm. Phenocrysts include predominant feldspar and subordinate biotite. Lithic clasts, typically smaller than 2 mm diameter, include light gray (N7) to colorless, variably hydrated, perlitic glass; pale red (5R6/2), devitrified volcanic rock; and rare, brownish black (5YR2/1) volcanic rock. The abundance of lithic clasts decreases upward from 5 to 7 percent near the deposit base to 2 to 3 percent near the upper contact. Slab-like fragments of locally derived pre-Yucca Mountain Tuff bedded tuff that are a few tens of centimeters long are incorporated into the deposit in exposures at Sta. 74+95.

The contact between the pre-Tiva Canyon Tuff bedded tuff and underlying pre-Yucca Mountain Tuff bedded tuff is depositional, sharp and planar to slightly irregular. Where the unit locally incorporates material from the substrate (Sta. 74+95), the contact is disturbed and gradational over 10 cm. The contact between pre-Tiva Canyon Tuff bedded tuff and unit G of the pre-Yucca Mountain Tuff bedded tuffs is recognized by the abrupt change from very light gray (N8), well-sorted pumice above to light brown (5YR6/4) poorly sorted, reworked material below.

Stratigraphic and Depositional Features

The pre-Tiva Canyon Tuff bedded tuff deposit is 0.85 to 0.95 m thick. The tuff is massive, ungraded and unstratified except in the basal 5 to 10 cm, where faint planar laminations are present. Exposures in the South Ramp generally lack the waviform structures and other evidence of high energy emplacement that are common in the North Ramp exposures (Barr and others, 1996).

Features of Welding, Secondary Crystallization, and Alteration

The pre-Tiva Canyon Tuff bedded tuff deposits are nonwelded and vitric to slightly altered. The increase in matrix content toward the upper contact of the deposit and change in color from grayish pink to moderate reddish orange suggest an incipient paleosol in locations where the unit was exposed on the surface prior to deposition of the Tiva Canyon Tuff.

Yucca Mountain Tuff

The Yucca Mountain Tuff (Tpy) (Fig. 3) is absent in the South Ramp (Table 1).

Pre-Yucca Mountain Tuff Bedded Tuff

The pre-Yucca Mountain Tuff bedded tuff (Tpbt3) deposits are exposed along the South Ramp tunnel walls from approximately Sta. 66+80.5 to 66+94, Sta. 66+88 to 66+91(left rib, incomplete section), and Sta. 70+51 to 70+58 (above springline, incomplete section) and Sta. 74+81 to 74+90 (Table 1). The unit consists of seven depositional subunits that were informally designated by letter symbols a through g (ascending stratigraphic order) by Moyer and others (1996). These strata are described below and shown in Photo 3 and Plate 1.

Rock Unit and Contact Descriptions

Nonwelded, reworked fall deposit (Tpbt3g). This light brown (5YR6/4, 5YR5/3), massive deposit has a thickness of 0.2 to 0.6 m. The deposit is moderately sorted, matrix supported, and composed of 15 to 25 percent pumice, 1 to 3 percent phenocrysts, 3 to 5 percent (locally 20 to 30 percent) lithic clasts, and 67 to 81 percent matrix. Burrow structures infilled with material from the overlying unit occur in the upper part of the deposit. Pumice clasts are very pale orange to white (10YR8/1 to N9), vitric, and subangular to subrounded, with diameters typically smaller than 12 mm. Phenocrysts are predominantly feldspar; crystal content is difficult to estimate due

to the similar appearance of phenocrysts and mm-sized glassy lithic clasts. Subangular to subrounded lithic fragments typically have diameters of 1 to 3 mm. Lithic types include predominant colorless, slightly perlitic glass; minor pale red (5R6/2), devitrified volcanic rock; and minor, medium to medium-light gray (N5, N6) glass. Matrix material is vitric and ashy. Where underlying subunits d and f are absent (Sta. 74+87), the basal 10 to 25 cm of the deposit contains 20 to 30 percent lithic fragments incorporated from the eroded strata. In such exposures, unit g is sandy to gravelly and may be composed entirely of reworked debris. The contact between units g and f is depositional, planar and sharp to gradational over 5 to 10 cm. The contact is marked by the downward change from matrix support to clast support and a change in rock color from light brown above to pale yellowish brown (10YR7/2) below. The contact between units g and c is erosional, irregular, and gradational over 5 to 10 cm.

Nonwelded, lapilli-fall deposit (Tpbt3f). This friable, massive to crudely stratified deposit is pale yellowish brown (10YR7/2) and is 0.28 m thick in an exposure at Sta. 66+99. The unit locally is removed by erosion (Sta. 74+91). The material is moderately sorted, clast supported, and composed of 60 to 70 percent pumice, 1 to 3 percent phenocrysts, and 30 to 40 percent lithic fragments. Pumice clasts are white (N9), vitric, and subangular to subrounded, with diameters typically smaller than 10 mm. Phenocrysts are predominantly feldspar, with rare biotite; crystal content is difficult to estimate due to the similar appearance of phenocrysts and mm-sized glassy lithic clasts. Subangular to subrounded lithic fragments of colorless and medium to medium-light gray (N5, N6), slightly perlitic glass and subordinate pale to moderate red (5R6/2) to grayish red (5R4/2), devitrified volcanic rock are typically smaller than 5 mm. The lower contact of this deposit is sharp, planar, and depositional, and is marked by an abrupt change in grain size from 1 to 5 mm above to 3 to 15 mm below.

Nonwelded ash-fall deposit (Tpbt3e). This unit is absent in the south ramp.

Nonwelded, lapilli-fall deposit (Tpbt3d). This unit is friable, crudely stratified on 10 cm intervals and is 0.66 m thick in an exposure at Sta. 66+96. The unit locally was removed by

erosion (Sta. 74+91). The very light gray (N8) deposit is moderately to well-sorted, clast-supported, and composed of 75 to 90 percent pumice, 3 to 5 percent phenocrysts, and 7 to 20 percent lithic fragments. The abundance of lithic clasts varies between beds. Pumice clasts are subangular to subrounded, very light gray (N8, 10YR8/1), vitric, and typically smaller than 10 mm, but occur to 20 mm. Phenocrysts include feldspar with traces of biotite. Angular to subangular lithic fragments are mostly smaller than 10 mm, but occur to 15 mm. Most are clasts of devitrified volcanic rock occurring in shades of grayish red and pale red (5R4/2, 5R6/2) or dark gray to grayish black (N3, N2). Colorless, perlitic glass forms a subordinate lithic population. Lithic clast content varies between beds. The lower contact of this unit is sharp, planar, depositional, and marked by an abrupt downward decrease in grain size.

Nonwelded, possibly reworked pumice-fall deposit (Tpbt3c). This massive, light brown to pale yellowish brown (5YR5/6, 10YR7/2), clast-supported unit is 0.32 to 0.50 m thick. The material is composed of 76 to 93 percent pumice, 2 to 4 percent phenocrysts, 5 to 10 percent lithic fragments, and 0 to 10 percent matrix. The moderately well sorted unit is composed of mm-sized material. Pumice clasts are very pale orange to white (10YR8/1 to N9), vitric, subrounded to rounded, and smaller than 2 mm. Phenocrysts, which are very difficult to distinguish from small glassy lithic clasts, are predominantly feldspar, with subordinate, partially oxidized biotite. Rounded to subrounded lithic fragments, typically smaller than 2 mm, include devitrified volcanic rock in shades of pale red (5R6/2), grayish red (5R4/2), and moderate to light brown (5YR4/4 to 5YR5/6); colorless, perlitic glass; and grayish black (N2) obsidian. Light brown (5YR5/6) matrix material is mostly absent in the lower part of the deposit, but increases in the upper 20 cm of the deposit and may represent a paleosol. Burrow structures infilled with material from the overlying unit occurs throughout the unit. The basal 4 cm of the unit is cemented by calcite at Sta. 66+95; calcite-cemented concretions of a few cm diameter occur in exposures at Sta. 74+86. The lower contact of the unit is gradational over 5 to 10 cm, planar to slightly undulatory or irregular, and marked by an abrupt downward change from very pale orange (10YR8/1) to light brown (5YR5/6) and an increase in the amount of matrix.

Nonwelded, reworked, lapilli-fall deposit (Tpbt3b). This massive, light brown (5YR5/6) to

moderate reddish orange (10R6/6), matrix-supported unit is 0.8 to 1.7 m thick. The material is composed of 7 to 15 percent pumice, 1 to 3 percent phenocrysts, 5 to 7 percent lithic fragments, and 75 to 87 percent matrix. Pumice clasts are vitric, subangular, and very light gray to white (N8 to N9) or grayish pink (5YR8/2). They are mostly smaller than 7 mm but occur to 20 mm. Phenocrysts include predominant feldspar and subordinate biotite. Subrounded to subangular lithic fragments, mostly smaller than 3 mm, include devitrified volcanic rock in shades of pale red to grayish red (10R6/2 to 10R4/2) and grayish black (N2), variably hydrated glass. The matrix is composed of fine sandy, friable ash. The lower 0.05 to 0.2 m of the deposit locally contains material incorporated from the underlying unit (Plate 1). The lower contact of the unit varies from depositional and planar to erosional and irregular. The contact, which grades over 5 to 20 cm, is marked by an abrupt downward change from matrix support to clast support, from light brown (5YR5/6) to very light gray (N8) color, and by an increase in the percentage of pumice and degree of sorting.

Nonwelded, pumice-fall deposit (Tpbt3a). This very light gray (N8), well-sorted, clast-supported, and reverse graded deposit is 0.5 to 0.9 m thick. The material is composed of 90 to 96 percent pumice, 2 to 3 percent phenocrysts, and 2 to 7 percent lithic fragments. Angular to subangular, vitric pumice clasts are very light gray to white (N8 to N9). The clasts increase in size upward from smaller than 5 mm to 2 to 15 mm. Phenocrysts include predominant feldspar and minor, partially oxidized biotite. In the basal portion of the deposit, lithic fragments form 2 to 4 percent of the unit and are smaller than 5 mm. Near the top of the unit, lithic fragments form 5 to 7 percent of the deposit and sizes range from 2 to 15 mm. Lithic types include devitrified volcanic rock in shades of pale red to grayish red (5R6/2 to 5R4/2) and medium-light gray (N6) and variably hydrated, feldspar- and biotite-bearing glass in shades of grayish black to dark yellowish brown (N2 to 10YR4/2). The lower contact of this unit is sharp, depositional, planar to slightly irregular, and marked by the abrupt downward transition from a well-sorted, very light gray (N8) pumice-fall deposit to a poorly sorted, light brown (7.5YR7/4), reworked or pyroclastic-flow deposit.

Stratigraphic and Depositional Features

The pre-Yucca Mountain Tuff bedded tuff deposits are a series of lapilli-fall deposits formed by a sequence of small eruptions (Moyer and others, 1996). A possible exception is unit b, which has incorporated material from the underlying unit, suggesting lateral flow (Plate 1). When compared to exposures in the North Ramp, the Tpbt3 units are thinner and finer grained in the South Ramp.

Reworking of the pre-Yucca Mountain Tuff bedded tuffs is more pronounced in South Ramp exposures than in North Ramp exposures. Minor erosional unconformities occur within the sequence, notably at Sta. 74+87, where units d and f are removed and incorporated into unit g (Photo 2 and Plate 1). Time breaks between depositional events are further indicated by burrows in units g and c (see Moyer and others, 1996).

Features of Welding, Secondary Crystallization, and Alteration

The pre-Yucca Mountain Tuff bedded tuffs are nonwelded, vitric, and unaltered except where paleosols developed at the tops of some units and where calcite-cemented concretions or calcite-cemented layers formed within units c and g.

Pah Canyon Tuff

The Pah Canyon Tuff is present in one exposure in the South Ramp from Sta. 74+77 to 74+81.3 (Table 1). The unit is described below and shown in Photo 4.

Rock Unit and Contact Descriptions

The Pah Canyon Tuff (Tpp) is a nonwelded, possibly reworked pyroclastic-flow deposit. The 1.15-m-thick unit comprises two matrix-supported deposits containing reverse graded pumice

clasts. Each deposit is composed of 59 to 68 percent matrix, 5 to 7 percent crystals, 2 to 4 percent lithic fragments, and 25 to 30 percent pumice. The vitric ash matrix varies from very pale orange to moderate orange-pink (10YR8/1 to 5YR8/4). Phenocrysts include predominant feldspar, subordinate partly to completely oxidized biotite, and trace pyroxene. Angular to subrounded lithic fragments of grayish red (5R4/2), pale reddish brown (10R4/4) and variegated pale red and light gray (5R6/2 and N7) devitrified volcanic rock and dark gray (N3) glass are mostly 1 to 4 mm (up to 10 mm). Subangular to subrounded, vitric pumice clasts are very light gray (N8), rarely grayish orange (10YR7/4), and mostly 3 to 20 mm grading to 15 to 150 mm at the top of each bed. The upper 5 to 10 cm is a light brown (5YR6/4), sandy, massive deposit. The lower contact is depositional, sharp, and planar to slightly irregular.

Stratigraphic and Depositional Features

Although the stratigraphic interval from the pre-Pah Canyon Tuff bedded tuffs (Tpbt2) to the pre-Yucca Mountain Tuff bedded tuffs (Tpbt3) is exposed in three locations in the South Ramp, the Pah Canyon Tuff is present in only one of these locations. Its uneven distribution is typical of the distal edges of pyroclastic-flow deposits, where flows may form finger-like projections that follow subtle variations in topography.

The Pah Canyon Tuff comprises units with reversely graded pumice clasts that appear to grade laterally into more massive (less graded) tuff at Sta. 74+82. It is unclear whether the reverse grading is a consequence of retransport and redeposition of primary pyroclastic-flow material or a result of primary pyroclastic-flow processes such as grain-flow that can occur near the distal edges of pyroclastic-flow deposits (Rowley and others, 1981). The generally subangular shapes of the pumice clasts and vitric, ashy matrix both suggest that, if retransport occurred, the material was not remobilized over a great distance.

The upper sandy deposit, which has a slightly irregular thickness, incorporates material from the underlying Pah Canyon Tuff, consistent with an origin by subaerial reworking.

Features of Welding, Secondary Crystallization, and Alteration

The Pah Canyon Tuff is nonwelded, vitric, and unaltered. Calcite-cemented concretions, which are scattered locally throughout the unit, are common near the base of the deposit.

Pre-Pah Canyon Tuff Bedded Tuffs and Non- to Partly Welded and Moderately Welded Subzones of the Topopah Spring Tuff Crystal-Rich Vitric Zone

The stratigraphic interval from the base of the Pah Canyon Tuff (or where the Pah Canyon Tuff is absent, from the base of the pre-Yucca Mountain Tuff bedded tuffs) to the top of the Topopah Spring Tuff pyroclastic-flow deposits comprises a thick, variably welded and altered pumice-fall deposit that underlies a deposit of reworked tephra. These two units are separated by an interval of red argillic alteration, informally designated as the "red clay layer" by Moyer and others (1996). The pumice-fall deposit contains two ash layers, the stratigraphically lowest of which is referred to as ash layer 1 and designated as the top of the Topopah Spring Tuff by Buesch and others (1996). This ash layer separates pre-Pah Canyon Tuff bedded tuff deposits (Tpbt2) from the underlying non- to partly welded (Tptrv3) and moderately welded (Tptrv2) subzones of the Topopah Spring Tuff crystal-rich vitric zone (Buesch and others, 1996). This stratigraphic interval is exposed in three locations in the South Ramp: Sta. 66+37.5 to 66+80.5; Sta. 69+96 to 70+58; Sta. 74+41 to 74+81.3 (Table 1).

Rock Unit and Contact Descriptions

Reworked Tephra Deposits

Moyer and others (1996) designated the interval of reworked tephra as unit d of the pre-Pah Canyon Tuff bedded tuffs (Tpbt2). This unit occurs as a single bed in South Ramp exposures at Sta. 66+78 and 70+55 and as a comparatively thick, massive deposit overlain by a thin, sandy bed at Sta. 74+77. The interval thickness varies along the South Ramp from 1 to 2 m (typically

1.3 m) at Sta. 66+78 to 0.8 to 1.2 m at Sta. 70+55 to 0.83 m at Sta. 74+76.

The reworked deposit is poorly sorted, matrix-supported, massive, ungraded and friable. The unit is composed of 48 to 70 percent matrix, 3 to 7 percent crystals, 2 to 5 percent lithic fragments, and 25 to 40 percent pumice. The grayish orange (10YR7/6 to 7.5YR7/4) to light brown (5YR7/4) matrix is composed of vitric particles that range from ash to fine sand sizes; glass shards are not present. Phenocrysts include predominant feldspar and fresh to partly oxidized biotite, and subordinate pyroxene. Angular to subrounded lithic clasts of grayish black (N2) glass and subordinate medium gray to medium light gray (N5, N6) devitrified volcanic rock are mostly smaller than 5 mm (max. of 15 mm). Vitric pumice clasts are very light gray to white (N8 to N9), subangular to subrounded, and smaller than 12 mm. Moderate orange-pink (10R7/4), slightly altered pumice clasts, which occur throughout the unit, are especially prevalent near the base of the deposit. The upper 20 to 50 cm of the deposit locally contains burrow structures and calcite-cemented concretions.

The coarse, sandy bed observed at Sta. 74+77 is a 2 to 3 cm-thick unit that has a sharp, planar contact with the underlying deposit. This bed is clast supported and composed of 30 to 40 percent crystals, 20 to 30 percent lithic fragments, and 30 to 50 percent pumice. Crystals are predominantly feldspar, with subordinate partly oxidized biotite and trace pyroxene. Lithic fragments include colorless glass and devitrified volcanic rock in shades of grayish red (5R4/2) and medium gray (N5). Most pumice clasts are white and vitric, but a few are moderate orange-pink (10R7/4) and argillically altered. Lithic and pumice clast sizes are typically 1 to 4 mm. Crystals and lithic fragments are subangular to subrounded; pumice clasts are subrounded to rounded.

The lower contact of the reworked deposits is sharp and planar to slightly undulatory. The contact is marked by the downward change from matrix-supported, poorly sorted material above to clast-supported, moderately well sorted pumiceous material below.

Pumice-Fall Deposits

These deposits of moderately well sorted, massive to crudely stratified, clast-supported pumice are variably altered and welded. The upper few tens of cm of the deposits comprise the informally designated "red clay layer" of Moyer and others (1996), which is not strongly developed in the South Ramp exposures. Stratification is defined by the crude alignment of slightly elongated pumice clasts, the subparallel alignment of discontinuous lithic trains, abrupt changes in grain size or clast composition, and interbedded ash horizons. Alteration varies in intensity and style vertically through the sequence and laterally at a given stratigraphic horizon. In a few locations, the degree of welding increases downward from nonwelded to moderately welded in the lower 0.5 m of the deposit. Moyer and others (1996) divided the pumice-fall deposits into three subunits based on laterally continuous changes in deposit color and degree of alteration. While these subunits can be recognized in the South Ramp, their stratigraphic relations are locally obscured by intense alteration. The pumice-fall deposits are exposed in three locations along the South Ramp: Sta. 66+37.5 to 66+75; Sta. 69+96 to 70+70+50.9; and Sta. 74+41 to 74+75.

The upper part of the pumice-fall deposits (designated as unit c by Moyer and others, 1996) generally is vitric and unaltered (for example, Sta. 66+69 to 66+80, 1.5 m above right invert). The unit, which typically has a very pale orange (10YR8/1) color, is composed of 10 to 15 percent phenocrysts, 5 to 12 percent lithic fragments, and 73 to 85 percent pumice. Phenocrysts include predominant feldspar, subordinate partly oxidized biotite, and minor pyroxene. Biotite is bronze-colored where the deposit is oxidized. Lithic fragments near the base of the unit compose 5 to 7 percent and range from 1 to 7 mm (maximum of 25 mm). In the central part of the unit, lithic fragments compose 10 to 12 percent and range from 1 to 15 mm (maximum of 40 mm). Near the upper contact, lithic fragments compose 5 to 10 percent and range from 1 to 15 mm, with clasts to 50 mm. Lithic fragments are angular to subrounded and include devitrified volcanic rock in shades of grayish red (5R4/2), medium gray to medium-light gray (N5 to N6) and pale reddish brown (10R5/4) and glassy volcanic rock in shades of moderate brown

(5YR4/4) and grayish black (N2). The ratio of glassy to devitrified clasts increases from 1:1 immediately below the ash layer 2 to 4:1 near the top of the unit. Vitric pumice clasts are white (N9) to very pale orange (10YR8/1, 10YR8/2), typically smaller than 25 mm, nondeformed, and subangular to subrounded. The color of unit c can vary abruptly depending on the intensity and style of oxidation and alteration. Color changes typically cut across bedding at steep angles (Plate 2). Where altered, the unit can appear pale yellowish brown (10YR7/2), dark yellowish orange (10YR6/6), dark reddish brown (10R3/4), grayish red to dusky red (5R4/2 to 5R3/4), or pale pink (10RP7/2). The upper meter of unit c is crudely stratified and variably altered to reddish clay-rich material (Photo 5). Pumice clasts in this zone appear moderate pink (5R7/4), moderate red (5R4/6), grayish pink (5R8/2), or white (N9).

Unit c typically includes ash layer 2 as described by Buesch and others (1996) and Moyer and others (1996) (Photo 6). In the South Ramp, ash layer 2 comprises 30 to 35 mm of grayish orange-pink (7.5YR8/2) to moderate orange-pink (10R6/4) vitric ash overlain by 25 to 30 mm of clast supported, lithic-rich fallout containing a 3:2 ratio of glassy:devitrified lithic fragments that have diameters of 1 to 5 mm.

The slight alteration that characterizes the central part of the pumice-fall deposit (unit b of Moyer and others, 1996) can create the impression of matrix support; however, the unit is a clast-supported deposit (for example, Sta. 66+59). The unit generally includes a thin ash horizon (ash layer 1) that marks the top of the Topopah Spring Tuff as defined by Buesch and others (1996). The unit, which is dark yellowish orange (10YR6/6), is composed of 10 to 12 percent crystals, 5 to 10 percent lithic fragments, and 78 to 85 percent pumice. Phenocrysts include predominant feldspar, subordinate partly oxidized biotite, and minor pyroxene. Biotite is bronze-colored where the deposit is oxidized. Angular to subrounded lithic fragments are mostly smaller than 15 mm, but they range to 25 mm. Below ash layer 1, fragments of devitrified volcanic rock in shades of grayish red (5R4/2) and medium to medium-light gray (N5 to N6) predominate fragments of glassy volcanic rock in shades of grayish black (N2). Above ash layer 1, devitrified and glassy lithic fragments occur in roughly equal proportions. Vitric pumice clasts are

predominantly dark yellowish orange to grayish orange (10YR6/6 to 10YR5/4) or light brown (5YR5/6), with subordinate white (N9) clasts. Yellowish orange pumice clasts have diameters of 5 to 45 mm and aspect ratios of 2:1. In contrast, white pumice clasts have diameters of 1 to 20 mm and aspect ratios of less than 2:1. The color of unit b can vary abruptly depending on the intensity and style of oxidation and alteration. Color changes typically cut across bedding at steep angles (for example, Sta. 70+09; Sta. 74+50). Where oxidized, the unit can appear dark reddish brown (10R3/4), grayish red to dusky red (5R4/1 to 5R3/4), or moderate red (5R5/4). Where locally opalized (Sta. 70+00, 1 m below right springline; Plate 2), the unit is grayish red to dusky red (10R3/1 to 5R2/2). Where locally vapor-phase altered and coated with MnOx (Sta. 74+40; Plate 3), the unit is pale pink (5RP7/2) to grayish black to light gray (N2 to N7), with grayish red (10R4/1), light brownish gray (5YR6/1), white to grayish pink (N9 to 5R8/2), or dark gray (N3) vapor-phase mineralized pumice clasts. Partially altered pumice clasts are pale pink to grayish red-purple (5RP8/2 to 5RP4/2).

Unit b includes ash layer 1 as described by Buesch and others (1996) and Moyer and others (1996) (Photo 6). In the South Ramp, ash layer 1 comprises 5 to 6 mm of grayish pink (5R8/2) to moderate orange-pink (10R6/4) vitric ash overlain by 3 to 10 mm of clast supported, lithic-rich fallout. Lithic fragments, which have diameters of 2 to 5 mm, are primarily devitrified volcanic rock in shades of pale red to grayish red (10R6/2 to 5R5/1) and medium gray (N5), and subordinate grayish black (N2) glass.

The lower part of the pumice-fall deposit (unit a of Moyer and others, 1996) consists of clast-supported material that varies from nonwelded to moderately welded (for example, Sta. 66+37.5 to 66+39). The unit grades downward to moderately welded only where overlying the Topopah Spring Tuff crystal-rich vitrophyre; the unit is nonwelded where overlying moderately welded, vapor-phase altered pyroclastic-flow material (for example, Sta. 70+02, 1 m above right invert; Sta. 74+41). The lower part of the fallout is moderately sorted and composed of 2 to 3 percent crystals, 1 to 2 percent lithic fragments, and 95 to 97 percent pumice. Phenocrysts include predominant feldspar and trace biotite; lithic fragments include predominant grayish red (5R4/2),

devitrified volcanic rock and grayish black (N2) glass. Vitric pumice clasts are medium-light gray (N6) to grayish orange (10YR7/4); slightly altered clasts are light gray to pinkish gray (N7 to 5YR7/1). Pumice clasts are 5 to 15 mm in diameter, angular, and slightly elongated. Opal locally forms a thin coating on pumice fragments and can impart a light gray (N7) color. Where intensively opalized (Sta. 70+00, 1 m below right springline; Plate 2), the unit is grayish red to dusky red (10R3/1 to 5R2/2). Where locally vapor-phase altered and coated with MnOx (Sta. 74+40; Plate 3), the unit is pale pink (5RP7/2) to grayish black to light gray (N2 to N7), with grayish red (10R4/1), light brownish gray (5YR6/1), white to grayish pink (N9 to 5R8/2), or dark gray (N3) vapor-phase mineralized pumice clasts. Partially altered pumice clasts are pale pink to grayish red-purple (5RP8/2 to 5RP4/2).

The lower contact of the pumice-fall deposit is depositional, sharp, and planar. The contact is marked by the downward change from clast-supported, pumice-fall material above to matrix-supported, pyroclastic-flow material below.

Stratigraphic and Depositional Features

The thickness of the reworked deposits varies along the South Ramp from 1 to 2 m (typically 1.3 m) at Sta. 66+78 to 0.8 to 1.2 m at Sta. 70+55 to 0.83 m at Sta. 74+76 (Table 2). The interval comprises a single massive and ungraded bed that is overlain by a thin deposit of coarse, sandy material at Sta. 76+77. The reworked deposits exposed in the South Ramp have a comparatively simple stratigraphy that is similar to that described by Moyer and others (1996) in contrast to the more complex stratigraphy exposed in the North Ramp at Sta. 10+20 to 10+40 (Barr and others, 1996). Although the basal contact of the reworked deposits does not show evidence of scouring or other erosional features, the units include moderate orange-pink pumice clasts clearly derived from the underlying "red clay layer".

The pumice-fall deposits have an aggregate thickness of 9.2 m at Sta. 74+50, 9.5 m at Sta. 70+00 and 9.95 m at Sta. 66+70. Although locally disrupted by minor faults, stratigraphic position

within the fall units can be discerned by noting the positions of the two ash layers and the "red clay layer". Table 2 shows that measured stratigraphic thicknesses from the fall-flow contact to ash layer 2 are very consistent in each of the exposures in the South Ramp. Stratigraphic thicknesses from ash layer 2 to the upper contact of the fall deposits (Table 2) are slightly more variable, perhaps as a consequence of subaerial exposure and erosion of this contact.

The pumice-fall deposits have vertical changes in crystal content and type and lithic fragment type. Near the base of the deposits, crystals of feldspar and trace biotite comprise 2 to 3 percent. Crystal content increases sharply upward to 10 to 12 percent by 2 m stratigraphically above the deposit base, where crystals include feldspar, subordinate biotite, and minor pyroxene. The transition in character from crystal-poor to crystal-rich is similar to that of the underlying pyroclastic-flow deposits. Lithic fragments of devitrified volcanic rock predominate those of glassy volcanic rock in the interval from the fall-flow contact to ash layer 1. The ratio of devitrified to glassy lithic fragments increases upward, with glassy clasts greatly predominant near the top of the deposit.

The pumice-fall deposits are clast supported and moderately well sorted. Nevertheless, they are more poorly sorted than many pumice-fall deposits (for example, unit a of the pre-Yucca Mountain Tuff bedded tuffs; see Fisher and Schmincke, 1984) which is consistent with a nearby source.

Features of Welding, Secondary Crystallization, and Alteration

The stratigraphic interval from the base of the Pah Canyon Tuff (or where the Pah Canyon Tuff is absent, from the base of the pre-Yucca Mountain Tuff bedded tuffs) to the top of the Topopah Spring Tuff pyroclastic-flow deposits is predominantly nonwelded. An exception locally occurs in the basal 0.5 m of the pumice-fall deposit, overlying the crystal-rich vitrophyre (for example,

Table 2. Stratigraphic Thicknesses of Units in the Pumice-Fall Deposit that Overlies the Pyroclastic-Flow Deposits of the Topopah Spring Tuff

	South Ramp			North Ramp
	Sta. 66+38 to 66+81	Sta. 69+96 to 70+58	Sta. 74+40 to 74+77	Sta. 10+21 to 10+76
Tpp or Tpbt3				
Reworked Tpbt2d	1.0-2.0 m	0.8-1.2 m	0.83 m	2.3 m
	4.9	4.4	4.0	2.3*
Ash layer 2				
	2.25	2.2	2.35	2.5
Ash layer 1				
	2.8	2.9	2.85	3.4
Fall/Flow				

Note: All stratigraphic thicknesses given in m.

* Unit may be structurally thinned.

Sta. 66+37.5). In these locations, the pumice-fall material grades downward from nonwelded to moderately welded. The sharp increase in welding that occurs directly above densely welded pyroclastic-flow material (called "sintered tuff" since it is caused by external rather than internal heat) is consistent with welding of the pumice-fall deposit by heat released from the underlying tuff sheet (Moyer and others, 1996).

The pumice-fall deposits are variably altered in the South Ramp. Tunnel exposures show abrupt changes from vitric to vapor-phase altered or argillically altered material. Intense oxidation, localized silicification or opalization, bleaching, and pervasive infiltration by manganese oxide minerals are also observed in the South Ramp.

The history of alteration and oxidation that affected the pumice-fall deposits is complex. It is clear that the processes of alteration were tied to the processes of cooling and degassing of the underlying pyroclastic-flow deposits. A subsequent section provides a more detailed discussion of the history of these "fumarolic zones". Observations include: 1) An increase in the degree of welding at the base of the pumice-fall deposits indicates that they were deposited atop hot pyroclastic-flow material. 2) Vapor-phase minerals and bleaching occur in the basal few meters of the pumice-fall deposits where they overlie a thin interval of moderately welded, vapor-phase altered pyroclastic-flow material. 3) Silicification and opalization of the pumice-fall deposits forms a carapace-like cap enclosing vapor-phase altered material (Plate 2). At Sta. 70+00, silicified material occurs where the underlying pyroclastic-flow deposit hosts a fracture lined with opal. 4) Fractures lined with manganese oxide minerals that can be traced from the pyroclastic-flow deposit into the pumice-fall deposit apparently served as a source of the pervasive MnOx mineralization in the pumice-fall deposit at Sta. 74+43.7 (Plate 3). 5) Oxidation and argillic alteration of the pumice-fall material occurs at stratigraphic levels above or laterally outside of vapor-phase altered zones (Plate 2). 6) Oxidation and alteration boundaries are abrupt features that can occur at sharp angles to bedding (Plate 2). Consequently, the alteration forms plumose structures that cut vertically through the pumice-fall deposits. 7) The regions of intense alteration are areally restricted and are not consistent with a deep-seated hydrothermal origin. They are consistent with localized zones of fumarolic and hydrothermal alteration that form at the tops of cooling pyroclastic-flow deposits (Sheridan, 1970; Keith,1991). 8) Subhorizontal zones of argillic alteration locally parallel crude bedding through the pumice-fall deposits, extending a distance of several meters through otherwise vitric and unaltered material (Photo 6).

Topopah Spring Tuff Pyroclastic-Flow Deposit

The South Ramp exposes pyroclastic-flow units of the Topopah Spring Tuff from the crystal-rich vitrophyre to the crystal-poor lower lithophysal zone in three intervals: Sta. 55+00 to 66+37.5; Sta. 67+91 to 69+96; and Sta. 70+58 to 74+41 (Table 1). This section provides summary rock unit and contact descriptions for the zones traversed by the tunnel, outlines the stratigraphic and depositional features observed in the tunnel walls, and describes general features of welding, secondary crystallization, and alteration.

Rock Unit and Contact Descriptions

Crystal-Rich Member

Moderately Welded Subzone (Tptrv2)

This unit comprises moderately welded, vapor-phase altered, devitrified, and locally silicified pyroclastic-flow material. The material is composed of 73 to 85 percent matrix, 5 to 7 percent crystals, less than 1 percent lithic clasts, and 10 to 20 percent pumice fragments (Photo 7). The interval varies from 0 to 1.0 m thick at Sta. 70+01 to 70+04 (1 m above right invert) and Sta. 74+40 to 74+41; the unit is absent in other South Ramp exposures. Where vapor-phase altered and silicified (Sta. 70+02, 1 m above right invert), the rock varies from grayish red to pale red (2.5YR4/2 to 10R6/1), but is pale pink (5RP7/2, 5RP7/1), grayish pink (5R8/2) or very light gray to very pale orange (N8 to 10YR8/1) where vapor-phase altered and bleached. Silicified rock retains variably preserved shard texture with angular intershard pores; bleached rock has a sugary texture. Phenocrysts include predominant feldspar, subordinate oxidized biotite, and minor altered pyroxene. Pumice fragments are medium dark gray to medium light gray (N4 to N6) or grayish red (10R5/1, 5R5/1, 5R6/2) and vapor-phase altered or silica-replaced, with a porous, spongy texture. A 1-to-8-cm thick interval of laminated tuff (surge deposit) composed of 30 to 40 percent crystals, 5 to 10 percent lithic fragments, and 50 to 65 percent blocky glass occurs

within the unit at Sta. 74+40.5. This surge horizon is stratigraphically equivalent to a surge horizon within the vitrophyre subzone at Sta. 69+95 as described below.

The lower contact of the moderately welded subzone is sharp and planar to irregular and can cross-cut bedding at high angles. The contact is marked by a downward loss of matrix porosity and increase in pumice elongation.

Vitrophyre Subzone (Tptrv1)

The crystal-rich vitrophyre is a densely welded, glassy pyroclastic-flow deposit that is composed of 73 to 80 percent matrix, 10 to 12 percent phenocrysts (locally 3 to 5 percent at the top of the unit) and 10 to 15 percent pumice. At Sta. 66+34, the unit has a stratigraphic thickness of 1.5 m and is composed of a basal interval of moderate reddish brown to dusky red (10R4/6 to 5R3/4) glass that is overlain by an interval of dark gray to grayish black (N2 to N3) glass. At Sta. 69+90.5 to 69+96, the unit has a stratigraphic thickness of 1.65 m, with a basal interval of black to grayish black (N1 to N2) glass overlain by an interval of grayish red (5R4/2) glass, the upper part of which has a vitroclastic texture. The unit is absent at Sta. 74+40. Phenocrysts include predominant feldspar, subordinate biotite, and minor pyroxene. Vitric pumice clasts are porphyritic, dense, black to grayish black, elongated (shape ratios of 3:1 to 10:1), and 30 to 100 mm long. Pumice clasts locally have moderate reddish brown (10R4/6) rims of argillically altered material. A swarm of large pumice fragments (max. 250 mm) occurs at the top of the unit at Sta. 66+37.5. A 2-to-10-cm thick interval of laminated tuff (surge deposit) composed of 30 to 40 percent crystals, 5 to 10 percent lithic fragments, and 50 to 65 percent blocky glass occurs within the unit at Sta. 69+95.

At Sta. 70+00 (1 m above right invert), the vitrophyre makes an abrupt lateral change to densely welded material that is devitrified, vapor-phase altered, and (possibly) silicified (Plate 3; Photo 7). Where this style of alteration occurs, the rock is grayish red (2.5YR4/2, 10R6/1) to brownish gray (5YR6/1) and contains spongy, silicified pumice clasts that have medium dark gray to

grayish brown (N4, 5YR3/2) colors. The matrix of this rock contains small intershard pores.

The contact between the crystal-rich vitrophyre and underlying crystal-rich nonlithophysal zone is sharp and slightly undulatory to irregular. The contact is marked by the downward change from glassy to devitrified rock. The lateral change from vitric to vapor-phase altered material is sharp and can cross-cut bedding at high angles.

Nonlithophysal Zone (Tptrn2)

This zone is composed of devitrified and vapor-phase altered pyroclastic-flow material that grades upward from densely welded to moderately to densely welded. The material is a poorly sorted, matrix supported deposit composed of 54 to 82 percent matrix, 12 to 15 percent phenocrysts, less than 1 percent lithic fragments, 5 to 30 percent pumice and 0 to 2 percent lithophysae (Photo 8). The unit varies downward from reddish brown (2.5YR4/3) or grayish red (10R4/2) to pale reddish brown (10R5/3) to pale red (5R6/2, 10R6/2, 10R5/1) to grayish orange-pink (5YR7/2 to 5YR6/1). The matrix is composed of dense, devitrified material in shades of grayish red (10R5/2, 10R4/2), pale reddish brown (10R5/4), reddish brown (2.5YR4/3) or light brown (5YR5/4 to 5YR7/4) with a variable amount of porous vapor-phase mineralization, commonly as blebs and stringers of grayish pink (5R8/2) or grayish orange-pink (5YR7/2) to very light gray (N8) or white (N9) material. Vapor-phase alteration locally pervades the matrix (for example, at Sta. 65+40 to 65+60) and typically diminishes in intensity upward. Phenocrysts include predominant feldspar, subordinate biotite, and minor pyroxene. Biotite varies from fresh to oxidized (bronze color); pyroxene is fresh in the upper part of the zone, but altered to lime-green pseudomorphs in the lower portion (the change occurs stratigraphically above Sta. 65+77 and Sta. 74+28); and feldspar is locally chatoyant. Pumice clasts are white, very light gray, or grayish pink (N9, N8, 5R8/2) and medium light gray, pale red, or grayish red (N6, 10R6/1, 10R5/1). They are replaced by euhedral vapor-phase minerals, and locally corroded (for example, from Sta. 65+50 to 65+58 and Sta. 68+85 to 69+04). Pumice content is typically between 10 to 25 percent in the basal third of the zone, 20 to 30 percent in central third of the

zone, and 10 to 15 percent in the upper third of the zone. In the upper and lower parts of the unit, pumice clasts typically are 20 to 250 mm (long axis), with clasts to 400 mm; in the central part of the unit, clasts typically are 20 to 500 mm. Shape ratios tend to decrease upward from 5:1 to 10:1 near the base of the zone to 3:1 to 7:1 near the top of the zone; clast alignment defines a flattening foliation.

The upper stratigraphic meter of the unit locally is dense and silicified, with a cherty fracture habit. Silicified rock is dusky brown (5YR2/2), grayish brown (5YR3/2), grayish red (5R4/2), or grayish orange-pink (5YR7/2). Vapor-phase minerals form less than 10 percent of the zone in this interval. Pumice clasts (7 to 15 percent) are pale to moderate reddish brown (10R5/4 to 10R4/6) or moderate pink to moderate reddish orange (5R7/4 to 10R6/6) and partly to wholly argillic, or moderate red (5R5/4) and devitrified.

The lower unit contact grades over 1 to 2 m and is marked by the downward increase in lithophysae from less than 2 percent above to 3 to 5 percent below.

Lithophysal Zone (Tptrl2, Tptrl1)

The crystal-rich lithophysal zone is a densely welded, devitrified and vapor-phase altered unit composed of 25 to 87 percent matrix, 5 to 15 percent phenocrysts, less than 1 percent lithic clasts, 5 to 20 percent pumice, and 3 to 40 percent lithophysae. The base of the unit includes the crystal transition zone (Sta. 68+47 to 68+66; Sta. 73+02 to 73+28). The matrix is a mix of devitrified and vapor-phase altered material. Rock colors grade upward from pale red-purple (5RP6/1) or grayish red-purple (5RP4/2, 5RP5/2) to light brownish gray (5YR5/1, 5YR6/1, 5YR7/1). Vapor-phase mineralization occurs as blebs, wisps, and pockets of white (N9) or medium dark gray (N4, 5R4/1) alteration that forms from 10 to 50 percent of the matrix and that increases upward through the unit. Crystal content increases gradually upward through the transition zone from 5 percent (feldspar with minor biotite) to 10 to 12 percent (predominant feldspar, subordinate partly oxidized biotite, and minor altered pyroxene); crystal content is 12 to

15 percent above the transition zone. Pumice clasts may be vapor-phase mineralized, devitrified, or both. Vapor-phase altered pumice clasts are white (N9) and medium light gray (N6). Devitrified clasts are dark yellowish brown (5YR5/2) and contain 7 to 10 percent crystals. Some clasts have pale brown (5YR5/2) devitrified margins with grayish red (5R5/1) vapor-phase mineralized interiors. Pumice clasts are typically 20 to 120 mm (long axis), but can exceed 200 mm. They have shape ratios that vary from 3:1 to 13:1 and their elongation can impart foliation to the rock. In general, lithophysae are lenticular, ellipsoidal, or subspherical, with linings of vapor-phase silica and rare hematite, and occasional overgrowths of tabular calcite. Lithophysal cavities vary in size and abundance throughout the zone. In the lower and central parts of the zone, the abundance of lithophysae ranges from 7 to 40 percent of the rock, but commonly falls between 15 and 30 percent. In these intervals, lithophysae generally are smaller than 210 x 250 mm, but they range to 330 x 500 mm. In the upper part of the zone, the abundance of lithophysae decreases upward from 7 to 10 percent to 3 to 5 percent. Cavities in the upper interval typically are smaller than 150 x 230 mm.

The lower contact grades over less than 1 m from a total phenocryst content of 2 to 4 percent below the contact to 5 percent above. In some locations (for example, Sta. 68+47), the contact also marks a change in the size of lithophysal cavities, from large (exceeding 50 cm diameter), irregularly shaped cavities below to smaller (less than 20 cm diameter), well-formed, ellipsoidal to lenticular cavities above.

Crystal-Poor Member

Upper Lithophysal Zone (Tptpul)

The crystal-poor upper lithophysal zone is a densely welded, devitrified and vapor-phase altered unit composed of 40 to 91 percent matrix, 1 to 4 percent phenocrysts, 1 percent lithic clasts, 5 to 15 percent pumice, and 3 to 40 percent lithophysae. Matrix is a variable mix of pale to grayish red-purple (5RP5/2 to 5RP4/2) and light brown (5YR6/4) to pale reddish brown (10R5/4)

devitrified material. The matrix contains less than 3 to 5 percent blebs, wisps and stringers of very light gray (N8) to grayish pink (5R8/2), vapor-phase material. Ellipsoidal to subspherical spots of grayish pink (5R8/2) to very light gray (N8), vapor-phase altered matrix, which compose from 5 to 30 percent of the rock, generally have diameters of 10 to 40 mm. Phenocrysts of feldspar and trace biotite compose 1 to 2 percent, except in the upper few meters of the unit, where crystal content increases to 2 to 4 percent (feldspars with minor biotite). Angular fragments of light gray (N7), devitrified volcanic rock occur to 40 mm diameter. In the lower part of the unit, elongated, devitrified pumice clasts (shape ratios of 3:1 to 7:1) are pale reddish brown (5R5/4) and 10 to 60 mm (long axis). In the upper part of the zone, elongated pumice clasts (shape ratios of 3:1 to 7:1) are grayish brown (5YR3/2), devitrified, and crystal-rich (10 to 12 percent crystals of feldspar, biotite, and pyroxene), with diameters of 20 to greater than 650 mm (long axis). Grayish brown clasts are present in exposures from Sta. 63+72 to 64+55, Sta. 67+91 to 68+47, and Sta. 72+38 to 73+02.

Lithophysae in the crystal-poor upper lithophysal zone range from moderately well formed to poorly formed, and have shapes that may be subspherical, lenticular, ellipsoidal, or irregular. Irregularly shaped cavities commonly have planar walls formed along fracture surfaces and blocky, quasi-pyramidal or slab-like interior surfaces that project into the lithophysal cavity; crudely formed concentric fractures surround some of these cavities. In contrast, lenticular, ellipsoidal, and subspherical lithophysae have relatively smooth, rounded interiors. Lithophysal cavities generally are enclosed by thin (less than 5 mm) rims of very light gray vapor-phase material. Lithophysae of all types have linings of white vapor-phase minerals; larger cavities may have platy calcite overgrowths atop the vapor-phase minerals.

Throughout most of the zone, lithophysae generally have diameters (long axis) of 20 to 150 mm, but they range from 10 to approximately 400 mm. The smallest cavities (those less than 20 mm) often occur as gash-like openings in the centers of ellipsoidal vapor-phase spots. Lithophysal cavities in the upper 3 to 7 m of the zone (stratigraphically) can exceed 1000 mm in size (for example, Sta. 68+23, left rib, 2 m above springline; Sta. 72+91 to 73+02). These intervals likely

are equivalent to the cavernous lithophysal subzone of Buesch and others (1996).

The percentages of lithophysae vary throughout the three South Ramp exposures. The abundance of lithophysae in the two exposures with complete stratigraphic sections of the zone (Sta. 63+08 to 64+55 and Sta. 71+68 to 73+02) increases inward from the upper and lower zone contacts. In a very general sense, the central part of the zone contains two intervals with comparatively high abundances of lithophysae separated by an interval of fewer lithophysae. Lithophysae content in the upper interval of high abundance varies between 10 and 20 percent from Sta. 63+80 to 64+34 and between 15 and 25 percent from Sta. 72+35 to 72+75. Lithophysae content in the lower interval of high abundance varies between 10 and 25 percent from Sta. 63+35 to 63+72 and between 15 and 40 percent from Sta. 71+76 to 72+12. In contrast, the intervening interval of fewer lithophysae contains between 5 and 10 percent lithophysae from Sta. 63+72 to 63+80 and between 10 and 15 percent lithophysae from Sta. 72+12 to 72+35.

The rock comprising the upper lithophysal zone may be broken and rubbly (for example, Sta. 72+35 to 72+91) and locally is shattered (for example, Sta. 68+29). The rock is intensely fractured near the Dune Wash fault (Sta. 67+91 to 67+95).

The lower contact of the zone grades over less than 1 m and is marked by a downward decrease in the abundance of lithophysae from greater than 5 percent above to 1 to 2 percent below, the presence of numerous vapor-phase partings below the contact, and an abrupt increase in smooth, high-angle fractures below the contact. At Sta. 67+91, the zone is fault-bounded (Dune Wash fault).

Middle Nonlithophysal Zone (Tptpmn)

The crystal-poor middle nonlithophysal zone is a densely welded, devitrified unit composed of 76 to 96 percent matrix, 1 to 2 percent phenocrysts, 1 to 5 percent lithic clasts, 2 to 15 percent pumice, and 0 to 2 percent lithophysae. The matrix occurs in shades of pale to grayish red

(5R6/2, 5R4/2), moderate to light brown (5YR4/3 to 5YR6/4), or grayish orange-pink (5YR7/2). The matrix may appear as a mottled mix of these colors and may include grayish red-purple (5RP4/2) material as feathery veinlets and stringers, some of which form centimeter-thick borders that enclose vapor-phase partings. Shard texture is variably preserved throughout the unit. Subspherical to slightly ellipsoidal spots of grayish pink (5R8/2) vapor-phase alteration, typically 3 to 30 mm in diameter, form 3 to 10 percent of the matrix from Sta. 70+58 to 71+40, 10 to 20 percent of the matrix from Sta. 71+40 to 71+68, and 0 to 3 percent elsewhere. Stringers of vapor-phase material and more continuous vapor-phase partings have central veinlets of white (N9) vapor-phase minerals 1 to 3 mm thick, enclosed in bands of grayish pink (5R8/2) alteration that vary from 3 to 10 mm. Vapor-phase partings and stringers generally form 0 to 3 percent of the rock mass; however, the upper few meters of the deposit (for example, at Sta. 71+44 to 71+68) may contain numerous (at least 17) laterally continuous, subparallel vapor-phase partings that occur at vertical spacings of 25 to 40 cm (Photo 9). Phenocrysts are primarily feldspar with a trace of biotite. Subangular to subrounded lithic fragments include predominant medium-light gray to white (N6 to N9) and pale red (5R6/2) foliated, devitrified volcanic rock, minor pale red, porphyritic volcanic rock, and rare medium-dark to dark gray (N4 to N3) or grayish brown (5YR3/2) volcanic rock. Lithic fragments typically have diameters of 3 to 15 mm, but locally occur to 80 mm. Pumice clasts occur in shades of grayish red to grayish brown (10R4/2 to 5YR4/2), light gray (N7), or pale red (5R5/2). In general, pumice clasts are devitrified (possibly spherulitic), and 3 to 90 mm (long axis), with shape ratios of 3:1 to 12:1. Pumice fragments are variably well preserved and locally obscured by secondary crystallization. A swarm of pumice clasts that occurs at Sta. 57+13 (1.5 m below right springline) may mark a flow unit boundary. Lithophysae occur as small lenticular or gash-like cavities of 10 to 25 mm (long axis) in the centers of some vapor-phase spots and stringers or, in the upper meter of the deposit, as ellipsoidal to lenticular cavities up to 70x90 mm.

This zone commonly contains high-angle, smooth, planar fractures that may contain a thin coating of grayish black (N2) MnOx, white (N9) vapor-phase minerals, opal, or calcite. Fracture faces may be altered to pale red (5R7/1 to 5R5/2) and have borders of grayish red-purple

(5RP4/2) devitrified material.

The lower contact of this zone grades over 30 to 60 cm and is marked by an abrupt downward increase in lithophysae and the downward termination of planar fracturing. The contact at Sta. 58+78 is marked by a continuous vapor-phase parting along which several lithophysae are aligned.

Lower Lithophysal Zone (Tptpll)

The crystal-poor lower lithophysal zone is a densely welded, devitrified and vapor-phase altered unit composed of 81 to 93 percent matrix, 1 to 2 percent phenocrysts, 1 to 2 percent lithic fragments, and 5 to 15 percent lithophysae. Pumice clasts are not evident and may be obscured by secondary crystallization. The devitrified matrix is a mottled mix of moderate brown (5YR4/4, 5YR5/4), pale red (10R6/3, 5R6/2) and grayish red-purple (5RP4/2). Subspherical spots of grayish orange-pink (10R8/2) vapor-phase alteration, which form 10 to 20 percent of the rock mass, are generally smaller than 25 mm. Phenocrysts include predominant feldspar and traces of biotite. Lithic fragments are primarily light gray to white (N7 to N9) and pale red (5R6/2) foliated, devitrified volcanic rocks with diameters typically smaller than 50 mm, but locally as large as 80 mm. Lithophysae are well-formed, lenticular to ellipsoidal, with diameters that generally range from 70 to 160 mm (long axis) but that vary to 500 mm. In the upper 1 to 2 meters of the zone, lithophysae have subspherical to irregular shapes and may merge into vapor-phase stringers that parallel foliation.

The lower contact of this zone is not exposed in the ESF.

Stratigraphic and Depositional Features

The pyroclastic-flow deposits of the Topopah Spring Tuff are composed of multiple flow units (Lipman and others, 1966). Although the flow deposits are generally ungraded, flow-unit

boundaries in the South Ramp exposures are marked by laterally continuous swarms of coarse pumice clasts that occur at the tops of flow units or by thin, crystal-rich surge deposits that occur between flow units. Examples of pumice swarms can be observed at the top of the crystal-rich vitrophyre at Sta. 66+37.5, near the top of the crystal-rich nonlithophysal zone at Sta. 74+39, within the crystal-poor upper lithophysal zone at Sta. 72+71, and within the crystal-poor middle nonlithophysal zone at Sta. 57+13. A surge deposit can be observed within the crystal-rich vitrophyre at Sta. 66+95 and within moderately welded, vapor-phase altered tuff at Sta. 74+40.5 (Plate 2).

Two features of the Topopah Spring Tuff that are related to the evacuation of the chemically zoned magma chamber (Lipman and others, 1966; Schuraytz and others, 1989) can be used to determine relative stratigraphic position within the deposit. These are the increase in crystal content that occurs stratigraphically upward through the crystal transition zone and the appearance of grayish brown, crystal-rich quartz latite pumice clasts in the crystal-poor upper lithophysal zone. Both features occur in exposures of the Topopah Spring Tuff in the North Ramp (Barr and others, 1996).

Features of Welding, Secondary Crystallization, and Alteration

Variations in the degree of welding, types of secondary crystallization, and style of alteration are related to cooling and degassing of the ash-flow sheet. The upper surface of the Topopah Spring Tuff pyroclastic-flow deposits varies from densely welded (crystal-rich vitrophyre) to moderately welded. The degree of welding generally decreases stratigraphically downward from the crystal-rich vitrophyre in the upper part of the crystal-rich nonlithophysal zone then generally increases to densely welded in the lower part of the crystal-rich nonlithophysal zone. Despite significant variability, changes in the degree of welding can be discerned through general changes in the aspect ratios of pumice clasts, the development of compaction (flattening) foliation, and the macroscopic porosity of pumice clasts and matrix. Pumice fiamme within the crystal-rich vitrophyre typically have aspect ratios of 5:1 to 10:1 that impart a strong compactional foliation

to the zone. In contrast, pumice clasts replaced by vapor-phase minerals in the upper part of the crystal-rich nonlithophysal zone have aspect ratios of 3:1 to 7:1 that define a moderately well developed foliation. As welding increases gradually downward, aspect ratios increase to 5:1 to 10:1 in the lower part of the crystal-rich nonlithophysal zone and to 5:1 to 12:1 in the crystal-poor middle nonlithophysal zone. Compaction foliation becomes more strongly developed as aspect ratios increase.

The crystal-rich vitrophyre contains densely welded, vitric pumice fragments that may have argillically altered margins. This subzone is underlain by a meter-thick interval of devitrified and locally silicified tuff that contains pumice clasts that are wholly altered to clay (Plate 3; Photo 10). Below this interval, pumice clasts are replaced by coarsely crystalline vapor-phase minerals. Vapor-phase crystallization appears to be most intense in the lower part of the crystal-rich nonlithophysal zone, where pumice clasts are locally corroded and the matrix contains pervasive blebs and pockets of vapor-phase minerals. Decreases in the amount of vapor-phase minerals in the matrix and changes in the textures of pumice clasts indicate that the intensity of vapor-phase crystallization gradually diminishes downward through the pyroclastic-flow deposits. The percentage of devitrified matrix increases stratigraphically downward and the style of vapor-phase alteration changes to spots, stringers, and partings of fine-grained material in the crystal-poor upper lithophysal zone. In this same stratigraphic interval, the texture of pumice clasts changes from predominantly coarsely crystalline to predominantly finely crystalline. The proportion of devitrified pumice clasts increases downward and becomes the predominant textural type in the lower part of the crystal-poor upper lithophysal zone.

Abrupt lateral and vertical variations in the degree of welding and character of secondary crystallization and alteration are typical of the upper 3 stratigraphic meters of the Topopah Spring Tuff pyroclastic-flow deposits (Photo 7). In some exposures (Sta. 66+44, 1.5 m below right springline), the crystal-rich vitrophyre is overlain by moderately welded, devitrified, and vapor-phase altered pyroclastic-flow material. In other exposures (Sta. 70+02, 1.5 m below springline), the crystal-rich vitrophyre grades laterally into densely welded, devitrified tuff that is overlain by

moderately welded, devitrified, and vapor-phase altered pyroclastic-flow material (Plate 3). In other locations (Sta. 74+40), the crystal-rich vitrophyre is missing and moderately welded, devitrified and vapor-phase altered pyroclastic-flow material overlies densely welded, argillically altered tuff (Plate 2). In all cases, these changes occur where the crystal-rich vitrophyre is offset along minor faults or cut by fractures that served as conduits for fluids. The character of these fumarolic zones is discussed in detail in a subsequent section of this report.

Lithophysae generally exceed 5 percent of the rock mass in the crystal-poor upper and lower lithophysal zones. The central portion of the upper lithophysal zone typically contains two intervals within lithophysal cavities exceeding 15 percent of the rock mass and locally approaching 40 percent of the rock. Although the upper and lower boundaries of the upper lithophysal zone are clearly gradational, the interval appears generally stratiform. Nevertheless, vertical and lateral variations in lithophysae abundance are apparent in the South Ramp exposures and suggest that lenticular or pod-shaped features occur locally within the lithophysal zones.

Any general model that describes the deposition and cooling history of the Topopah Spring Tuff pyroclastic-flow deposits must explain the welding, secondary crystallization, and alteration features present in the South Ramp. The variations in degree of welding and style of secondary crystallization at the top of the pyroclastic-flow deposits appear to be related to localized zones of fumarolic alteration. It is important to note that these features occur only where the crystal-rich vitrophyre is offset along faults or cut by fractures (although alteration is not observed to occur in the absence of fractures, not all fractures and faults are associated with alteration). As discussed by Barr and others (1996), the densely welded character of the upper few meters of the pyroclastic-flow deposits points to the influence of the overlying pumice-fall material, which presumably acted as a thermal blanket that minimized conductive heat loss from the top of the pyroclastic-flow deposits. In contrast, the downward change to significantly less welded, devitrified, and vapor-phase altered material that occurs below the crystal-rich vitrophyre may reflect the relative timing of devitrification and compactional deformation near the upper

boundary of the flow deposits (Barr and others, 1996). The presence of argillically altered material directly beneath the crystal-rich vitrophyre and the downward change from fresh to altered pyroxene phenocrysts in the crystal-rich nonlithophysal zone may be related to the temperature and amount of fluids released from the cooling tuff sheet and their ability to migrate through the sheet during cooling.

The Nature and Style of Fumarolic Alteration

The top of the Topopah Spring Tuff pyroclastic-flow deposits is exposed in three South Ramp locations. In each case, the overlying pumice-fall deposits are intensely altered and oxidized in a restricted area. Although the style of alteration varies to some extent between and within exposures, there are numerous similar features that combine to support a general model for the origin of the alteration zones. Significant observations regarding the styles of alteration observed in the pumice-fall deposits and upper 3 m of the pyroclastic-flow deposits are summarized in previous sections of this report. Photomosaics of two alteration zones in the South Ramp are included as Plates 2 and 3; a third location is shown in Photo 10.

The South Ramp exposures indicate that the altered zones are the interiors of fossil fumaroles formed during degassing and cooling of the Topopah Spring Tuff pyroclastic-flow deposits. Four observations are crucial to this interpretation: 1) Localized welding of the basal portion of the post-Topopah Spring Tuff pumice-fall deposits indicates deposition shortly (perhaps immediately) after the emplacement of the underlying pyroclastic-flow deposits. 2) Alteration of the upper few meters of the pyroclastic-flow deposits is near intensely altered pumice-fall deposits; this alteration is not observed in locations where the lower pumice-fall deposits are pristine and unaltered. 3) Alteration of the upper pyroclastic-flow deposits and overlying pumice-fall deposits occurs where their contact is offset along minor faults or cut by fractures that served as conduits for fluids (Photo 10; Plates 2 and 3). Although alteration is not observed without fractures, not all fractures and faults are associated with alteration. 4) Opalization of pumice-fall material at Sta. 70+00 occurs directly above an opal-lined fracture in the underlying

pyroclastic-flow deposit (Plate 3). Pervasive manganese oxide minerals within bleached and altered pumice-fall materials at Sta. 74+43.7 are associated with a MnOx-coated fracture that penetrates into the underlying pyroclastic-flow deposit (Plate 2).

The geometry of alteration zones within the pyroclastic-flow deposits varies within and between exposures. Plate 3 shows complex relations between densely welded vitric material, densely welded, devitrified material, and moderately welded, vapor-phase altered material. The alteration zones in the pyroclastic-flow deposits apparently are not necessarily related to the locations of fractures through which fluids migrated during cooling (Plates 2 and 3).

The geometry of alteration zones within the pumice-fall deposits are localized, have plumose shapes, and have abrupt margins that cut across strata at a high angle to bedding. The zones appear to be quasi-concentric. Plates 2 and 3 illustrate the outward zonation from a core of vapor-phase alteration to a region of silicification and oxidation to a region of argillization and intense hematite staining. The vapor-phase altered cores of the fossil fumaroles are near fractures that penetrate downward into the underlying pyroclastic-flow deposits.

The South Ramp exposures suggest mound-like or ridge-like alteration features within the pumice-fall deposits that were fed by fluids escaping from the underlying pyroclastic-flow deposits. The transition from a core of vapor-phase alteration to an outer shell of argillic alteration suggests a decrease in temperature with distance from the fluid source.

The alteration features in the South Ramp are strikingly similar in geometry and alteration style to the fossil fumaroles described by Keith (1991) in the pyroclastic deposits of the Valley of Ten Thousand Smokes (VTTS), Alaska. Like the deposits in the South Ramp, the VTTS fumaroles also formed at the interface of a welded pyroclastic-flow deposit with an overlying pumice-fall deposit. The controlling influence of the porosity and permeability contrast between the flow and fall deposits on the distribution of alteration above fumarolic fractures, delineated mound-like and ridge-like features that have sharp outer boundaries beyond which tephra is vitric and

unaltered, and features with cores of vapor-phase alteration that grade outward to zones of argillic alteration and intense hematite staining. The VTTS fumaroles are an excellent analog to the features observed in the ESF.

Comparisons with Exposures in the North Ramp

This section briefly compares the stratigraphic relationships, depositional histories, and features of welding, secondary crystallization, and alteration observed in the South Ramp with those in the North Ramp (Barr and others, 1996).

Tiva Canyon Tuff

The Tiva Canyon Tuff is composed of multiple flow units in both the North and South Ramps. In both locations, flow-unit boundaries are marked by swarms of coarse pumice or thin pyroclastic-surge beds. Table 3 shows the measured or estimated stratigraphic thicknesses of flow units in both ramps. Although variations in unit thicknesses are apparent, the changes do not appear to be laterally consistent.

Several differences are apparent in the South and North Ramp exposures of the Tiva Canyon Tuff. 1) The crystal-poor lower lithophysal zone is absent in the South Ramp, an observation corroborated by field mapping of surface exposures (Day and others, in press). Although the middle nonlithophysal zone in the South Ramp contains a thin interval with less than 1 percent lithophysae (Sta. 76+60 to 76+73), it is not known if this interval grades laterally into the lower lithophysal zone. 2) The estimated thickness of the interval of argillically altered pumice clasts in the crystal-poor lower nonlithophysal zone is slightly thicker in the South Ramp (15.2 m from Sta. 75+14 to 75+70) than in the North Ramp (11.4 m from Sta. 6+30 to 6+85). 3) Argillic alteration of the upper part of the crystal-poor vitric zone is notably more intense in the North Ramp than in the South Ramp.

The PTn Hydrogeologic/Thermal-mechanical Unit

The PTn hydrogeologic/thermal-mechanical unit is markedly thinner in the South Ramp than in the North Ramp. Estimated stratigraphic thicknesses for the PTn unit in the South Ramp are 24.5 to 26.3 m from Sta. 66+37 to 67+28 and 19.8 to 23.0 m from Sta. 74+40 to 75+16. In contrast, the stratigraphic thickness of the PTn unit in the North Ramp is estimated at between 50 and 66 m from Sta. 7+50 to 10+76 (repetitive faulting complicates estimates of stratigraphic thickness). Although most of the difference (23 m) is due to the general absence of Pah Canyon Tuff in South Ramp exposures, the absence of Yucca Mountain Tuff (0.4 to 1.0 m thick in North Ramp) and thinning of the pre-Yucca Mountain Tuff bedded tuffs (3.7 to 4.2 m thick from Sta. 66+81 to 66+94; 2.2 to 2.4 m thick from Sta. 74+81 to 74+88; 5.1 to 6.0 m thick from Sta. 8+75 to 9+10) also contribute to a thinner PTn unit. Nevertheless, some stratigraphic intervals, notably the pre-Tiva Canyon Tuff bedded tuff and the pumice-fall deposits that overlie the Topopah Spring Tuff pyroclastic-flow deposits, have consistent stratigraphic thicknesses.

The depositional and alteration histories of the PTn units exposed in the North and South Ramps also differ slightly. 1) Disruption along the lower contact of the pre-Tiva Canyon Tuff bedded tuffs, which is spectacularly displayed in the North Ramp, generally is absent in South Ramp exposures (an exception occurs near Sta. 74+87). 2) The pre-Yucca Mountain Tuff bedded tuffs have a greater degree of reworking in the South Ramp. In particular, units d and f are locally eroded and incorporated into overlying unit g (Sta. 74+87) and the contact of units a and b locally is highly irregular and disturbed (Sta.74+82, left rib). 3) The pre-Yucca Mountain Tuff bedded tuffs exposed in the South Ramp locally contain calcite-cemented concretions and calcite cement in the basal few centimeters, which are not present in the North Ramp. 4) The reworked interval that comprises the upper portion of the pre-Pah Canyon Tuff bedded tuffs has markedly more complex stratigraphic relations in the North Ramp than in the South Ramp. Many of these differences can be attributed to the effects of fumarolic alteration visible in the North Ramp exposures. 5) The North Ramp exposes an interval of zeolitic alteration that affects the lower part of the Pah Canyon Tuff and the reworked tephra of the pre-Pah Canyon Tuff bedded tuffs.

Table 3. Tentative Correlation of Flow Units in the Lower Tiva Canyon Tuff

	South Ramp		North Ramp
	Sta. 66+98 to 67+60	Sta. 74+96 to 75+76	Sta. 7+28 to 8+69
pumice swarm	13.9[a]	22.6[a]	18.1[a]
surge horizon	n.p.	21.3[a]	n.p.
pumice swarm	10.8*‡	20.1¶‡	16.0§‡
dense/moderate weld	6.9*‡	5.4¶‡	13.5§‡
pumice swarm	n.p.	n.p.	4.6[b]
surge horizon	4.7*‡	2.25[b]	1.7[b]
Tpc/Tpbt4 contact	0.0	0.0	0.0

Notes: Thicknesses given in meters. n.p. = flow-unit boundary is not present.

* Calculated using measured dip of 13° for the interval above Tpc/Tbpt4 contact.

¶ Calculated using measured dip of 16° for the interval above Tpc/Tpbt4 contact.

§ Calculated using estimated dip of 12° for the interval above the lowermost pumice swarm (Sta. 7+93).

‡ Thickness is not corrected for minor faults through the interval.

[a] Measured thickness above central pumice swarm.

[b] Measured thickness above Tpc/Tpbt4 contact.

A similar zone of zeolitic alteration is absent in the South Ramp exposures.

Topopah Spring Tuff

Many features of the zones and subzones comprising the pyroclastic-flow deposits of the Topopah Spring Tuff are similar in the North and South Ramps. Included are the general pattern of welding and secondary crystallization, the location and general character of lithophysal zones, and the style of alteration that occurs beneath the crystal-rich vitrophyre.

Several features described in the North Ramp (Barr and others, 1996), however, either were not observed in the South Ramp or differ in some manner. 1) The base of the cavernous lithophysal subzone of the crystal-poor upper lithophysal zone is not as sharp in South Ramp exposures and the underlying flow-unit boundary (Sta. 19+50) is not evident. The interval is present in the South Ramp, but large cavities are not well developed. 2) The stratigraphic thickness of the interval of crystal-poor upper lithophysal zone from the base of the crystal-transition zone to the base of abundant quartz latite pumice clasts is estimated to be thinner in the South Ramp (23 m at Sta. 63+72 to 64+55; 18 m at Sta. 72+38 to 73+02) than in the North Ramp (39 m at Sta. 17+97 to 20+80). 3) In North Ramp exposures, the crystal-rich nonlithophysal zone includes a distinct interval of intense vapor-phase alteration with a sharp lower contact at Sta. 13+36. Although variations in the intensity of vapor-phase alteration do occur within the crystal-rich nonlithophysal zone in the South Ramp, an interval with a discrete lower boundary is not evident. 4) The upper few meters of the pyroclastic-flow deposits are notably more complex in South Ramp exposures and contain features not observed in the North Ramp. In one location (Sta. 74+40), the crystal-rich vitrophyre is absent. In other locations (Sta. 70+01, Sta. 74+40), the top of the pyroclastic-flow deposits include an interval of moderately welded, vapor-phase altered tuff.

Exposures of the Topopah Spring Tuff in the ESF reveal the complex relationships that can occur at the top of a thick, welded pyroclastic-flow deposit. They also show that in some locations, the

nomenclature of Buesch and others (1996) can't describe these variations. The contact between the pyroclastic-flow deposits and overlying pumice-fall deposits is a key to explaining the variations within this interval. This prominent depositional contact is not completely described by the present nomenclatural system. The timing of deposition and alteration of the pumice-fall and upper pyroclastic-flow deposits as exposed in both ramps indicates that the upper contact of the Topopah Spring Tuff should be revised (see Moyer and others, 1996). Exposures in the ESF and throughout the proposed site area (Moyer and others, 1996) suggest a formation contact at the top of the pumice-fall deposits (top of unit Tpbt2C of Moyer and others, 1996). In the proposed repository area, this would restrict the pre-Pah Canyon Tuff bedded tuffs to the interval of reworked tephra (unit Tpbt2D of Moyer and others, 1996).

Fumarolic Alteration

The North and South Ramps cross intervals of fumarolic alteration that occur within the pumice-fall deposits that overlie the Topopah Spring Tuff pyroclastic-flow deposits. In both ramps, the alteration is restricted to mound-like features that have complex internal stratigraphic relations and within which an interval of intense argillic alteration and hematite staining overlies a zone of silicification. The North Ramp exposure, which cuts through intense alteration near the top of the pumice-fall deposits, exposes alteration features that occur at a slightly higher stratigraphic level than those in the South Ramp. The South Ramp cuts through intense alteration near the base of the pumice-fall deposits. Consequently, the South Ramp exposures more clearly reveal the intimate relationships between mounds of alteration and fractures originating in the pyroclastic-flow deposits, display deeper portions of the alteration zone that are dominated by vapor-phase crystallization, and demonstrate that fumarolic alteration also affected the upper few meters of the pyroclastic-flow deposit. In contrast, the North Ramp exposures reveal complex geological relationships that involve slumping of the vent walls of the fumarole, infilling of the vent by windblown or waterlaid deposits, and subsequent zeolitic alteration of the overlying strata as ground water presumably ponded atop the altered, clay-rich pumiceous material (Barr and others, 1996; Levy and others, 1996; Peterman and others, 1996).

STRUCTURE

Comparative Cross Section

The Comparative Geology Cross Section Along The South Ramp (Drawing OA-46-301) was developed by the underground mapping team from as-built geology mapped in the South Ramp. The as-built cross section was compared to the pre-construction cross section, "Stratigraphic Cross Section Along The ESF South Ramp", assembled by Agapito and Associates for Sandia National Laboratories. Of the three comparative sections completed at the ESF the South Ramp shows the most difference between the pre-construction and as-built sections. The pre-construction section is based almost entirely on surface mapping. Stratigraphic thicknesses for the pre-construction section were developed using drill holes H-3, 1220 meters west of the South Ramp, and SD-7, about 700 meters northwest of the South Ramp.

Stratigraphic and Structural Differences Between the Sections

Pre-construction	Station	As-built	Station
Normal Fault	62+20	Normal Fault	63+25
Tptpmn/Tptpul	63+25	Tptpmn/Tptpul	63+08
Tptpul/Tptrn	65+55	Tptpul/Tptrn	65+07
		Normal Fault	65+24
Normal Fault	66+65	Normal Fault	66+45
Tptrn/Tpbt	67+70	Tptrn/Tpbt	66+49
		Normal Fault	67+61
Dune Wash Fault	67+60	Dune Wash Fault Zone	67+88 to 67+91
Tptpul/Tptrn	69+15	Tptpul/Tptrn	68+47
Tptrn/Tpbt	70+40	Tptrn/Tpbt	70+07
Normal Fault	70+50	Normal Fault	70+58
		Normal Fault	71+30
		Tptpmn/Tptpul	71+68

Stratigraphic and Structural Differences Between the Sections			
Reverse Fault	72+05		
Normal Fault	72+25	Normal Fault	72+70
Normal Fault	73+30		
Tptpul/Tptrn	73+90	Tptpul/Tptrn	73+02
Tptrn/Tpbt	75+00	Tptrn/Tpbt	74+50
Tpbt/Tpcpv	75+50	Tpbt/Tpcpv	74+96
Tpcpv/Tpcun	75+65	Tpcpv/Tpcun	75+15
Normal Fault	75+90		
Reverse Fault	77+90	Reverse Fault	77+80

Table 4: Stratigraphic and Structural Differences Between the Sections

In a general sense these sections are comparable, with the most significant differences at about Sta. 72+00 and Sta. 78+00. At Sta. 72+00 the pre-construction section shows a down- dropped block or graben bounded by a closely-spaced reverse fault and a normal fault. This block was not encountered during excavation of the South Ramp. Since these faults are mapped on the surface, the configuration of the block was added to the as-built section. The block was shown as pinching out above the tunnel. At Sta. 78+00 the pre-construction section shows a low-angle reverse fault intersecting the tunnel alignment. During the excavation of the South Ramp a much steeper dipping fault was encountered at this location. The projection of this structure is based on the geometry of the surface trace, therefore it must steepen with depth as is shown on the as-built section.

Faults and Shears in the South Ramp

Faults are defined as discontinuities displaying more than 0.1 m of offset (U.S. Bureau of Reclamation and U.S. Geological Survey, 1997, p.11). Shears are defined as discontinuities displaying less than 0.1 m of offset or having an undeterminable offset. Offset is determined visually in the tunnel by offset of reference features. For faults with displacement greater than

the diameter of the tunnel (7.62 m), offset is defined from correlation of stratigraphic units.

Faults and shears with less than 4.0 meters of offset

In the ESF from Sta. 55+00 to 78+77 there are 710 features from the full periphery geologic map and the detailed line survey are faults and shears with less than 4.0 meters of offset. Of these features, 288 have less than 0.1 meters and 191 have offset unknown, for a total of 479 shears. The average offset for shears is 0.045 meters. There are 234 faults with less than 4.0 meters offset. The average offset of these faults is 0.31 meters.

The sense of displacement for all faults and shears with less than 4.0 meters of offset is as follows; 366 - normal, 109 - reverse, 21 - left lateral, 18 - right lateral, 6 - normal/right lateral, 1 - reverse/left lateral, and 189 with undeterminable offset. The orientation plotted against frequency of these structures is shown in Fig. 4. The dips of these structures are as follows; $6 < 40°$, $21 < 50°$, $49 < 60°$, $89 < 70°$, $236 < 80°$, $292 < 90°$, $16 = 90°$, and 1 with unknown dip. The average distance between structures in the various stratigraphic units is; 3.77 m in the Topopah, 0.63 m in the bedded tuffs, 2.85 m in the Tiva. The overall average distance between structures in the South Ramp is 3.35 m. The distribution of faults and shears is shown in Fig. 5.

Faults with greater than 4.0 meters of offset

In the South Ramp of the ESF there are six faults with an offset greater than 4.0 meters. Two of these faults have greater than 50 meters of offset. These two faults are located at Sta. 67+87 to 67+91 (Dune Wash fault) and at Sta. 70+58. The rest have offsets less than 15 meters. With the exception of the reverse fault at Sta. 77+95, all these faults have normal down to the west movement. The Ghost Dance Fault, and the fault at Sta. 71+31 have less than 4.0 meters of offset, however they are significant features.

The Ghost Dance Fault (GDF) crosses the ESF Main Drift on the right wall springline at Sta.

Figure 4

Distribution of Fault and Shear azimuths in the South Ramp

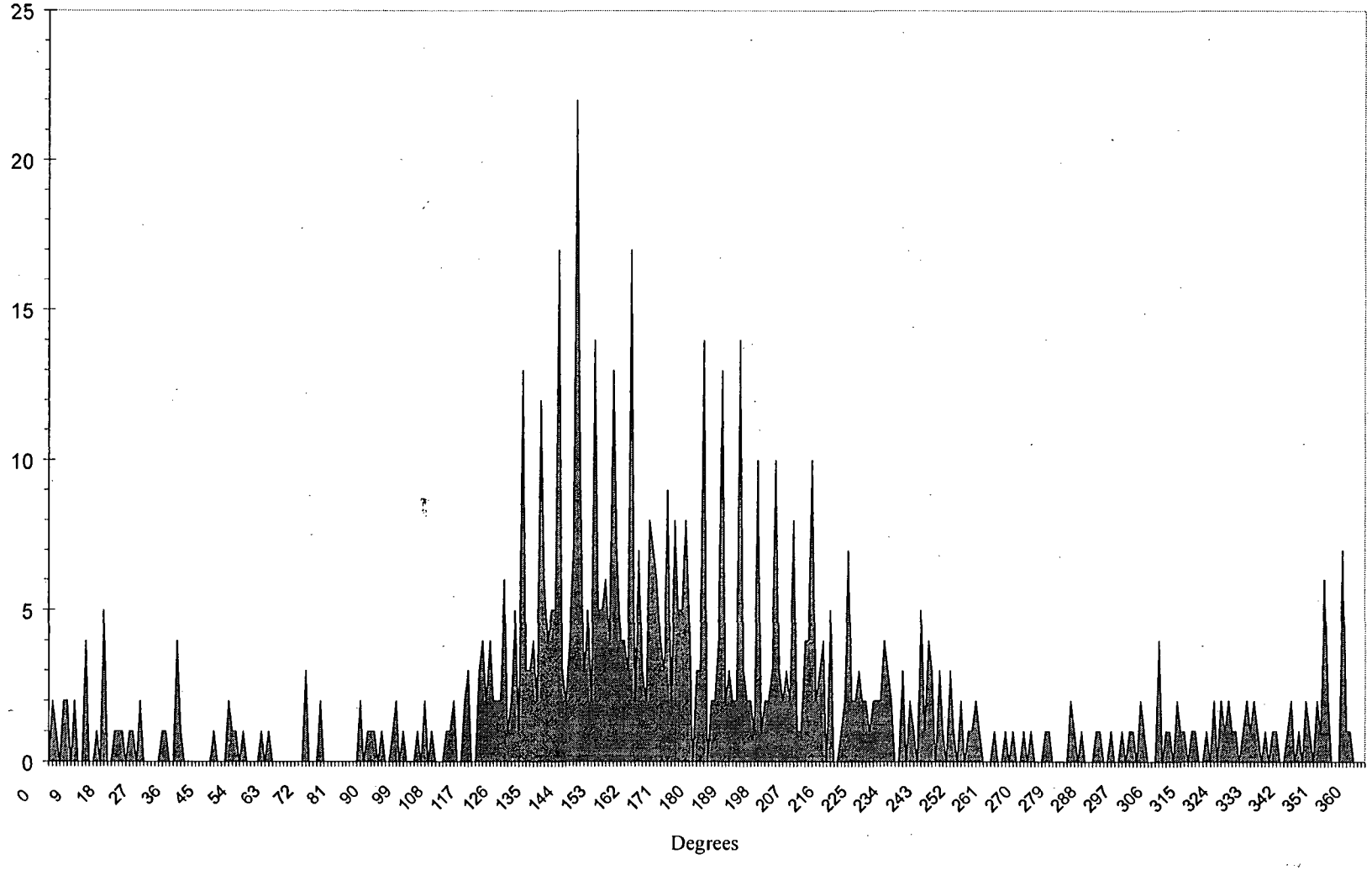

Distribution of Faults and Shears in the South Ramp

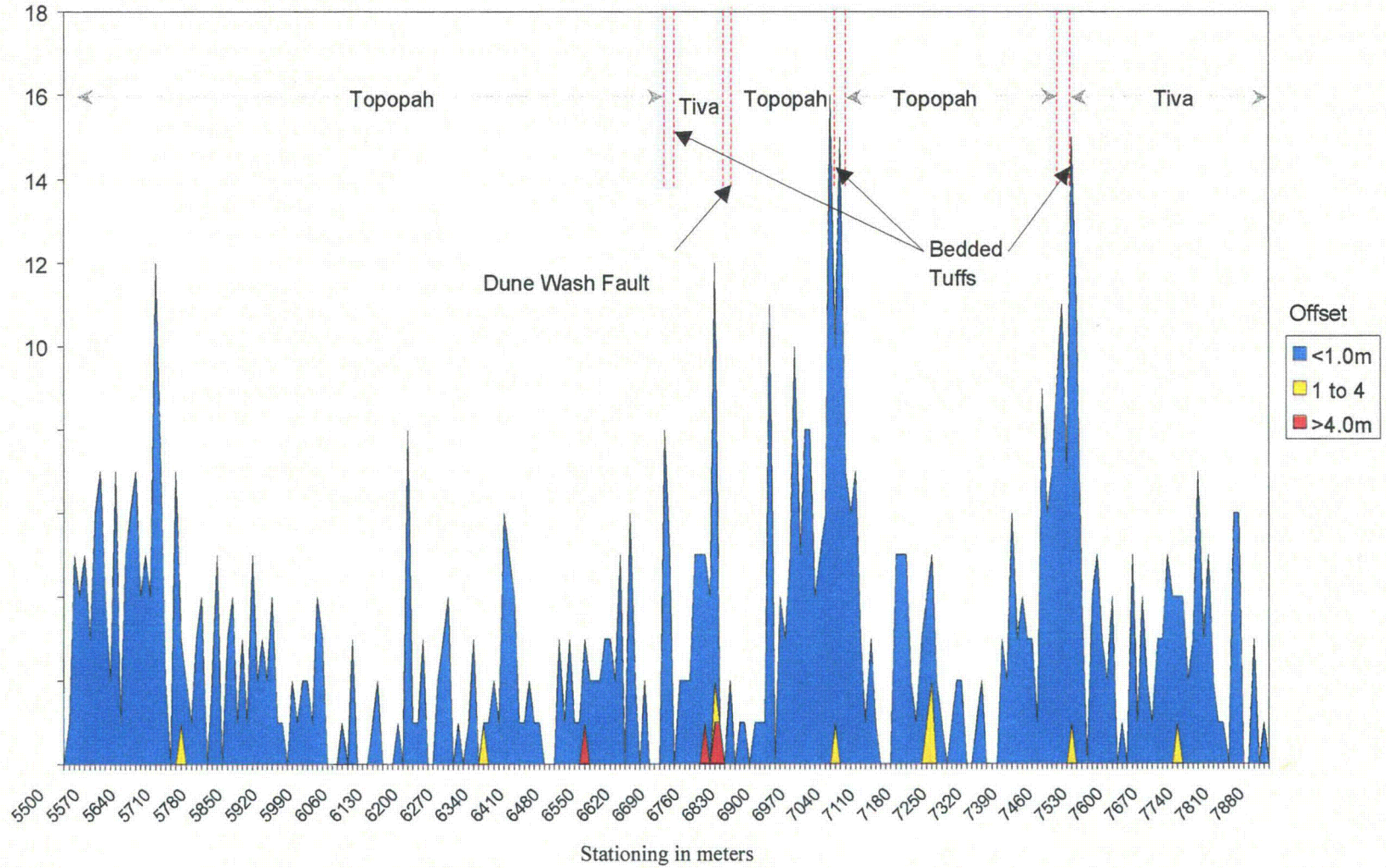

Figure 5

57+30. Compared to the exposure of the fault in Testing Alcove #6 (p.168) the GDF in the Main Drift is rather non-descript. In the Main Drift the GDF is oriented 205°/90° and has 1.2 meters of down to the west normal offset. The fault zone consists of an uncemented breccia zone about 0.25 meters wide. The breccia is composed of wall rock derived from the Tptpmn and Tptpll. The breccia is clast supported, with clasts that are angular to sub-angular and sizes range from <0.5 cm to >15 cm. The average clast size is about 5 cm. The breccia matrix is composed of clay to sand sized fine sand, and clay, possibly kaolinite. Minor goethite staining can be found throughout the breccia. The hanging wall of the fault is moderately to intensely fractured out to about 2.5 meters from the fault. The footwall shows only about 0.5 meters of fracturing. The ground support at the fault is 3x3" welded wire with steel channels and rock bolts.

The fault at Sta. 65+24.74 is oriented 130°/82°. This fault has 7.8 meters of down to the west normal offset. This fault places the Tptrl in the hanging wall against the Tptrn in the footwall. On the right wall the fault is a discrete zone about 10 cm wide. The 10 cm wide zone is composed of an uncemented, clast supported breccia. The breccia is about 90 percent clasts which are angular to sub-angular with sizes ranging from <1.0 cm to 5.0 cm. The average clast size is about 1.5 cm. The matrix is composed of clay to sand sized fine sand, and clay, possibly kaolinite. Fracturing related to the fault extends about 1.0 meter into the footwall and about 4.0 meters into the hanging wall. On the left wall, fracturing in the footwall is moderate to intense to about 2.5 meters from the fault plane. Fracturing in the hanging wall is intense to about 1.5 meters from the fault plane. The ground support at the fault is 3x3" welded wire with steel channels and rock bolts.

The fault at Sta. 67+61.40 is oriented at 135°/73°. The fault has 11.0 meters of down to the west normal offset. This fault places the Tpcpv in the footwall against the Tpcpln in the hanging wall. The fault plane is tight with little brecciation. What breccia there is, is uncemented, and clast supported. Clasts make up about 95 percent of the breccia. The clasts are angular to sub-angular, with sizes ranging from <1.0 cm to 3.0 cm. The matrix is a combination of clay to sand sized fine sand, and clay. The hanging wall shows fault related fracturing out to 2.0 meters from

the fault. The footwall shows very little fracturing related to the fault. The ground support at the fault is 3x3" welded wire with steel channels and rock bolts.

The Dune Wash Fault (DWF) crosses the South Ramp at Sta. 67+87.25 (see Plate 5). The DWF is composed of two distinct planes which have a combined down to the west normal offset of approximately 52 meters. On the right wall the fault is composed of two discrete planes. The first plane is located at Sta. 67+87.25 and is composed of a clast supported breccia up to 0.5 meters wide. The breccia is 70 percent clasts which are angular to sub-angular with sizes ranging from <1.0 cm to 20 cm. The average clast size is about 10 cm. Clasts are a combination of Tiva, Topopah and bedded tuff. The second plane is located at Sta. 67+91.15 and is similar to the first plane, however, the breccia is only about 0.25 meters wide.

Between the two fault planes is a steeply tilted, broken and sheared block. Because of tilting and shearing in the crown, the right and left ribs expose markedly different rock units. Units of the Topopah Spring Tuff are exposed along the right rib. These include the upper part of the crystal-rich nonlithophysal zone (right invert to approximately 2 m above right springline) which is overlain by the crystal-rich vitrophyre. The contact between the pyroclastic-flow and -fall deposits occurs along the upper right rib, approximately 0.3 m below the ends of the channels in the crown. In contrast, the left rib exposes units of the pre-Pah Canyon Tuff bedded tuffs and pre-Yucca Mountain Tuff bedded tuffs. Identified units include the upper part of the post-Topopah Spring Tuff pumice-fall deposits (unit c of Moyer and others, 1996; left invert to approximately 1 m above springline) which are overlain by reworked tephra of the pre-Pah Canyon Tuff bedded tuffs (unit d of Moyer and others). The contact between the pre-Pah Canyon Tuff bedded tuffs and pre-Yucca Mountain Tuff bedded tuffs is evident on the upper left rib, immediately below the channel ends. Units a (pumice-fall deposit) and b (reworked deposit) of the pre-Yucca Mountain Tuff bedded tuffs (Moyer and others, 1996) can be recognized along the upper left rib, bordering the western margin of the fault zone. These units are sheared against the lower part of the post-Topopah Spring Tuff pumice-fall deposits in the crown. Tpcpln is exposed in the hanging wall, with fault related fracturing extending out about 8.0 meters. In the

footwall the lithology is Tptpul with fault related fracturing extending out from the fault for about 1.0 meter. The ground support at the fault is 3x3" welded wire with steel channels and rock bolts.

The fault at Sta. 70+58 (right wall) is oriented approximately 170°/60°. The fault places Tpbt2 on the hanging wall against the middle nonlithophysal zone on the Tptpmn. The amount of offset along the zone is estimated at approximately 50+ m. On the left wall above springline the fault plane is a damp zone. For a complete description of this zone see the section on damp zones (p.171). The fault zone varies across the width of the tunnel in both thickness and orientation. Two meters above the right springline, the fault zone consists of gouge 20 cm thick, composed of reddish orange to purplish gray clay with occasional 1-2 cm clasts derived from the Tptpmn wall rock. Fault related fracturing extends into the hanging wall about 13 meters and into the footwall about 1.0 meter.

At Sta. 71+31 the TBM encountered a fault with relatively small offset – approximately 2 m (see Photo 12). The zone is not visible in the tunnel due to the large amount of continuous lagging installed as part of the ground support system during excavation. The fault zone is approximately 2 m thick and composed of uncemented and loose fault rubble. The fault rubble is an uncemented matrix-supported breccia, with angular Tptpmn clasts generally 10-20 cm in size. The matrix is composed of primarily sand-size material with no secondary mineralization visible. The fault rubble is soft to very soft, and because of the fallout in the tunnel crown prior to the fault, allowing the TBM to "nose down" approximately 1.5 m while excavating through the zone.

The fault at Sta. 77+95 is difficult to discern because the rock is highly fractured and steel sets and lagging obscure most of the tunnel. The fault is oriented 150°/72° and is a tight plane with little brecciation. Refer to the section on the comparative cross sections for a description of this feature.

Fractures

Effect of Tunnel Bearing on DLS Fracture Data

The South Ramp Report includes the portion of the ESF beginning at Sta. 55+00 to the end of the tunnel at Sta. 78+77 (Fig. 2). ESF Sta. 55+00 to 59+35.47 is actually part of the Main Drift (tunnel oriented along bearing 183°). ESF Sta. 59+35.47 to 64+25.21 is the curved section, and Sta. 64+25.21 to 78+77 is the true South Ramp (tunnel oriented along bearing 091°).

There are few DLS fractures in the Main Drift with strike azimuths near 183°(the Main Drift bearing). Similarly, DLS fractures near 091° azimuth (the South Ramp bearing) are scarce in the South Ramp. Two stereonets on the following pages show these phenomena. An example of the Main Drift section, Fig. 6 shows the tunnel from Sta. 56+00 to 57+00 including the Main Drift tunnel bearing of 183°. Fractures with strike azimuths near 183° are plotted on the East side of the stereonet, and any reciprocals are plotted on the West side. An example of the South Ramp section, Fig. 7 represents the tunnel from Sta. 70+00 to 71+00 including the South Ramp tunnel bearing of 091°. Fractures with strike azimuths near 091° are plotted near the North, and any reciprocals are plotted near the South. These stereonets illustrate the bias against the collection of DLS fractures with strike azimuths parallel or subparallel to the bearing of the tunnel. This is further borne out by examining each of the stereonets on the 100 meter FPGM's.

Lithology was taken into consideration in examining the changing fracture patterns going from the Main Drift through the curve and into the South Ramp. A section of Tptpmn in the Main Drift was compared with a very similar section of Tptpmn within the curve, eliminating any differences in the two sections due to a change in lithology. Also, a section of the curve was compared with a section in the South Ramp with similar lithologies (i.e. predominantly lithophysal rock).

Changes in fracture patterns due to differing structural forces acting upon the rock are not so

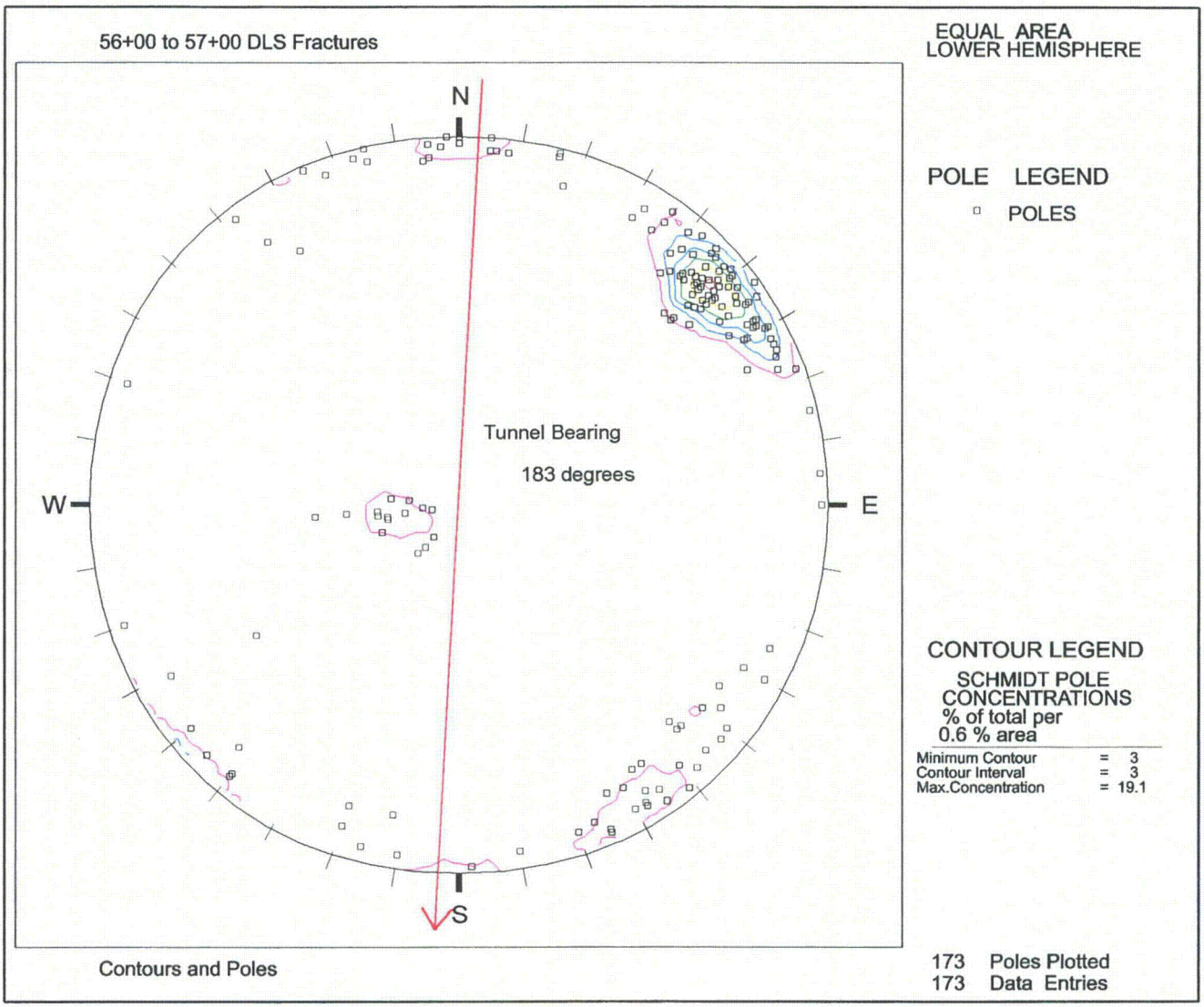

Figure 6: Stereonet plot of contours, poles, and Main Drift tunnel bearing of 183 degrees. This represents DLS fractures collected between Sta. 56+00 and 57+00, as an example of the bias in the Main Drift against the collection of fractures with strike azimuths parallel or subparallel to 183 degrees. Consequently few poles are plotted on the East or West of the stereonet.

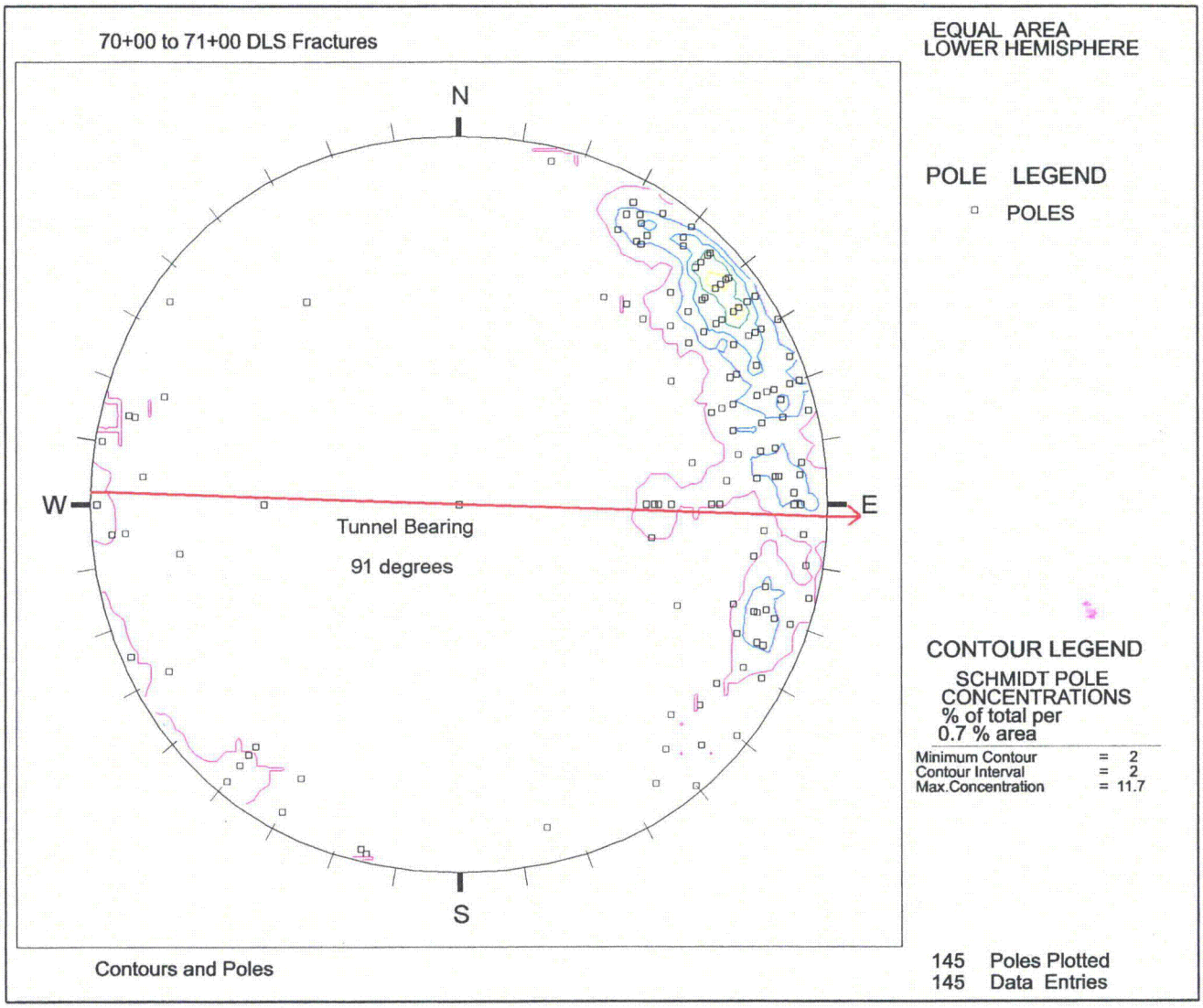

Figure 7: Stereonet plot of contours, poles, and South Ramp tunnel bearing of 91 degrees. This represents DLS fractures collected between Sta.70+00 and 71+00, as an example of the bias in the South Ramp against the collection of fractures with strike azimuths parallel or subparallel to 91 degrees. Consequently few poles are plotted on the North or South of the stereonet.

easily dismissed. DLS's show that there is a trend for fractures with strike azimuths that are parallel or subparallel to the tunnel bearing to be under represented in any given section of tunnel. This trend can be easily seen by examining stereonet plots and scatter plots of strike azimuth vs. stationing (of DLS fractures). The trend, or bias, is present only for fractures recorded on the DLS, and does not affect fractures mapped on the FPGMs.

Figure 8 shows the section of the tunnel between Sta. 59+00 and 65+00, which includes the curve. The scatter plot was made after eliminating all fractures with dips less than 70° in order to clarify the identification of reciprocals in the high angle fracture sets. Reciprocals are those poles that plot on the opposite side (180°) from an identified set or concentration of fractures.

A tight concentration of fractures in the 130°-160° azimuth range (see Fig. 8) represents the dominant fracture set. With the tunnel bearing plotted on this illustration, it can be seen that very few fractures are recorded where the tunnel bearing is 183°. Where the bearing changes as the tunnel curves and intersects the dominant fracture set (130°-160°), the set thins out significantly. Then, as the bearing changes to 91° in the south ramp, no fractures are recorded near this bearing. However, some fractures centered around 91° azimuth can be seen prior to about Sta. 62+00, since the bias against observing these fractures does not exist in this section of the tunnel. Additionally, more fractures can be seen in the curve and into the south ramp that are centered around 183°, because the bias against these fractures is gone since the tunnel bearing is no longer parallel or subparallel to the fractures.

As illustrated on Fig. 8, fractures approaching 091° can be found up to approximate Sta. 62+00, which is near the midpoint of the curve. After Sta. 62+00, fractures approaching 091° are absent. From the last half of the curve and beyond, the tunnel orientation is biased against fractures near 091° azimuth. The reciprocal tunnel bearing is also plotted on Fig. 8, showing only a few fractures plotted anywhere near the reciprocal bearing. The few that come near this bearing are reciprocals of the dominant fracture set (130°-160°).

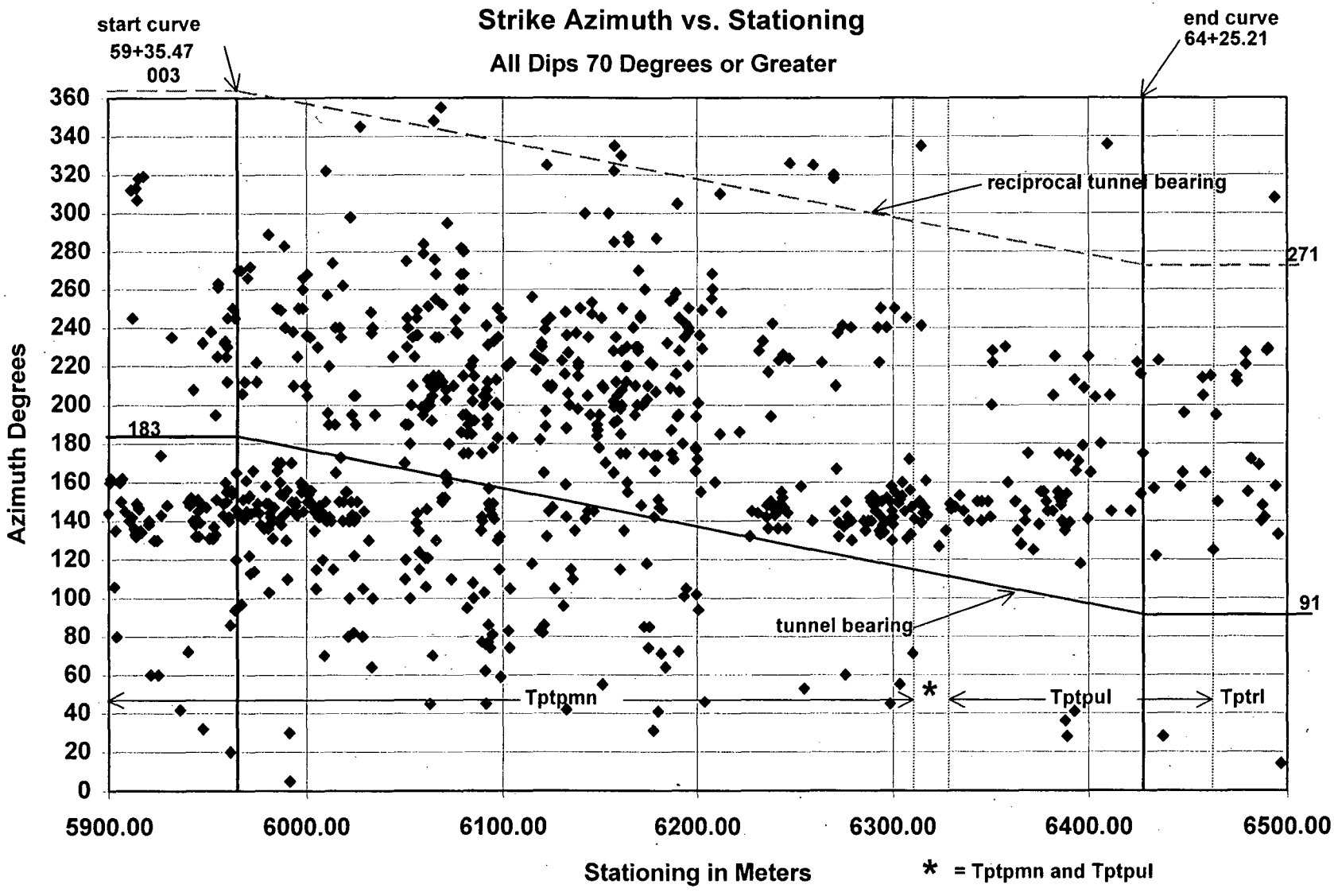

Figure 8: Scatter plot of strike azimuth vs. stationing. DLS fractures collected from Sta. 59+00 to 65+00 excluding those with dips less than 70°. Tunnel bearing is plotted, illustrating the "blind zone".

The bias against sampling DLS fractures with azimuths parallel or subparallel to the tunnel bearing is illustrated on Fig. 8. However, it doesn't explain all of the factors involved. Fractures in a given set either dominate or thin out due to other factors. Fractures near 91° are more easily observable in the Main Drift section, but they are not persistent throughout the Main Drift. Likewise, fractures near 183 ° are not found consistently throughout the South Ramp section, or in the last portion of the curve. In fact, Fig. 8 illustrates the existence of considerably more fractures near 183° azimuth in the first portion of the curve, than in the last portion, which is farthest from the 183° tunnel bearing. This contrasts sharply with the pattern of fractures near 091° azimuth, which are found in the first portion of the curve (farthest from the 091° tunnel bearing).

Analysis of DLS Fracture Data

The South Ramp is characterized by frequent changes in lithology, and units are often repeated due to normal faulting. Where lithologic units are repeated along the tunnel in large enough intervals and where significant numbers of data points (at least 50) exist, stereonets were constructed to observe variations in fracture patterns. Units which have too few data points to be considered in this type of analysis include the bedded tuff units (Tpbt), both the Tiva and Topopah vitric units (Tpcpv and Tptrv), the Tptrl (Topopah Spring crystal rich lithophysal zone), and the Tptpll (Topopah Spring crystal-poor lower lithophysal zone). This analysis is based upon visual characteristics of contour plots. A statistical approach using poles is used in the Cluster Analysis section (see p.89). Further statistical analysis is contained in Appendix IV (Descriptive Statistics for Fractures, Shears, and Faults) in which strike, dip, trace length, aperture, and roughness are analyzed.

"Less than one meter" fracture data was collected at 500 meter intervals for 50 meters (for the section of the ESF covered by this report these intervals include: 55+00 to 55+50, 60+00 to 60+50, 65+00 to 65+50, 70+00 to 70+50, and 75+00 to 75+50). This analysis was performed after removing all fractures less than one meter long to avoid any bias that could be introduced by

the additional data points.

Topopah Spring Tuff

Crystal-Poor Middle Nonlithophysal Zone (Tptpmn)

Stereonets were constructed for each of the 3 Tptpmn areas in the South Ramp:

A - Sta. 55+00 to 57+20.92 (Fig. 9)

B - Sta. 58+95.76 to 63+30.72 (Fig. 10)

C - Sta. 70+58 to 71+69.20) (Fig. 11)

All three show a dominant set comparable to Set 1 described in the Main Drift Report (Albin and others 1997), and the Cluster Analysis section of this report. The peak concentrations of strike azimuths shifts clockwise from Stereonet A to B, and then in C, the concentration becomes more diffuse:

A - 135°

B - 146°

C - 122° and 138°

A secondary dominant set corresponds to Set 2 described in the Main Drift Report and the Cluster Analysis section of this report. This set is seen in Stereonet A with a concentration of 241°, in B 236°, and in C the poles are too few to form a contour in this azimuth vicinity. However, in B, a new concentration occurs (201°) not seen in A, which continues in C as 203°. Stereonet A has very few poles in this range (201°) due to the bias against azimuths near 183° (Main Drift bearing).

The new concentration of poles seen in Stereonet B can also be seen when comparing the 100 meter stereonets (refer to Drawings OA-46-257 through -282, and OA-46-293 through -294). This concentration (201°) is either a distinct fracture set, or a shift of the set represented by poles in the 230°-245° range. The stereonets for Sta. 60+00-61+00 and Sta. 61+00-62+00 each have a

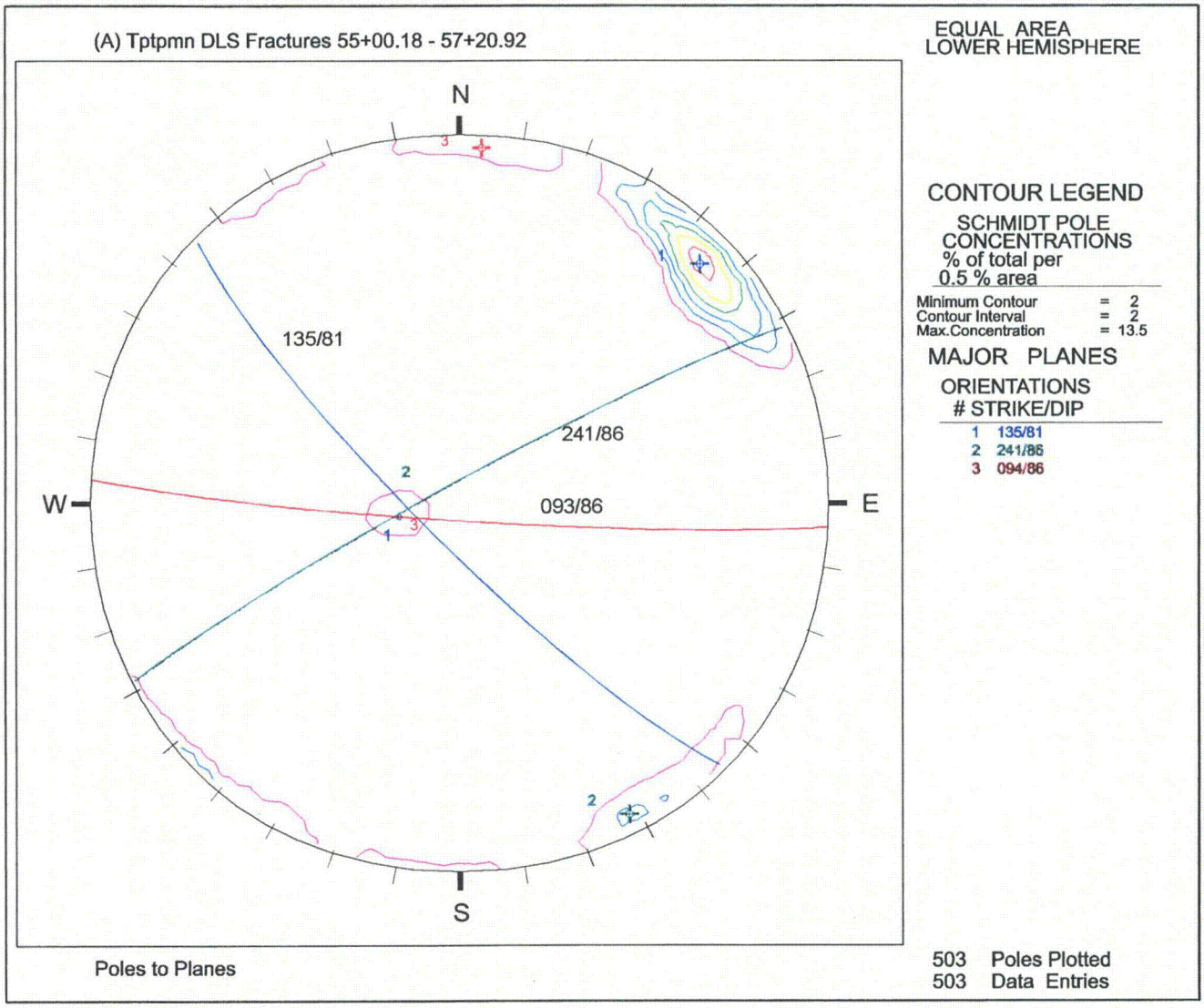

Figure 9: Stereonet A. Contour plot of DLS fractures in the first of three Tptpmn intervals. This section from Sta. 55+00 to 57+20.92 is located in the Main Drift of the ESF (bearing 183 degrees).

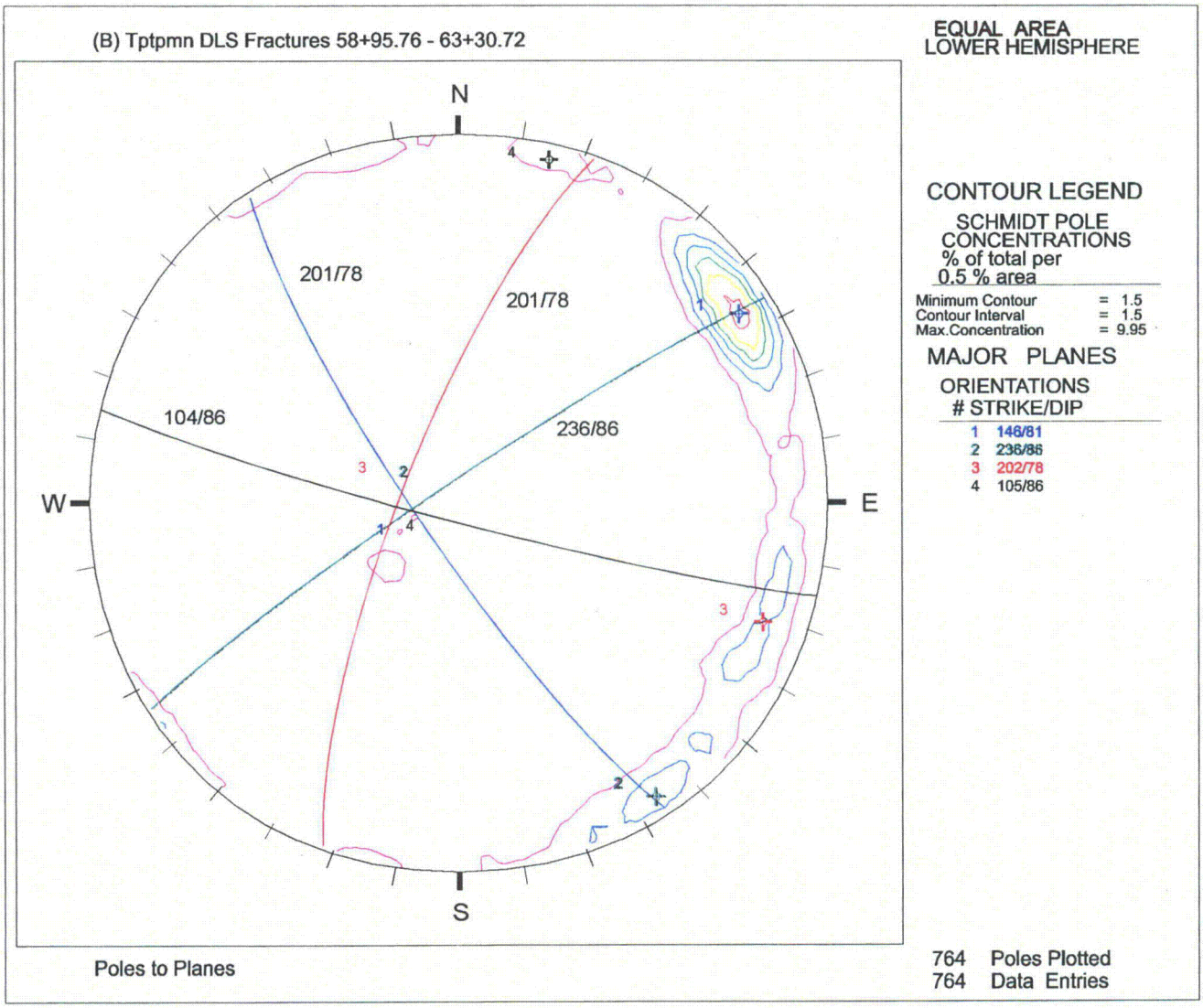

Figure 10: Stereonet B. Contour plot of DLS fractures in the second of three Tptpmn intervals. This section from Sta. 58+95.76 to 63+30.72 is located partly in the Main Drift (bearing 183 degrees) and mostly in the curved section.

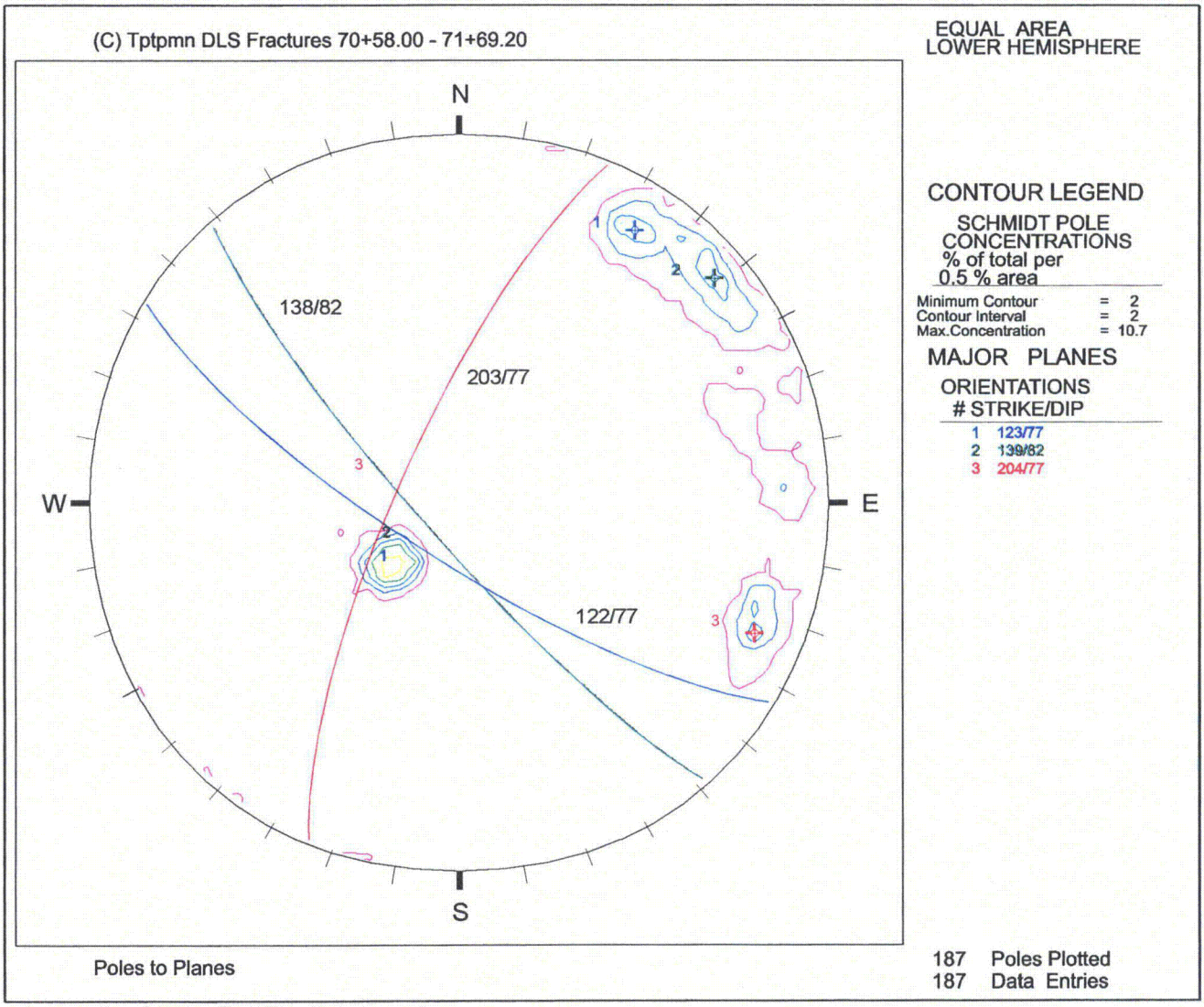

Figure 11: Stereonet C. Contour plot of DLS fractures in the third of three Tptpmn intervals. This section from Sta. 70+58 to 71+69.20 is located in the South Ramp (bearing 91 degrees).

significant concentration of poles in the 185°-220° azimuth range, as well as in the 220°-250° azimuth range. This section of the tunnel (Sta. 61+00-62+00) is within the curve, and the manifestation of fractures in this range (185°-220°) may be an effect of the slightly more favorable tunnel alignment, since this portion of the curve is still close to the Main Drift tunnel bearing. This set (185°-220°) does not come into prominence again until past Sta. 65+00. After Sta. 65+00 this set (185°-220°) dominates poles in the 220°-250° azimuth range. This may be a distinct set or a shift in the peak concentration. Stereonet plots similar to A, B, and C covering the three occurrences of Tptpmn can be seen on Drawing OA-46-308. These stereonet plots show the poles as well as contours, and also illustrate an approximate 20° "blind zone" of influence due to the tunnel orientation in these intervals.

Stereonet A has poles centered around azimuth 090°, forming a contour. Stereonet B also has fewer poles centered around 090°, and these entirely disappear in C. The disappearance of these poles in C is a reflection of the bias against these azimuths in this range in the true south ramp, oriented at 091°. Stereonet A is located in the main drift, while B is partly in the main drift and partly in the curve.

All three stereonets show a low angle set which generally corresponds to vapor-phase partings, and which is the dominant set in Stereonet C since the uppermost portion of the Tptpmn is characterized by closely-spaced vapor-phase partings.

Crystal-Rich Nonlithophysal zone (Tptrn)

A comparison using stereonets was made for Tptrn areas in the south ramp:

a - Sta. 65+12.24 - 66+33.59 (Fig. 12)

b - Sta. 68+90.35 - 69+92.85 (Fig. 13)

c - Sta. 73+44.72 - 74+39.09 (Fig. 14)

The dominant set falls in the azimuth range 180°-210°. In Stereonet a the peak concentration is at 194°, in b the peak is 203°, and in c the peak is 198°, indicating minor shifts.

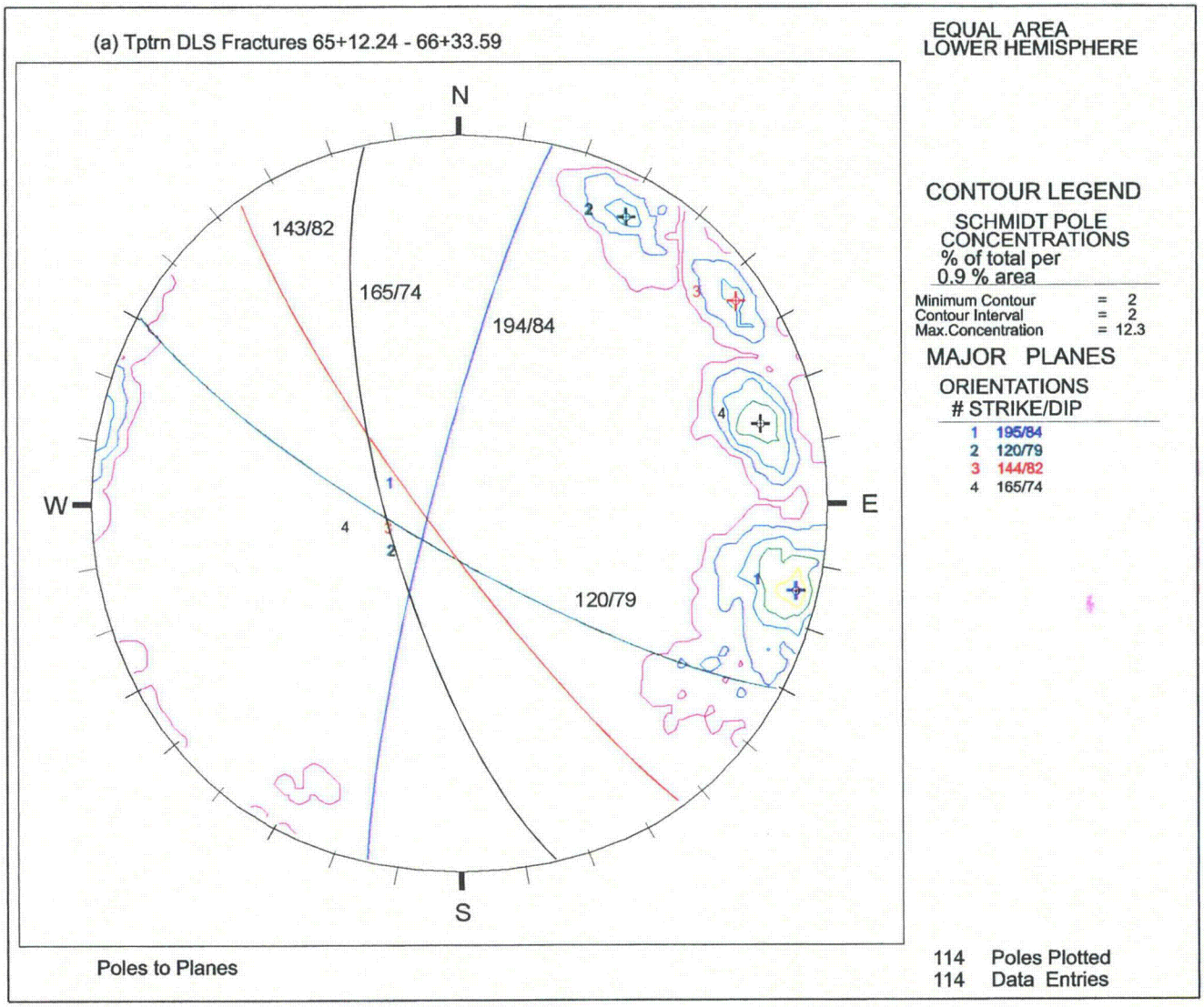

Figure 12: Stereonet a. Contour plot of DLS fractures in the first of three Tptrn intervals in the South Ramp.

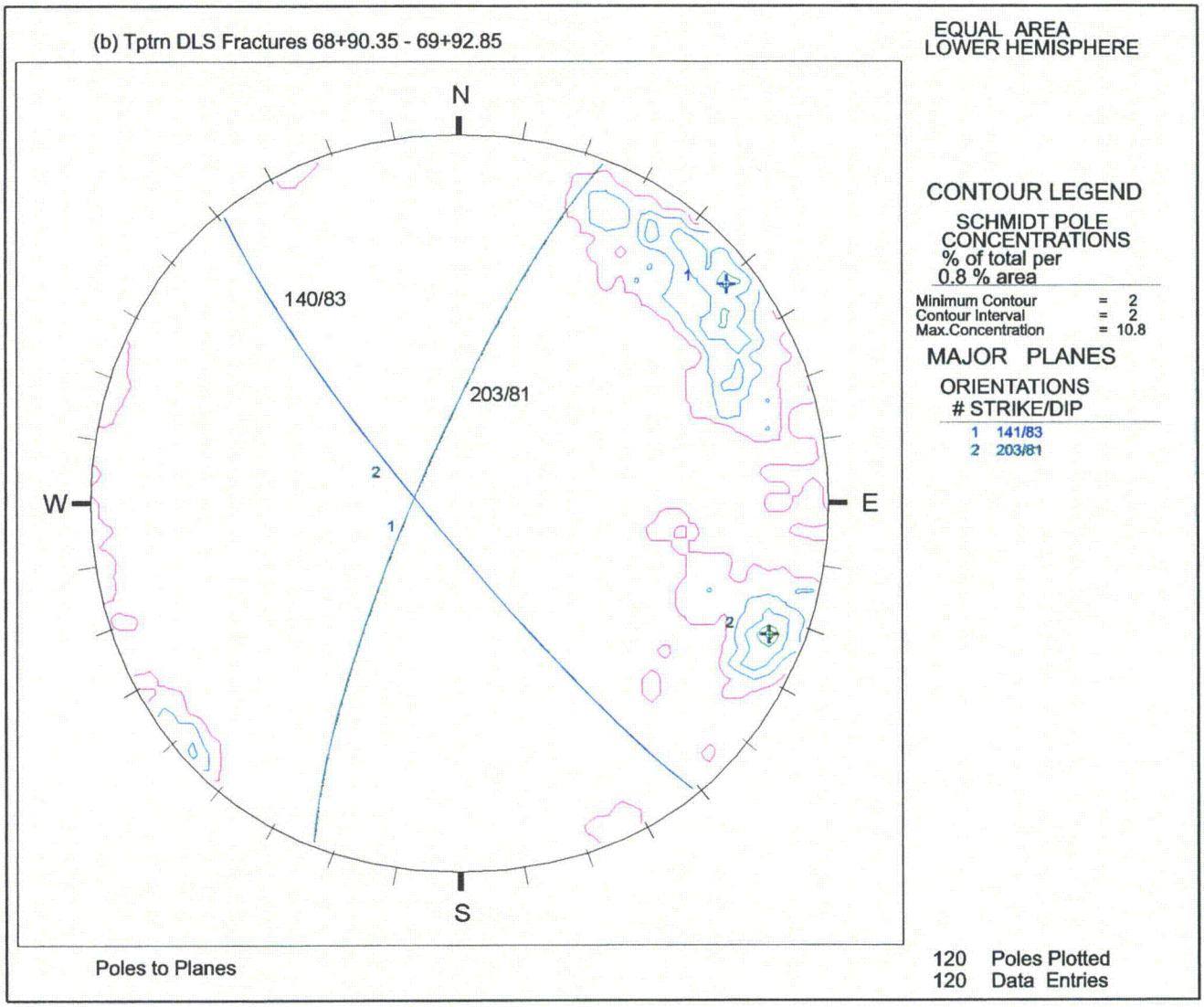

Figure 13: Stereonet b. Contour plot of DLS fractures in the second of three Tptrn intervals in the South Ramp.

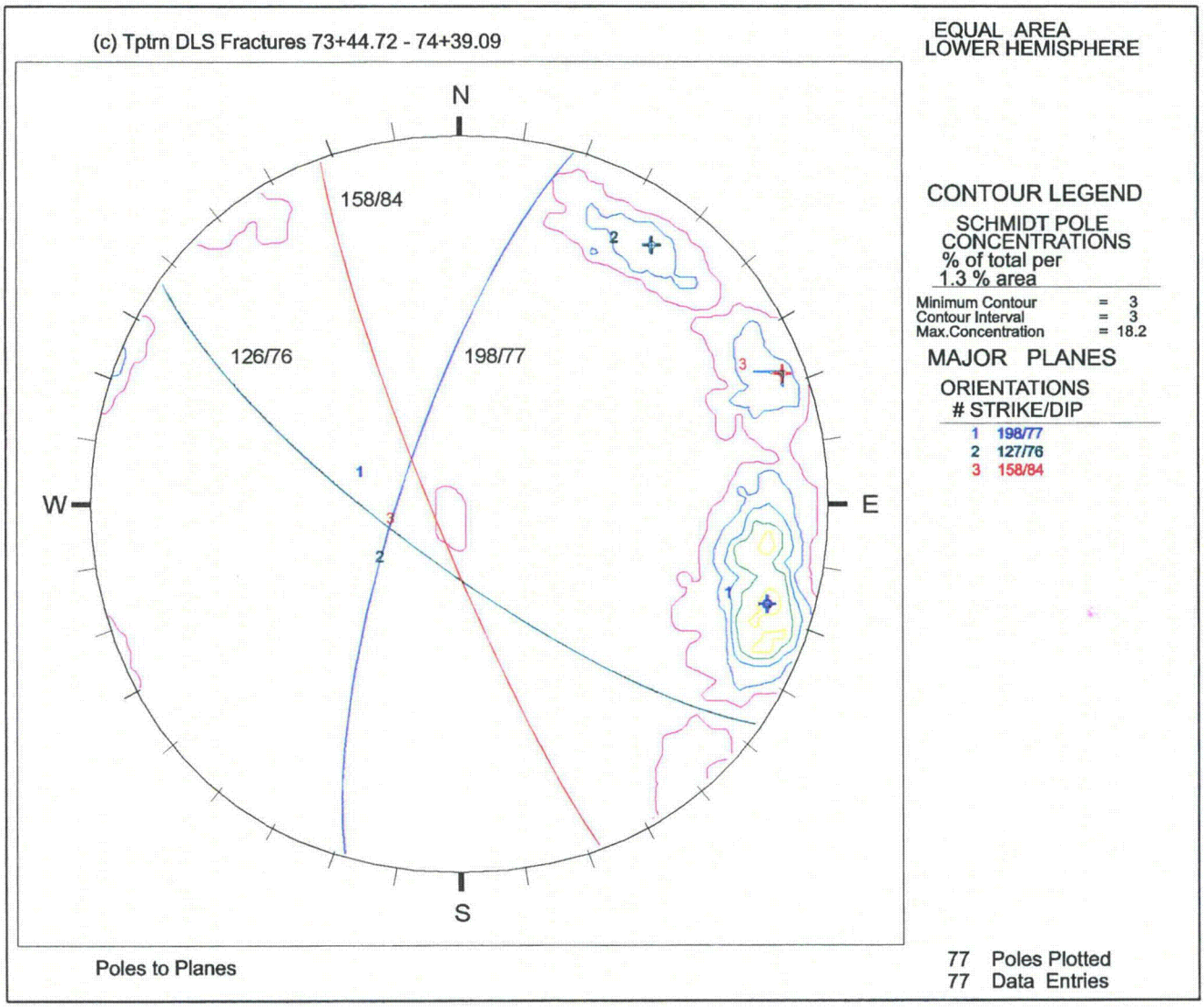

Figure 14: Stereonet c. Contour plot of DLS fractures in the third of three Tptrn intervals in the South Ramp.

A secondary concentration covers a large range from 110° to 175°. In Stereonet a this is broken up into 3 divisions, with peaks at 120°, 143° and 165°; in b is homogenized into one concentration with the peak at about 140° and in c is two, with peaks at 126°, and 158°. All of the intervals have a few low angle poles, but only Stereonet c has enough for these to form a contour.

Crystal-Poor Upper Lithophysal Zone (Tptpul)

A comparison was made using two composite intervals of Tptpul:
1 - Sta. 63+11.12-63+18.50 and Sta. 63+32.18-64+57.65 (Fig. 15)
2 - Sta. 67+93.80-68+47.38 and Sta. 71+70.29-73+02.86 (Fig. 16)
Stereonet 1 has a dominant concentration of azimuths ranging from 130° to 170° azimuth, with a peak at 150°. Stereonet 2 has a similar concentration with the peak at 155°. Both stereonets have concentration ranging from 200-230°. In Stereonet 1 the peak is about 209°, while in 2 it is at 215° azimuth. Stereonet 2 shows the strongest concentration between 180° and 200° azimuth, with the peak at about 192°. Stereonet 1 has a few poles in this area (180°-200°), but not a strong concentration, and not enough to form a contour. Stereonet 2 has enough low angle poles to form a contour (corresponding to vapor-phase orientations), while Stereonet 1 has a more diffuse spread of low angle poles, not forming contours.

Tiva Canyon

Crystal-Poor Lower Nonlithophysal Zone (Tpcpln)

Two sections of Tpcpln have fractures with poles plotting in a generally unbroken arc on the right side of the stereonets (110° to 250°):
i - Sta. 67+26.63 - 67+86.90 (Fig. 17)
ii - Sta. 75+17.35 - 76+05.33 (Fig. 18)
Each section has about four significant contour peaks. There are only a few low-angle poles

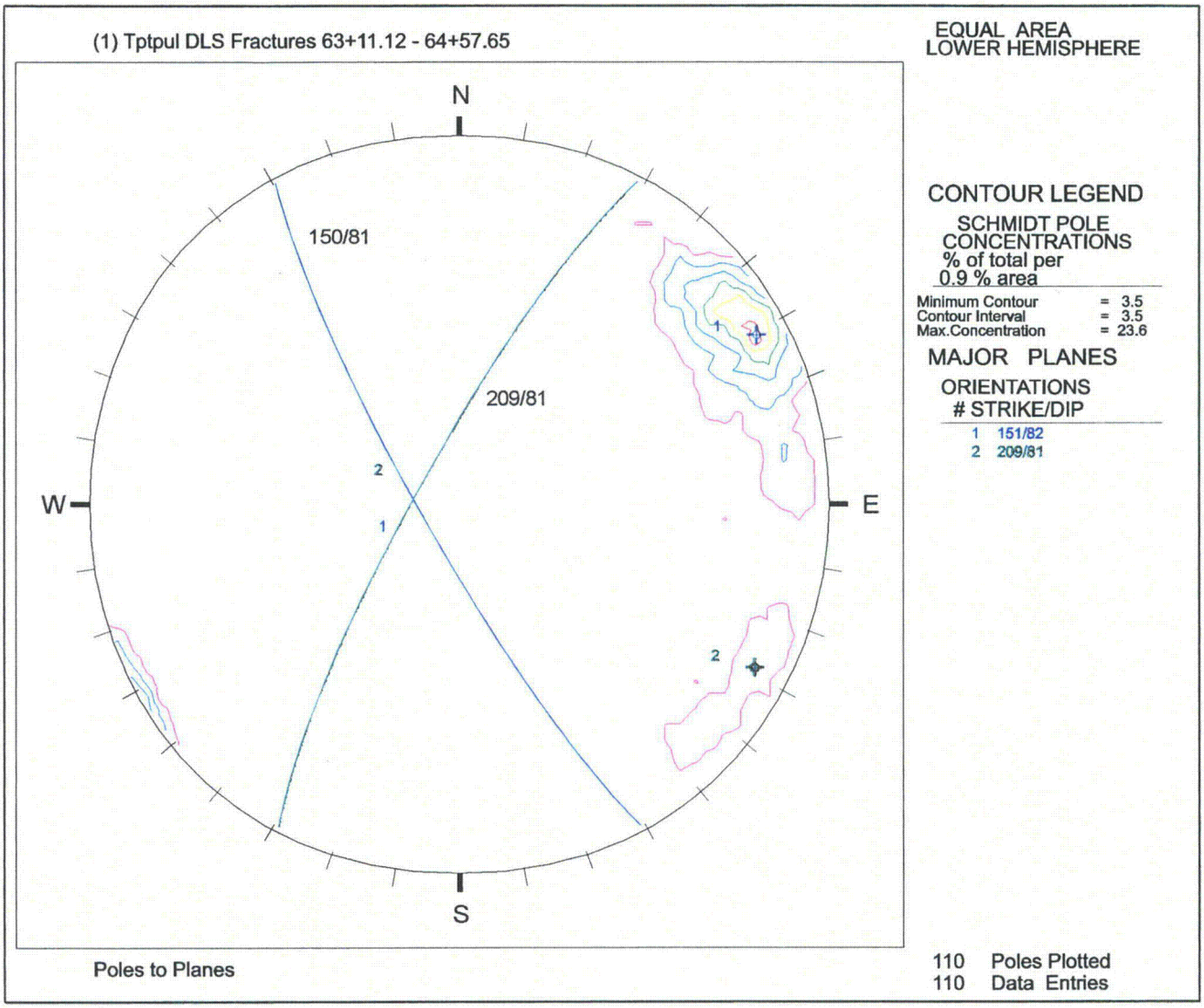

Figure 15: Stereonet 1. Contour plot of DLS fractures in the first of two composite intervals of Tptpul. This composite interval combines the section from Sta. 63+11.12 to 63+18.50 (within the curve) with the section from Sta. 63+32.18 to 64+57.65 (partly in the curve, and partly in the South Ramp - bearing 91 degrees).

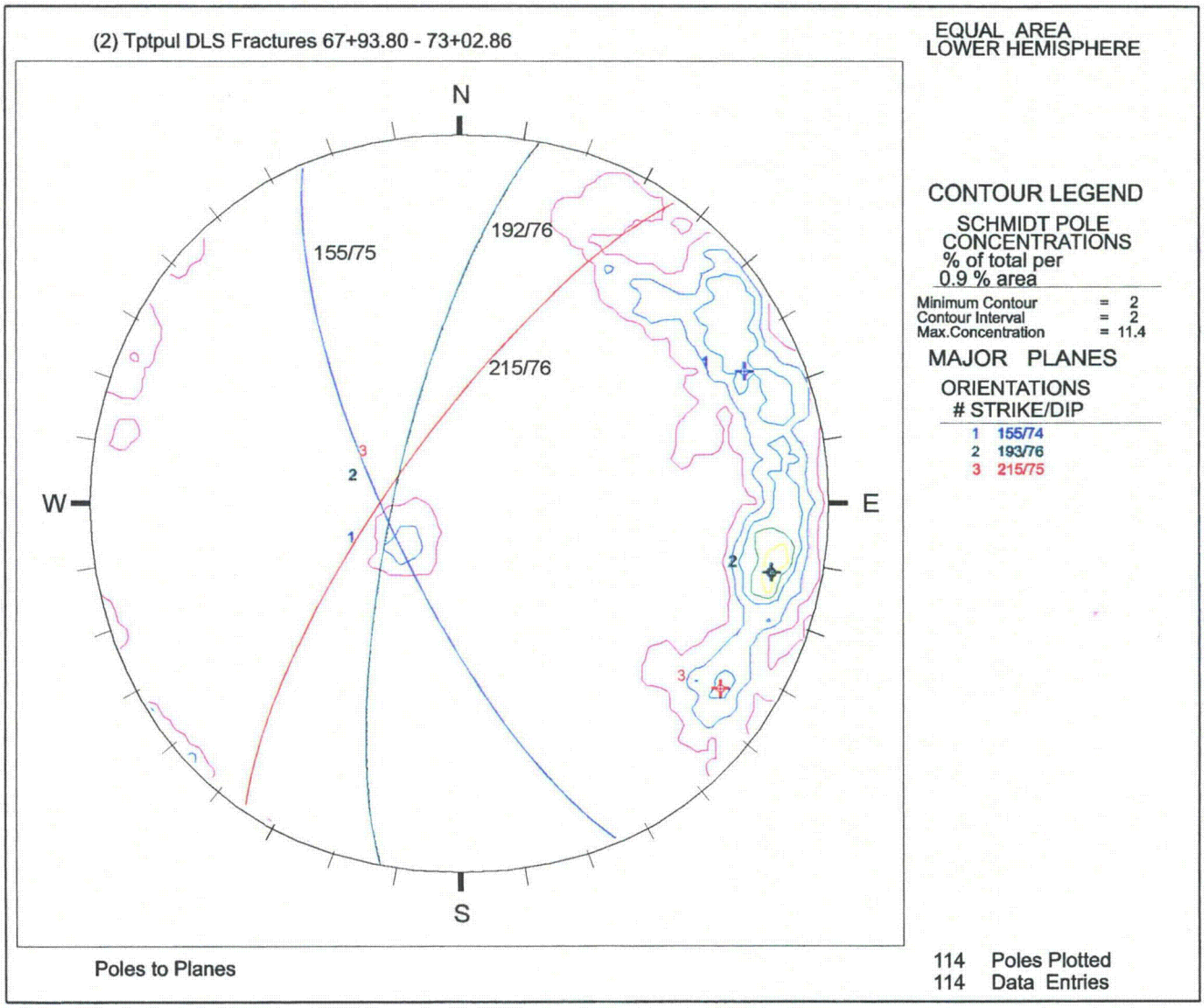

Figure 16: Stereonet 2 Contour plot of DLS fractures in the second of two composite intervals of Tptpul. This composite interval combines the section from Sta.67+93.80 to 68+47.38 with the section from Sta. 71+70.29 to 73+02.86 (both sections in the South Ramp - bearing 92 degrees).

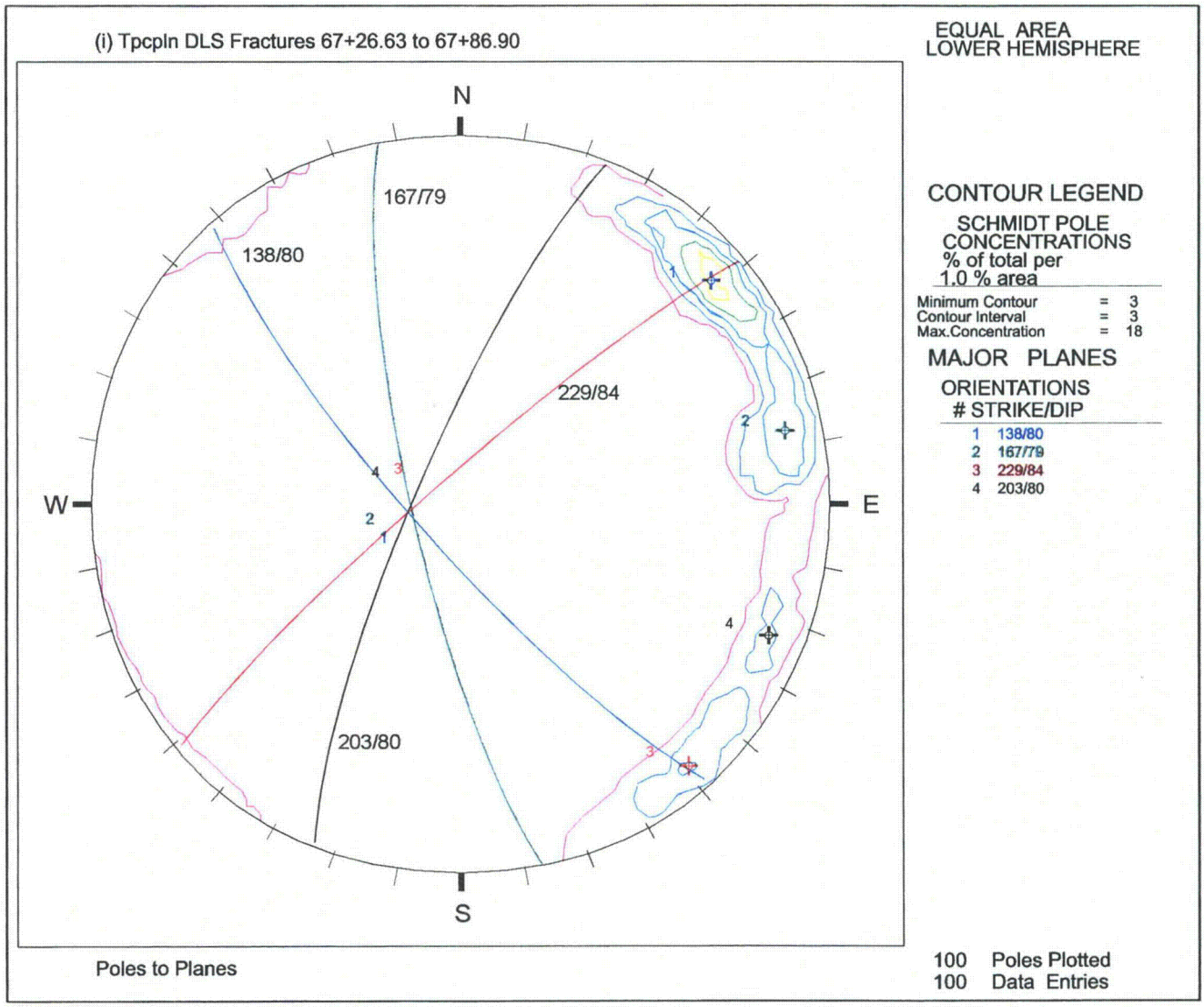

Figure 17: Stereonet i. Contour plot of DLS fractures in the first of two intervals of Tpcpln in the South Ramp. This section is from Sta. 67+26.63 to 67+86.90.

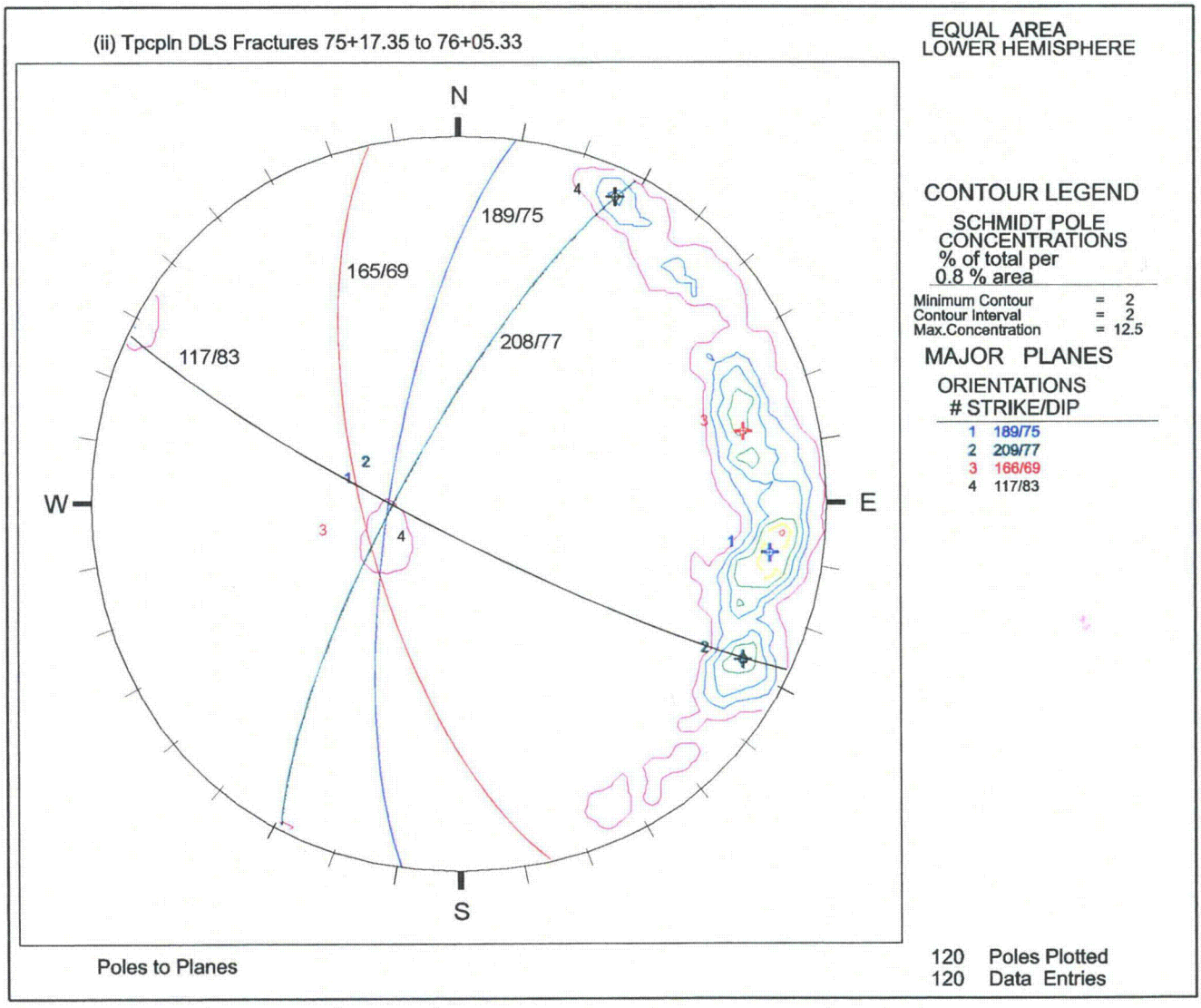

Figure 18: Stereonet ii. Contour plot of DLS fractures in the second of two intervals of Tpcpln in the South Ramp. This section is from Sta. 75+17.35 to 76+05.33.

(vapor-phase partings). There do not appear to be any other similarities between the two sections of Tpcpln. The dominant set in Stereonet i peaks at 138°, contrasting with the dominant set in Stereonet ii peaking at 189°. The second most dominant peak in i at 167°, corresponds to the third most predominant peak in ii at 165°.

Crystal-Poor Middle Nonlithophysal (Tpcpmn) and Upper Lithophysal (Tpcpul)

Data points within the Tpcpmn are combined with those within the Tpcpul (too few to be considered separately) in Figure 19. The dominant set is low- angle vapor-phase partings. The secondary set peaks at 165°. No other significant contours are formed.

The approach taken in this analysis has been to compare intervals of the same lithologic unit, and discuss similarities and differences. Overall, the contrasts between intervals of the same lithology have been minor. Further analysis using Clustran (p.89) uses a somewhat different approach, in which intervals of the same lithology have been grouped for analysis due to basic similarities in the intervals. Some intervals of lithologic units which contained too few data points to be effectively portrayed as individual intervals on stereonet plots, have adequate data points to be analyzed using Clustran, when combined.

Comparison With Main Drift and North Ramp Fracture Sets

Set 1 in the Main Drift (Albin and others 1997), centers around 120° in contrast with major contour peaks of 122°, 135°, 138°, 146°, and 150°, found in the South Ramp. The same is true for Set 2 in the Main Drift, centered at 220°, which is rotated clockwise in the South Ramp with peaks of 236° and 241°. Another significant difference in the South Ramp is the appearance of the set generally ranging from 185-220°. Set 3 in the Main Drift (310°/30°) corresponds to the low-angle fractures, mostly identified as vapor-phase partings, which are found in some of the lithologic units in the South Ramp. The south ramp has no corresponding set with peak azimuth orientations of 254° to 258° as found in the North Ramp (Barr and others, 1996) as the dominant

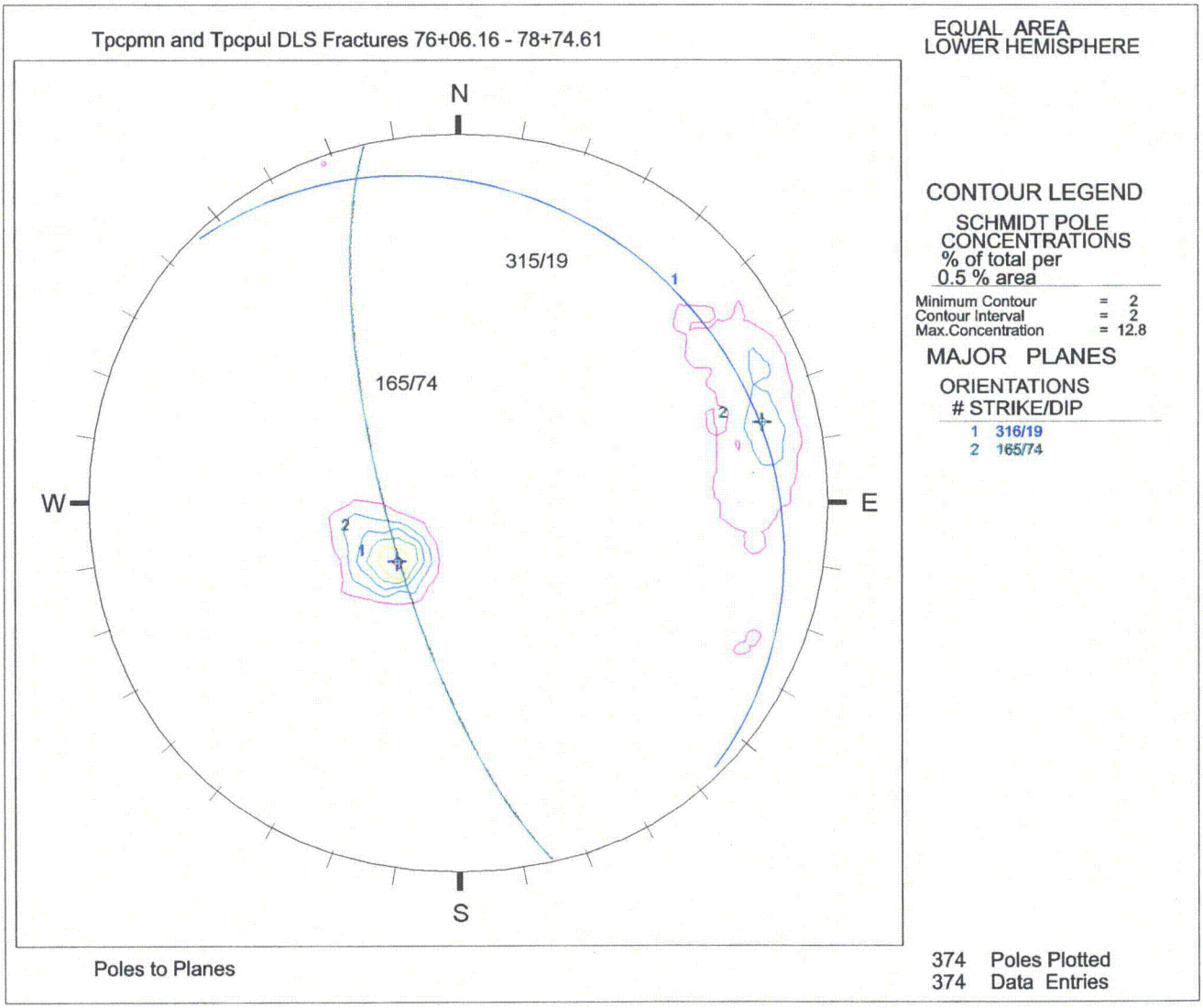

Figure 19: Stereonet Contour plot of DLS fractures from Sta. 76+06.16 to the end of the South Ramp at Sta. 78+77. The lithology of this interval is mostly Tpcpmn, with some Tpcpul.

fracture set (the closest peak concentration for the South Ramp is 229°). The second most prevalent fracture set in the North Ramp, with peak concentrations ranging from 215° to 219° is similar to some minor peak concentrations in the South Ramp ranging from 208° to 215°.

Cluster Analysis

The relative timing and mode of rock failure is important in interpreting the structural fabric of the rock, and these parameters may be determined by separating the fractures into sets with similar characteristics. Sets may be distinguished by differences in measurable parameters such as those recorded in the DLS. These parameters may include trace length, orientation, continuity, roughness, and aperture. This study describes the statistical analysis of the fractures observed on the right-wall-DLS data between Sta. 55+00 and Sta. 78+77. Drawing OA-46-306 shows the variations in azimuth, dip, and fracture frequency along the stationing interval of the South Ramp. Also shown on this drawing are the lithologic boundaries and the tunnel orientation. The presence of a bias or "blind zone", a range of fracture attitudes parallel or subparallel to the tunnel alignment that is poorly represented, should be considered when evaluating these results. On the stereonets, the "blind zone" is the region perpendicular to the tunnel alignment. This is due to the stereonet projection of poles normal to planes, rather than the planes of the fractures themselves. This "blind zone" is shown on some of the stereonets on Drawings OA-46-307 and -308 defining a 20°-wide zone (10° on either side of the tunnel alignment). The azimuth range affected by this "blind zone" is subjective, and the choice of 20° to represent the zone is intended only to suggest a possible range of influence, and not to quantify that range precisely. On the stereonets defining sets derived by cluster analysis, 10°, 15°, and 20° cones are shown centered on the mean set orientation to show the amount of concentration of each set.

Directional fracture data can typically be divided into several clusters representing different fracture sets. Statistical cluster analysis can help to overcome the large scatter of natural data sets and objectively separate sets for further analysis. The PC application Clustran, a commercially available software package, was used to perform the cluster analysis.

Like two-dimensional trend plots, poles plotted on stereonets need statistical analysis to substantiate relationships. Problems are likely when using only the contoured stereonet to pick the number and positions of sets. Results are sensitive to the algorithm used, and this sensitivity may not be apparent to the user. Set selection from contoured plots is subjective, and visually apparent trends may not be statistically significant.

Clustran avoids these problems by testing the set for nonrandomness, thus eliminating non-significant clusters. The directional data are analyzed directly and not contoured. The user specifies different clustering radii for the algorithm to identify the resulting clusters using an "objective function" that is minimized at the "best" radius. This process produces an identification of sets that is more objective than observing contoured pole plots. Statistical fits are made by Clustran to the extracted clusters of directions, and includes their means and confidence intervals. Clustran allows the user to write the clusters into new data files, which may be used for further analysis (Gillett, 1987). Cluster analysis provides a statistical approach to resolving sets, but cannot apply a knowledge of geological concepts. Sets derived from cluster analysis must then be viewed in terms of geological relevance. If sets derived by using the "best radius" as determined by the minimized "objective function" are not geologically significant, it may be necessary to choose the next higher "minimized function" and it's corresponding radius.

Clustran initially tests the directional fracture data for randomness using the chi square test, Poisson analysis, and log likelihood ratio test for quality of fit. Data from the ESF are found to be nonrandom. This nonrandomness is expected because the poles plotted show clusters, not a uniform scatter. Thus, the data can be analyzed for clusters, removing outlying data and selecting statistically significant clusters.

Because of the size of the data set (2842 fractures with greater than 1 m trace length) it was necessary to separate them into smaller intervals due to limitations in the Clustran program and the increasing scatter in larger data sets. Major structural fractures and the parameters recorded in the DLS were considered when determining how to divide the data set. All types of fractures

recorded in the DLS were included in this analysis; therefore, the sets do not distinguish between fractures, shears, faults, cooling joints, and vapor-phase partings.

Interval Selection

Variations in DLS-recorded parameters were analyzed when defining homogenous intervals in the South Ramp. Multiple repetition of units due to the number of faults with significant offset in the South Ramp necessitate evaluating the presence or absence of changes in fracture characteristics across these structural boundaries. Drawing OA-46-306 shows the strike versus stationing and dip versus stationing scatter plots as well as the fracture frequency histogram of the South Ramp data. In comparing same-unit fracture characteristics at each occurrence of the same unit, there were no significant variations observed between the occurrences except for the Tptpmn. This suggests that faults have caused no significant rotation of fracture orientations. Variations in Tptpmn orientations are discussed later, however, structural rotation of blocks in the South Ramp is not believed to be a significant factor in this fracture analysis. The most significant factors in evaluating differences in orientation data appear to be the internal characteristics of each lithostratigraphic unit and the potential bias introduced by tunnel orientation. Therefore, the fracture data collected in the DLS of the South Ramp is analyzed by separating it into lithostratigraphic units. This approach also serves to divide the fracture data into smaller data sets which are better suited to Clustran's capabilities. A detailed comparison of occurrences of the same unit is presented in the previous section, Analysis of DLS Fracture Data p.73

Topopah Spring Tuff

Crystal-Rich Vitrophyre (Tptrv)

The Tptrv is exposed from Sta. 55+00 to 78+77 at 3 locations. There were no distinguishable differences in fracture orientations between the occurrences, so these were considered as one

group. Clustran identified 2 sets in the 46 fractures which make up this group, and Drawing OA-46-307 shows the orientation distribution of these fractures and sets. There are 2 subzones within this zone. The first subzone is moderately welded, vapor-phase altered, devitrified, and locally silicified, and the second subzone is a densely welded, glassy pyroclastic-flow material. Fractures tend to be short (<5 meters in length), and commonly terminate at the under- or overlying zone.

Set 1 is a widely dispersed set containing all fractures in this lithologic unit except the low-angle fractures. Set 1 contains 42 fractures widely dispersed around a mean orientation of 173°/74°. The azimuths range from 110° to 230°, and the dips range from 45° to 88°.

Set 2 contains 4 fractures centering on a mean orientation of 342°/20°. Azimuths range from 328° to 352° and the dips range from 12° to 27°. This set contains fractures mapped as low-angle vapor-phase partings and features subparallel to the foliation.

Crystal-Rich Nonlithophysal Zone (Tptrn)

The Tptrn is exposed from Sta. 55+00 to 78+77 at 3 locations. There were no distinguishable differences in fracture orientations between the occurrences, so these were considered as one group, which consists of 295 fractures. The sets identified by Clustran are believed to have no geological significance, and Drawing OA-46-307 shows the orientation distribution of all of these fractures. This zone is composed of devitrified and intensely vapor-phase altered pyroclastic-flow material that grades upward from densely welded to moderately to densely welded. Fractures in the second occurrence of the Tptrn (Sta. 68+85 to 69+90) tend to be shorter than the first and third occurrences (<5 meters in length), and the maximum apertures in the Tptrn are proportionally higher than those in any other zone.

Crystal-Rich Lithophysal Zone (Tptrl)

The Tptrl is exposed from Sta. 55+00 to 78+77 at 3 locations. There are no distinguishable differences in fracture orientations between the occurrences, so these were considered as one group. This group consists of 71 fractures. Clustran identified 2 sets in this group, and Drawing OA-46-307 shows the orientation distribution of these fractures and sets. Although this zone is densely welded, devitrified and vapor-phase altered, the presence of lithophysae inhibit fracture propagation. This results in a zone with a lower fracture intensity and generally shorter fractures (<3 meters in length). Fracture zones within areas with a high lithophysal content may not be observed in the DLS as the fracture lengths may not meet the minimum fracture length criteria of one meter.

Set 1 is a northwest-trending set of fractures that contains 43 fractures dispersed around a mean orientation of 144°/78°. The azimuths range from 117° to 187°, and the dips range from 51° to 88°.

Set 2 is a northeast-trending set of fractures that contains 27 fractures dispersed around a mean orientation of 217°/80°. Azimuths range from 195° to 237° and the dips range from 56° to 88°.

This set contains only one fracture mapped as a low-angle vapor-phase parting or feature subparallel to the foliation.

Crystal-Poor Upper Lithophysal Zone (Tptpul)

The Tptpul is exposed from Sta. 55+00 to 78+77 at 3 locations. There were no distinguishable differences in fracture orientations between the occurrences, so these were considered as one group which consists of 238 fractures. The sets identified by Clustran are believed to have no geological significance, and Drawing OA-46-307 shows the orientation distribution of all of these fractures. Although this zone is densely welded, devitrified and vapor-phase altered, the

presence of lithophysae inhibit fracture propagation. This results in a zone with a lower fracture intensity and generally shorter fractures (<5 meters in length).

Even though Clustran did not distinguish significant sets in this zone, it is visually apparent that this zone contains a set of low-angle vapor-phase partings not observed in the Tptrl.

Crystal-Poor Middle Nonlithophysal Zone (Tptpmn)

The Tptpmn is exposed from Sta. 55+00 to 78+77 at 3 locations. The tunnel intersects the Tptpmn throughout the Main Drift, briefly intersects the top of the underlying Tptpll, and then proceeds up section through the Tptpmn again in the turn into the South Ramp. The first and second occurrences are not repeated sections due to faulting. The third occurrence of the Tptpmn is repeated due to faulting.

The three separate occurrences were evaluated, and some similarities and differences were found. Drawing OA-46-308 shows the stereonets for each occurrence, as well as their "blind zones". This study is complicated by comparing data from Sta. 55+00 to 57+30 which has a tunnel orientation of 183° (occurrence 1), Sta. 58+78 to 63+08 which is mostly in the south turn from the Main Drift to the South Ramp and has a gradually changing tunnel orientation (occurrence 2), and Sta. 70+58 to 71+68 which has a tunnel orientation of 093° (occurrence 3). The dominant set in all three occurrences is a northwest trending set. In the first and third occurrence, the peaks are roughly similar with an azimuth of approximately 135°. In the second occurrence, the peak azimuth is approximately 145°. Note that in the second occurrence, the tunnel orientation changes from 183° to 127°, and changes through the entire quadrant that contains this primary set. This causes an apparent shift in the peak location.

The three occurrences of the Tptpmn are believed to all represent the same fracture network for the following reasons. 1) Peak orientations for the primary set in the first and third occurrences are similar, whereas the second occurrence is probably affected in some way by the DLS "blind

zone". 2) The 30-40° difference in peak orientation of the northeast trending set (Set 2, approximately 210° to 250° range) is possibly due to the "blind zone" influence on the edges of the fracture sets in each occurrence. 3) All other zones within the Topopah Spring Tuff showed no changes in peak fracture orientations along the stationing interval considered in this study. For these reasons, all three occurrences of the Tptpmn are treated as representing the same fracture network, and are combined together for analysis.

Cluster analysis of the 1439 fractures in the Tptpmn from Sta. 55+00 to 78+77 produced no geologically significant clusters. As there were visually apparent clusters, further evaluation was indicated. The problem that Clustran appeared to face was the increased scatter of fractures in the 165° - 200° range that prohibited Clustran from statistically separating the denser northwest- and northeast-trending, visually-apparent fracture sets. Further analysis showed these fractures to generally be less than 2 meters long. Analysis of all of the Tptpmn fractures less than 2 meters long showed this set to be evenly dispersed over the 110° - 250° azimuth range. These are not believed to be a geologically relevant set of fractures, and cluster analysis was completed on a data set excluding these short fractures.

This abbreviated group consists of 691 fractures. Clustran identified 3 sets in this group, and Drawing OA-46-308 shows the orientation distribution of these fractures and sets. Sets 1 and 2 may visually appear to have smaller clusters within, and the fractures in these sets scatter widely around a central cluster, however, cluster analysis on each set individually does not support further separation.

Set 1 is a northwest-trending set of fractures that contains 427 fractures around a mean orientation of 137°/81°. The azimuths range from 080° to 170°, and the dips range from 59° to 90°.

Set 2 is a northeast-trending set of fractures that contains 198 fractures dispersed around a mean orientation of 222°/82°. Azimuths range from 171° to 261° and the dips range from 60° to 90°.

Set 3 is a low-angle set of fractures that contains 66 fractures dispersed around a mean

orientation of 326°/17°. Azimuths range from 007° to 360° and the dips range from 2° to 39°. This set contains fractures mapped as low-angle vapor-phase partings or features subparallel to the foliation and is widely dispersed around the center of the stereonet.

Crystal-Poor Lower Lithophysal Zone (Tptpll)

The Tptpll is exposed from Sta. 55+00 to 78+77 at one location. Clustran identified 2 sets in this group, and Drawing OA-46-308 shows the orientation distribution of these fractures and sets. Although this zone is densely welded, devitrified and vapor-phase altered, the presence of lithophysae inhibit fracture propagation. This results in a zone with a lower fracture intensity. The presence of the same 2 predominant sets as observed in the Main Drift (Albin and others, 1997) may be a result of the "blind zone" resulting from a tunnel orientation of 183°.

Set 1 is a northwest-trending set of fractures that contains 29 fractures dispersed around a mean orientation of 147°/80°. The azimuths range from 111° to 172°, and the dips range from 70° to 90°.

Set 2 is a northeast-trending set of fractures that contains 9 fractures dispersed around a mean orientation of 226°/85°. Azimuths range from 208° to 252° and the dips range from 77° to 89°.

This set does not contain fractures mapped as low-angle vapor-phase partings or features subparallel to the foliation.

Bedded Tuffs

The bedded tuffs are exposed from Sta. 55+00 to 78+77 at 3 locations. There were no distinguishable differences in fracture orientations between the occurrences, so these are considered one group. This group consists of 75 fractures. The sets identified by Clustran are believed to have no geological significance, and Drawing OA-46-308 shows the orientation

distribution of all of these fractures. The nonwelded or moderately welded tuffs undergo more intergranular deformation and flexing thus producing fewer fractures and inhibiting the formation of smaller fractures with shorter trace lengths. This was observed in the bedded tuffs of the North Ramp (Barr and others, 1996).

Tiva Canyon Tuff

The Tiva Canyon Tuff is exposed from Sta. 55+00 to 78+77 at 2 locations. Individual zones within the Tiva Canyon Tuff showed no discernable differences. There were no distinguishable differences in fracture orientations between occurrences, so these were considered as one group of 640 fractures. The sets identified by Clustran are believed to have no geological significance other than the distinct low-angle set, and Drawing OA-46-308 shows the orientation distribution of all of these fractures. The Tiva Canyon Tuff fractures are distributed widely over an azimuth range of roughly 103° to 255°. There are several possible peaks observed visually in this set defined by contouring the data points (Drawing OA-46-308). However, statistical cluster analysis does not break these out into significant sets. This unit does not have the distinct 3 sets observed in most of the Topopah Spring Tuff in the South Ramp and all of the Topopah Spring Tuff in the Main Drift (Albin and others, 1997). The degree of welding, crystallization, and vapor-phase alteration is not significantly different between the two tuffs, and therefore is not likely to be the explanation for this difference in fracturing. This suggests that the fracturing in the two tuffs is probably related to differing stress environments.

Comparisons with Fractures in the North Ramp and Main Drift

This section briefly compares the fracture characteristics in the South Ramp with those in the North Ramp (Barr and others, 1996) and Main Drift (Albin and others, 1997). Stereonets of the North Ramp DLS data separated by lithologic unit are show on Drawings OA-46-307 to -308 next to their South Ramp counterparts for comparison purposes. Comparisons with the North Ramp are based upon further review of the North Ramp data. A more detailed comparison

involving extensive field and statistical analysis to better understand regional implications is recommended for future work, and is beyond the scope of this report.

Topopah Spring Tuff

Crystal-Rich Vitrophyre (Tptrv)

Fracture intensity is higher in the North Ramp Tptrv fractures than in the South Ramp. Fracture orientations are widely dispersed in both exposures, however the fractures in the North Ramp have azimuths that range from 155° to 260° and dips that range from 30° to 90°. The South Ramp azimuths range from 110° to 230°, and the dips range from 45° to 88°.

In the North Ramp there is a north-south trending set of fractures which is not observed in the Main Drift or the South Ramp. Also present in the North Ramp is a set of fractures similar in orientation to the Set 2 fractures of the Main Drift and the South Ramp. Fractures with orientations corresponding to the Main Drift and South Ramp Set 1 are not observed in the North Ramp, however this may be due to the "blind zone" corresponding to this tunnel orientation.

Crystal-Rich Nonlithophysal Zone (Tptrn)

Fracture intensity is generally higher in the North Ramp Tptrn fractures than in the South Ramp. Fracture orientations are widely dispersed in both exposures, although some peaks are visually present. Fractures in the North Ramp have azimuths that range from 130° to 250° with one peak azimuth at 218°. The South Ramp azimuths range from 118° to 247° with several minor peak azimuths at 202°, 167°, and 143°.

The dominant set observed in the North Ramp correlates with the Set 2 fracture orientations observed in the Main Drift and the South Ramp. There is a smaller concentration of fractures with a north-south orientation, not observed in the Main Drift or the South Ramp, and no set

corresponds to the Set 2 fractures of the Main Drift and the South Ramp. As in the other lithostratigraphic units present in the North Ramp, this may be due to under-represented fractures closely paralleling the tunnel orientation.

Crystal-Rich Lithophysal Zone (Tptrl)

Fracture intensity is generally similar in the North Ramp and South Ramp Tptrl fractures. Fracture orientations appear to be randomly dispersed in the North Ramp fractures, which may be due to the few number of fractures present. Fractures in the South Ramp fall into two clusters, with peak azimuths of 217° and 144°, roughly correlating to the Set 1 and Set 2 fractures described in the Main Drift.

Crystal-Poor Upper Lithophysal Zone (Tptpul)

Fracture intensity is consistently low in the North Ramp and South Ramp Tptpul fractures. Fracture orientations are randomly dispersed over almost a 180° range in both occurrences, however the North Ramp has a peak azimuth at about 182°, while the South Ramp has a peak azimuth at 145°.

The highest concentration of fracture orientations in the North Ramp are a north-south trending set not observed in the Main Drift or the South Ramp. A secondary peak fracture orientation in the North Ramp correlates with the north-east trending Set 2 of the Main Drift and the South Ramp. A small concentration of fracture orientations in the North Ramp correlates to the Set 1 fractures of the Main Drift and the South Ramp. In this interval within the North Ramp, these Set 1 fractures first develop as an identifiable set. This set appears within the Tptpul from approximately Sta. 22+00 and on. This represents the lower portion of the Tptpul exposed in the North Ramp. There are several possibilities for the appearance of this set. 1) The tunnel orientation shifts from the 299° of the North Ramp to the 183° of the Main Drift. This rotates the "blind zone" away from a range which may obscure any appearance of this set. 2) The Set 1

orientations observed in the Main Drift and the South Ramp may be due to a structural change in fracturing across the Drill Hole Wash area which cuts through this interval of Tptpul exposed in the ESF. 3) The Set 1 fracturing may extend up from the Tptpmn in the Main Drift into only the lower portion of the Tptpul.

Crystal-Poor Middle Nonlithophysal Zone (Tptpmn)

Fracture orientations in the South Ramp fall into three distinct sets (Sets 1, 2, and 3) with peak orientations of 137/81, 222/82, and a low angle set of 326/17. North Ramp orientations fall into two distinct sets (Sets 1 and 3) with peak orientations of 123/80, and 294/15. There is a small scattering of fractures with orientations possibly belonging to a north-south trending set.

Crystal-Poor Lower Lithophysal Zone (Tptpll)

The Tptpll is not exposed in the North Ramp, so a comparison is not possible.

Bedded Tuffs

The Bedded Tuffs in the South Ramp range in azimuth from 125° to 189° and range in dip from 42° to 90°. These show a north-westerly to north-south orientation. Bedded Tuffs in the North Ramp have a more north-easterly to north-south orientation with azimuths ranging from 149° to 239° and dips ranging from 47° to 90°. Bias due to the tunnel orientation does not appear to explain this variation.

Tiva Canyon Tuff

The South Ramp Tiva Canyon Tuff fractures are distributed widely over an azimuth range of roughly 103° to 255° with several possible peaks observed visually in this set. Statistical cluster analysis does not break these out into significant sets, and these peaks do not appear to correlate

to any fracture pattern observed elsewhere in the ESF. In the North Ramp fractures within the Tiva Canyon Tuff, peaks occur in the distribution of fracture orientations which possibly correlate to those seen in the Topopah Spring Tuff in the North and South Ramps. The predominant set is a north-south trending set which is observed in many of the North Ramp units. A secondary set is Set 2, a north-east trending set observed in the Main Drift and the South Ramp. A third small peak is observed in an orientation which may correlate with Set 1, a north-west trending set observed in the Main Drift and the South Ramp.

Regional Implications

Study of the North Ramp DLS data shows the presence of a north-south trending set throughout much of the North Ramp. This set disappears from the DLS data at approximately Sta. 26+00 to 28+00. The north-west trending set referred to as Set 1 in the Main Drift Report (Albin and others, 1997) and in this report is not clearly present in the North Ramp until approximately Sta. 22+00. This fundamental change in fracture orientations occurs beneath the Drill Hole Wash area, and surface features also demonstrate a possible change in fracture character. Set 1 orientations in the Main Drift rotate from an approximate azimuth of 110° to 140° from north to south (Albin and others, 1997). The South Ramp Set 1 orientations correlate with the orientations observed in the southern portion of the Main Drift. The North Ramp Set 1 orientations which do not appear to be present before approximately Sta. 22+00 correlate with the more west-north-westerly orientations observed in the north part of the Main Drift. This supports a regional rotation of this fracture set from north to south, and possibly constrained to the south-west of the Drill Hole Wash area.

GEOTECHNICAL CHARACTERIZATION

Introduction

The purpose of this report is to summarize the results of rock mass rating data collected during excavation of the South Ramp in the ESF from Sta. 55+00 to 78+77. These data may be used as part of the overall assessment of the stability of current and proposed underground excavations at Yucca Mountain. Data were collected for two empirical rock mass classification systems: the Norwegian Geotechnical Institute (Q system), and the Rock Mass Rating (RMR), system. These rock mass classification systems were developed in response to the demand for numerical design tools. Bieniawski (1989) lists the benefits of rock mass classification:

- improve the quality of site investigations by recognizing parameters important to the geotechnical classification of the rock mass.
- provide quantitative information for design purposes.
- enable better engineering judgment and achieve a common standard for more effective communication.

Kirkaldie (1987) suggests that the rock material field classification procedure consists of two primary steps: the classification process and the performance assessment. The classification process includes (1) the identification of the *rock unit* and (2) the description of the rock in terms of *classification elements*. Classification elements describe the physical properties of the rock units that are most relevant to engineering activities. These elements include rock material, rock mass, and geohydrologic properties of the rock units. This geotechnical characterization reports rock mass properties in terms of the classification elements of the Q and RMR systems. Data presented in other sections of the South Ramp Report may be used for geohydrologic modeling; however, this section of the report includes rock material and rock mass, but does not specifically present geohydrologic information. Performance assessment of the rock mass is not a part of the South Ramp Report.

Performance assessment includes erosion resistance, construction quality, fluid transmission, and

long-term rock mass stability.

The data presented here:

- describes rock mass properties for each thermal-mechanical unit
- compares the installed ground support with that predicted using rock mass classification systems

Methodology

The data base used for this report is a summary of observations and data collected and documented under a technical procedure titled *Rock Mass Classification* (U.S. Bureau of Reclamation and U.S. Geological Survey, 1997). Descriptions of the rock mass are based on two empirical rock mass classification systems: the Norwegian Geotechnical Institute Q rock quality system (Barton and others, 1974) and the Geomechanics Rock Mass Rating or RMR system (Bieniawski, 1989). Ratings are assigned to a five meter interval of tunnel using both rock classification systems.

The use of this relatively short rating interval may have the disadvantage of introducing variations in some evaluated parameters which may be expected to be stable; yet it has the advantage of capturing variations in more unstable parameters. For example, considering the Q system, one might assume the number of joint sets would be constant over a long interval of tunnel. Using a five meter rating interval permits evaluation of the actual occurrence of a particular joint set within the rating interval; therefore the rating value for the number of joint sets may vary within a ten meter interval of tunnel. On the other hand, the five meter rating interval permits a description of the changes in fracture frequency represented by RQD. Overall, the five meter rating interval emphasizes changes in rock quality from one interval to the next. When longer intervals of the tunnel or various stratigraphic units are compared, differences in the trends of the five meter ratings and differences in the average ratings are meaningful.

Thermal-Mechanical Units in the South Ramp

The rock material at Yucca Mountain have been grouped into thermal-mechanical units which exhibit similar physical and mechanical properties. The South Ramp passes through four such units; TSw2, TSw1, PTn, and TCw. Table 5 lists the locations of the thermal-mechanical units encountered in the South Ramp. The stratigraphic units included in each thermal-mechanical unit are also shown in the table.

MECHANICAL UNIT	STRATIGRAPHY	STATIONS	LENGTH IN METERS
TSw2	Tptpmn, Tptpll	55+00 → 63+10	810
TSw1	Tptpul, Tptrl, Tptrn	63+10 → 66+30	320
PTn	Tptrv, Tpbt, Tpcpv	66+30 → 67+25	95
TCw	Tpcpln	67+25 → 67+60	35
PTn	Tpcpv	67+60 → 67+70	10
TCw	Tpcpln	67+70 → 67+90	20
TSw1	Tptpul, Tptrl, Tptrn	67+90 → 69+90	200
PTn	Tptrv, Tpbt	69+90 → 70+55	65
TSw2	Tptpmn	70+55 → 71+70	115
TSw1	Tptpul, Tptrl, Tptrn	71+70 → 74+40	270
PTn	Tptrv, Tpbt, Tpcpv	74+40 → 75+15	75
TCw	Tpcpln, Tpcpmn, Tpcpul	75+15 → 78+77	362

Table 5: South Ramp Thermal-Mechanical Units

Rock Mass Classification Data

The following sections describe data collected in the South Ramp for the Q and RMR systems.

While RQD alone is not considered to be an adequate classification system, RQD is a parameter in both the Q and RMR systems so Rock Quality Designation data are reviewed in the same detail as the Q and RMR data.

Rock Quality Designation (RQD)

The rock quality designation (RQD) index is a rating parameter of both the Q and RMR systems for drill core. It was introduced over 20 years ago as a quantitative measure of rock quality (Deere, 1989). The total length of core pieces which are 4 inches (about 10 cm) and longer is divided by the length of the core run. RQD is calculated as follows:

$$RQD\ \% = \frac{\sum \text{Length of Core Pieces} > 10\ \text{cm}}{\text{Interval Length}} * 100$$

Following is the sequence for calculating RQD from observation of the tunnel wall. Intervals of intact rock adjacent to the DLS tape are estimated or calculated as the percentage of core pieces 10 centimeters or longer which would be recovered in an imaginary horizontal drill hole along the right wall of the excavation. The fundamental assumption for RQD calculation with the DLS data is that the interval of rock between recorded fractures is intact rock. From that assumption, the total of intact rock pieces longer than 10 cm are determined from the fracture spacing. That interval, expressed as a percentage of the total length, is the line survey RQD. Where RQD within a 5 meter section is less than or equal to a rating of 10 or less (including 0), a nominal value of 10 is assigned to the interval. Table 6 below shows the qualitative description associated with ranges of RQD percentages.

In areas supported by steel sets, an accurate station for fractures behind the sets cannot be recorded. Where fracturing on either side of the steel sets suggests fracturing behind the steel sets, an estimated station for the inferred fractures is recorded and RQD is calculated using these

fractures.

RQD Ranges	Rock Quality Description
< 25%	Very Poor
25% - 50%	Poor
51% - 75%	Fair
76% - 90%	Good
91% - 100%	Excellent

Table 6: RQD Percentages and Descriptions

Lithophysae encountered in core drilling samples produce a interval of drill hole with no core recovery. Similarly, lithophysal zones are treated as void spaces and therefore excluded from the theoretical length of intact rock. This procedure of "zeroing out" lithophysal cavities reduces the computed RQD. The rock mass with a high concentration of lithophysal cavities is not characterized well by the empirical systems.

Summary of RQD in the South Ramp

Table 7 below summarizes the RQD values encountered in each of the thermal-mechanical units in the South Ramp of the ESF.

Mechanical Units	Stratigraphy	Stations	Meters Rated	RQD Mean	RQD Median	RQD Range
TSw2		55+00 → 63+10	810	52	53	10-99
	Tptpmn	55+00 → 57+30 58+80 → 63+10	230 430	59	58	10-99
	Tptpll	57+30 → 58+80	150	24	21	10-54
TSw2		70+55 → 71+70	80	60	61	38-70
	Tptpmn	70+55 → 71+70 71+10 → 71+45	80 35	60 NR	61 NR	38-70 NR

Mechanical Units	Stratigraphy	Stations	Meters Rated	RQD Mean	RQD Median	RQD Range
TSw1		63+10 → 66+30	320	64	71	19-100
	Tptpul	63+10 → 64+55	145	51	45	21-82
	Tptrl	64+55 → 65+05 65+25 → 65+30	50 5	47	50	19-73
	Tptrn	65+05 → 65+25 65+30 → 66+30	20 100	88	90	56-100
TSw1		67+90 → 69+90	200	65	74	23-98
	Tptpul	67+90 → 68+50	60	39	37	23-77
	Tptrl	68+50 → 68+85	35	64	67	40-96
	Tptrn	68+85 → 69+90	105	81	80	51-98
TSw1		71+70 → 74+40	270	57	57	10-100
	Tptpul	71+70 → 73+00	130	35	32	10-70
	Tptrl	73+00 → 73+40	40	54	55	38-68
	Tptrn	73+40 → 74+40	100	86	91	58-100
PTn		66+30 ≈ 67+70	30	95	96	92-100
	Tptrv	66+30 → 66+45	15	95	95	95-96
	Tpbt	66+45 → 66+80	35	NR	NR	NR
	Tpcpv	66+80 → 67+20 67+20 → 67+25 67+60 → 67+70	40 5 10	NR 100 95	NR 100 95	NR 100 92-97
TCw		67+25 ≈ 67+90	55	83	87	42-100
	Tpcpln	67+25 → 67+60 67+70 → 67+90	35 20	83	87	42-100
PTn		69+90 → 70+55	15	79	82	59-96
	Tptrv	69+90 → 70+05	15	79	82	59-96
	Tpbt	70+05 → 70+55	50	NR	NR	NR
PTn		74+40 → 75+15	5	77	77	77-77

Mechanical Units	Stratigraphy	Stations	Meters Rated	RQD Mean	RQD Median	RQD Range
	Tptrv	74+40 → 74+50	10	NR	NR	NR
	Tpbt	74+50 → 74+95	45	NR	NR	NR
	Tpcpv	74+95 → 75+10 75+10 → 75+15	15 5	NR 77	NR 77	NR 77
TCw		75+15 → 78+77	362	71	72	37-95
	Tpcpln	75+15 → 76+05	90	79	85	52-95
	Tpcpmn	76+05 → 78+40	235	69	74	37-95
	Tpcpul	78+40 → 78+77	37	61	68	39-72

Table 7. Summary RQD Ratings in the South Ramp

Figure 20 shows the RQD through the entire South Ramp. Figures 21 through 24 portray the distribution of RQD values for each of the four thermal-mechanical units identified within the South Ramp.

RQD in TSw2: Unit TSw2 is encountered twice within the South Ramp. The first occurrence is 810 meters from Sta. 55+00 - 63+10 and includes the stratigraphic units Tptpmn and Tptpll. The second interval is 115 meters and contains only Tptpmn. Both sections of Tptpmn have significantly higher RQD values than the Tptpll. The Tptpmn zone is characterized with only 0-3 percent lithophysae, where-as the Tptpll is generally composed of from 15-25 percent lithophysae. Lithophysal cavities within the Tptpll are not counted as intact rock, so the RQD value for Tptpll includes reduction for both void spaces and closely spaced fractures.

Between Sta. 55+00 and 63+10 the average RQD rating of 52 represents the rating of a *fair* quality rock, with the Tptpmn being reduced by the rating of the *poor* quality Tptpll. RQD in the TSw2 is best represented by

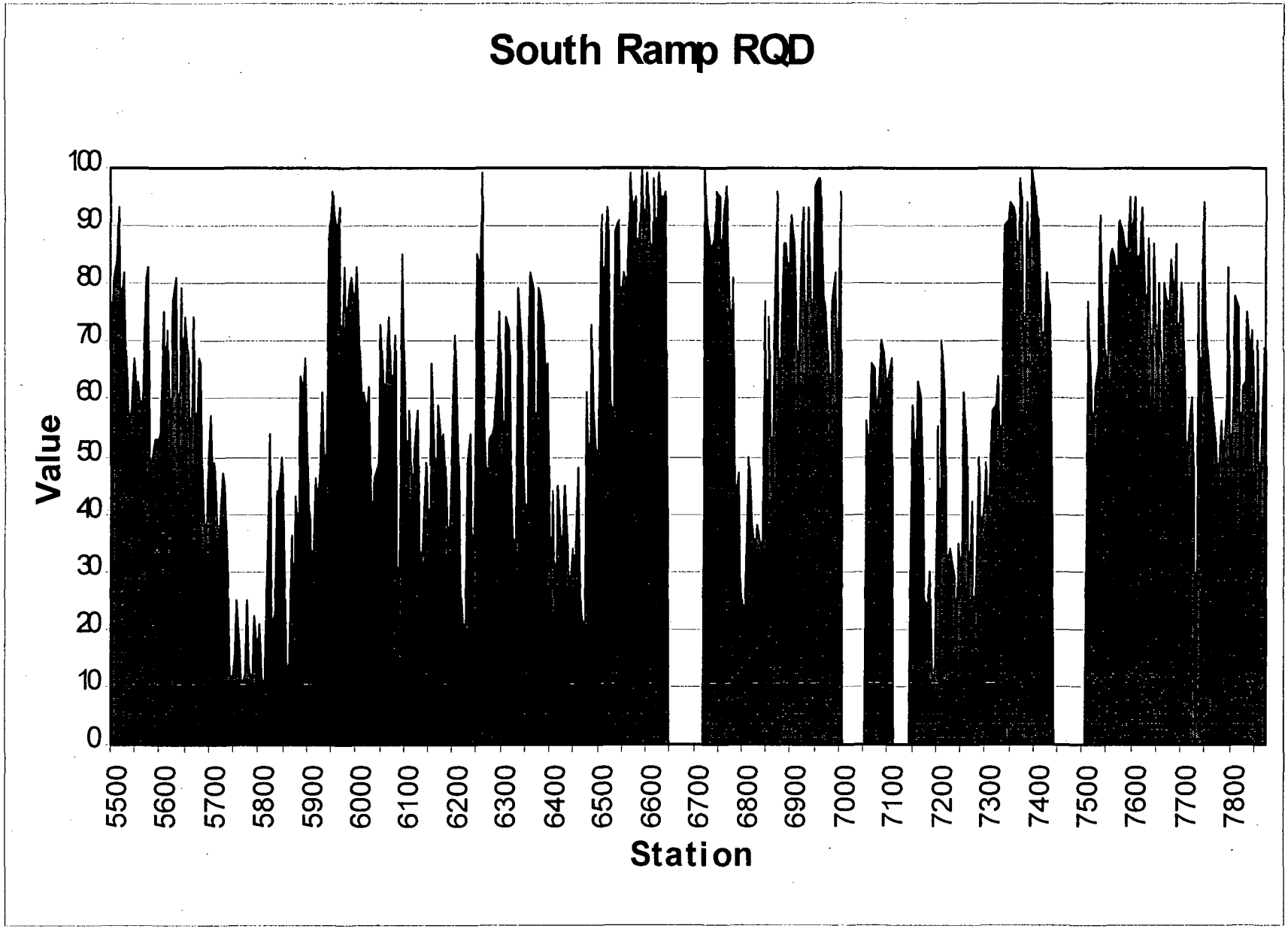

Figure 20: South Ramp RQD

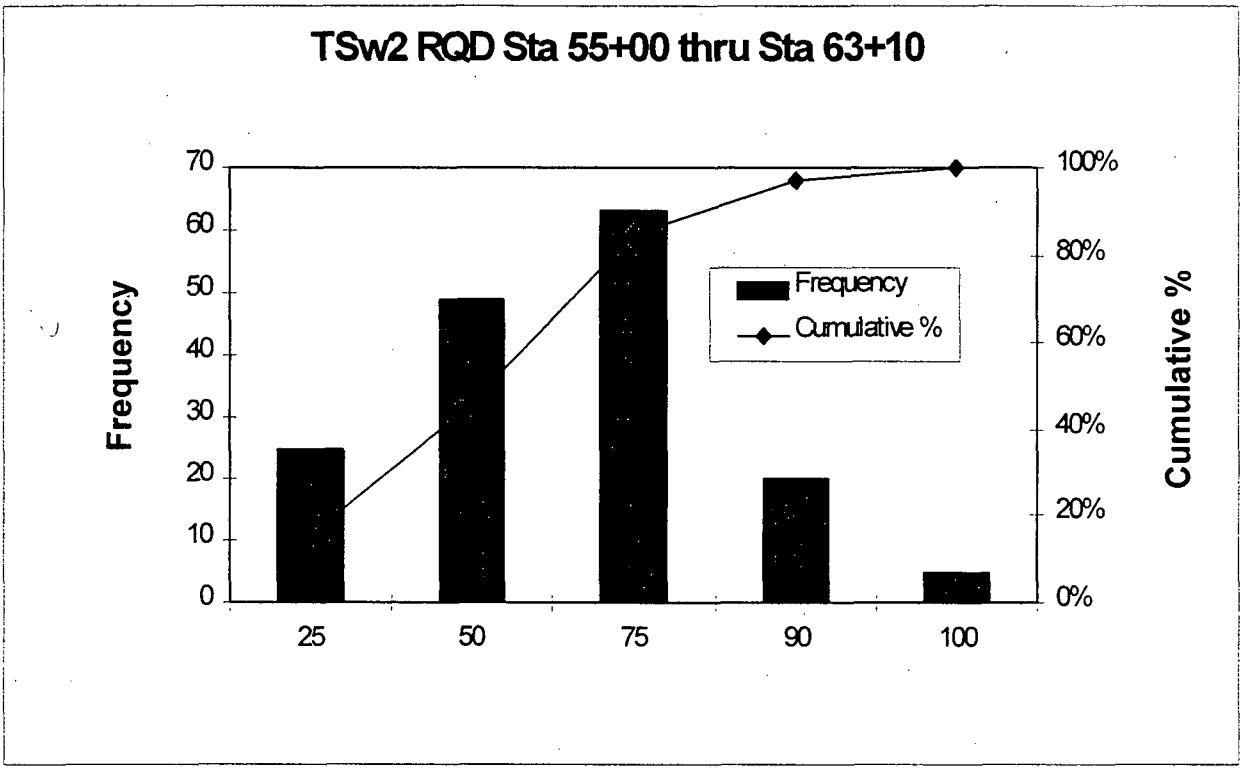

Figure 21a: Distribution of RQD in TSw2 (Sta 55+00 - 63+10)

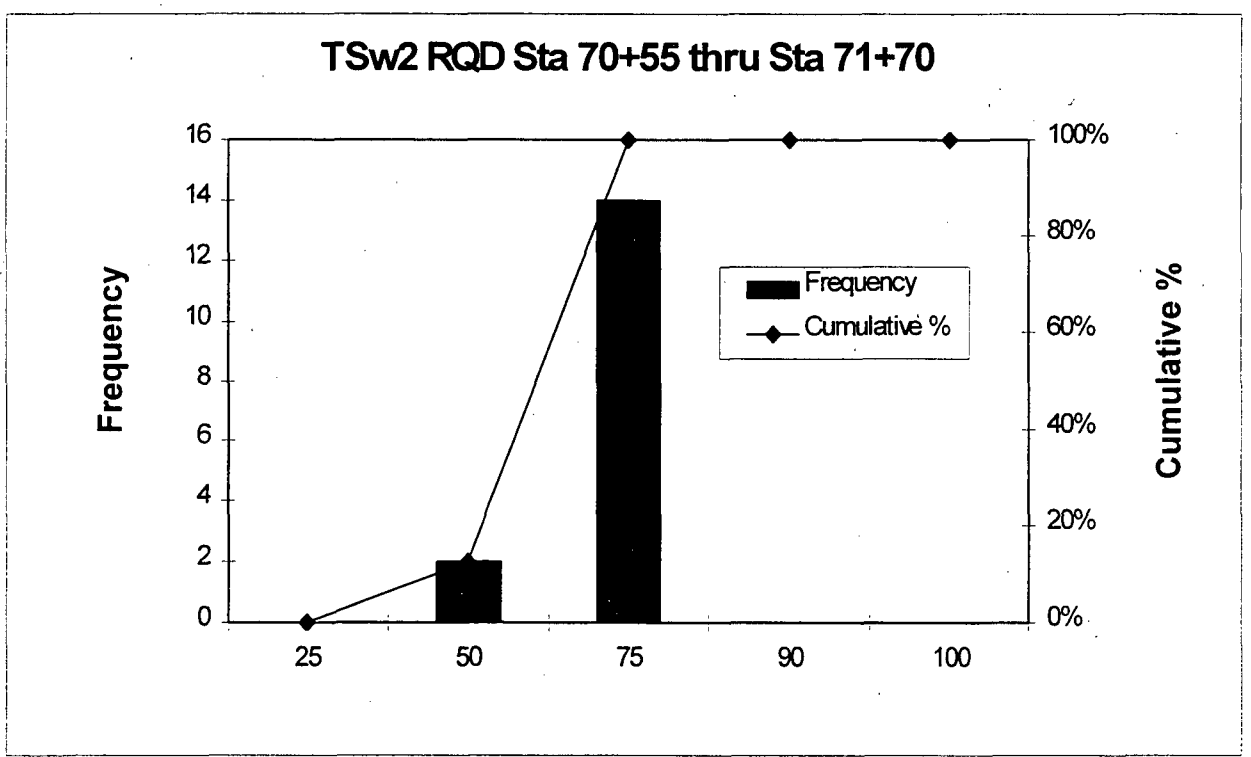

Figure 21b: Distribution of RQD in TSw2 (Sta 70+55 - 71+70)

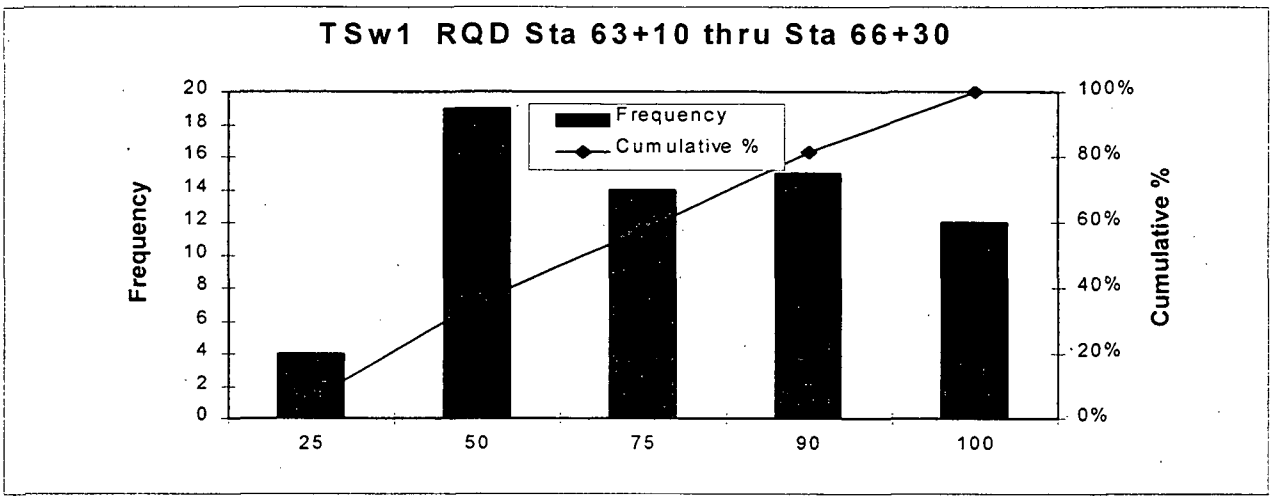

Figure 22a: Distribution of RQD in TSw1 (Sta 63+10 - 66+30)

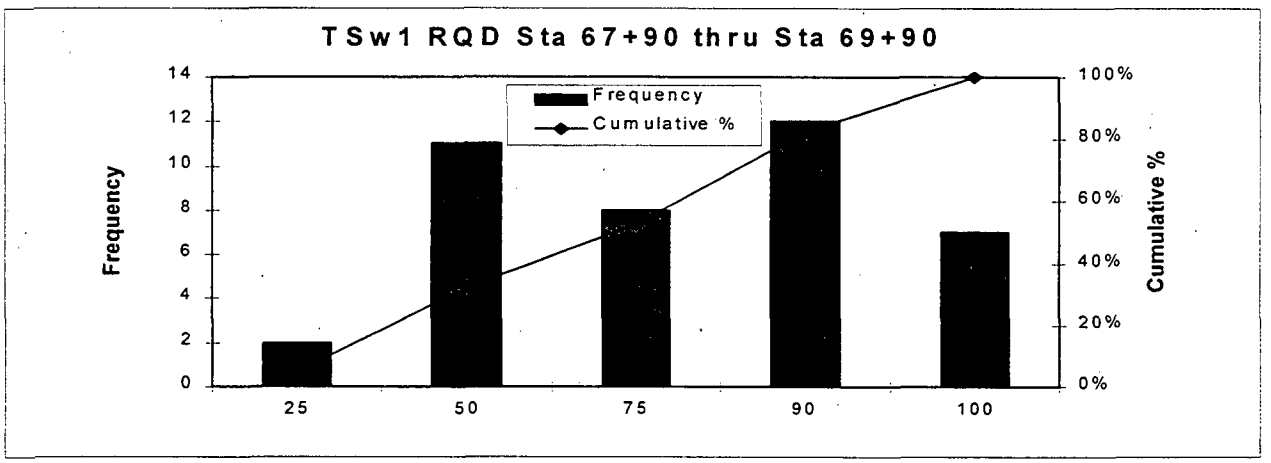

Figure 22b: Distribution of RQD in TSw1 (Sta 67+90 - 69+90)

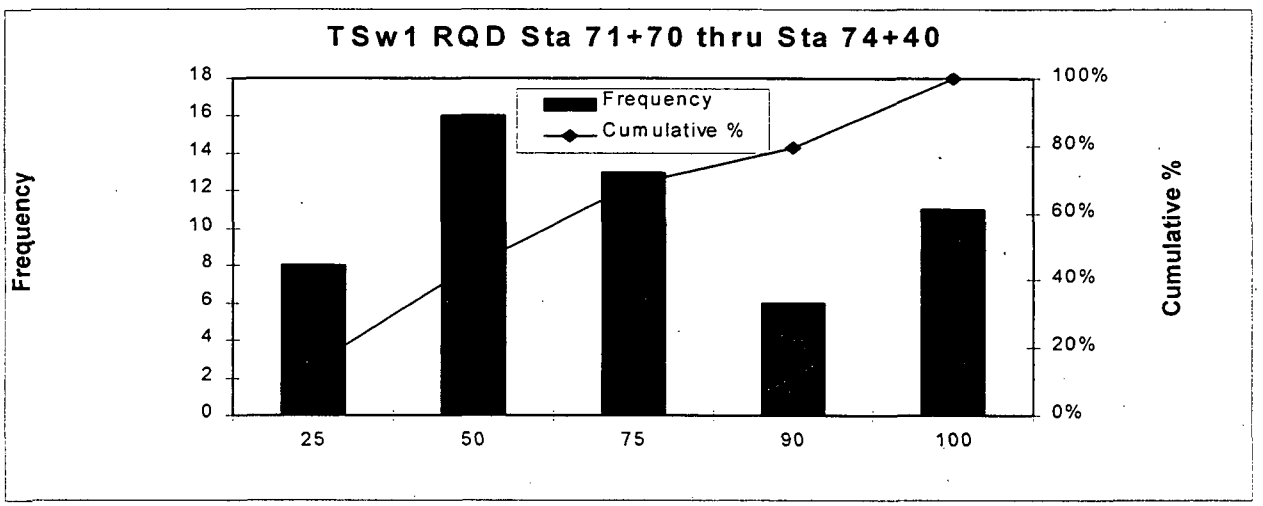

Figure 22c: Distribution of RQD in TSw1 (Sta 71+70 - 74+40)

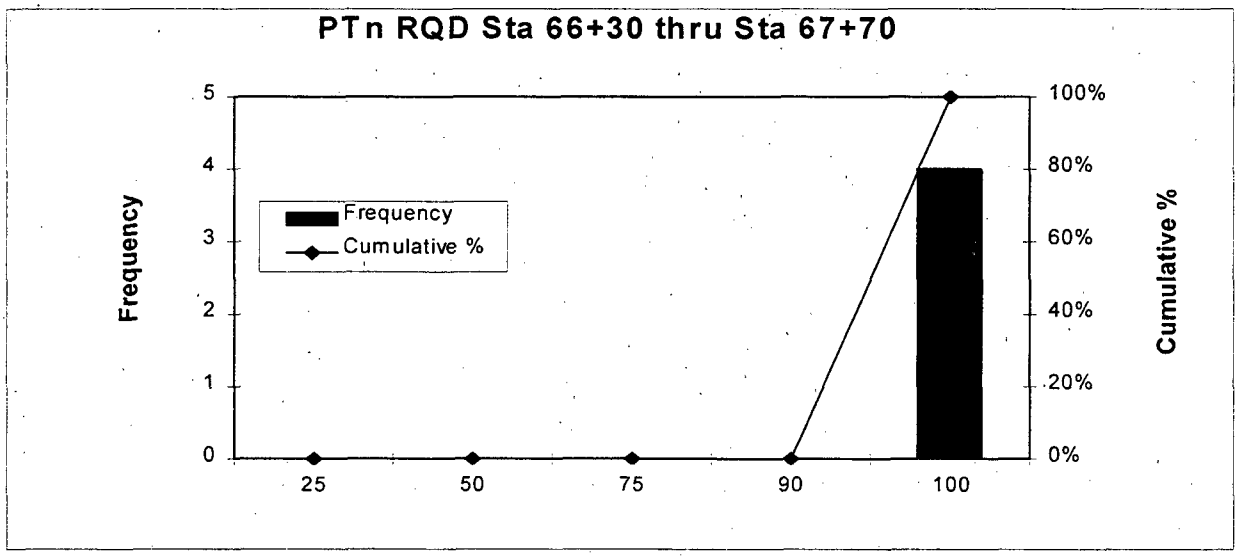

Figure 23a: Distribution of RQD in PTn (Sta 66+30 - 67+70)

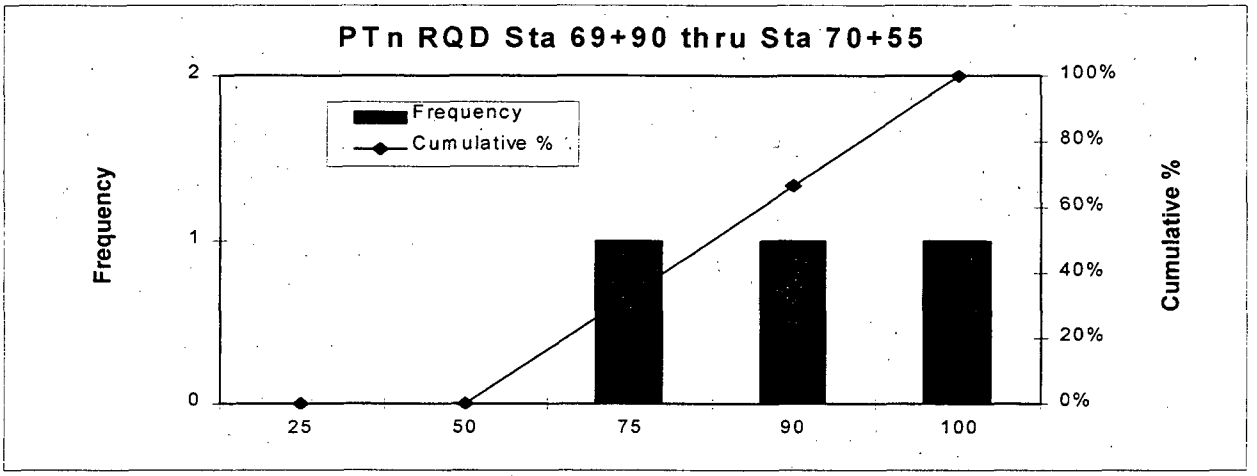

Figure 23b: Distribution of RQD in PTn (Sta 69+90 - 70+55)

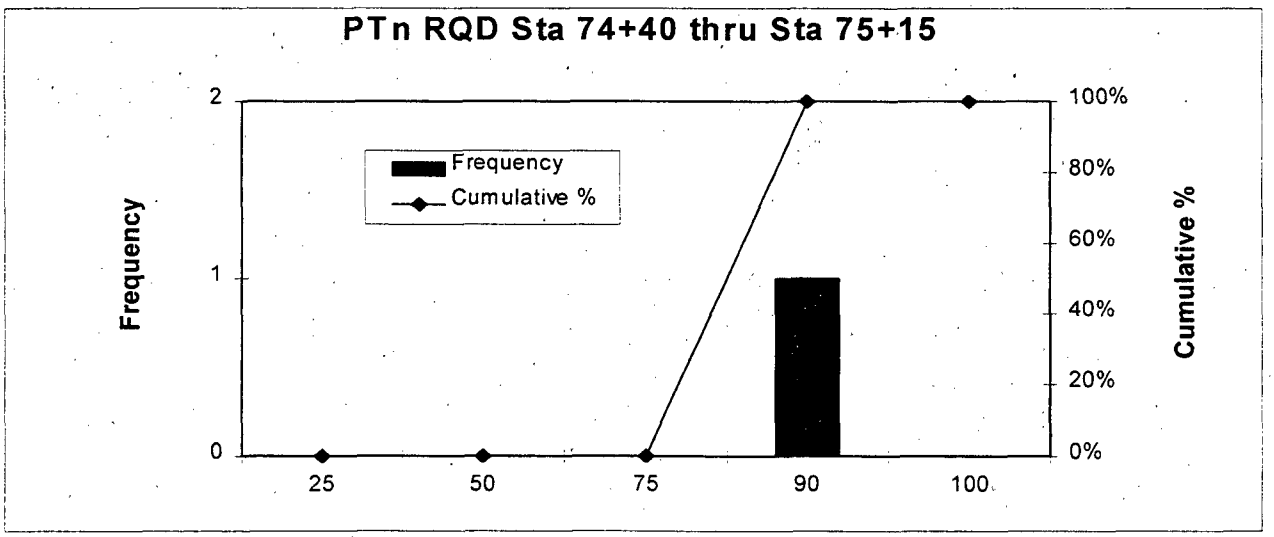

Figure 23c: Distribution of RQD in PTn (Sta 74+40 - 75+50)

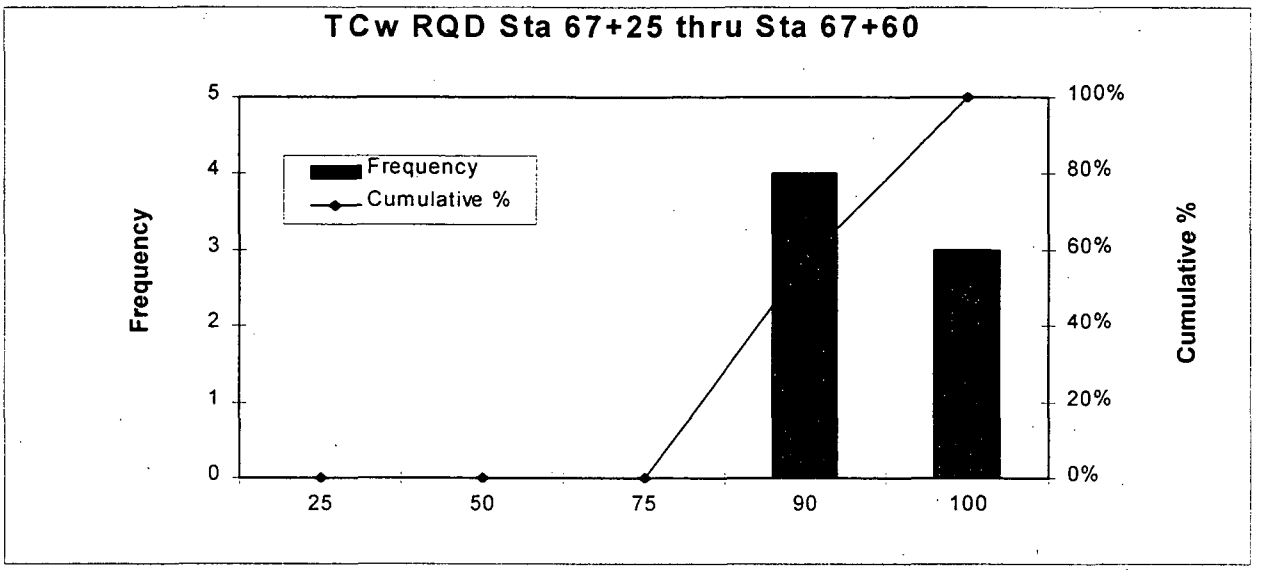

Figure 24a: Distribution of RQD in TCw (Sta 67+25 - 67+60)

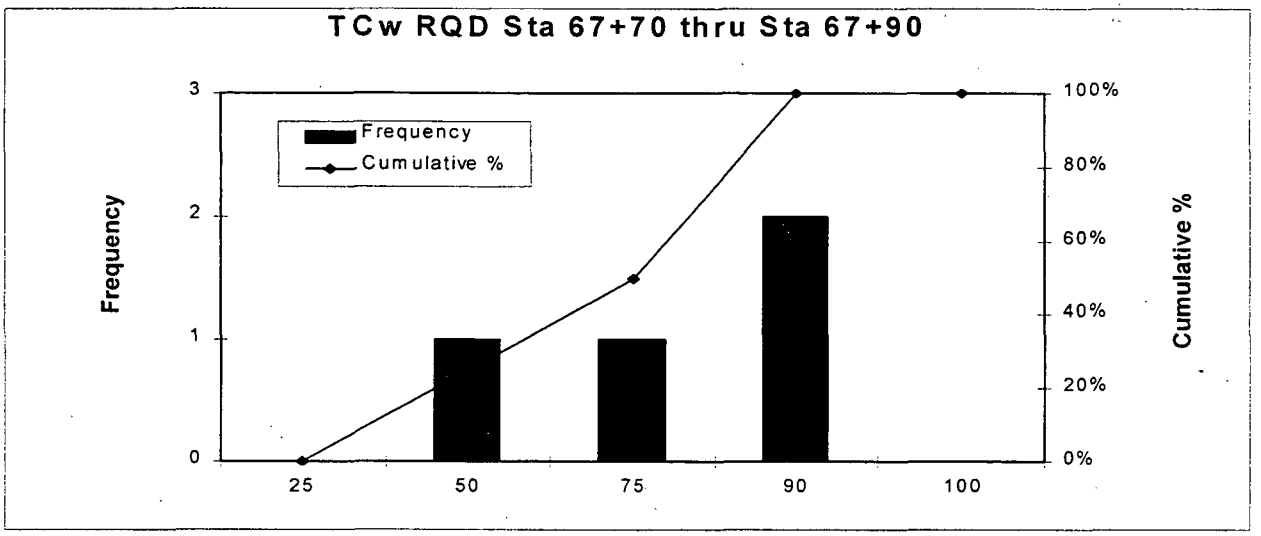

Figure 24b: Distribution of RQD in TCw (Sta 67+70 - 67+90)

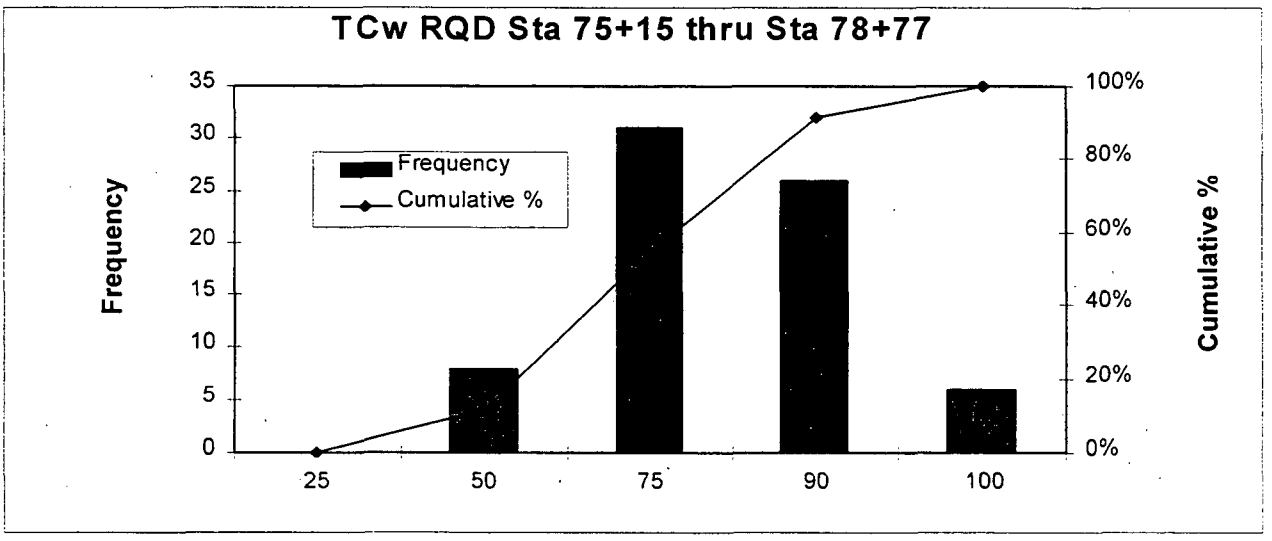

Figure 24c: Distribution of RQD in TCw (Sta 75+15 - 78+77)

two values:

- For Tptpmn the average RQD is nearly 60 percent describing a *fair* quality rock.
- For Tptpll the average RQD of 24 percent describes a rock quality on the borderline of *very poor* to *poor*.

Figure 21 shows the distribution of RQD ratings in TSw2 undifferentiated by stratigraphic unit. Note that Figure 21b shows the distribution of RQD for the rated sections as if all sections were rated a *fair* quality rock. Unstated in the figure is that only 80 of 115 meters are rated, due to extensive lagging and shotcrete over 35 meters.

RQD in TSw1: TSw1 occurs in 790 meters of the South Ramp. This interval includes stratigraphic units of Tptpul, Tptrl, and Tptrn. The lithophysal units, Tptpul and Tptrl have lower RQD's than the non lithophysal Tptrn. Table 7 shows that the three intervals of Tptrn all have average RQD values above 80, indicating a *good* quality rock. Figure 22 plots the distribution of RQD values for the intervals of TSw1. Without segregating the stratigraphic units the figures imply a nearly uniform distribution of RQD between 25 and 100. Again, the distribution of *poor* quality rock is defined by stratigraphic units. Tptpul with an overall mean RQD of 43 percent and Tptrl with an overall mean RQD of 54 percent both rate on the *poor* to *fair* borderline. Tptrn with an overall mean RQD of 85 percent rates as a *good* quality rock.

RQD in PTn: There are 245 meters of PTn within the South Ramp, 195 meters are unrated. In some of the PTn units, actual RQD based on drill core may vary significantly from that calculated for this report. The method of RQD calculation cannot describe the reaction of the rock to actual core drilling. Recognizing mechanical damage is to be discounted, the act of drilling

may actually break the core on natural weaknesses in the rock which are not observable. Figure 23a suggests a RQD rating of *good*, but only 30 meters of the 105 meters from Sta. 66+30 to 67+70 is actually rated. Figure 23b has only 15 meters of ratings, so, the high RQD values aren't statistically representative. Figure 23c, from Sta. 74+40 to 75+15, only 5 meters of a possible 75 meters were rated. There is no best interval which represents the overall RQD ratings within the PTn. A more detailed discussion on non-rated (NR) areas is presented later within this report.

RQD inTCw: This unit consists of 55 total meters slivered in between the PTn from Sta. 66+30 to 67+90. Additionally, the South Ramp ends in this unit, from Sta. 75+15 to 78+77, for a total of 362 meters. All the sections within the TCw are rateable material, with the exception of 5 meters covered with shotcrete and lagging. The 55 meters of Tpcpln in Figures 24a and 24b suggest a rating of 83 *good* . Figure 24c is comprised of Tpcpln, *good*; Tpcpmn, *fair*; and Tpcpul, *fair*. Note that the lithophysae-riddled Tpcul rates from 10-20 percent lower than the other two stratigraphic units.

Rock Mass Rating (RMR)

The RMR system, also known as the Geomechanics Classification, is an empirical rating system based on the sum of six rock mass parameters. Bieniawski (1989) developed this system in 1973 and, with the addition of case histories, revised it to its present form. The numerical rock mass rating, RMR, is calculated according to the following equation:

$$\mathbf{RMR = C + RQD + Js + Jcd + JwR + AJO}$$

where

C is a numerical index associated with the intact-rock compressive strength. The rock-wall compressive-strength rating is assigned using laboratory test data as a

reference and sounding the tunnel rib with a rock hammer. This procedure is not sensitive to changes in the numerical index in borderline cases.

RQD is a numerical index associated with the rock mass RQD from procedures previously discussed, (the index is not the actual RQD value). RQD is determined and a numerical index is assigned based on that RQD.

Js is a numerical index associated with the fracture spacing of a given joint set. The spacing of discontinuities is the mean distance between the planes of weakness in the rock mass in the direction perpendicular to the discontinuities.

Jcd is a numerical index associated with the condition of discontinuities. This parameter includes roughness of the discontinuity surfaces, their separation, length or continuity (persistence), weathering of the wall rock of the planes, and the infilling material. The joint condition most often is assigned by rating five individual parameters. The total of length, separation, roughness, joint filling, and weathering ratings yields a Jcd rating as shown below:

Jcd = CDl + CDs + CDr + CDf + Cdw

JwR is a numerical index dependent on groundwater or inflow conditions (the "R" is used to distinguish this rating from the Q system joint water rating).

AJO is a numerical index associated with the orientation of discontinuities. The rating of discontinuity orientations depends on the engineering application. Tunnels, slopes, and foundations use different rating values for joint orientations.

Table 8 below shows ratings for joint orientations in tunnels. Concentration is on unfavorable and very unfavorable conditions as this is significant for tunnel support.

Estimates of compressive strength, RQD, joint spacing, joint condition, groundwater and joint orientation parameters are gathered and calculated for each 5 meter interval. For this report, the

	Dip of Discontinuity (degrees)					
Orientation of joints with respect to tunnel axis and direction of tunnel excavation	0 - 20	20 - 45	45 - 90	Condition for tunneling	Category	AJO_{index}
Strike-versus-Tunnel axis / Drive-versus-Dip direction			normal / with	Very Favorable	AJO. 1	0
Strike-versus-Tunnel axis / Drive-versus-Dip direction		normal / with		Favorable	AJO. 2	-2
Strike-versus-Tunnel axis / Drive-versus-Dip direction	any / either	parallel / either	normal / against	Fair	AJO. 3	-5
Strike-versus-Tunnel axis / Drive-versus-Dip direction		normal / against		Unfavorable	AJO. 4	-10
Strike-versus-Tunnel axis / Drive-versus-Dip direction			parallel / either	Very Unfavorable	AJO. 5	-12

Table 8. RMR Index Values for Joint Orientation in Tunnels

joint set with the lowest total rating for spacing, joint condition, and orientation is used to calculate the RMR. Qualitative rock descriptions are associated with numerical RMR values in Table 9.

RMR	RMR Description
< 20	Very Poor
20 - 40	Poor
41 - 60	Fair
61 - 80	Good
81 - 100	Very Good

Table 9: RMR Values and Descriptions

Summary of RMR in the South Ramp

Most of the RMR ratings fall in the *fair* category. Table 10 summarizes the ratings of RMR throughout the South Ramp.

Mechanical Units	Stratigraphy	Stations	Meters Rated	RMR Mean	RMR Median	RMR Range
TSw2		55+00 → 63+10	810	54	56	32-73
	Tptpmn	55+00 → 57+30 58+80 → 63+10	230 430	56	56	39-73
	Tptpll	57+30 → 58+80	150	46	47	32-65
TSw2		70+55 → 71+70	80	54	54	44-63
	Tptpmn	70+55 → 71+70 71+10 →71+45	80 35	54 NR	54 NR	44-63 NR
TSw1		63+10 → 66+30	320	55	55	37-71
	Tptpul	63+10 → 64+55	145	50	48	37-63
	Tptrl	64+55 → 65+05 65+25 → 65+30	50 5	51	52	45-62
	Tptrn	65+05 → 65+25 65+30 → 66+30	20 100	64	67	48-71
TSw1		67+90 → 69+90	200	54	55	36-70
	Tptpul	67+90 → 68+50	60	45	44	36-54
	Tptrl	68+50 → 68+85	35	56	54	46-66
	Tptrn	68+85 → 69+90	105	59	59	46-70
TSw1		71+70 → 74+40	270	53	53	38-70
	Tptpul	71+70 → 73+00	130	48	48	38-61
	Tptrl	73+00 → 73+40	40	54	52	49-65
	Tptrn	73+40 → 74+40	100	59	59	46-70
PTn		66+30 ≈ 67+70	30	63	62	57-69

Mechanical Units	Stratigraphy	Stations	Meters Rated	RMR Mean	RMR Median	RMR Range
	Tptrv	66+30 → 66+45	15	63	68	62-69
	Tpbt	66+45 → 66+80	35	NR	NR	NR
	Tpcpv	66+80 → 67+20 67+20 → 67+25 67+60 → 67+70	40 5 10	NR 62 59	NR 62 59	NR 62-62 57-61
TCw		67+25 ≈ 67+90	55	57	61	28-67
	Tpcpln	67+25 → 67+60 67+70 → 67+90	35 20	57	61	28-67
PTn		69+90 → 70+55	15	59	58	58-62
	Tptrv	69+90 → 70+05	15	59	58	58-62
	Tpbt	70+05 → 70+55	50	NR	NR	NR
PTn		74+40 → 75+15	5	56	56	56-56
	Tptrv	74+40 → 74+50	10	NR	NR	NR
	Tpbt	74+50 → 74+95	45	NR	NR	NR
	Tpcpv	74+95 → 75+10 75+10 → 75+15	15 5	NR 56	NR 56	NR 56-56
TCw		75+15 → 78+77	362	61	61	49-73
	Tpcpln	75+15 → 76+05	90	60	60	49-67
	Tpcpmn	76+05 → 78+40	235	61	61	51-73
	Tpcpul	78+40 → 78+77	37	63	63	54-72

Table 10. Summary of RMR Ratings in the South Ramp

Figure 25 graphs the fluctuation in RMR for the entire South Ramp.

Figures 26 through 29 depict the distribution of RMR ratings for each of the four thermal-mechanical units in the South Ramp.

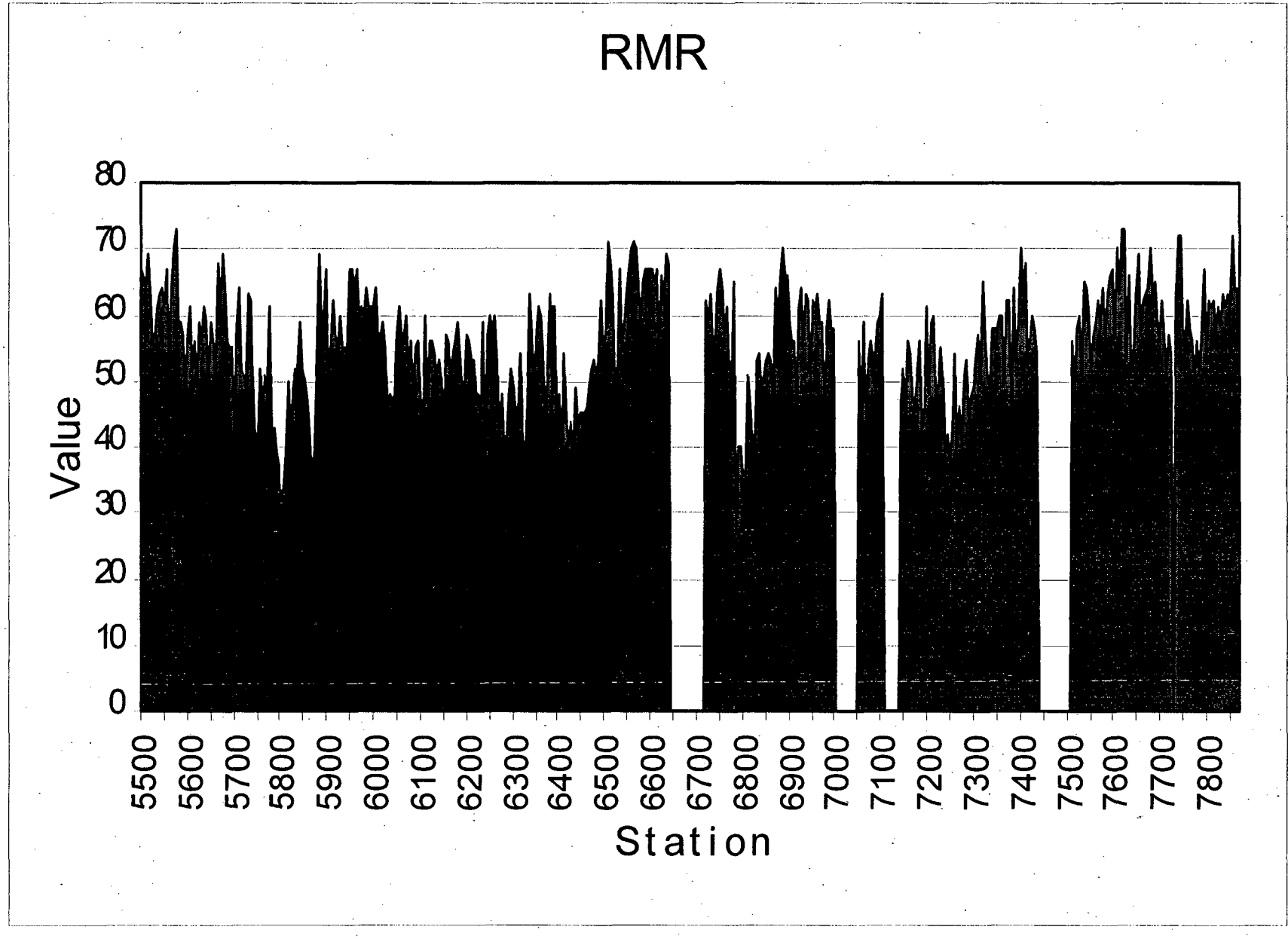

Figure 25: South Ramp RMR

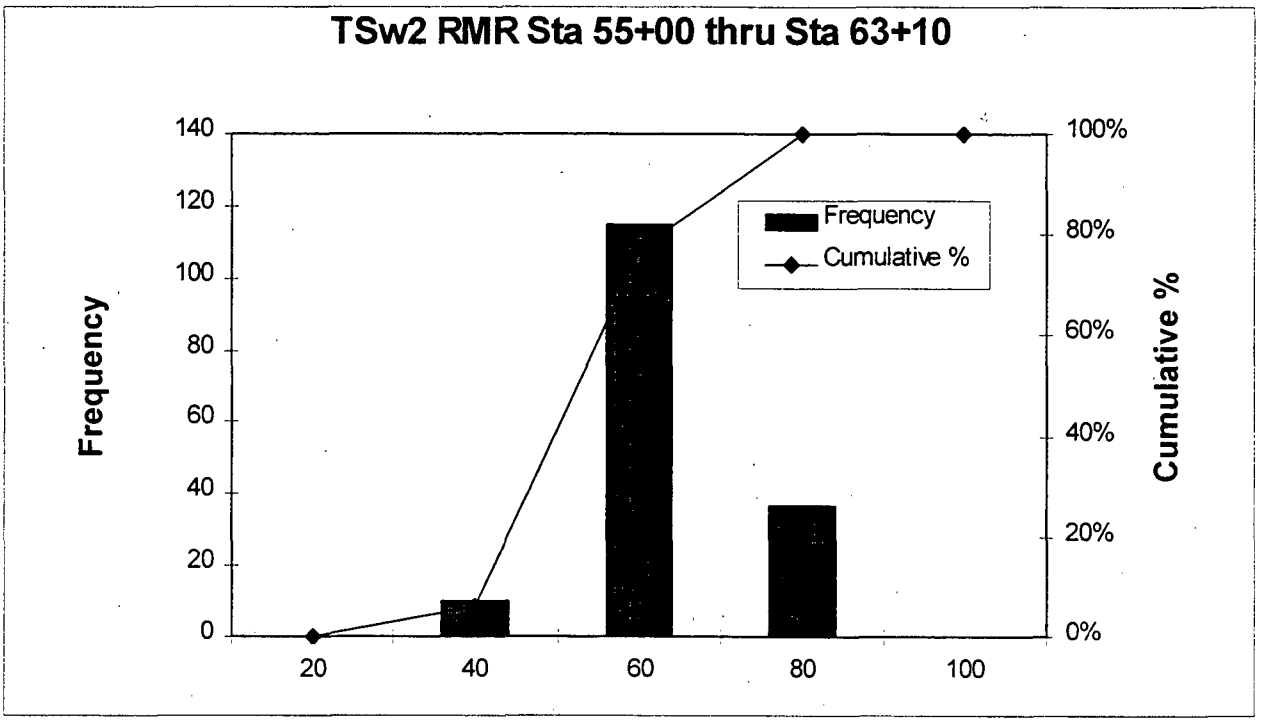

Figure 26a: Distribution of RMR in TSw2 (Sta 55+00 - 63+10)

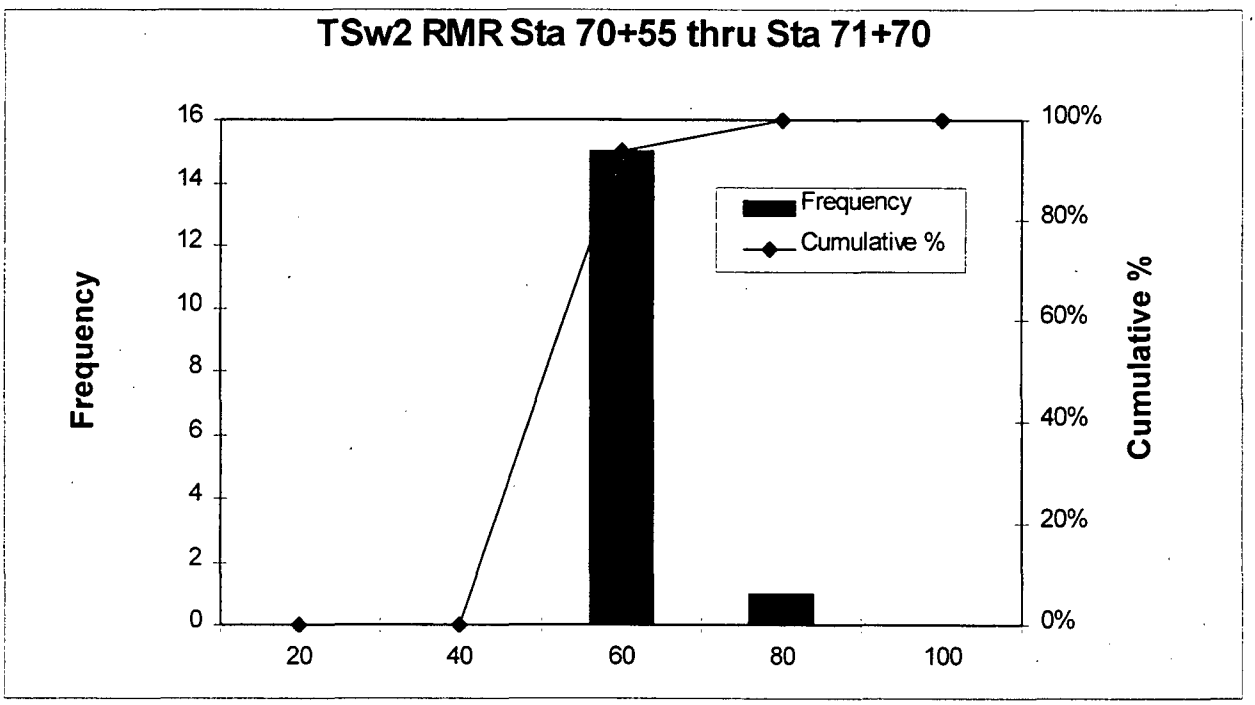

Figure 26b: Distribution of RMR in TSw2 (Sta 70+55 - 71+70)

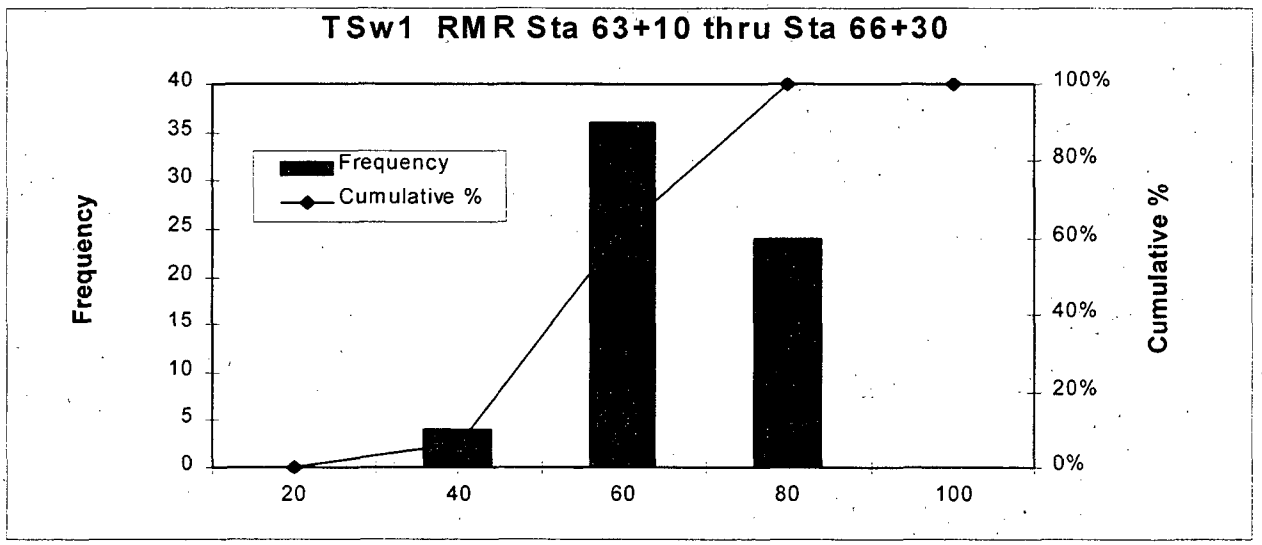

Figure 27a: Distribution of RMR in TSw1 (Sta 63+10 - 66+30)

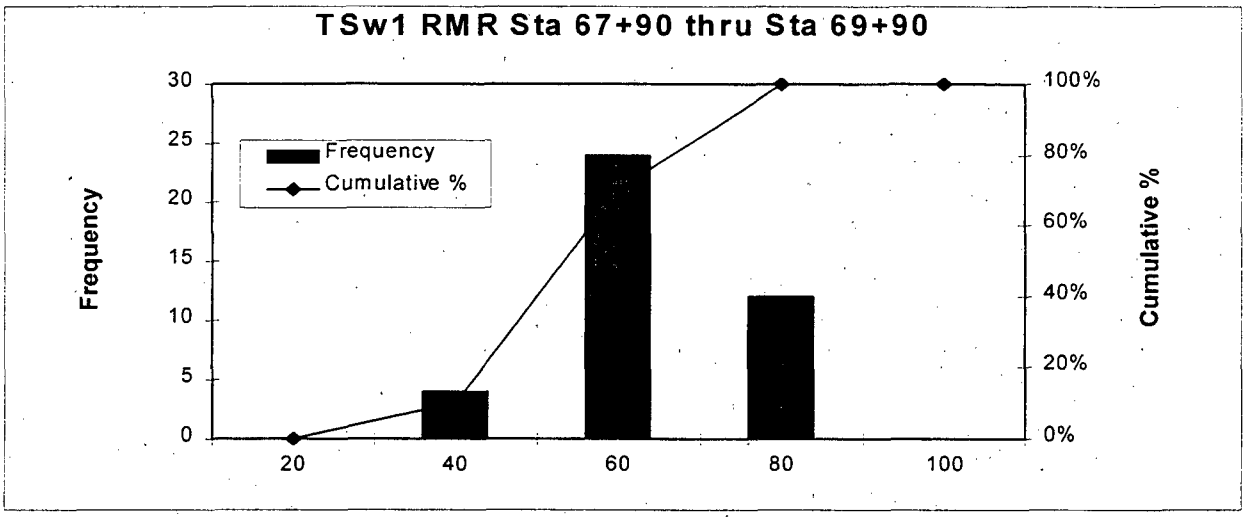

Figure 27b: Distribution of RMR in TSw1 (Sta 67+90 - 69+90)

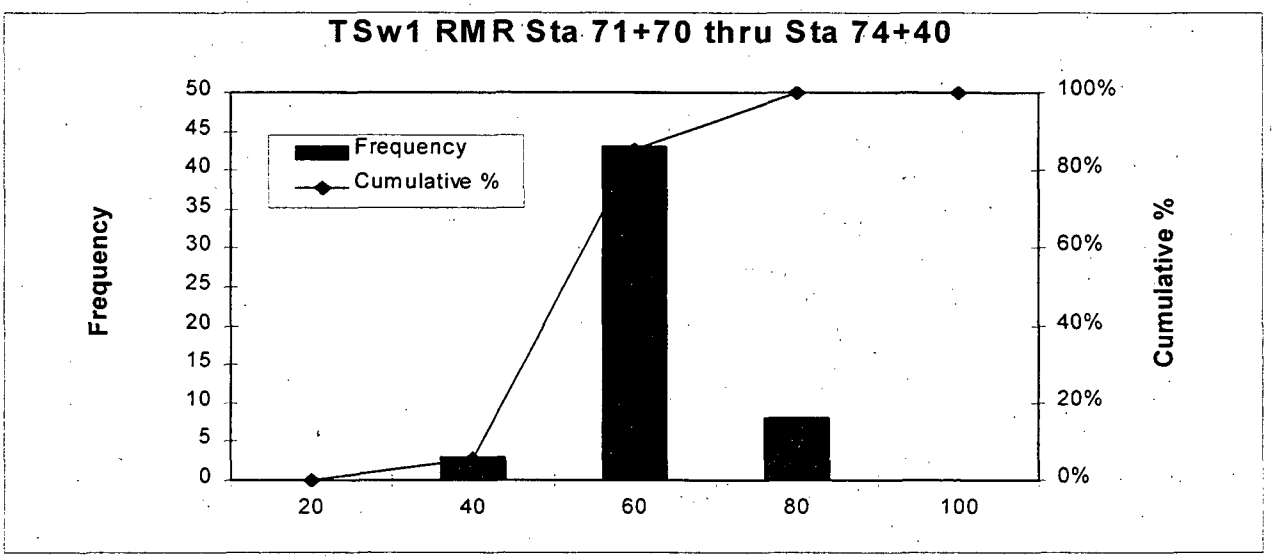

Figure 27c: Distribution of RMR in TSw1 (Sta 71+70 - 74+40)

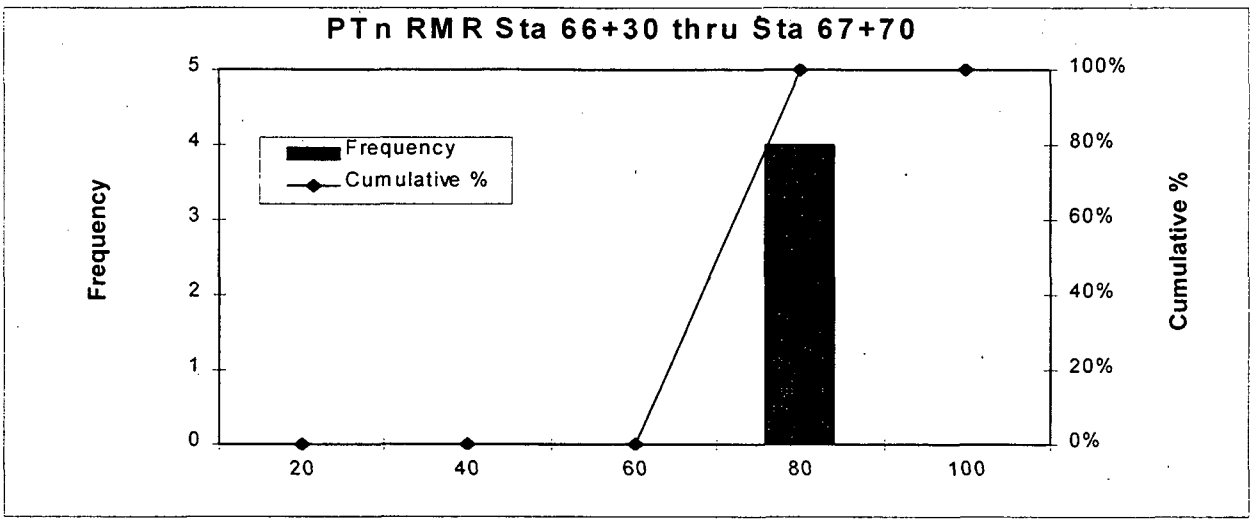

Figure 28a: Distribution of RMR in PTn (Sta 66+30 - 67+70)

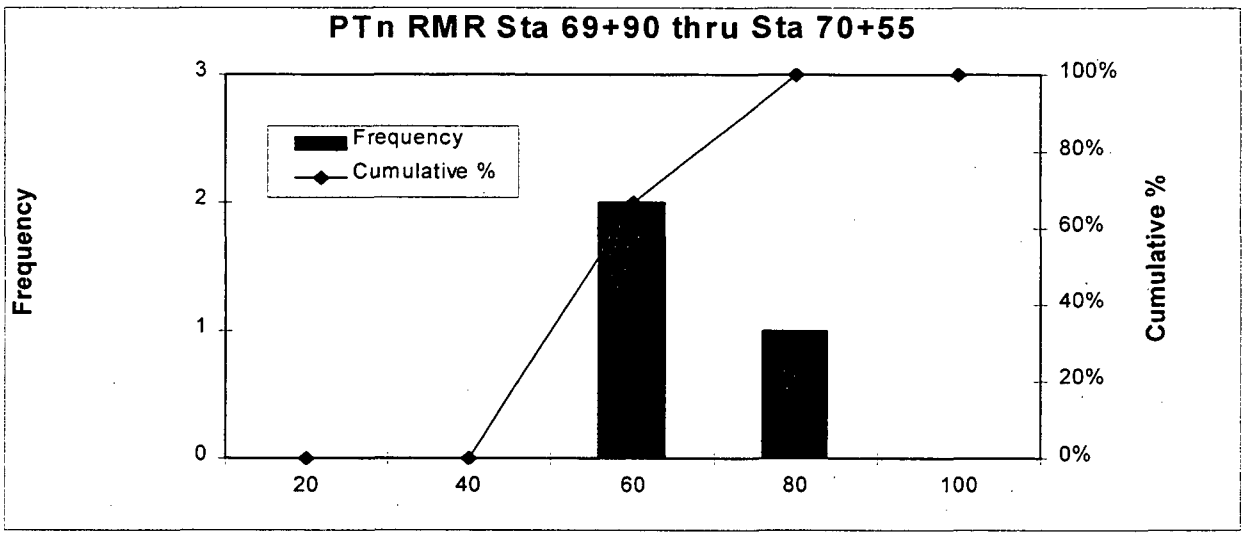

Figure 28b: Distribution of RMR in PTn (Sta 69+90 - 70+55)

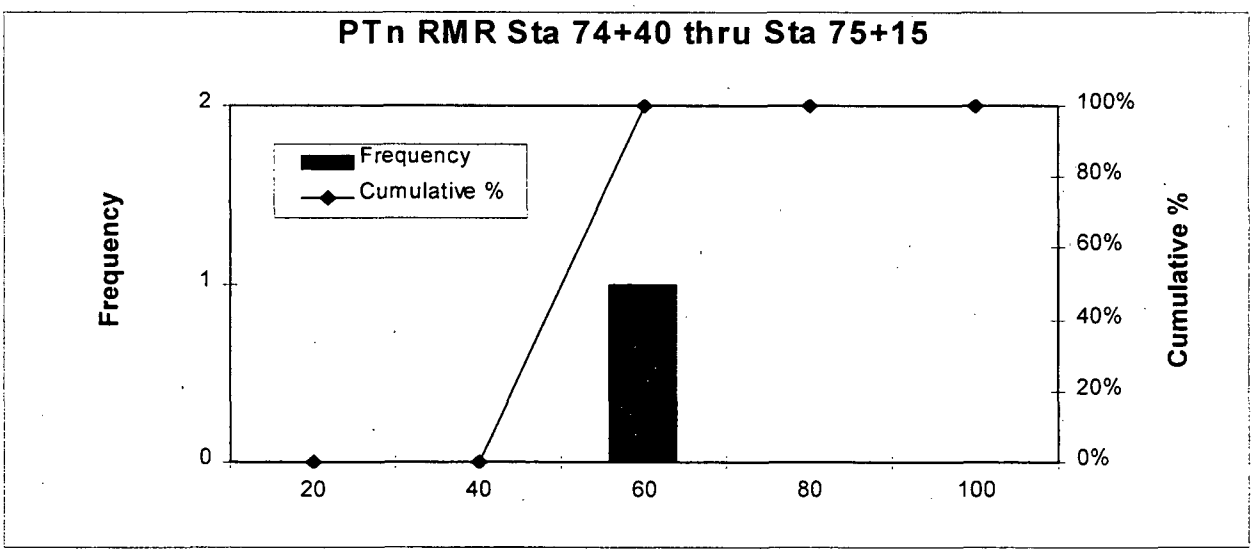

Figure 28c: Distribution of RMR in PTn (Sta 74+40 - 75+15)

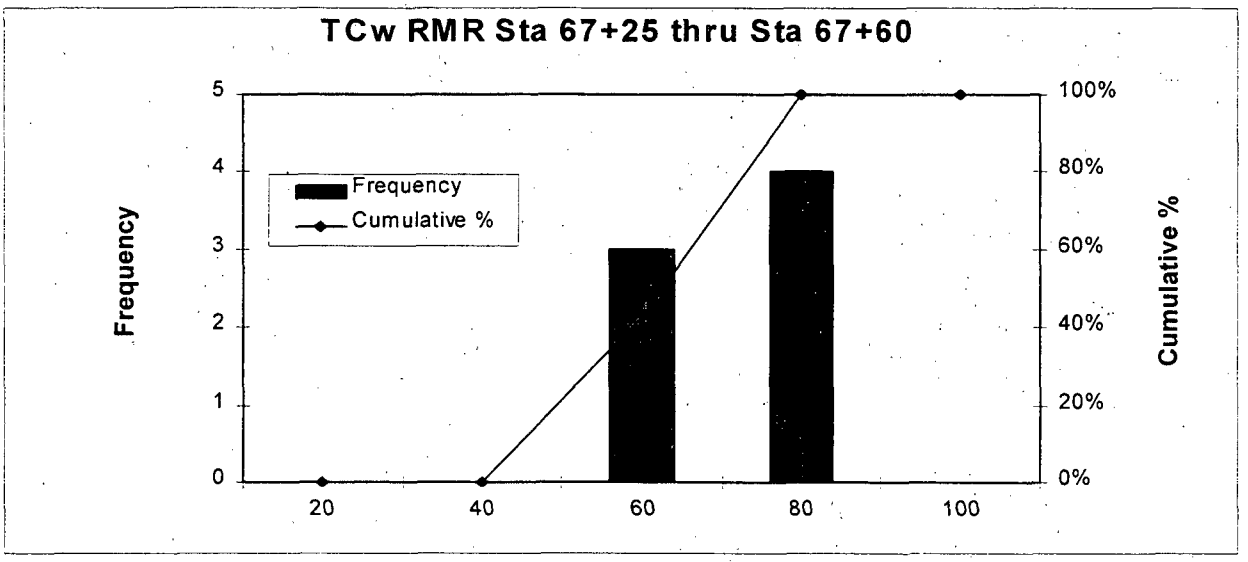

Figure 29a: Distribution of RMR in TCw (Sta 67+25 - 67+60)

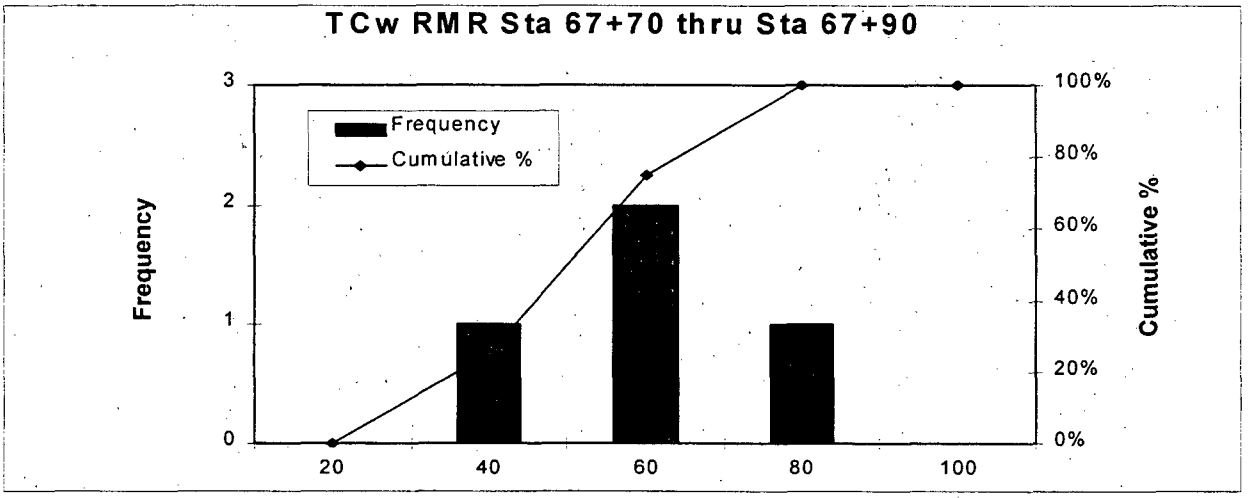

Figure 29b: Distribution of RMR in TCw (Sta 67+70 - 67+90)

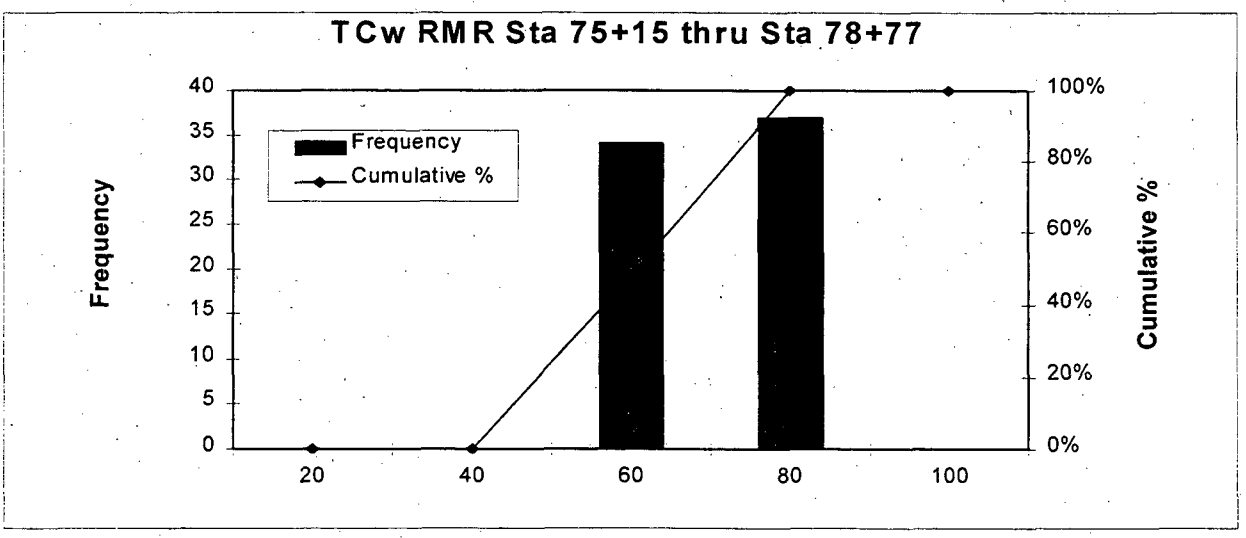

Figure 29c: Distribution of RMR in TCw (Sta 75+15 - 78+77)

RMR in TSw2: The first 810 meter interval has a mean RMR rating of 54 (*fair*). The second interval of 115 meters also scores a mean rating of 54 (*fair*); however, 35 meters of this section are not rated due to extensive lagging. Consistent with the RQD ratings, the RMR of 46 (*fair*) in stratigraphic unit Tptpll still ranks below the 56 of unit Tptpmn. The RMR differences between the two units reflect the RQD differences discussed previously. The addition of rock mass characteristics like the intact rock compressive strength and joint water condition tends to equalize numerical values of RMR. The differences are still explained by RQD. Figure 26a shows 71 percent of the first occurrence of TSw2 rates between 40 and 60.

RMR in TSw1: The mean RMR rating in 790 meters of the TSw1 is 54 (*fair*). All occurrences of the TSw1 were rated. The 325 meters of unit Tptrn have a mean RMR of 61 (*fair-good borderline*). The lithophysal units Tptpul and Tptrl have a mean RMR of 48 (*fair*) and 53 (*fair*) respectively. The distributions of RMR presented on Figures 27a, 27b, show that for these two occurrences of TSw1 62 percent and 70 percent of the ratings are in the *fair* (40-60) range with more variation into the *good* (60-80) range rather than the *poor* (20-40) range.

RMR in PTn: Since 195 of the 245 meters within the PTn are not rated, the mean ratings for the three separate PTn units of 63 (*fair*), 59 (*fair*), and 56 (*fair*) do not completely represent conditions in these units. Figures 28a, 28b, and 28c display the distribution of RMR in the PTn. Ratings are generally distributed around the *fair-good borderline* (60). As noted above, 80 percent of the PTn is not rated. The high ratings result from low fracture frequencies in these units.

RMR in TCw: Figures 29a and 29b show the 55 meters of Tpcpln which is sandwiched in

around the PTn (Tpcpv). Overall, this 55 meters has a mean RMR of 57 (*fair*). The longest Tcw unit is found from Sta 75+15 to 78+77. This section is composed of three stratigraphic units, with over 50 percent rated *fair* or better, as seen in Figure 29c.

Norwegian Geotechnical Institute Rock Quality, Q, System

The Q ratings assigned here are a conservative estimate of the rock mass quality in that the 5-m ratings are based on the lowest quotient of observed joint roughness, Jr divided by joint alteration, Ja. The Q value is calculated with the following equation:

$$\mathbf{Q = (RQD/Jn) * (Jr/Ja) * (JwQ/SRF)}$$

where:

RQD is an integer number equal to the RQD percentage. In the equation above, the numerical value of 90 is used for an RQD of 90 percent.

Jn is an index number based on assessment of the number of joint sets within the 5-meter rating interval considered. The number of joint sets is a parameter related to the extent of fracturing in the rock mass. The number of joint sets for a given 5-m rating interval is determined primarily from observations of the right rib of the tunnel along the DLS tape. However, discontinuities which are subparallel to the tunnel axis are more easily observed in the crown of the tunnel; therefore the observed Jn includes joint sets exposed in the crown, and/or left rib. The right rib of the tunnel is emphasized so that observed ratings may be compared with the data gathered in the Detailed Line Survey. Visual inspection to determine the number of joint sets requires engineering-geological judgment. Ratings are based strictly on observations within a 5-m interval. The use of a short interval to determine this parameter leads to oscillations in the joint-number rating. Intuitively, one might assume this parameter would be more or less constant in a

structural region. That constancy is not the case using a short rating interval. Variation in Q ratings between two adjacent intervals of tunnel are most often due to the quotient RQD/Jn and the parameter SRF which is discussed later. Fracture zones including crushed rock or intensely jointed rock may be evident on the left rib of the tunnel and not on the right. In these cases, notes describing fracture zones or fallout on the left rib are entered on the data form, and the Q rating is based on the overall tunnel observations, not just along the right wall. If there are only a few joints visible, the joints are counted as "random joints" when evaluating Jn.

RQD/Jn The quotient, RQD/Jn, represents the overall structure of the rock mass and is a crude measure of the relative *block size*. The larger the ratio, the higher the values (Barton, 1974)

Jr is an index number representing the roughness of the joint set. Joint roughness is related to the shear strength of the rock. The joint-roughness rating considers the small-scale roughness of the fracture surface in combination with the large-scale roughness. The rating may not include the single worst joint condition but will always indicate roughness below the average for the set.

Ja is an index number based on the alteration or filling of a given joint set. Joint alteration describes conditions which may reduce the stability of rock blocks in the tunnel.

Jr/Ja The quotient, Jr/Ja, represents the roughness and frictional characteristics of the joint walls or filling materials. This quotient is weighted in favor of rough, unaltered joints with little or no separation (in direct contact). Such surfaces will be close to peak strength, tend to dilate significantly when sheared and, therefore, be especially favorable to tunnel stability. This quotient is a fair approximation of the actual *shear strength* expected of the various combinations of wall roughness and alteration. The larger the ratio, the higher the values (Barton,1974)

JwQ is an index number based on groundwater conditions. The "Q" is used to distinguish this index from the RMR system groundwater rating. The South Ramp

excavation is dry.

SRF is an index number based on in-situ conditions which influence the stability of the excavation. The stress reduction factor considers loosening loads, *in situ* stress, and squeezing or swelling loads. For field-form notation, the category SRF.40, was added to the original system to indicate no stress-related reduction in the rock-quality rating. Stress-reduction factors at Yucca Mountain are most often related to fracture zones intersecting the excavation. Rock quality is reduced for shear zones which influence the surrounding rock. One would expect an influence zone of, for example, 1 to 2 meters wide for a stress reduction. Given that size zone and a rating interval of 5 meters, significant multiple shear zones are not a probability. If longer rating intervals were used, multiple shear zones would often be encountered.

Jw/SRF The quotient, Jw/SRF consists of two stress parameters. Jw is a measure of water pressure, which has an adverse effect on the shear strength of joints because of a reduction in normal stress. The parameter SRF is a measure of (1) loosening load in the case of excavation through shear zones and clay bearing rock, (2) rock stress in competent rock, and (3) squeezing or swelling loads in plastic, incompetent rock. It can be regarded as a total-stress parameter. The quotient (Jw/SRF) is a complicated empirical factor describing the Q-system "active stresses". The term does not refer specifically to the in situ state of stress in the rock, but includes mechanical effects, effects of shears, and chemical behavior, as well as strength of material and in situ stress. The larger the ratio, the lower the values.

Qualitative rock descriptions associated with numerical Q values are shown in Table 11.

Q Ratings in the South Ramp

Two Q values were calculated for each 5-m section of the South Ramp. The value reported as the

Rated Q Value	Rock Quality Description
0.1 - 1	Very Poor
1 - 4	Poor
4 - 10	Fair
10 - 40	Good
40 - 100	Very Good

Table 11: Q Ratings and Qualitative Descriptions

Q rating for any section is called the Rated Q. This value is determined using the lowest Jr/Ja ratio from within the 5-m interval. The second Q value, called Q Max is calculated using the highest Jr/Ja ratio within the 5-m interval. All other parameters, RQD/Jn and Jw/SRF, within the Q equation remain constant for both Rated Q and Q Max. Table 12 summarizes the mean, median and range of Rated Q for four thermal-mechanical units and their related stratigraphic units in the South Ramp.

Mechanical Units	Stratigraphy	Stations	Meters Rated	Rated Q Mean	Rated Q Median	Rated Q Range
TSw2		55+00 → 63+10	810	1.81	1.31	0.11-13.5
	Tptpmn	55+00 → 57+30 58+80 → 63+10	230 430	1.97	1.54	0.11-13.5
	Tptpll	57+30 → 58+80	150	1.12	1.0	0.27-3.33
TSw2		70+55 → 71+70	80	1.37	0.86	0.31-7.0
	Tptpmn	70+55 → 71+70 71+10 → 71+45	80 35	1.37 NR	0.86 NR	0.31-7.0 NR
TSw1		63+10 → 66+30	320	7.48	4.03	0.34-74.25
	Tptpul	63+10 → 64+55	145	4.19	3.53	0.34-14.81

	Tptrl	64+55 → 65+05 65+25 → 65+30	50 5	4.2	1.97	0.75-15.25
	Tptrn	65+05 → 65+25 65+30 → 66+30	20 100	12.95	5.89	0.69-74.25
TSw1		67+90 → 69+90	200	5.34	3.01	0.37-37.0
	Tptpul	67+90 → 68+50	60	2.69	1.18	0.39-9.63
	Tptrl	68+50 → 68+85	35	16.58	12.8	6.0-37.0
	Tptrn	68+85 → 69+90	105	3.1	2.43	0.37-11.6
TSw1		71+70 → 74+40	270	4.04	1.93	0.29-35.25
	Tptpul	71+70 → 73+00	130	2.02	1.48	0.29-11.25
	Tptrl	73+00 → 73+40	40	12.54	8.27	0.85-35.25
	Tptrn	73+40 → 74+40	100	3.27	2.33	0.52-8.17
PTn		66+30 ≈ 67+70	30	6.55	4.78	0.61-15.83
	Tptrv	66+30 → 66+45	15	8.47	6.4	3.17-15.83
	Tpbt	66+45 → 66+80	35	NR	NR	NR
	Tpcpv	66+80 → 67+20 67+20 → 67+25 67+60 → 67+70	40 5 10	NR 11.11 1.38	NR 11.11 1.38	NR 11.11-11.11 0.61-2.16
TCw		67+25 ≈ 67+90	55	8.39	7.63	0.12-24
	Tpcpln	67+25 → 67+60 67+70 → 67+90	35 20	8.39	7.63	0.12-24
PTn		69+90 → 70+55	15	2.54	1.82	0.98-4.8
	Tptrv	69+90 → 70+05	15	2.54	1.82	0.98-4.8
	Tpbt	70+05 → 70+55	30	NR	NR	NR
PTn		74+40 → 75+15	5	1.28	1.28	1.28-1.28
	Tptrv	74+40 → 74+50	10	NR	NR	NR
	Tpbt	74+50 → 74+95	45	NR	NR	NR
	Tpcpv	74+95 → 75+10 75+10 → 75+15	15 5	NR 1.28	NR 1.28	NR 1.28-1.28

TCw		75+15 → 78+77	362	4.07	2.27	0.34-23.33
	Tpcpln	75+15 → 76+05	90	3.84	2.15	0.52-15.33
	Tpcpmn	76+05 → 78+40	235	2.8	1.84	0.34-14.5
	Tpcpul	78+40 → 78+77	37	12.96	14.63	2.27-23.33

Table 12: Summary of Rated Q Values in the South Ramp

Figure 30 shows the rated Q for the entire South Ramp. Figure 31 compares the Rated Q value and a computed Maximum Q value based on the highest Jr/Ja ratio.

Rated Q in TSw2: Within the 810 meters of the two TSw2 units, Q in the first section of Tptpmn averages 1.97 (*poor*). The Tptpll and the second section of Tptpmn average 1.12 and 1.37 respectively. Both those ratings are also *poor*. The differences in Q between Tptpmn and Tptpll are less dramatic than the RQD differences discussed previously. The Tptpll displays a lower - and more favorable - joint set number than the first Tptpmn, so differences in RQD are partially offset by Jn. The overall Q average of 1.81 (*poor*) may be a generous characterization of TSw2 in the South Ramp. Figure 32a indicates that 40 percent of the Q ratings are less than 1.0. For the second occurrence of TSw2, Figure 32b shows 69 percent of Q values less than 1.0.

Rated Q in TSw1: The mean Q ratings for three occurrences, 790 meters of the TSw1 are 7.48 (*fair*), 5.34 (*fair*), and 4.04 (*fair*). These values produce an overall average of 5.8 (*fair*). Stratigraphic units Tptrl and Tptrn exhibit high mean ratings. For example, 35 meters of Tptrl in the second occurrence averages 16.58 (*good*), while 120 meters of Tptrn in the first occurrence has a mean Q of 12.95 (*good*). In all three sections of TSw1 the lowest mean ratings belong to Tptpul with a means of 4.2, 2.69, and 2.02 giving a 335 meter average

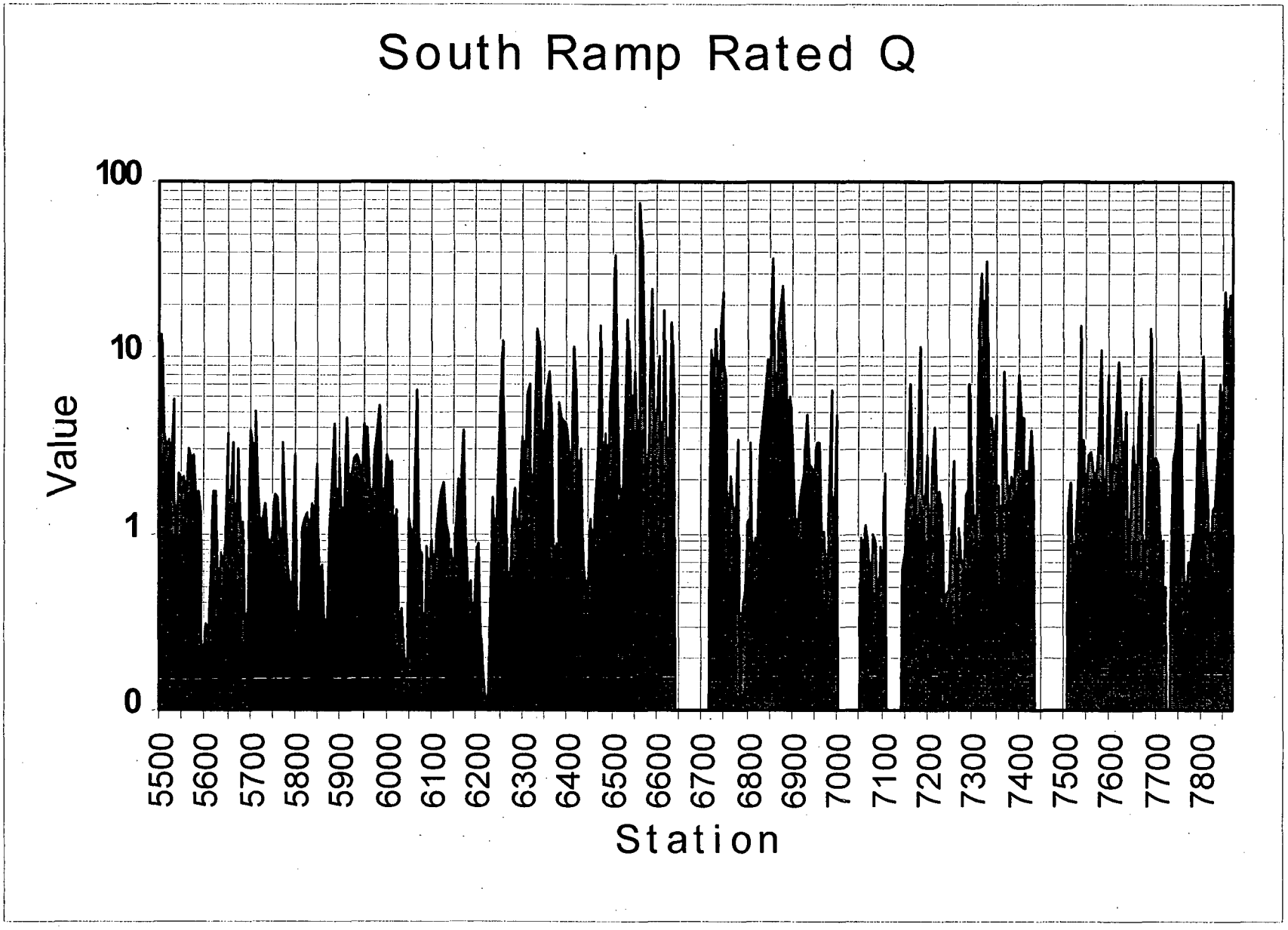

Figure 30: South Ramp Rated Q

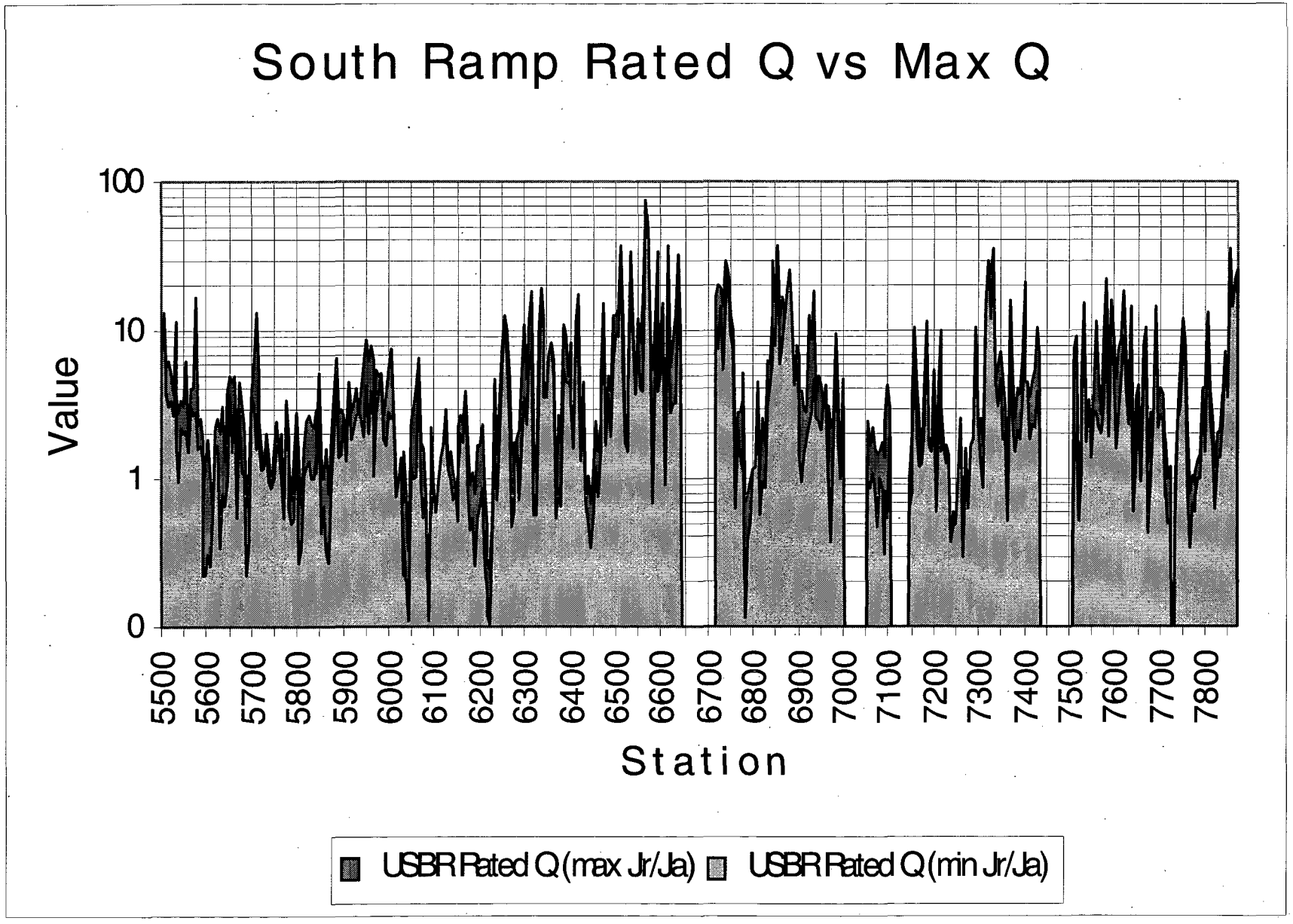

Figure 31: South Ramp Rated Q and Max Q

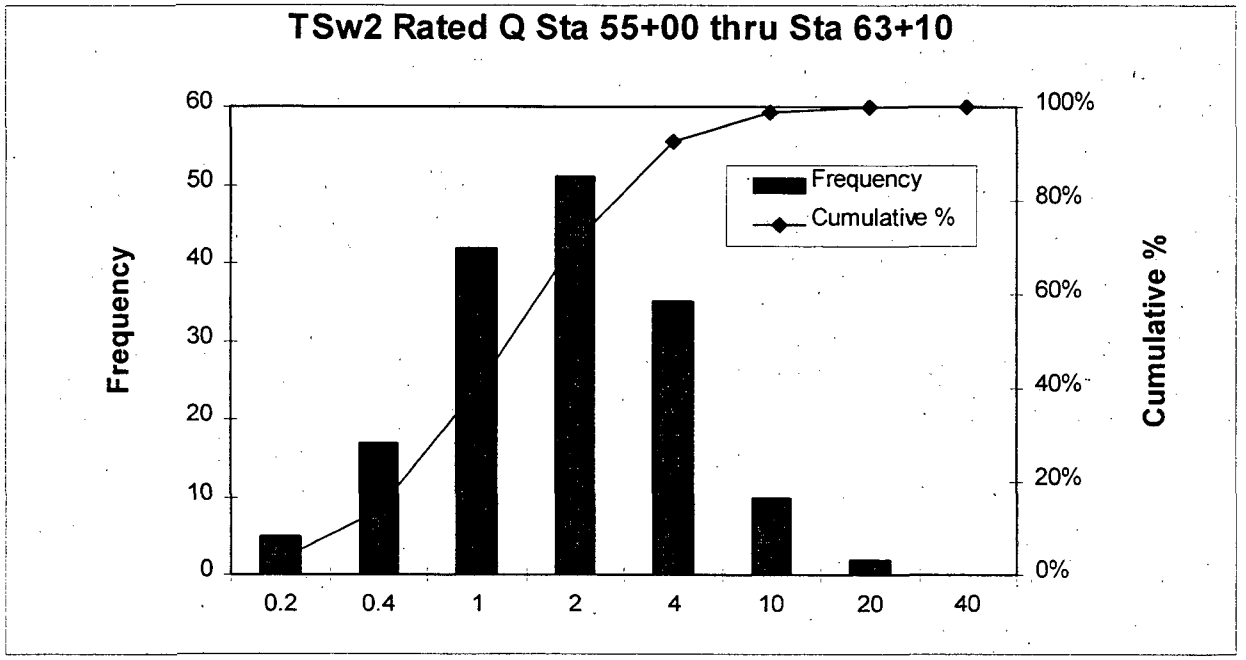

Figure 32a: Distribution of Q in TSw2 (Sta 55+00 - 63+10)

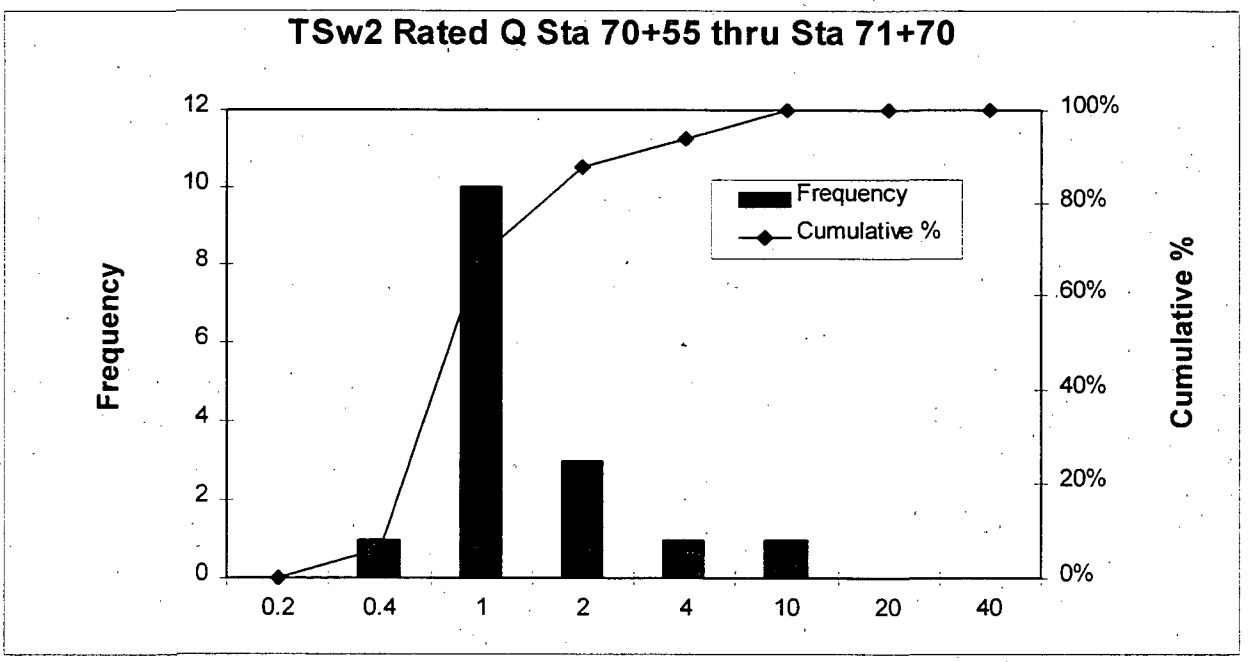

Figure 32b: Distribution of Q in TSw2 (Sta 70+55 - 71+70)

of 3.1 (*poor*). Figures 20 and 27 show high RQD values and spikes of relatively high Q ratings in all three occurrences of the TSw1. Figure 33 displays the distribution of Q values throughout the TSw1. Favorable conditions cause a geometric increase in the numerical Q rating. When these high Q values are averaged, the means are skewed. Table 12 gives medians roughly one-half to two-thirds the mean. From Figure 33a nearly 75 percent of the rated Q values fall below 2.0. The second and third occurrences of TSw1 contain more sections of higher rated rock. In Figure 33b 37 percent, and in Figure 33c 51 percent of the rated Q's are less than 2.0. The median values of 2 to 4 represent the middle ground in the TSw1.

Rated Q in PTn: Since 195 of the 245 meters within the PTn were not rated, the mean ratings for 50 meters of PTn of 6.55 (*fair*), 2.54 (*poor*), and 1.28 (*poor*) are not statistically representative of the whole section. These Q system descriptions do not describe the condition of the lower compressive strength sections of the PTn. For the omitted Q ratings, a section of this report titled "Non-Rated Areas" discusses of the reasons ratings were not assigned in this unit. For the intervals of tunnel which were rated, Figure 34 presents the distribution of Q ratings.

Rated Q in TCw: This unit is the third longest section in the South Ramp; 427 m is rated. The mean Q ratings for the three separate sections are 4.6 (*fair*), 5.6 (*fair*), and 12.96 (*good*). The most even distribution is in Figure 35c, where nearly 78% of the ratings exceed a Q value of 4.0 and rates as high as 23. The Tpcpul rates exceptionally high; 12.96 (*good*). The lithophysal voids here make it very difficult to see joint sets. As a result, this lower joint set number results in a higher Q value.

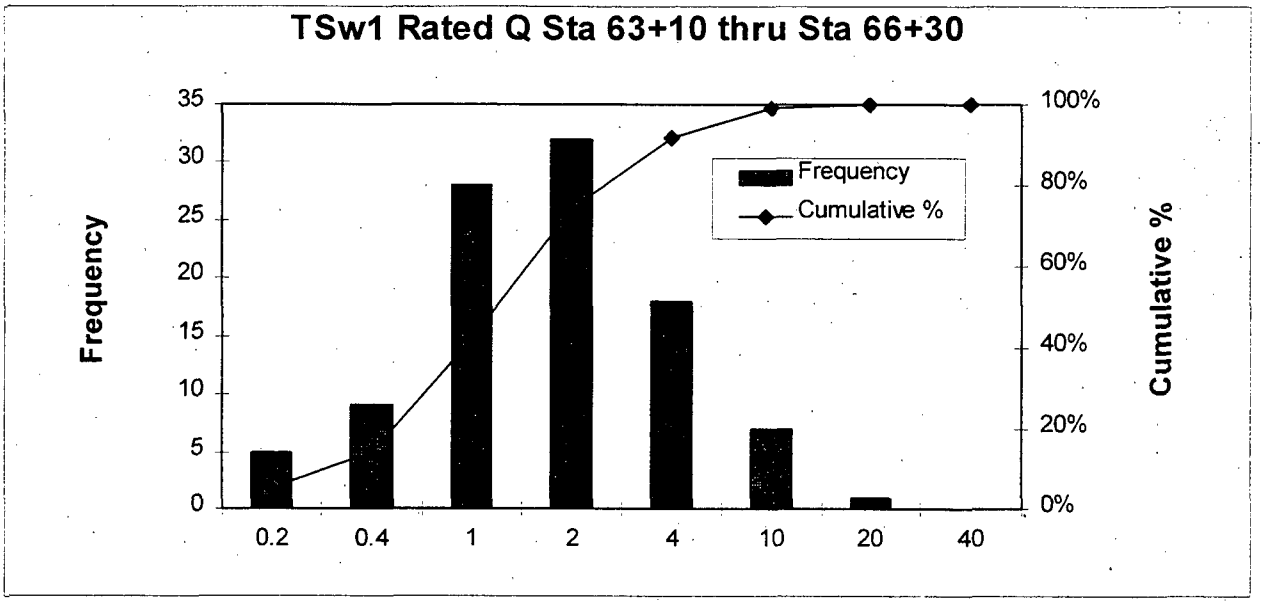

Figure 33a: Distribution of Q in TSw1 (Sta 63+10 - 66+30)

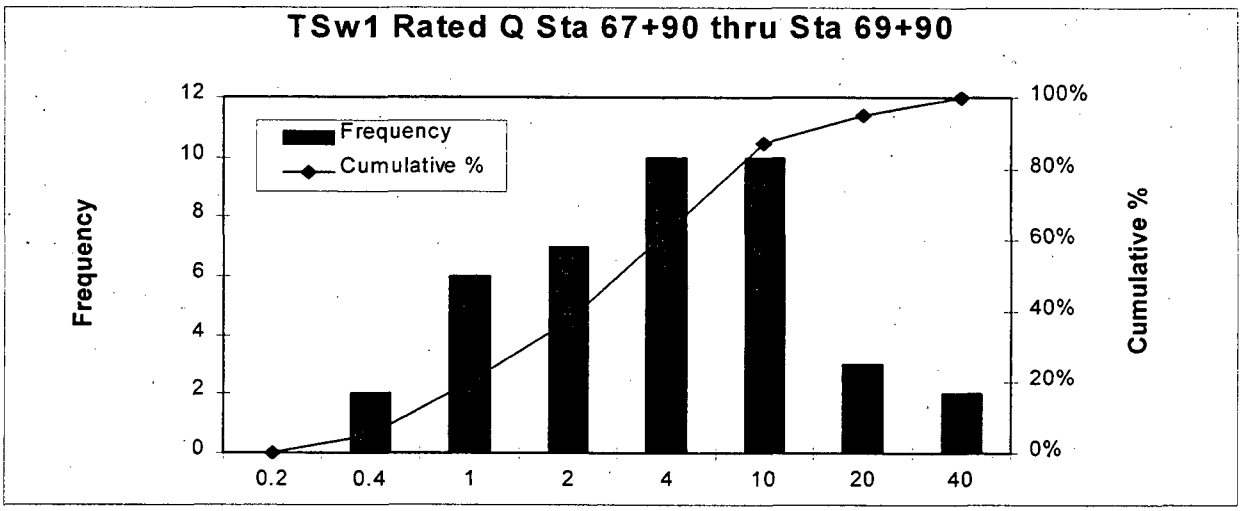

Figure 33b: Distribution of Q in TSw1 (Sta 67+90 - 69+90)

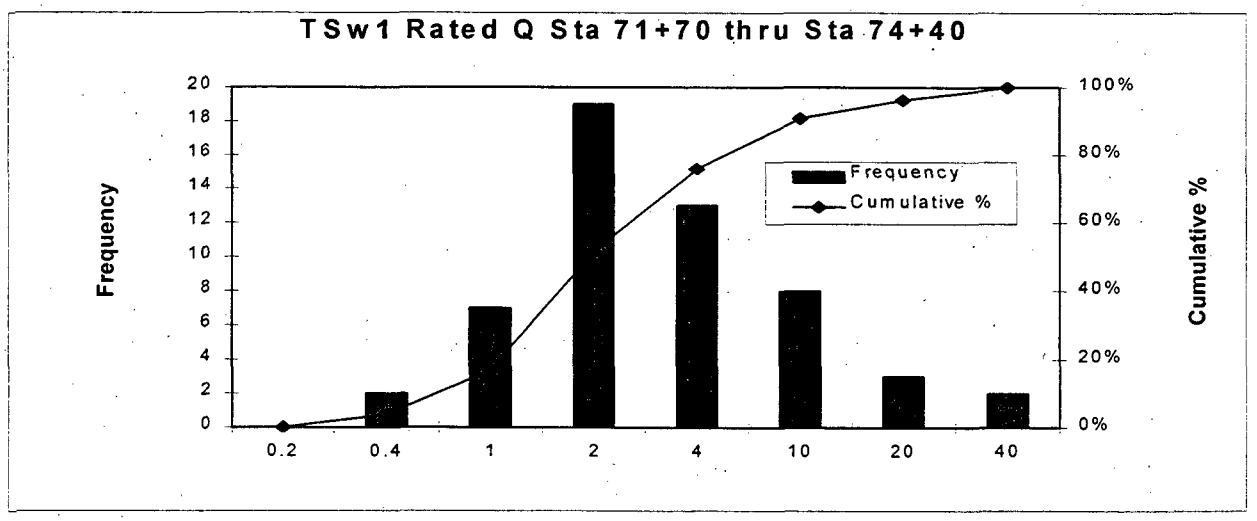

Figure 33c: Distribution of Q in TSw1 (Sta 71+70 - 74+40)

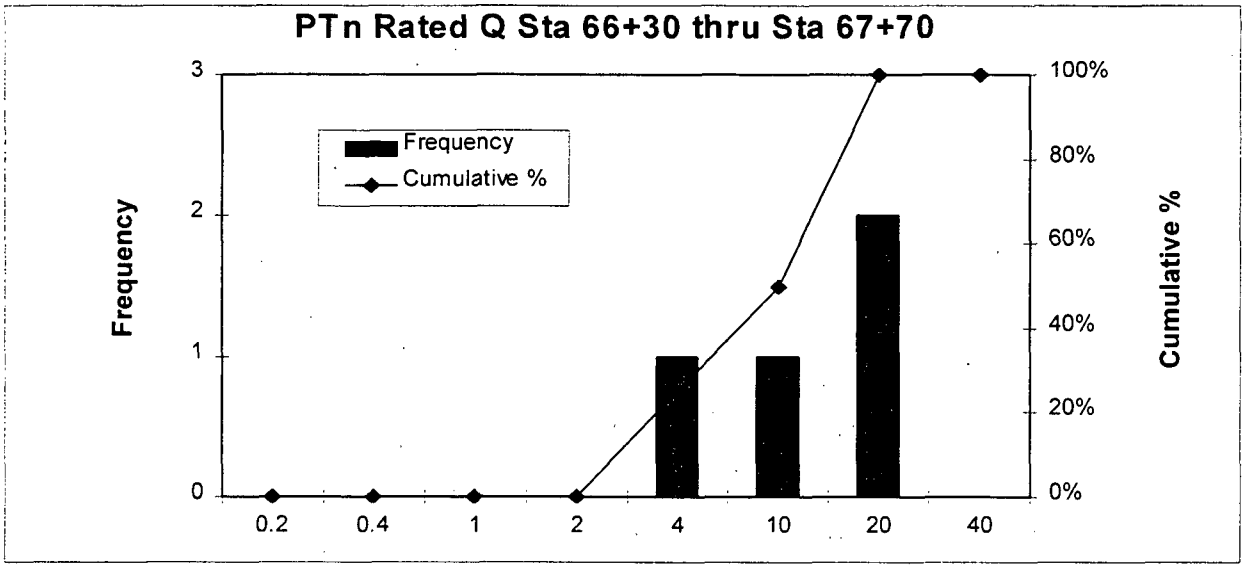

Figure 34a: Distribution of Q in PTn (Sta 66+30 - 67+70)

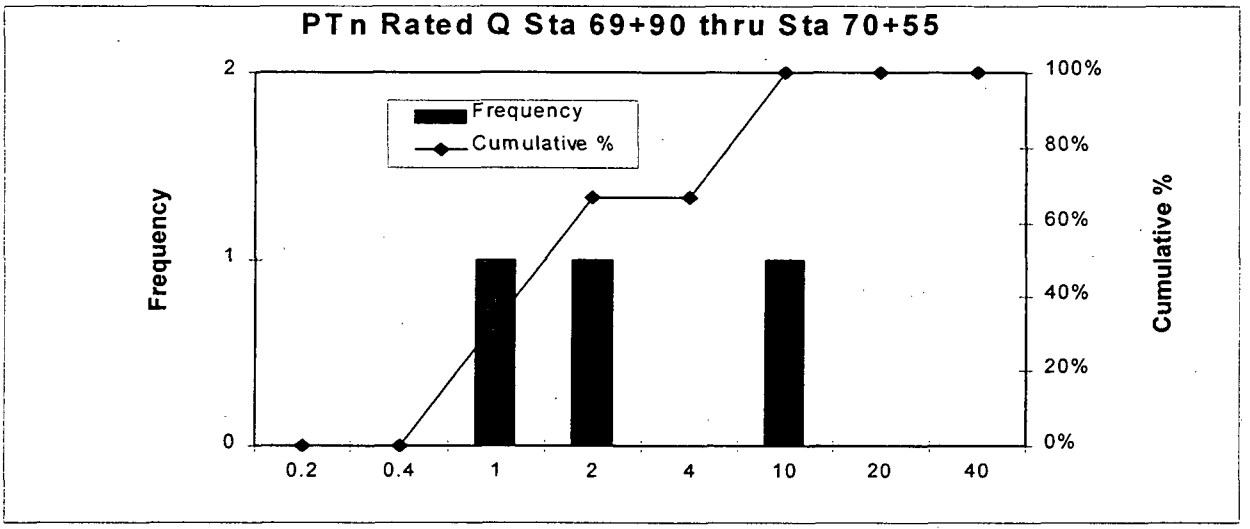

Figure 34b: Distribution of Q in PTn (Sta 69+90 - 70+55)

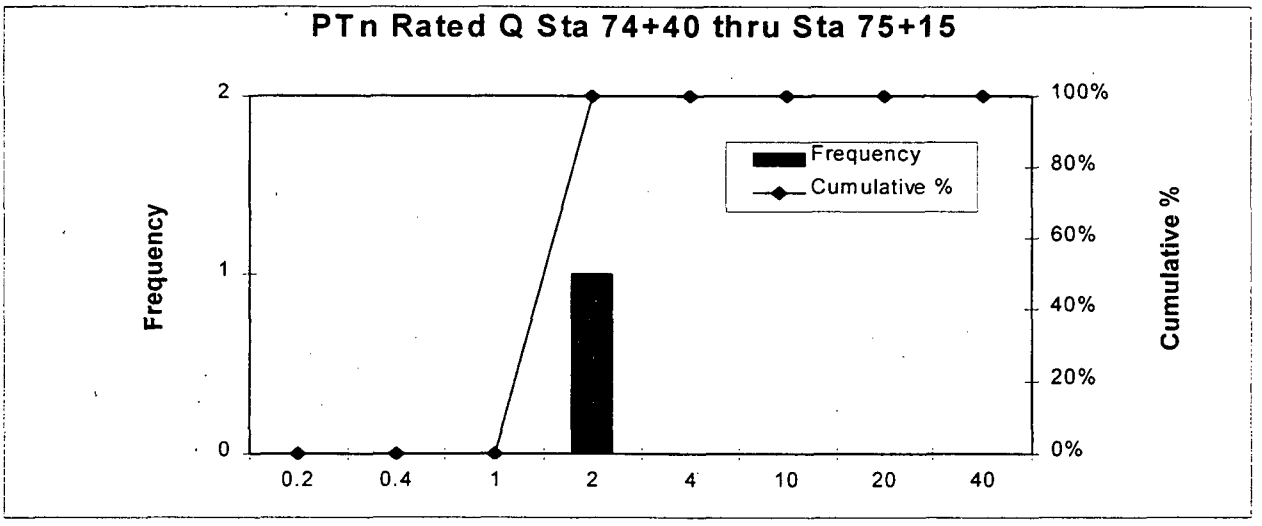

Figure 34c: Distribution of Q in PTn (Sta 74+40 - 75+15)

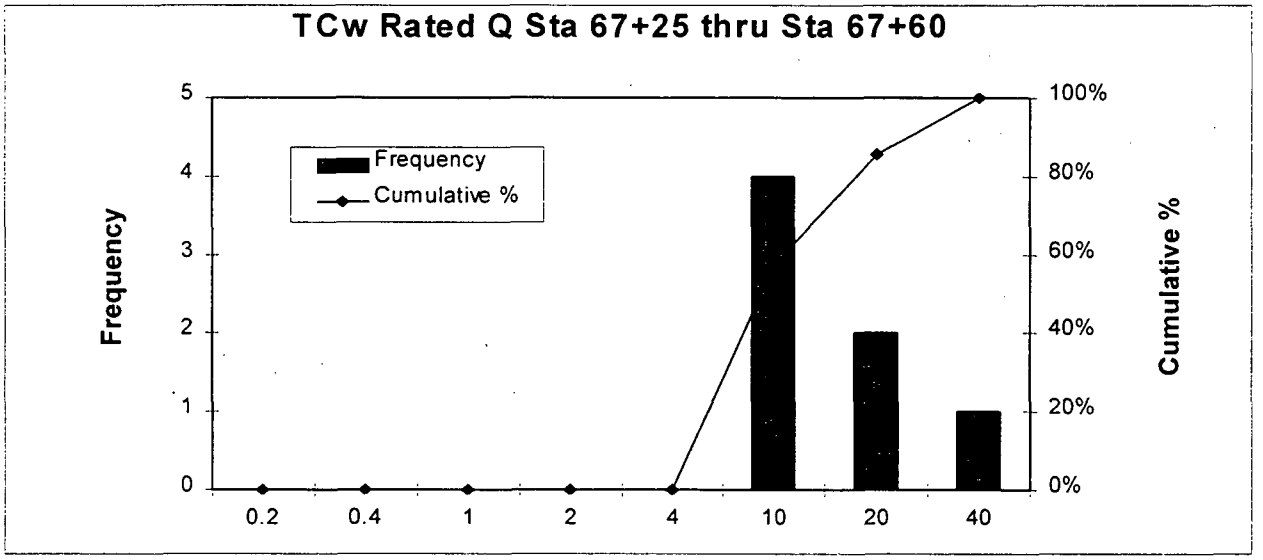

Figure 35a: Distribution of Q in TCw (Sta 67+25 - 67+60)

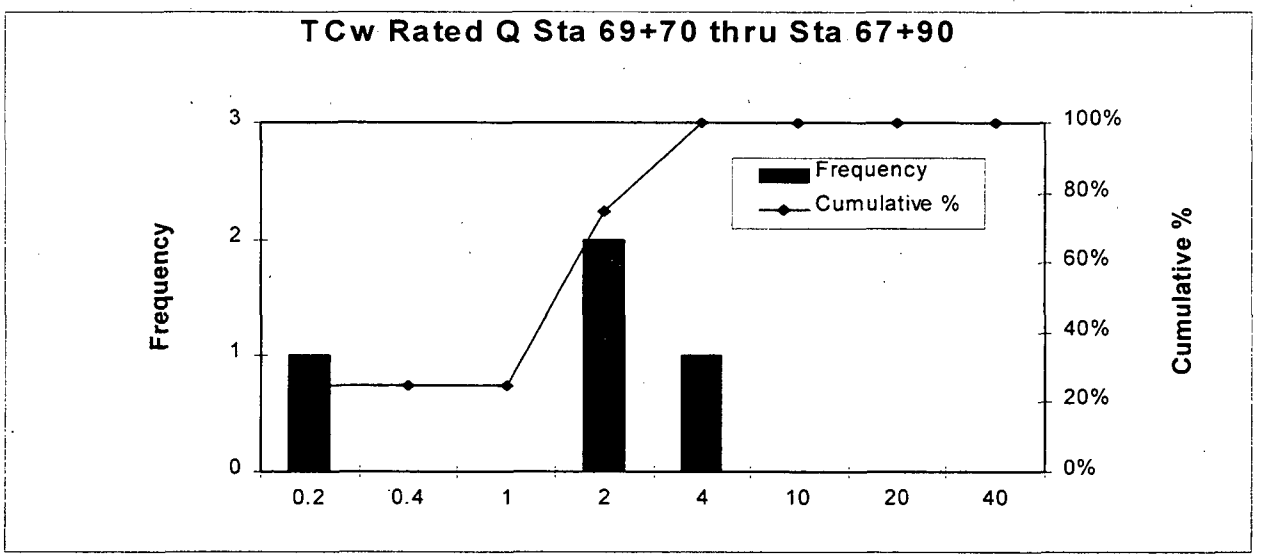

Figure 35b: Distribution of Q in TCw (Sta 69+70 - 67+90)

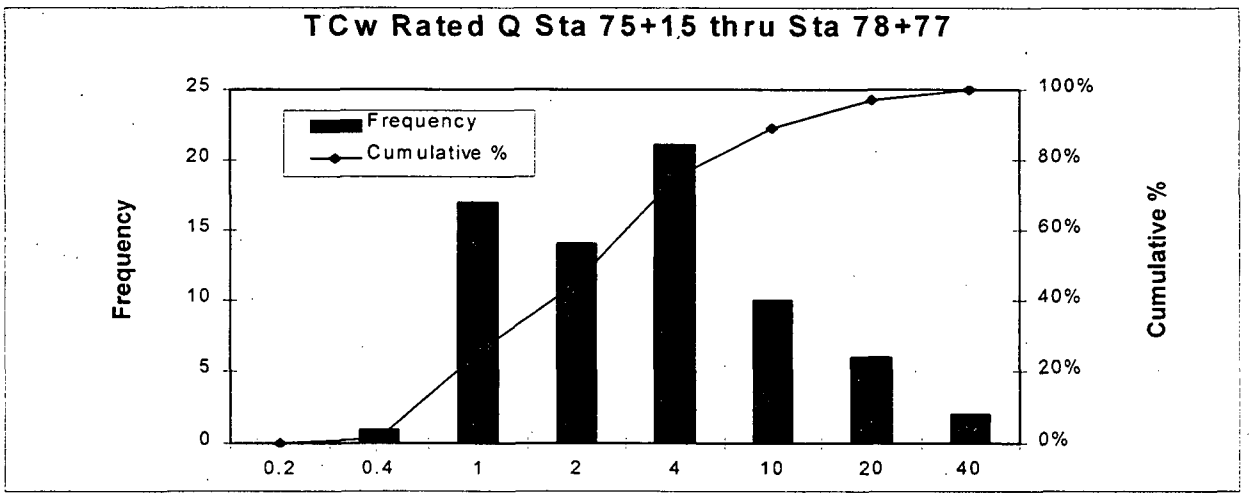

Figure 35c: Distribution of Q in Tcw (Sta 75+15 - 78+77)

Q Parameters in the South Ramp

Figures 36 thru 38 show ratios and individual parameters derived in the calculation of Rated Q. Table 13 shows mean and median values of Q rating parameters. Additionally, these parameters; Jn, Jr, Ja, Jw, and SRF are indexes which represent various descriptions extracted from Barton's Q procedures.

- Jn ranges from an index of 1 (massive occurrence) to 2 (1 joint set) to 4 (2 joint sets) to 9 (three joint sets) to 12 (3 + random joint sets) to 15 (4 or more joint sets).
- Jr ranges from an index of 1 (smooth & planar) to 2 (smooth & undulating) to 3 (rough & undulating).
- Ja ranges from an index of 2 (slightly altered, non-softening coating, sandy particles) to 3 (silty or sandy clay coatings, little clay) to 4 (softening or clay mineral coating).
- Jw index of 1 indicates a dry excavation.
- SRF ranges from an index 1 (no stress problems) to 2.5 (single shear zone or low stress) to 5 (loose open joints, heavily jointed) to 7.5 (multiple shear zones).

Non-Rated Areas

There are some areas within the South Ramp that were not rated. Some areas are not suitable for rating using the current principles and procedures of the Q and RMR systems. Other areas were obstructed from view by lagging. See Table 14 for a summary of these areas.

Ground Support

As encountered in the North Ramp, using the Q system ratings, *poor* to *good* quality rock was excavated through most of the South Ramp excavation. This section describes the classes of support defined in the construction documents, and compares the theoretical support based on Q system ratings (rated support) with the actual ground support installed in the South Ramp

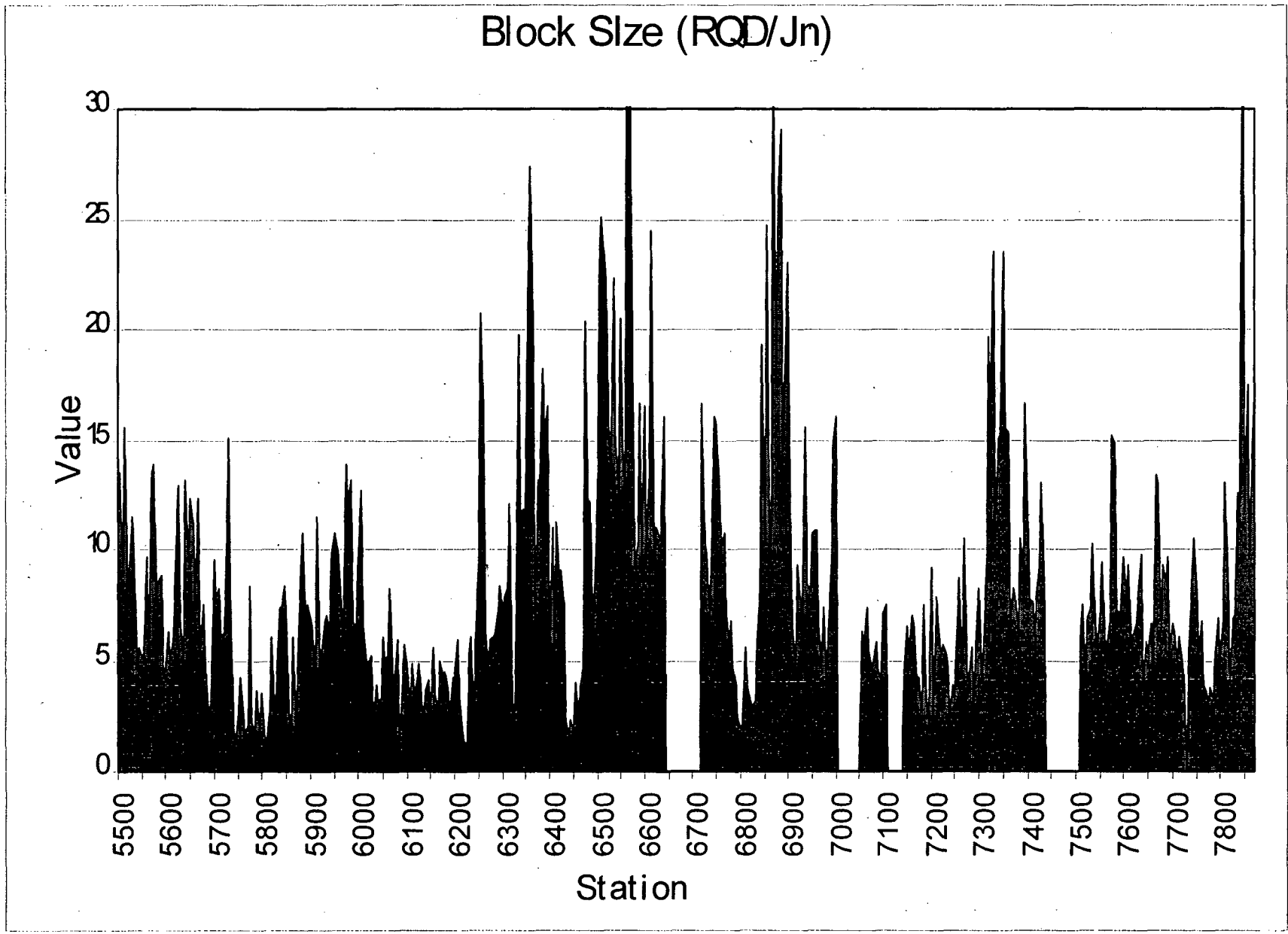

Figure 36: Q System RQD/Jn

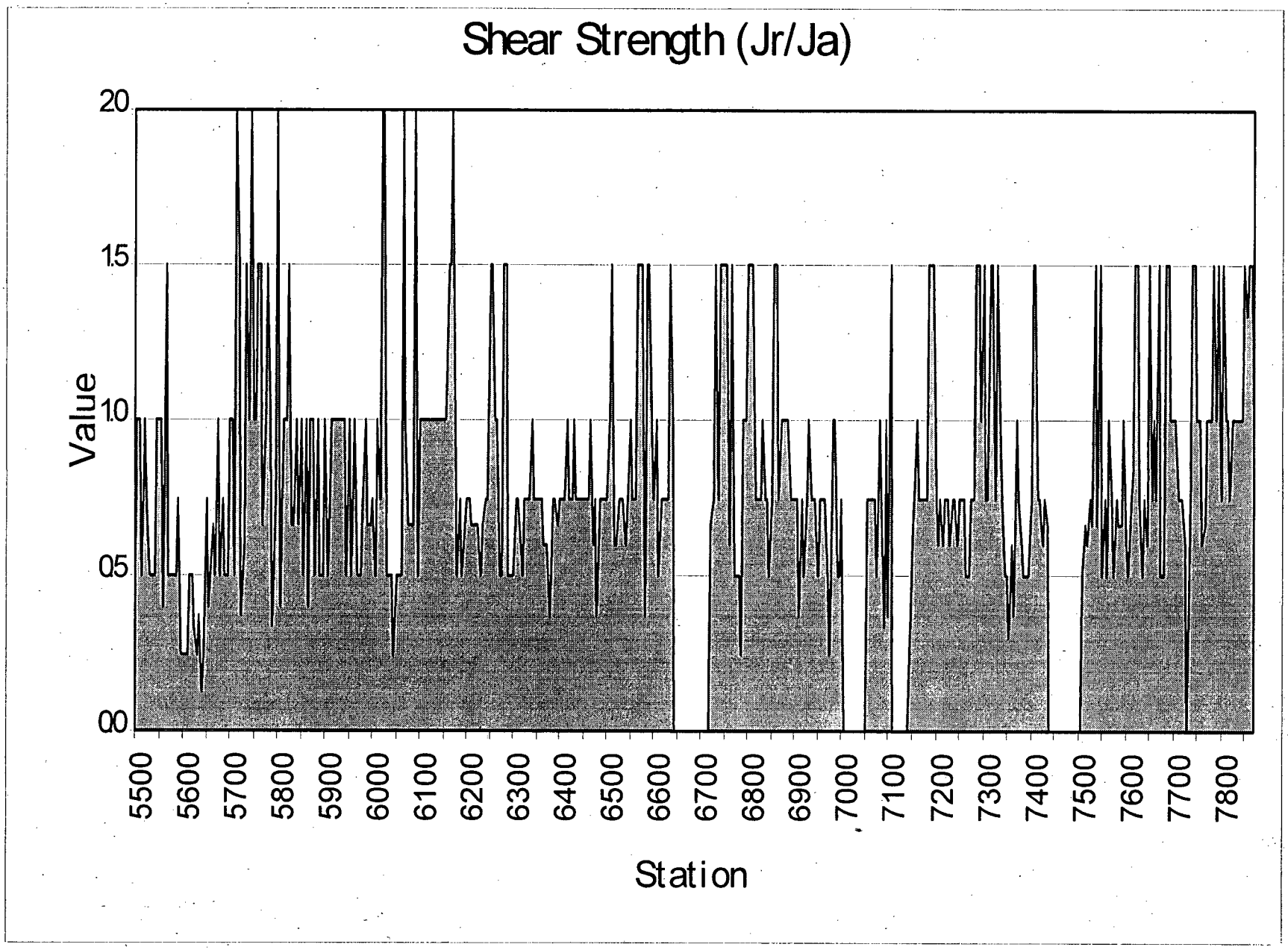

Figure 37: Q System Jr/Ja

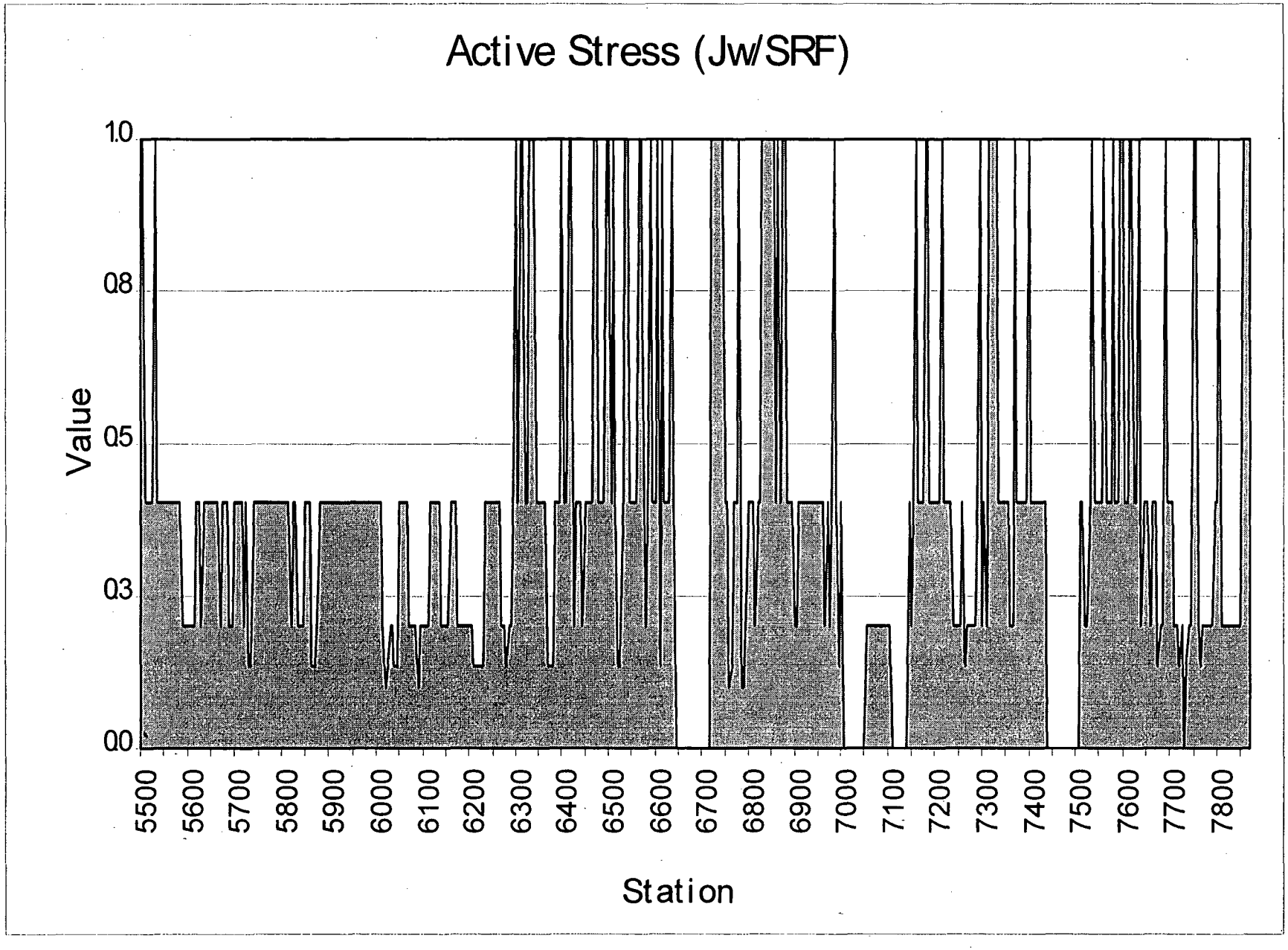

Figure 38: Q System Jw/SRF

(installed support).

South Ramp Average Rated Q Parameters for each Thermal-Mechanical Unit								
Parameters	**TSw2**		**TSw1**		**TCw**		**PTn**	
	Mean	**Median**	**Mean**	**Median**	**Mean**	**Median**	**Mean**	**Median**
RQD	53	54	62	65	72	76	88	95
Jn	9.3	9	7.5	6	10	9	7.6	7.5
Jr	2	2	2.8	3	2.5	3	2.4	2.5
Ja	2.9	2	3.7	4	3.0	3	3.5	3.5
Jw	1	1	1	1	1	1	1	1
SRF	3.7	2.5	2.7	2.5	3.2	2.5	2.8	2.5
RQD/Jn	6.3	5.8	10.8	9.11	8.4	7	12.5	12.7
Jr/Ja	0.82	0.75	0.83	0.75	0.96	1.0	0.77	0.71
Jw/SRF	0.33	0.40	0.51	0.40	0.48	0.40	0.52	0.40

Table 13: Q Parameters in the South Ramp

STATIONS	REASONING FOR NOT RATING	NO. METERS
66+45 - 67+20	Material too soft and soil-like. (PTn)	75
70+05 - 70+55	Material too soft and soil-like. (PTn)	50
71+10 - 71+45	Lagging (TSw2)	35
74+40 - 75+10	Material too soft and soil-like. (PTn)	70
77+30 - 77+35	Lagging & shotcrete. (TCw)	5

Table 14: Non Rated Areas

The design support includes rock reinforcement with welded wire fabric (class 1), to rock reinforcement with welded wire fabric and shotcrete (class 3), to structural steel supports (steel sets) with lagging (class 4) (see Table 15). Class 3 which utilizes shotcrete is never used in the

Ground Support Class	Description of Class of Support
1	8 rock bolts 1.5- x 1.5-m spacing with welded-wire fabric (wwf)
2	15 rock bolts 1.0- x 1.0-m spacing with wwf
2a	w6 steel sets 1220-mm spacing with wwf
3	15 rock bolts 1.0- x 1.0-m spacing with wwf and shotcrete
3a	w6 x 20 steel sets 1220-mm spacing with wwf and lagging
4	w8 x 31 steel sets 610 - 1220-mm spacing with wwf and crown lagging
5	w8 x 31 steel sets 610-mm spacing with full lagging

Table 15. YMP Design Ground-Support Classes

South Ramp or any other section of the ESF. Understanding the reluctance to use shotcrete is critical to a reasonable interpretation of the figures presented later in this section. Shotcrete was not used in the ESF for two reasons:

1) For construction convenience and efficiency, the contractor elected to install either rock bolt reinforcement or steel sets and to forego the use of shotcrete for ground support.

2) The routine use of shotcrete for ground support would be detrimental to geologic mapping, full periphery photography, and rock-characterization efforts. Shotcrete was also considered detrimental to hydrochemistry, geochemistry and isotopic studies, especially carbon-14 dating of liquids and gases in the rocks.

During excavation of the tunnel, two classes of ground support were added to the construction procedures:

1. Class 2a, identified in this section as class 2.1, uses steel sets with interlocking wire mesh as an alternative to the 15 rock bolts of class 2 support.

2. Class 3a, uses w6x20 steel sets (6"0 with steel lagging as an alternative to the 15 rock bolts and shotcrete of class 3.

The stability of the excavation and, consequently, the required ground support is significantly affected by the method of excavation. Tunnel-boring machine excavation in the South Ramp produces a much more stable excavation than that produced by the drill-and-blast method. Theoretical ground support based on the Q rock mass quality rating does not directly consider the method of excavation. TBM excavation may explain some of the apparent differences in rated and actual support.

One final consideration with regard to ground support involves the plan to immediately supplement the actual support installed during excavation. Throughout the tunnel, many 5-m intervals indicate the need for class 3 support. Based on observations of the opening stability, the difference between rated and installed support does not require immediate action. Potential performance problems may be detected by simple visual observation of the opening and by monitoring structural instrumentation data. The decision to install shotcrete for ground support should include at least two considerations:

1) The final lining requirements for the tunnel should be established before an extensive program of supplemental ground support is undertaken. If a final lining is planned for the entire tunnel, the permanent lining can be designed as supplemental ground support.

2) The positive effect of the TBM excavation vs. drill-and-blast excavation should be evaluated. Such an empirical analysis is beyond the scope of this data collection effort; however, the interval of tunnel considered for additional ground support may be minimized by careful consideration of the rock structure data collected in the tunnel, coupled with analysis of structural instrumentation data and mathematical models of the excavation.

Classes of Support

Support categories used in comparisons of installed versus calculated ground support are described in Table 15. These descriptions are taken from Drawing BAABEE0000-01717-2100-40151-00, titled " 7.2 m Tunnel Ground Support Master Sections" effective April 16, 1996. The original ground-support drawings used the term "category" and did not include Classes 2a and 3a. In this report, the terms "ground-support class" and "ground-support category" are used interchangeably, and both refer to the descriptions in table 15..

Installed versus Rated Ground Support

Figure 39 provides a comparison of installed and rated ground support in the entire south ramp. The theoretically required ground support, designated rated support, is based on a calculation of

the rock quality rating, Q and two parameters of the Q rating RQD/Jn and Jr/Ja. The methodology used to determine support is described on Drawing BABEAB0000-01717-2100-40151, titled "TS North Ramp Ground Support Master Elevation and Sections," accepted for construction October 13, 1991.

The ground support actually installed in the South Ramp is determined by the excavation contractor. The heading crew selects rock reinforcement or steel sets and lagging for support based on their experience in similar conditions and their estimate of loosening loads. Table 16 gives the percentage of various classes of support shown in Figure 39. The table shows that in the South Ramp the theoretical requirement for class 2, 3, or 4 ground support is 80 percent. Actual installation of the classes was 36 percent. Figures 40 thru 46 show rated and installed support in each thermal-mechanical unit.

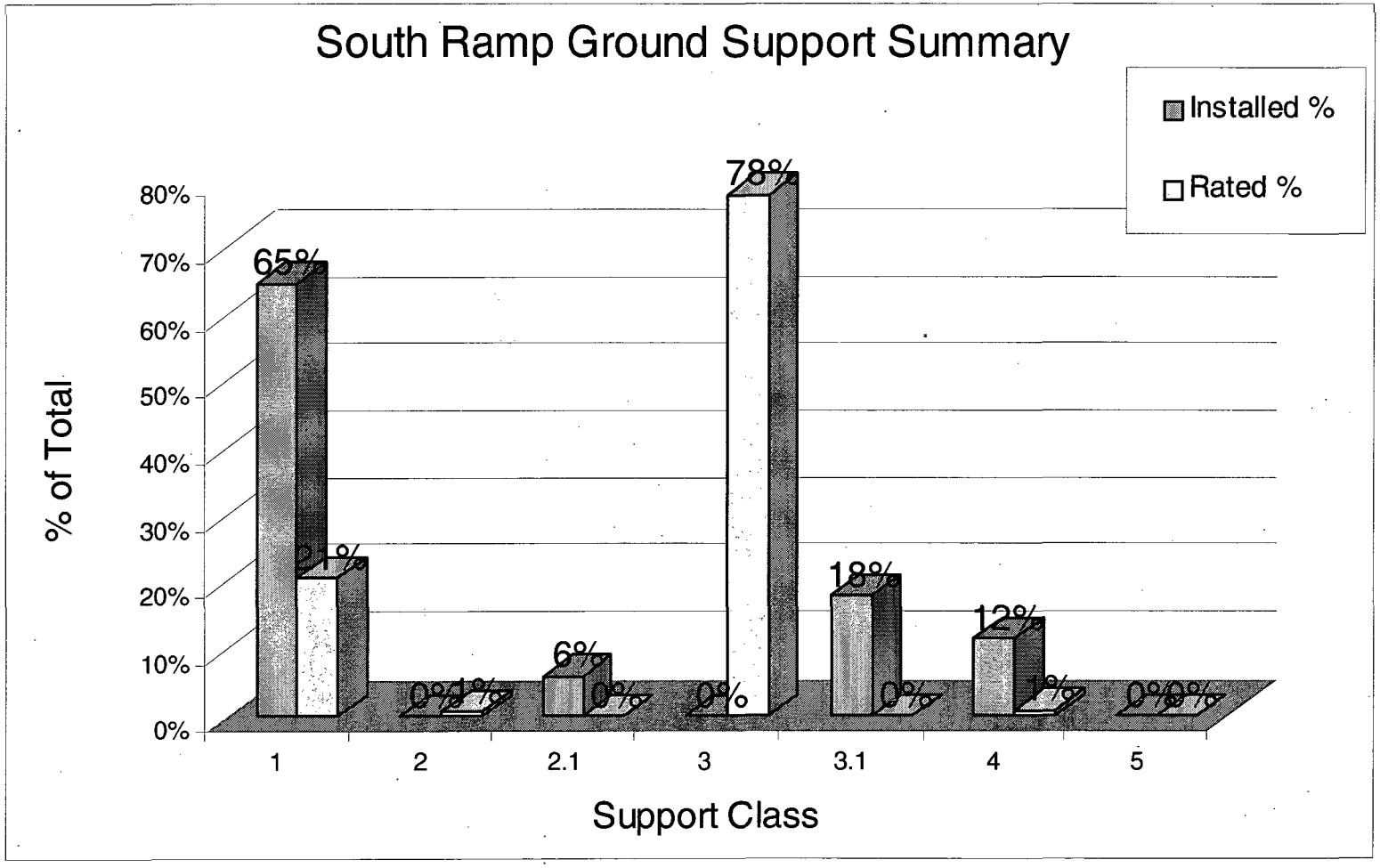

Figure 39: South Ramp Summary of Ground Support

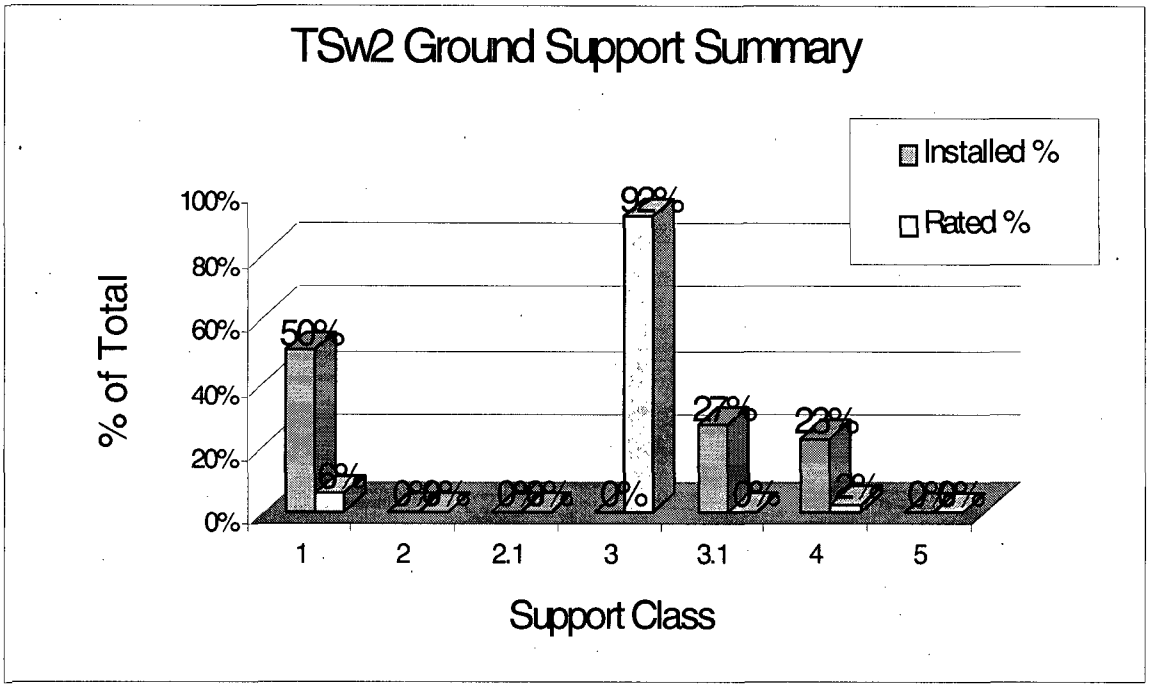

Figure 40a: Summary of Ground Support in TSw2

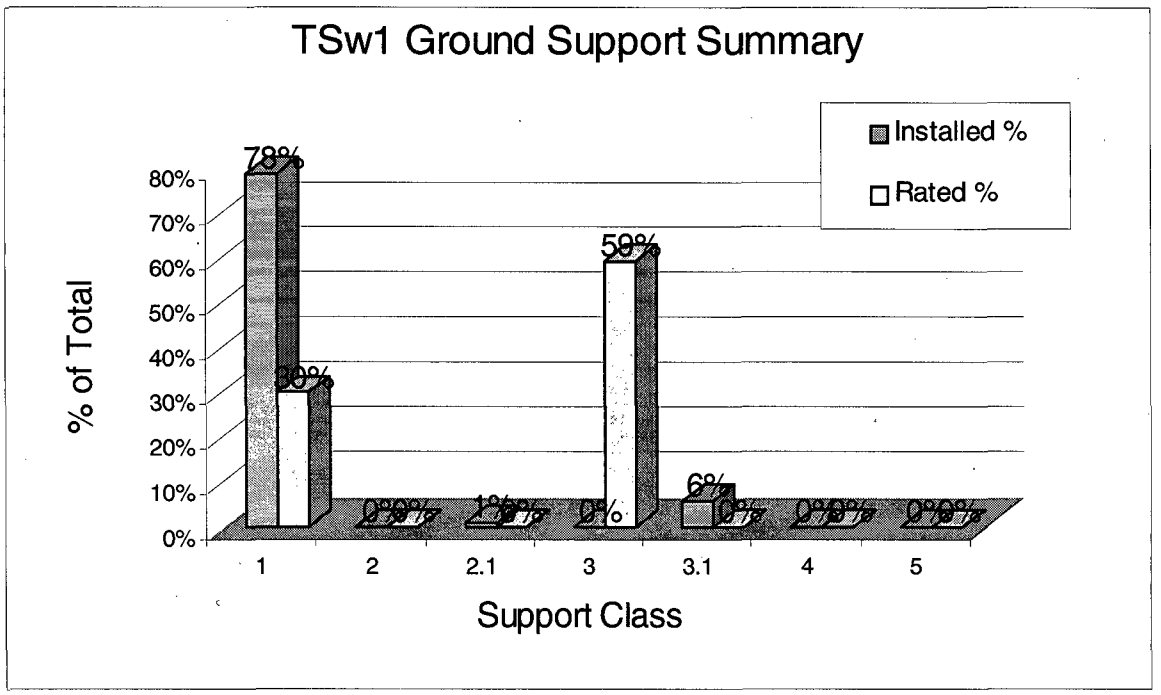

Figure 40b: Summary of Ground Support in TSw1

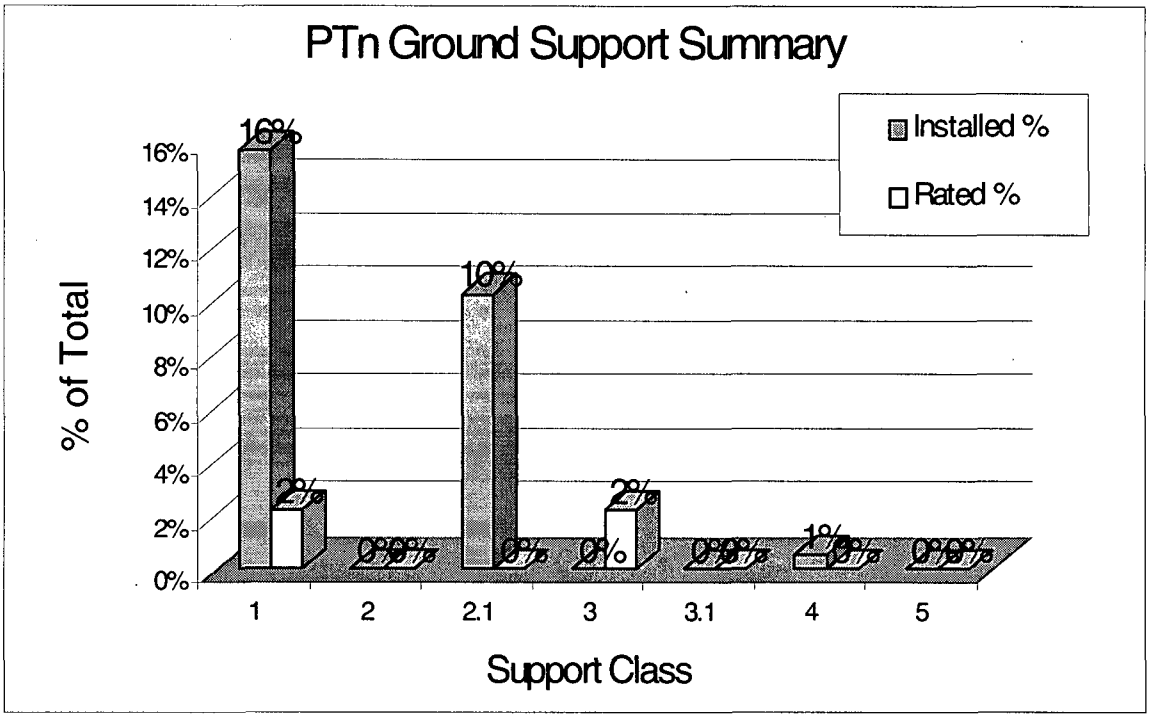

Figure 41a: Summary of Ground Support in PTn

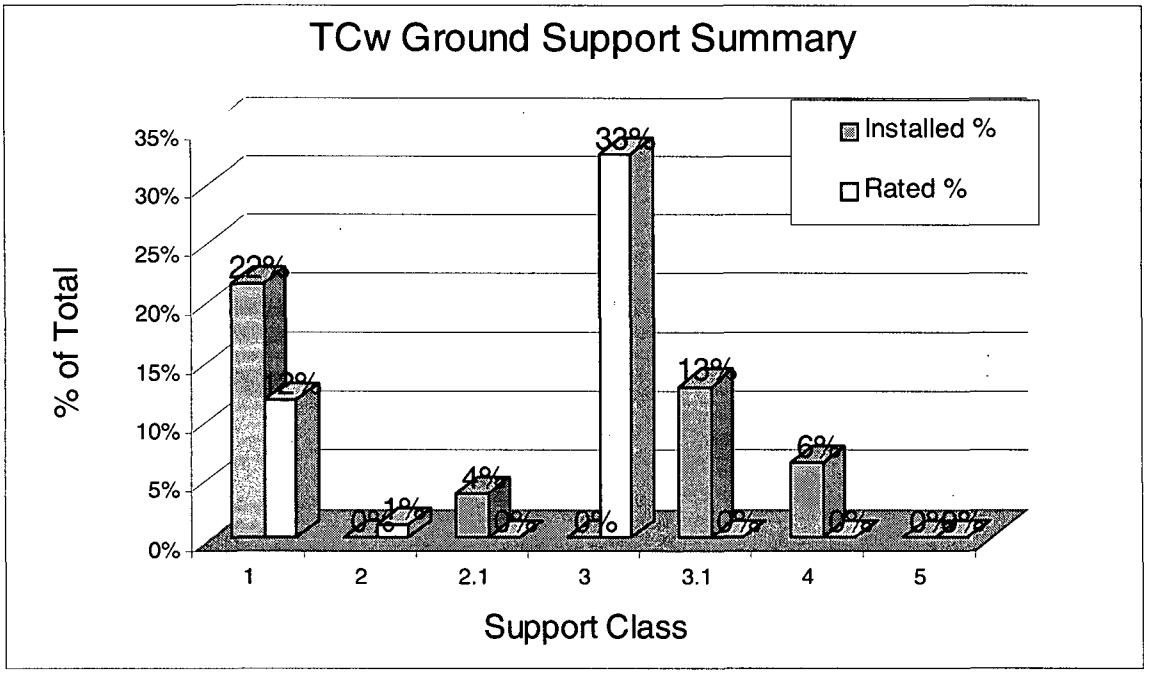

Figure 41b: Summary of Ground Support in TCw

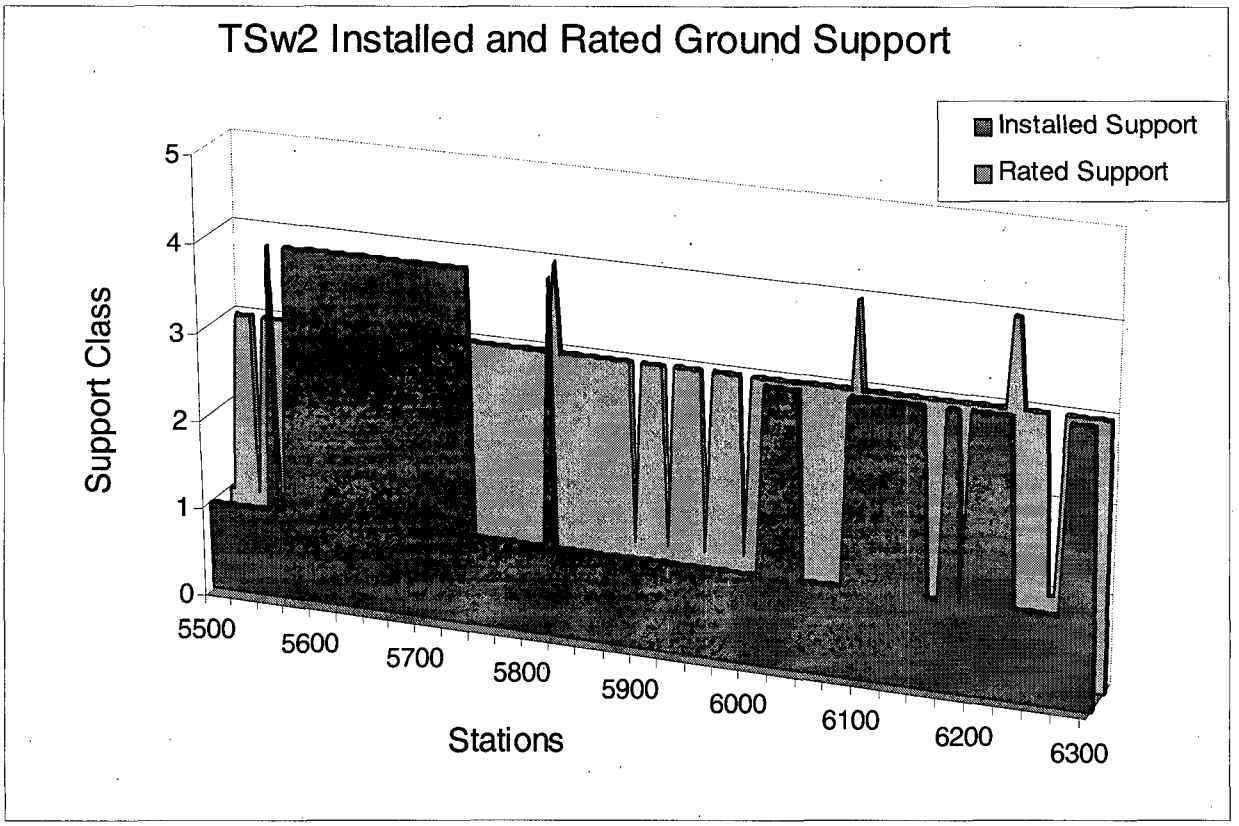

Figure 42a: TSw2 Installed and Rated Ground Support

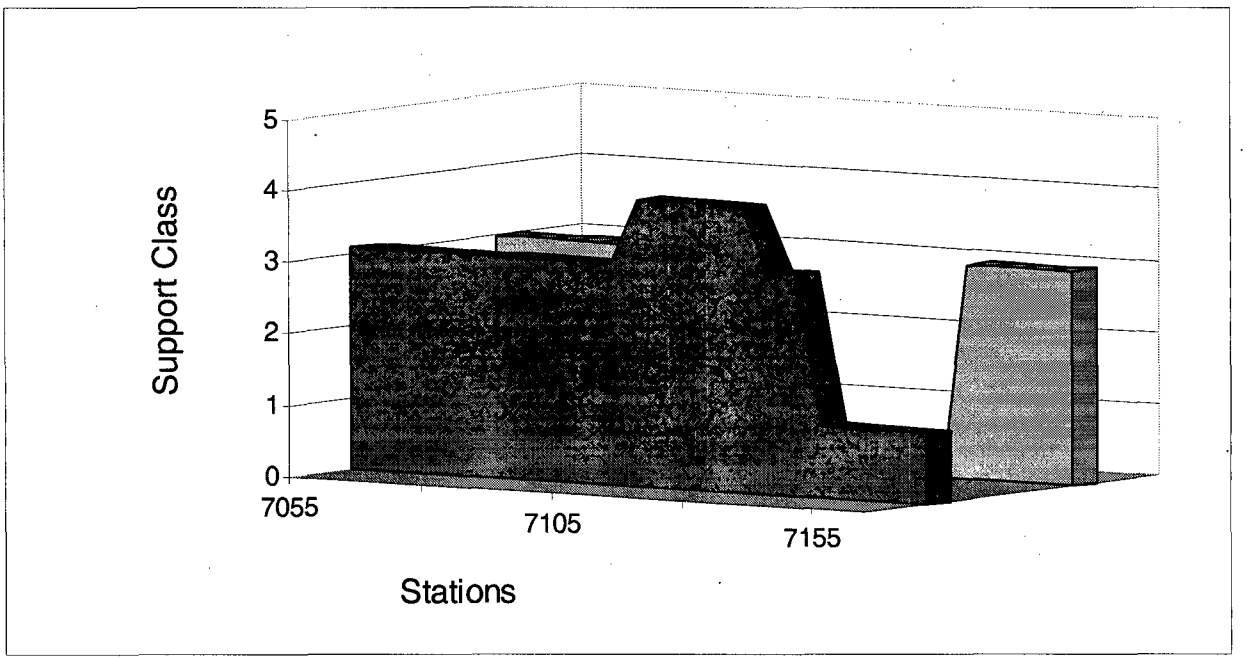

Figure 42b: TSw2 Installed and Rated Ground Support Continued

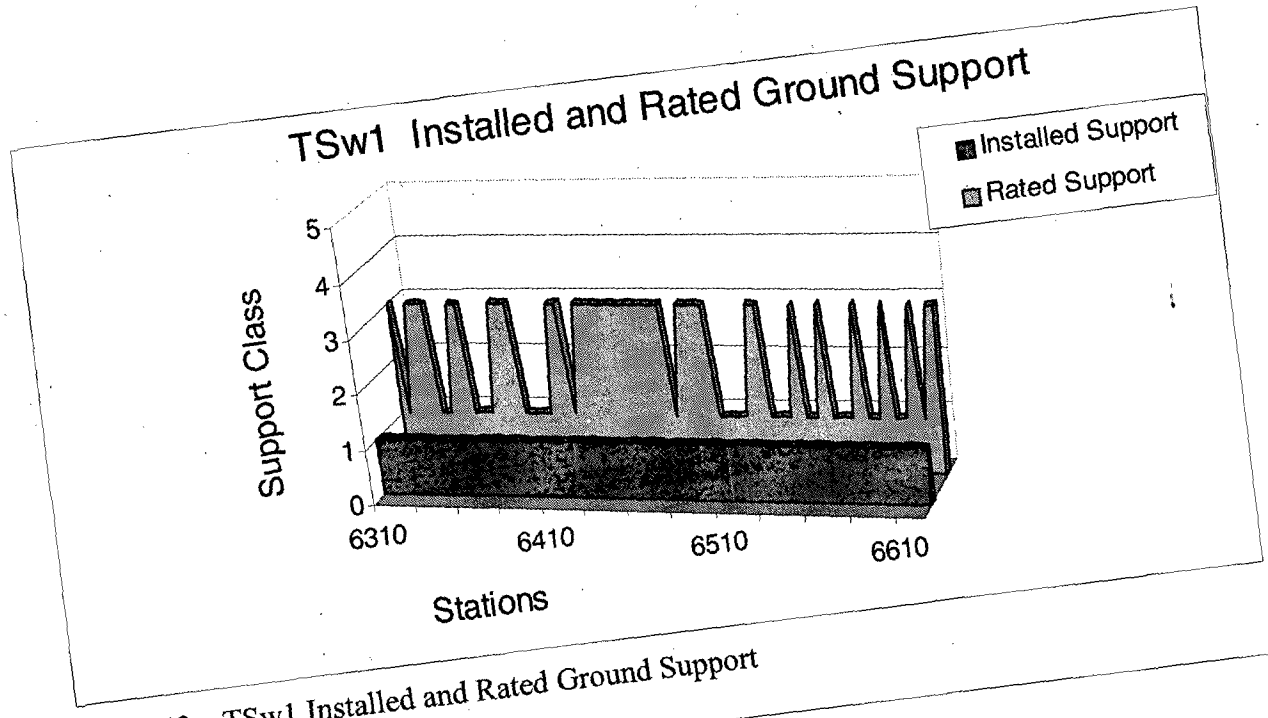

Figure 43a: TSw1 Installed and Rated Ground Support

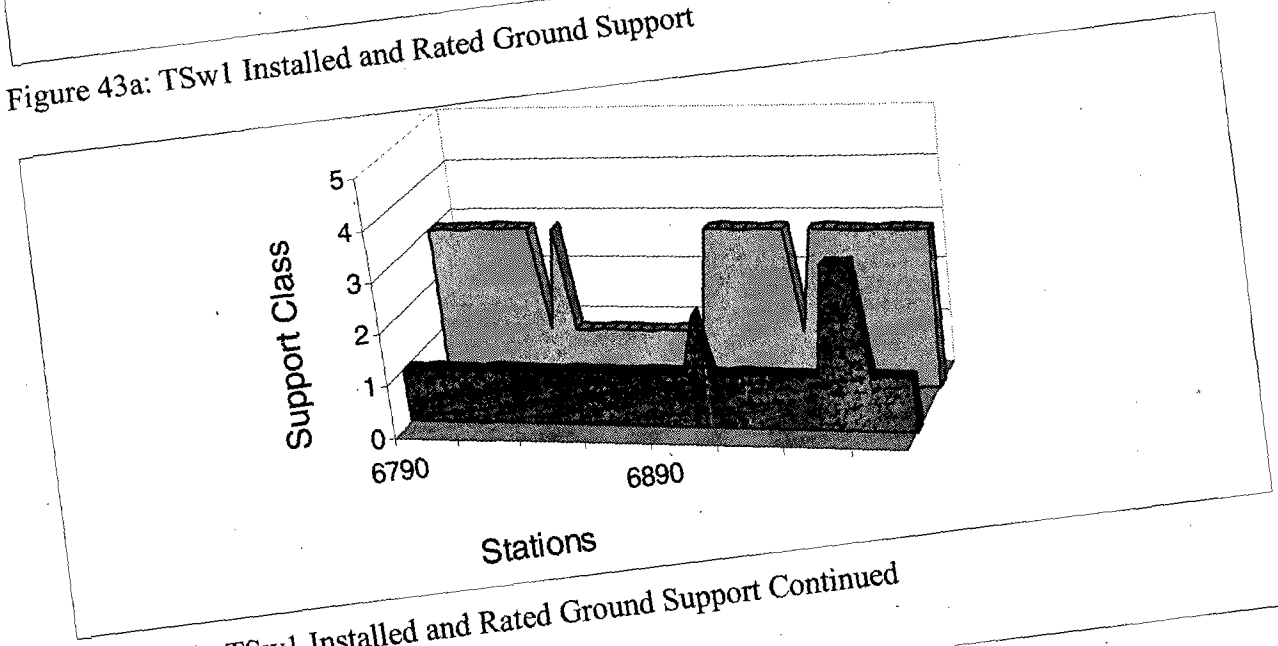

Figure 43b: TSw1 Installed and Rated Ground Support Continued

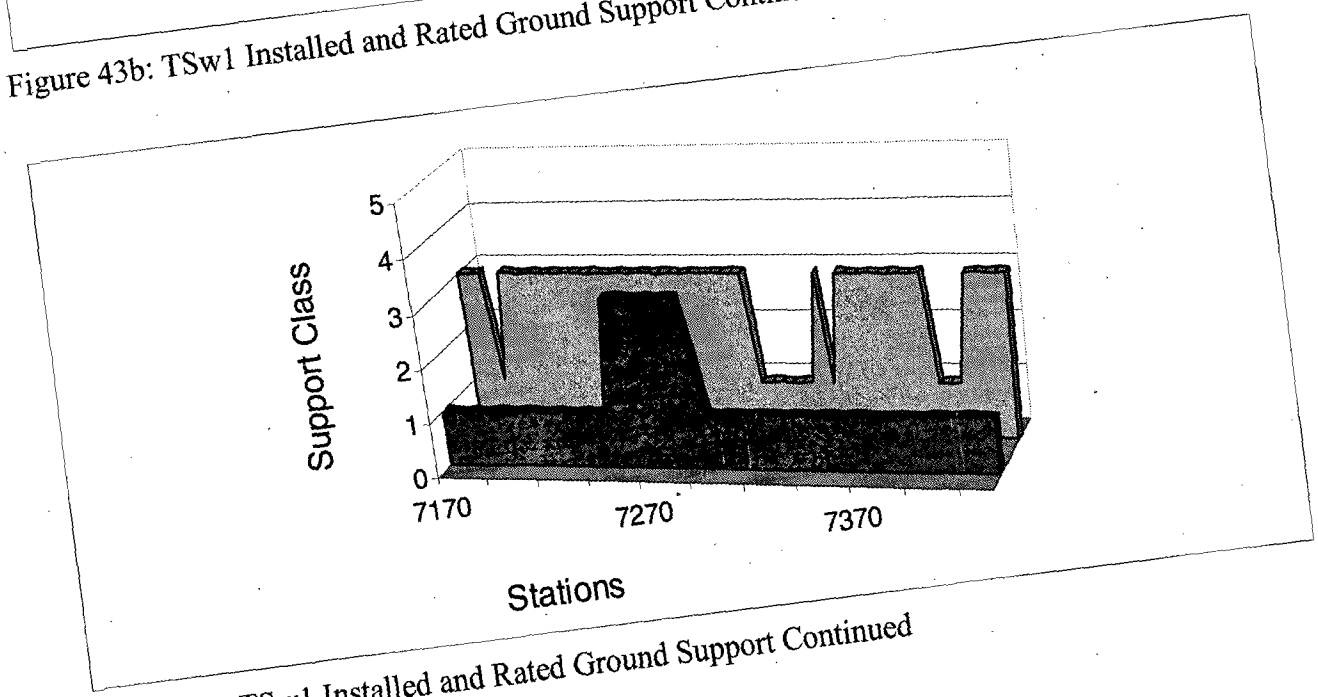

Figure 43c: TSw1 Installed and Rated Ground Support Continued

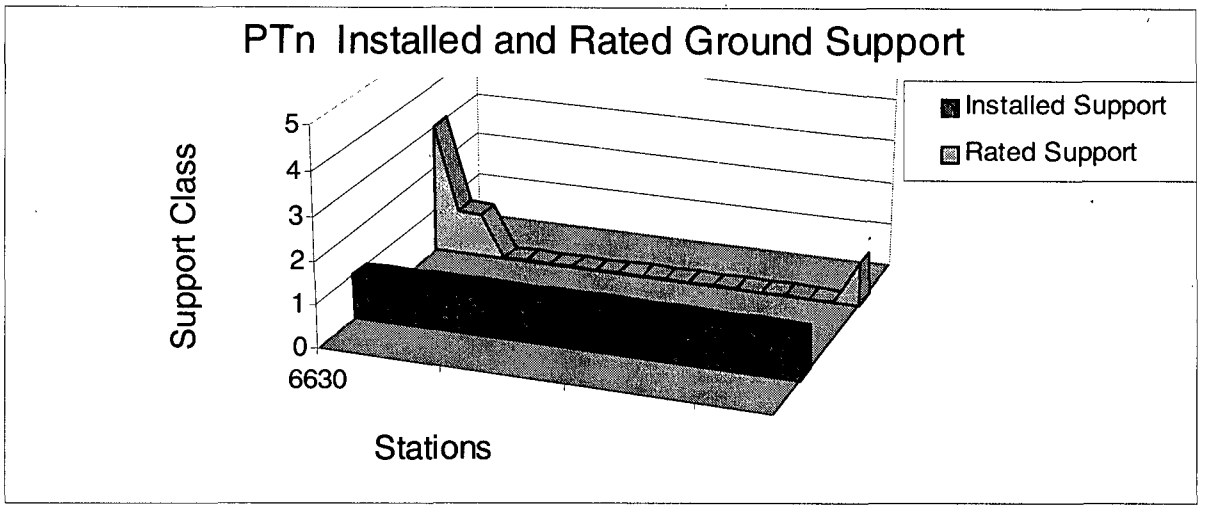

Figure 44a: PTn Installed and Rated Ground Support

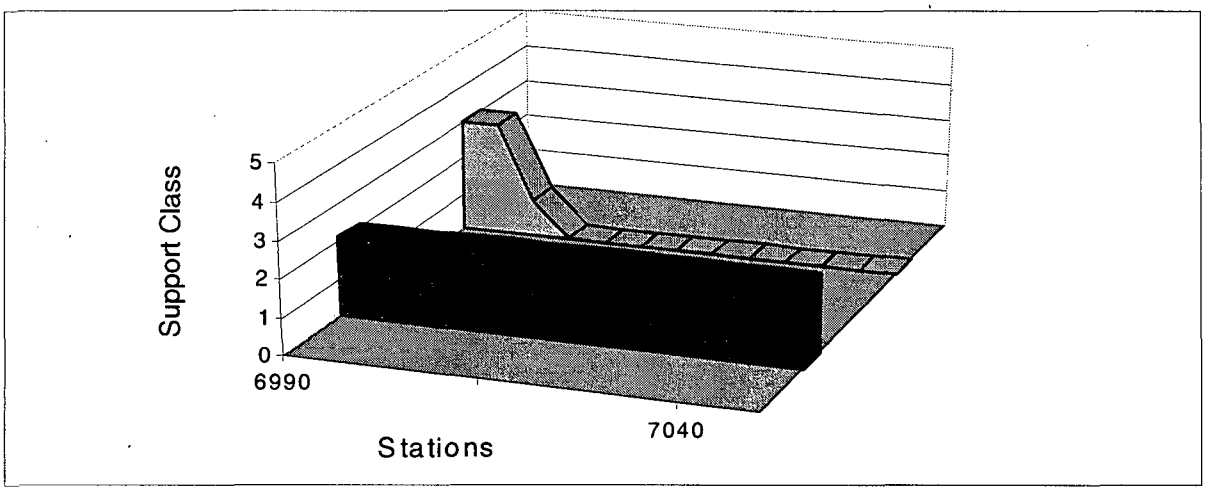

Figure 44b: PTn Installed and Rated Ground Support Continued

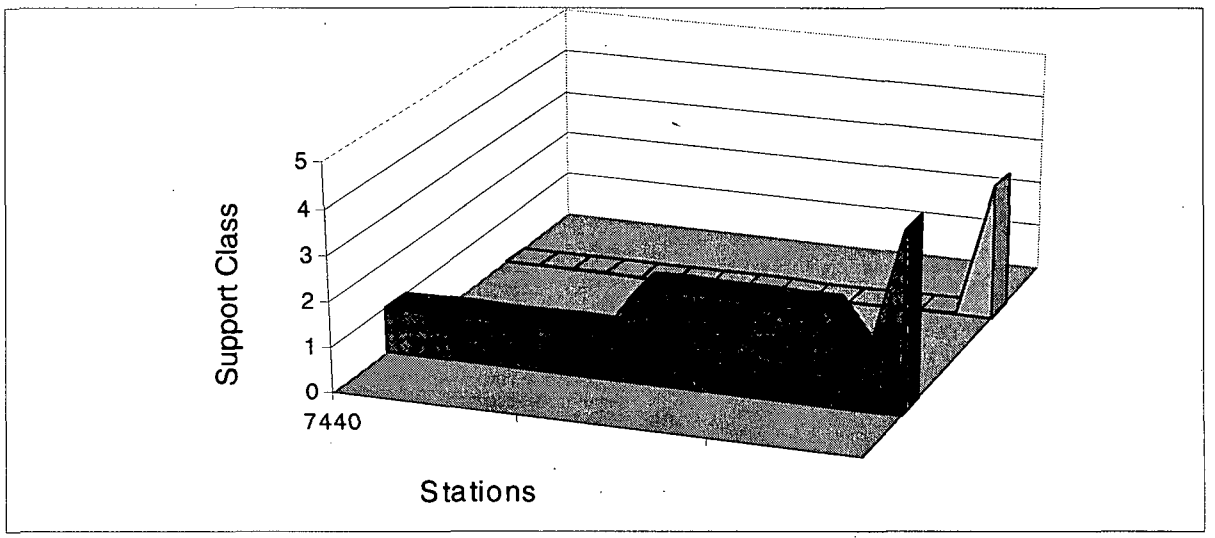

Figure 44c: PTn Installed and Rated Ground Support

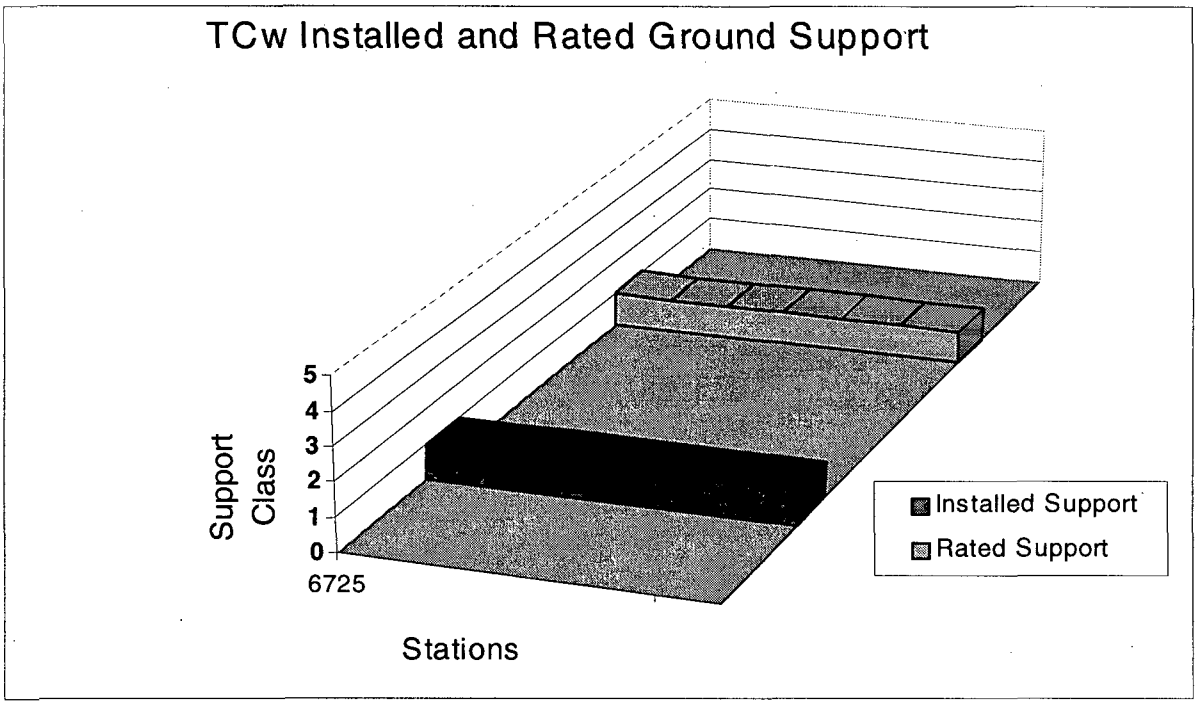

Figure 45a: TCw Installed and Rated Ground Support

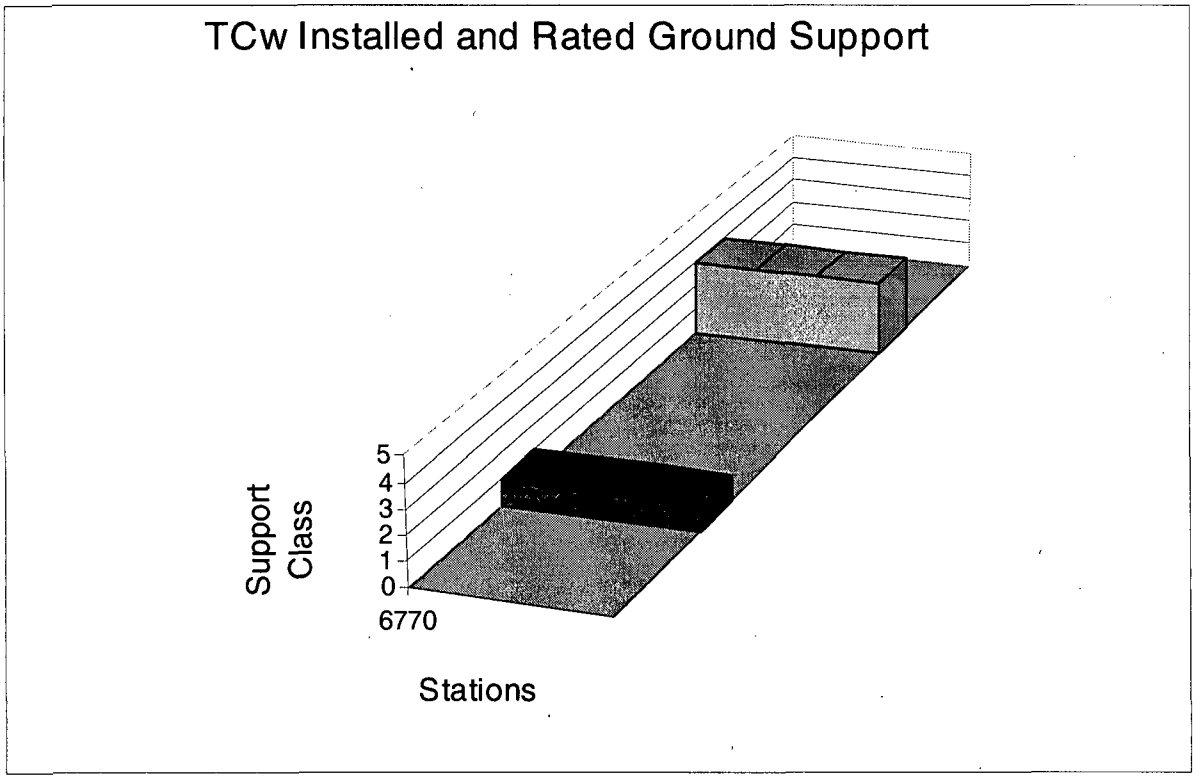

Figure 45b: TCw Installed and Rated Ground Support Continued

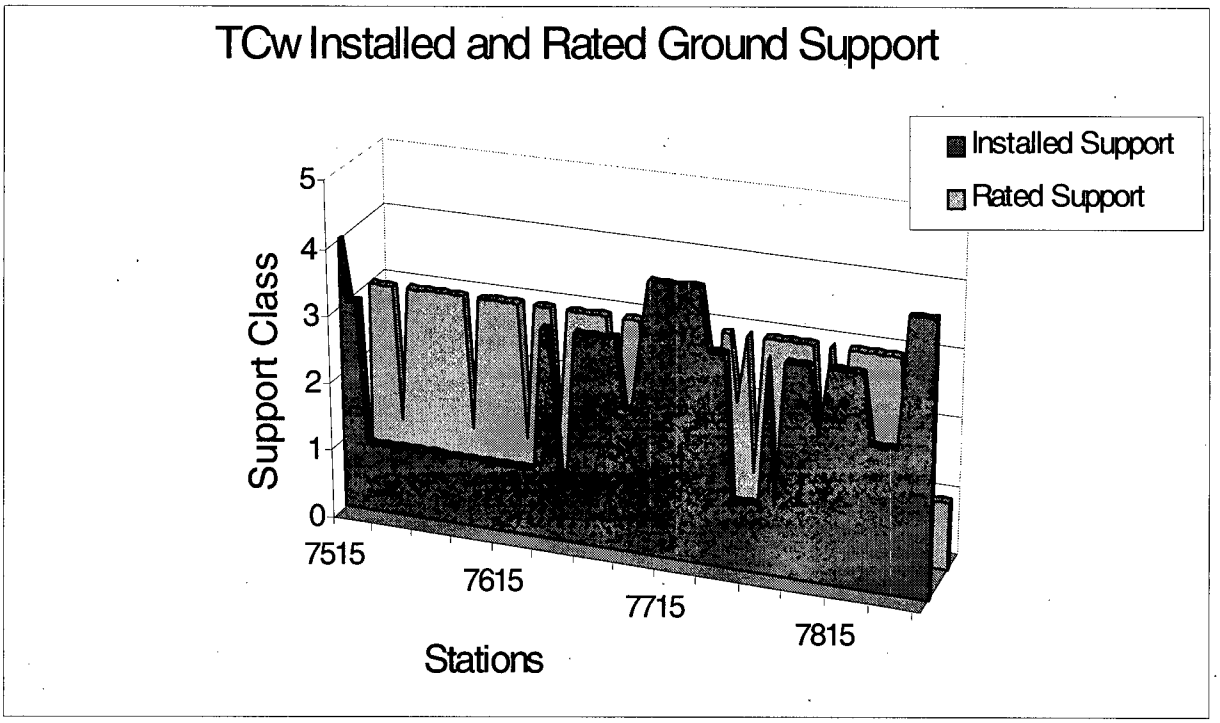

Figure 46: TCw Installed and Rated Ground Support Continued

Summary of Ground Support

The following paragraphs provide more detail on the apparent discrepancy between theoretically rated and installed ground support. These paragraphs broadly describe areas which may warrant consideration for additional ground support. While calculation of the theoretical support requirement suggests a significant interval of the tunnel may require additional support, the decision to add ground support should be based on an analysis of the excavation. Considerations include the nearly undamaged periphery due to TBM excavation, the results of tunnel instrumentation, and environmental factors (i.e., long-term dust control).

Class of Support	No. Meters	Rated percent	No. Meters	Installed percent
1	440	21%	1535	65%
2	15	1%	0	0%
2a	0	0%	140	6%
3	1665	78%	0	0%
3a	0	0%	425	18%
4	20	1%	275	12%
5	0	0%	0	0%

Table 16: Rated and Installed Ground Support in the South Ramp

TSw2

Within the TSw2, this section has an mean Q value of 1.8 (*poor*) and a mean block-size ratio (RQD/Jn) of 6.3. The summary of 5-m sections, Figure 40a, shows 92 percent class 3 ground support is required in the TSw2, where only 50 percent of class 3 or 3a is actually installed. ESF TS North Ramp Ground Support Guidelines indicate that for rock quality Q between 1.0 and 4.0 and RQD/Jn < 10 class 3 support or up to class 2 quantity of rockbolts is required.

- Based on mean rated Q parameters and Figure 42a, the rated class 3 or 3a support appears to be required in the Tptpll (Sta. 57+30 - 58+80) and just beyond to about Sta. 60+50. This could be considered for additional ground support. From about Sta 60+50 thru 63+10, installed support appears to be adequate. However, these empirical systems don't accurately quantify lithophysal zones as in the Tptpll.

- The median Q ratings provide a more accurate picture of the tunnel, however, using a median Q of 1.27 and a block-size ratio of 5.8 makes no difference in recommendations. Additional ground support will not be required through most of this section.

TSw1

Throughout the South Ramp the TSw1, has a mean rated Q value of 5.8 (*fair*) and a median block-size ratio (RQD/Jn) of 10.8. The ESF TS North Ramp Ground Support Guidelines indicate that for Q ratings between 5.5 and 10.0 and RQD/Jn $\geq$10, class 1 support is required. Using the median Q values of 3.1 and a block-size ratio of 9.1 provides a different perspective to the overall support requirements. The ESF TS North Ramp Ground Support Guidelines indicate that for Q ratings between 1.0 and 4.0 and RQD/Jn < 10, class 3 support or up to class 2 quantity of rock bolts is required. This borderline case overall area is depicted in Figure 40b, where percent class 3 ground support is required.

- In 30 percent of this section, the installed support equals or exceeds the theoretical support requirement (30 percent rated class 1).

- Average values imply significant intervals of class 1 support in this reach. The difference between rated support and installed support in this section may be resolved by review of the theoretical support-rating system. A significant portion of the 5 meter Q values are above 5.5, and RQD/Jn values greater than 10 would

require class 1 support. Q values below 4.0, RQD/Jn values less than 10 would indicate class 3 support. The averages fall in a range between the border of class 1 to class 3 support. Additional ground support would not be required through most of this section.

PTn

Within the PTn, this small section has an mean rated Q value of 4.8 and a block-size ratio (RQD/Jn) of 12.5. The ESF TS North Ramp Ground Support Guidelines indicate that for Q ratings between 4.0 and 5.5 and RQD/Jn $\geq$5, class 1 support is required. However, using the median Q values of 3.5 and a block-size ratio of 12.7 provides a slightly different perspective to the overall support requirements. The ESF TS North Ramp Ground Support Guidelines indicate that for Q ratings between 1.0 and 4.0 and RQD/Jn greater than 10, class 2 support is required. This borderline case overall area is depicted in Figure 41a, where support appears to be adequate.

- Based on average Q parameters and empirical formulas, the rated class 2 support appears to be on the borderline with class 1. Additional ground support will not be required through most of this section, however, for long-term stability, additional rock bolts should be considered.

TCw

Within the TCw, this section has an mean rated Q value of 4.6 and a block-size ratio (RQD/Jn) of 6.4. The ESF TS North Ramp Ground Support Guidelines indicate that for Q ratings between 4.0 and 5.5 and RQD/Jn greater than 5, class 1 is required. But using the more representative median value of 3.0 and an RQD/Jn ratio of 7, better represents the Q ratings. This would require class 3 support or at least up to class 2 quantity of rock bolts.

- Based on average Q parameters and empirical formulas, the Tpcpln from about

Sta 75+15 thru 76+15 requires additional ground support. The rest appears to be sufficient.

Summary and Conclusions

Rock Mass Quality

Table 17 summarizes representative ratings for each of the thermal units judged to represent central values. Along with tabulation of the mean and median rock quality ratings, the distribution of these ratings were discussed previously. Mean values are considered to be representative except in the Q ratings. Median Q ratings in the TSw1, PTn, and TCw appear to better represent the true picture.

Conclusions

- Those sections of the PTn thermal-mechanical unit which could be rated have a mean RMR of 61 (*good*) rock quality, and a median Q rating of 3.5 (*poor*) quality rock mass.

- Over three-fourths of the PTn is unrated. Of the rated sections, empirical formulas, at best, provide a questionable guide in such soft material. These unrated sections of PTn may exhibit long term deformations which cannot be evaluated by observation.

- In the South Ramp the TSw2 thermal-mechanical unit contains two stratigraphic units with significantly different fracture frequencies represented by RQD. The addition of measures of fracture orientation, shear strength and stress conditions tends to compensate for RQD differences. Mean RMR ratings of 54 indicate a

MECHANICAL UNIT	STRATIGRAPHY	Meters Rated	REPRESENTATIVE RATINGS			
			Mean RQD	Mean RMR	Mean Rated Q	Median Rated Q
TSw2		890	53	54	1.8	1.3
	Tptpmn	740	59	56	1.9	1.5
	Tptpll	150	24	46	1.1	1.0
TSw1		790	62	54	5.8	3.1
	Tptpul	335	43	48	3.1	2.3
	Tptrl	130	54	53	10.0	6.8
	Tptrn	325	85	61	6.8	3.7
PTn (rated areas)		50	88	61	4.8	3.5
	Tptrv	30	87	61	5.5	4.1
	Tpcpv	20	92	59	3.8	3.8
TCw		417	73	60	4.6	3.0
	Tpcpln	145	81	58	5.6	4.2
	Tpcpmn	235	69	61	2.8	1.8
	Tpcpul	37	61	63	13.0	14.6

Table 17: Representative Rock Mass Quality Ratings for Mechanical Units (South Ramp)

fair quality rock mass. Based on a median Q of 1.3 the TSw2 is described as *poor* quality rock mass.

- Thermal-mechanical unit TSw1 contains the best quality rock mass in the South Ramp. Of the three stratigraphic units in TSw1, Tptpul has the lowest average ratings. High ratings in all three units, Tptpul, Tptrl and Tptrn often exceed a Q value of 10. An RMR average rating of 54 indicates a *fair* quality rock mass. The median Q rating is 3.1 defining a *poor* quality rock mass.

- The TSw1 contains the highest quality rock mass encountered in the South Ramp excavation.

- The TCw is the second best quality rock encountered in the South Ramp with an overall median of 3.0 *poor*.

- The qualitative rock mass description *poor* does not infer performance problems in the excavation; quite the opposite is true as noted in the following conclusions. The qualitative descriptions result directly from the numerical evaluation of the rock mass.

- Based on Q ratings, the theoretical ground support requirement is that 79 percent of the interval of South Ramp should be Class 2 or heavier support. Class 1 support was actually installed in 65 percent of the South Ramp. It is not the conclusion of this report that ground support in the South Ramp is inadequate. Ground support generally appears to be adequate. It is assumed that the differences in installed and theoretical support may be almost entirely reconciled when the beneficial effect of the tunnel boring machine excavation is evaluated.

ADDITIONAL FEATURES

Description of Alcoves 5, 6 and 7

Alcoves 5, 6, and 7 were excavated from the Main Drift toward the east (Fig. 47). All of the Alcoves are entirely within the Tptpmn. The Alcoves were excavated primarily with an Alpine Miner with some drill and blast. The Alcoves were excavated to conduct a variety of scientific tests. Alcove 5 is primarily devoted to heating experiments but also includes a plate loading drift. Alcoves 6 and 7 were excavated to assess the characteristics of the Ghost Dance fault which is parallel to and approximately 150 m east of the Main Drift. Scientific tests including hydrochemistry tests and hydrologic properties of the fault are being conducted. Full-Periphery Geologic Mapping, Detail Line Surveys, and Stereo Photography were done in all the Alcoves.

Alcove 5

Alcove 5, located at Sta. 28+27, consists of several drifts. The Access Observation Drift extends from the Main Drift on a bearing of 108° for approximately 133 meters. The drift descends on a -11.5 percent slope, approximately parallel to and approximately 6.5 m below the top of the TSw2 thermal-mechanical unit, the Tptpul/Tptpmn lithostratigraphic contact.

There are no significant lithological differences between the rock exposed in Alcove 5 and that exposed in the Main Drift adjacent to Alcove 5. For description and discussion of the lithology, fracture, fault and other characteristics of the Main Drift in the ESF, see Albin and others (1997). Because Alcove 5 is only a few meters below the contact with the Tptpul, lithophysal cavities and vapor-phase partings are relatively common in the alcove.

The distribution of fractures in Alcove 5 is similar to that of the Main Drift. The differences in the distribution can largely be attributed to the effects of sampling bias. The bias arises from the

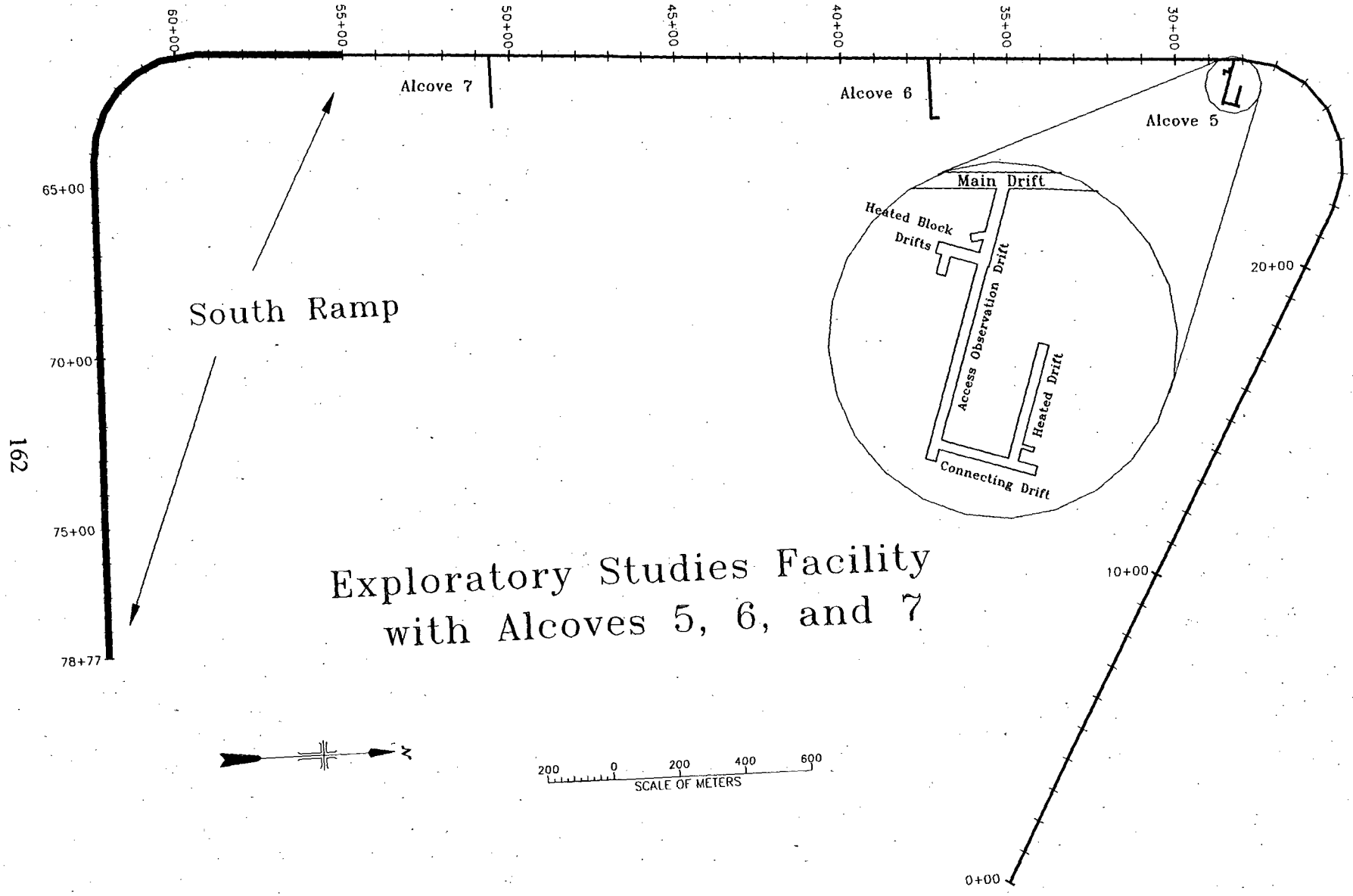
60+00
55+00
50+00
45+00
40+00
35+00
30+00
Alcove 7
Alcove 6
Alcove 5
65+00
70+00
75+00
78+77
South Ramp
Main Drift
Heated Block Drifts
Access Observation Drift
Heated Drift
Connecting Drift
20+00
10+00
0+00
Exploratory Studies Facility
with Alcoves 5, 6, and 7
N
200 0 200 400 600
SCALE OF METERS

Figure 47

tendency for fractures striking nearly parallel to the tunnel to be observed less frequently than fractures striking more directly across the tunnel. This bias is evident when the stereonet plots of fracture data from Alcove 5 and the Main Drift near Alcove 5 are compared (Fig. 48). On stereonet plots, poles representing fractures striking parallel to the tunnel plot at right angles to the bearing of the tunnel and poles representing fractures striking across the tunnel plot near the bearing of the tunnel. A comparison of the two plots reveals that there are more data points plotting near the arrows indicating the bearing of the tunnel, or alcove, and fewer points 90° to the right or left of the arrows than are plotted in the same area. This bias is also evident in plots of data from the individual drifts in Alcove 5 (not shown).

The sampling bias can be nullified by combining data from traverses that are at high angles to each other. The bearing of the Access-Observation drift in Alcove 5 is 75° from that of the Main Drift. The drifts that comprise Alcove 5 form a rectangular network (Fig. 47). By combining data from the Main Drift and Alcove 5, the sampling bias is effectively eliminated. The stereonet plot of the combined data (Fig. 49) shows well-defined clusters representing the four sets of fractures identified in the Main Drift in the area of Alcove 5 (p. 34 Albin and others 1997). Set 1 is the most prominent and is comprised of fractures striking 118° ±15° and dipping greater than 70°. Sets 2 consists of fractures striking 220° ± 20° and dipping greater than 70°. Poles representing Set 3 fractures cluster near the center of the stereonet. Set 3 fractures strike 310° ±30° and dip less than 30°. Set 4 fractures strike similarly to Set 3 fractures, 300° ±20° and dip between 30° and 60°. A fifth cluster centered at 92° represents a set of fractures that strike 182° ± 15° is prominent in Fig. 49. This set of fractures does not appear as a cluster in Fig. 48(a) or elsewhere in the Main Drift where collection of this data would be greatly effected by the sampling bias. Data collected in Alcove 5 nullified the effect of the bias and revealed the presence of this set of fractures.

Drill holes were drilled in arrays from the Access Observation Drift toward the heated drift. Examination of down-hole videos taken in those drill holes reveal that lithophysal cavities are present. Borehole fractures oriented similar to fractures mapped in the alcove can be projected

48a

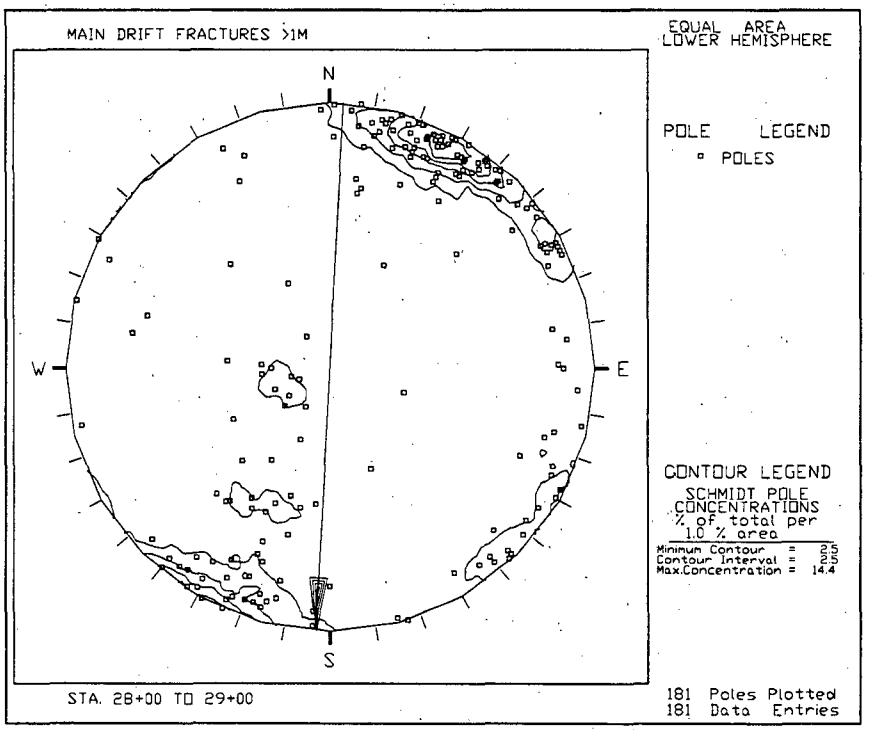

48b

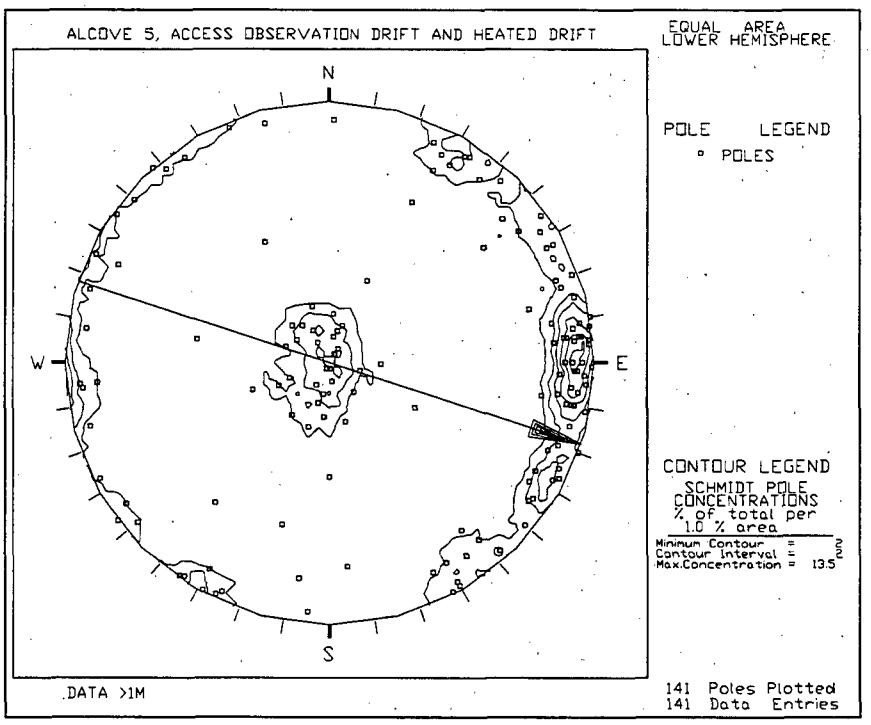

Figure 48. Stereonet plots of DLS data from the Main Drift between Sta. 28+00 and 29+00 (48a) and Alcove 5 (48b). The Alcove 5 data shown was collected in the Access-Observation Drift and the Heated Drift. The two drifts are parallel to each other and at a 75° angle to the Main Drift. The arrows indicate the bearing of the Main Drift and the drifts in the alcove. A comparison of the two stereonets shows a general similarity in the distribution of poles. The differences in the two plots can largely be attributed to a sampling bias. The effect of the bias can be seen by comparing the two plots. In each stereonet, more poles plot near the arrow than in the same location on the accompanying plot. Conversely, there are fewer poles plotting approximately 90° from the arrow than in the accompanying plot.

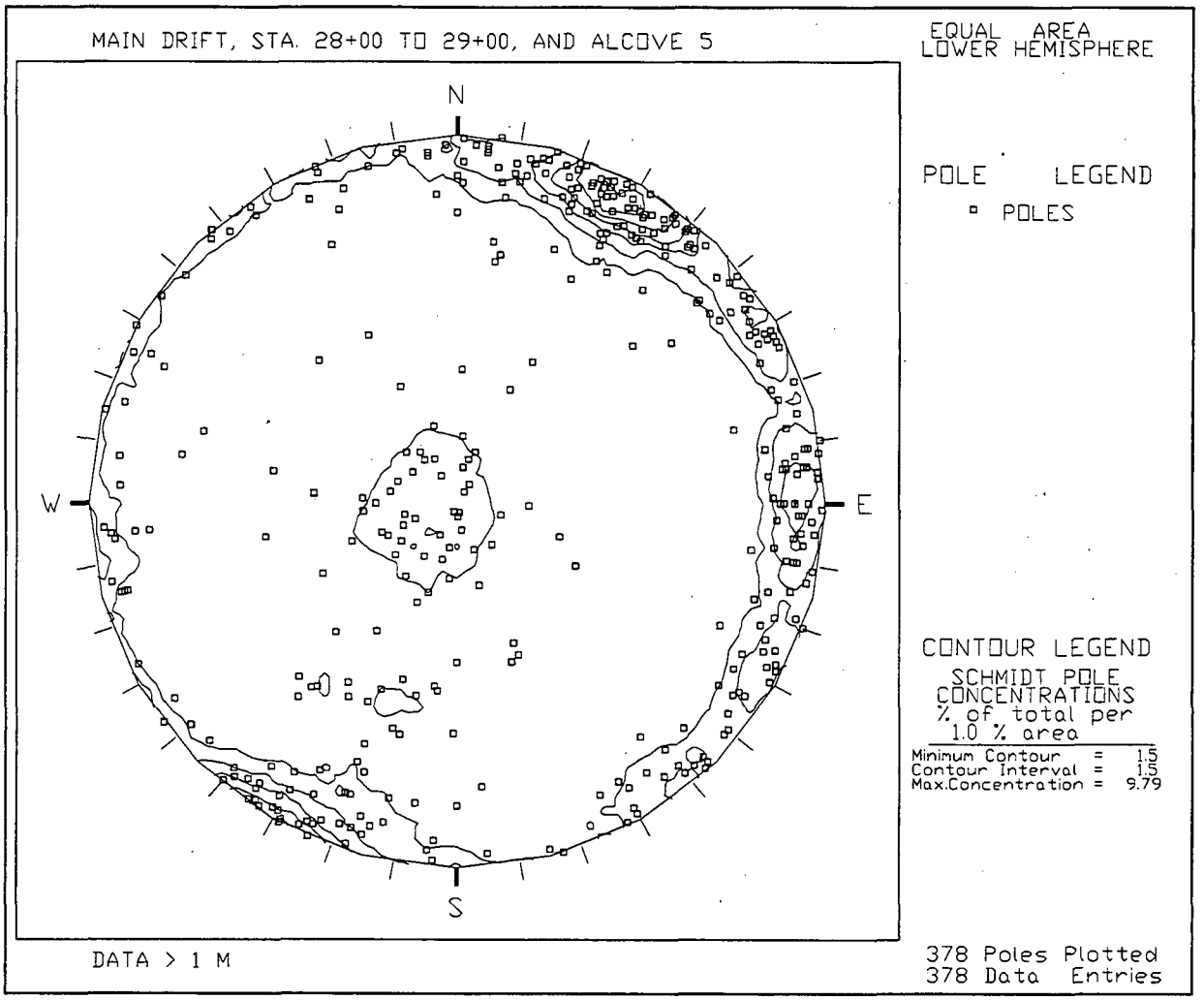

Figure 49. The stereonet showing data from the Main Drift between Sta. 28+00 and 29+00 combined with data from all of the drifts in Alcove 5 has a distribution that more closely represents the actual distribution of fractures in that area. The sampling bias has largely been nullified by combining several orthogonal or nearly orthogonal transects from Alcove 5 and the adjacent Main Drift.

to their mapped locations in the alcove.

Few faults and shears were observed in Alcove 5; two are in Set 1, two are in Set 2 and three are random. One Set 1 fault has left lateral offset. The two Set 2 shears had one reverse and one normal offset.

Alcove 6

Alcove 6, at Sta. 37+37, extends 160 m from the Main Drift on a bearing of 90° and a -5 percent slope. Alcove 6 was initially excavated to Sta. 1+34, less than 20 m from the Ghost Dance fault. A hole was drilled horizontally from the end of the alcove across the fault to conduct hydrologic and other tests. Alcove 6 was then extended across the fault to approximate Sta. 1+64. A side drift approximately 20-m long was excavated at the end of Alcove 6 on a bearing of 000°.

There is no significant lithologic difference between the rock exposed in Alcove 6 and that exposed in adjacent areas of the Main Drift. The distribution of fractures in Alcove 6 is similar to that seen in the Main Drift (Fig. 50). The sampling bias, discussed above in relation to the Alcove 5 data, is also evident in the comparison figures. The fifth set of fractures identified in the Alcove 5 data does not appear as a cluster in Alcove 6, although Alcove 6 data does include fractures that would be included in that set.

The DLS recorded 9 faults and 29 shears in Alcove 6. Three faults and three shears are in Set 1. One normal and three reverse offsets were observed and one set of slickensides raking 9° was observed. In Set 2, there are 2 faults and 10 shears. Three normal, four reverse and one right lateral offset was observed. Two Set 3 shears were present, both with reverse offset. Random faults and shears are the most numerous, 4 and 14 respectively. Normal offsets outnumber reverse offsets by a 2 to 1 margin. The relative numbers of faults and shears in the four sets and the offsets are comparable to that found in the Main Drift in the area of Alcove 6.

50a

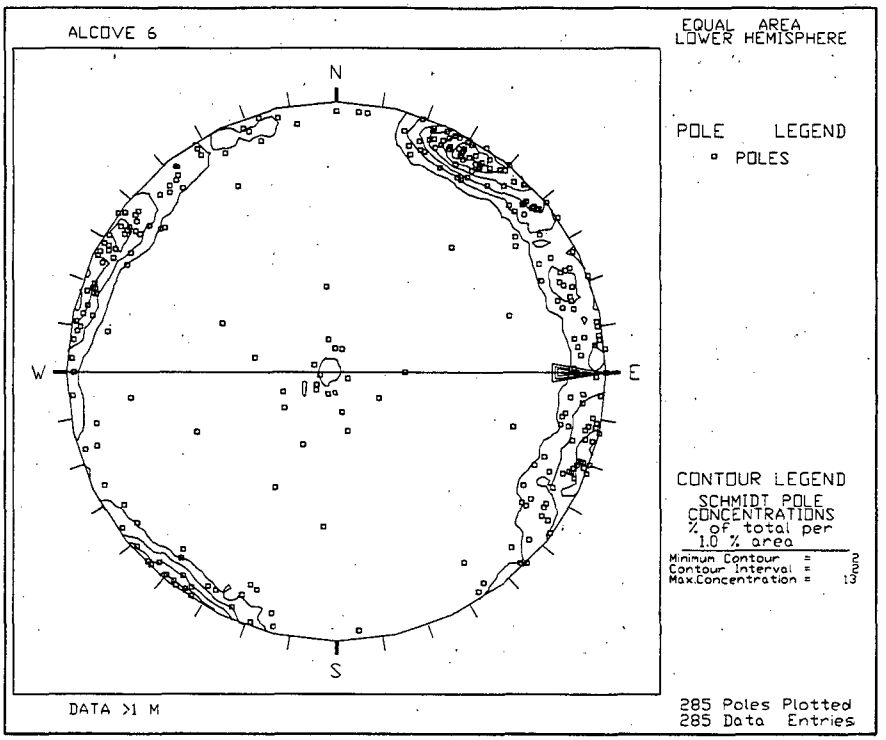

50b

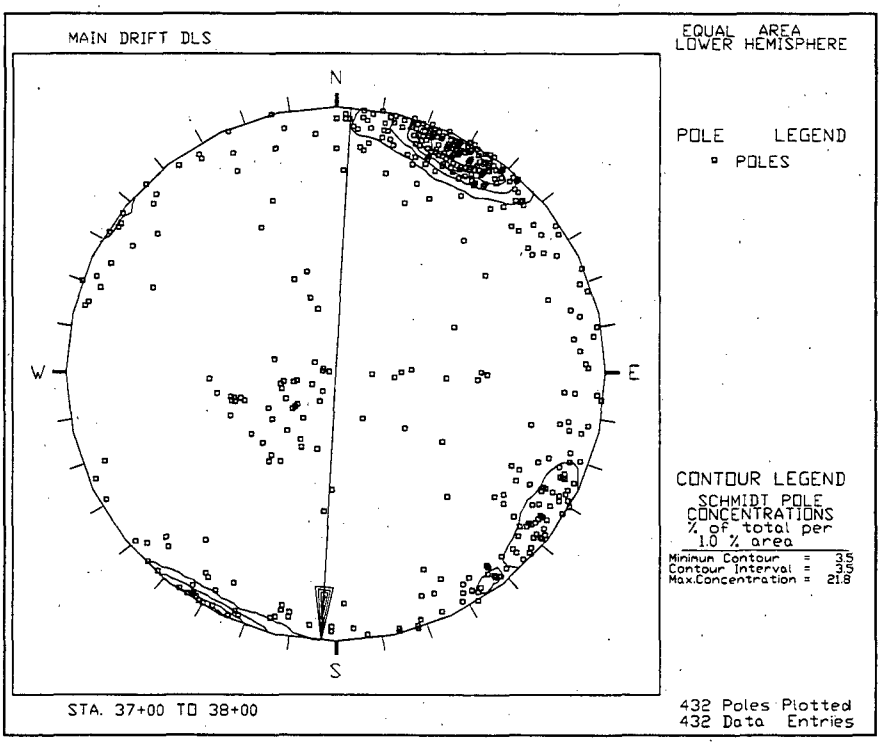

Figure 50. Stereonet plots of Alcove 6 (50a) and the Main Drift between Sta. 37+00 and 38+00 (50b). The arrows indicate the bearing of the Main Drift and Alcove 6. The distributions shown in the two plots are generally similar. The differences in the two plots can largely be attributed to sampling bias, as described above.

Description of the Ghost Dance fault in Alcove 6

The fault zone intercepts the right (south) wall of Alcove 6 (Northern Ghost Dance Fault Alcove) between Sta. 1+52.1 and 1+52.7 at springline. The zone contains 0.6-1m-thick matrix-supported, uncemented fault breccia derived from the wall rock. Orientation of the fault at 180°/80° on the footwall, and 175°/82° on the hanging wall. Distinct planes along the hanging wall and footwall are not evident, and no slickensides were visible. The breccia is approximately 60 percent matrix composed primarily of clay- to sand-size particles; and approximately 40 percent angular to subangular rotated clasts to 20 cm in size. Average clast size is approximately 5 cm, and clasts are derived from the wall rock. No secondary calcite or silica/opal are visible in the breccia or surrounding rock.

The wall rock on both sides of the fault is densely welded, devitrified, rhyolitic composition, ash-flow tuff of the Topopah Spring, crystal-poor, middle nonlithophysal zone. The rock on either side of the breccia is intensely fractured, but the characteristics of the fracturing differ from the footwall to the hanging wall. The footwall is very intensely fractured for a distance of about 1 m diminishing to slightly fractured over a distance of 4 m. The wall rock has a crushed appearance, with tight, anastomosing fractures of relatively short trace length. For a distance of about 10 m the hanging wall is moderately to intensely fractured, but the fractures tend to be long, discrete fracture surfaces of various orientations. Many of the fractures in the hanging wall have measurable apertures. The rock in the hanging wall is intact, with pumice and lithic fragments clearly visible.

Alcove 7

Note: *Alcove 7 data are preliminary (subject to change); the data have not been technically reviewed.* Alcove 7, the Southern Ghost Dance fault access drift was excavated to conduct tests including hydrochemistry tests and hydrologic properties of faults. Alcove 7, at Sta. 50+64, extends 145 m from the Main Drift on a bearing of 90° and a +6.7 percent slope.

Alcove 7 is within the fracture zone exposed in the Main Drift between Sta. 42+00 and 51+50. Fracturing in Alcove 7 is similar, both in orientation and intensity, to that observed in the Main Drift adjacent to Alcove 7. The stereonet of DLS data from Alcove 7 shows a strong cluster of poles representing fractures striking between 120° and 155° (Fig.51). These are the Set 1 fractures that make up the Fracture Zone. Fracture density is as high as 11 fractures per meter, the average is nearly 5 fractures per meter. Set 2 and 3 fractures are also present but in far fewer numbers than Set 1 fractures. Set 1 fractures make up over 77 percent of all fractures while Sets 2 and 3 make up approximately 7 percent and ½ percent respectively. Approximately 15 percent are random fractures.

Four faults and 60 shears are present in Alcove 7. Unlike the distribution of fractures, Set 2 faults and shears make up a majority with 35 faults and shears. There are 22 Set 1 faults and shears and 7 random shears. Set 3 shears are not present in Alcove 7. The greatest offset was 0.20 m normal offset on a Set 1 fault. Offsets on Set 1 faults and shears is predominantly normal. Left lateral offsets predominate on Set 2 faults and shears with some normal offsets.

Damp Areas in the South Ramp

During the excavation of the South Ramp, the tunnel walls appeared completely dry for most of the length of the ramp. Some limited areas were damp at the time of excavation. In each of these areas, the excavation surface was damp prior to cleaning of the walls for geologic mapping. At none of these locations was "free" water observed, i.e. no running or dripping water was present at the time of excavation. The concentrations of water were frequently observed near the base of the Tiva Canyon Tuff (Tpcpv1), or near the stratigraphic top of the Tiva Canyon, crystal-poor, vitric, just below the densely welded portion of the ash-flow unit. At two locations, damp areas were also associated with individual discontinuities in the densely welded Tiva Canyon and Topopah Spring Tuffs.

At Sta. 66+91, dampness was observed on the right wall of the excavation, along a pair of small

51a

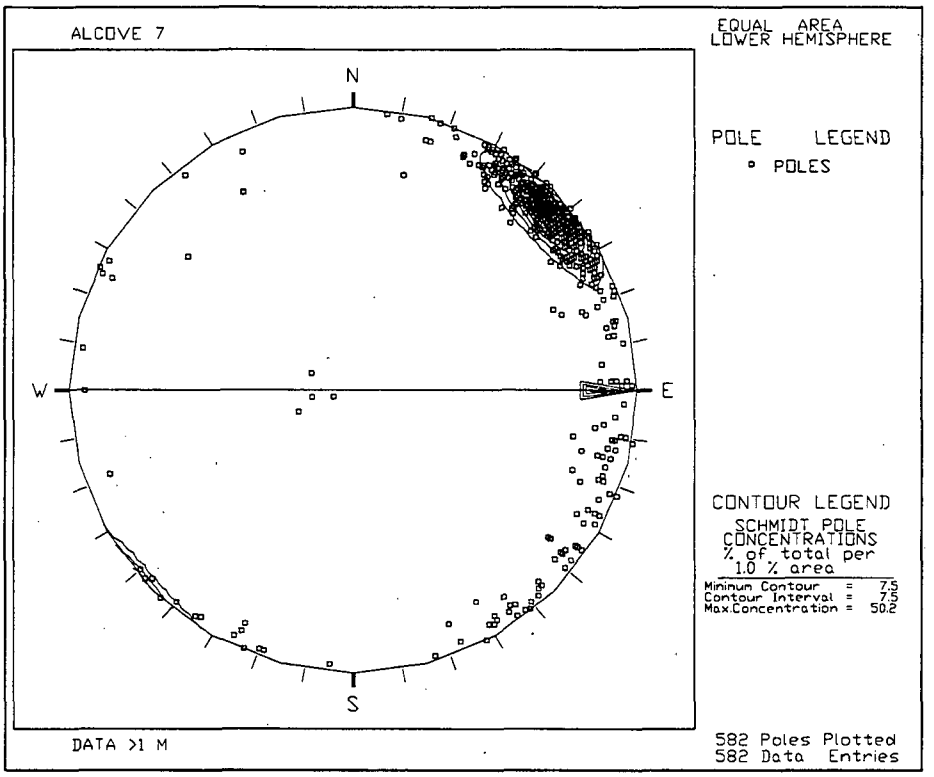

51b

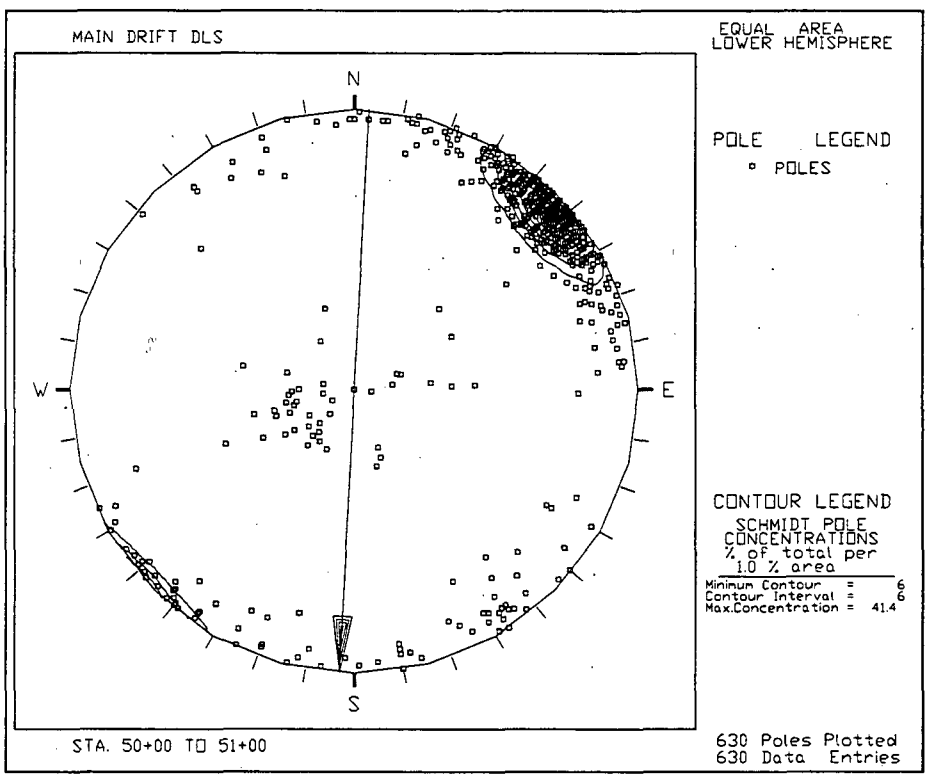

Figure 51. Stereonet plots of Alcove 7 (51a) and the Main Drift between Sta. 50+00 and 51+00 (51b). The arrow indicates bearing of the Main Drift and Alcove 6. The distributions shown in the two plots are generally similar. The differences in the two plots can be largely attributed to sampling bias, as described above.

faults oriented 329°/71° and 318°/57°. The faults have 0.1 m and 0.19 m normal offset, respectively, and are 10-20 cm apart. These faults intersected a stratigraphic contact between the pre-Tiva bedded tuffs (Tpbt4) and the nonwelded, reworked fall deposits of the pre-Yucca Mountain Tuff bedded tuff (Tpbt3), about 1 m above the right wall springline. This area originally was damp along these two faults which extended about 10 cm horizontally from the faults.

At Sta. 66+95 to 67+01, a damp zone is present paralleling the contact noted above, dipping about 17° toward the portal. This contact is about 1 to 1.2 m below the stratigraphic base of the Tiva Canyon Tuff (Tpcpv1) which is marked by a basal lag deposit about 4 cm thick. The damp zone appeared just below the pre-Tiva bedded tuffs (Tpbt4) in nonwelded, reworked fall deposits of the pre-Yucca Mountain Tuff bedded tuff (Tpbt3)(see Plate 4). For detailed descriptions of these units see p. 24 and 26. The top of the damp zone follows the dipping upper contact of the Tpbt3.

Another damp area was encountered in the base of the Tiva Canyon Tuff crystal-poor, lower nonlithophysal zone (Tpcpln) between Sta. 67+32 and 67+35. The moisture was usually present just below the change in the Tpcpln from densely welded (above) to moderately welded. Across this change in welding, the porosity changes slightly from approximately 8 percent in the densely welded material to approximately 30 percent in the moderately welded material (Flint and others, 1997). The changes in matrix porosity result directly from the change in welding (see Tiva Canyon Tuff, Features of Welding, Secondary Crystallization, and Alteration, p.23). The observed zone of dampness on the wall follows this densely welded/moderately welded boundary exactly, climbing up the wall along the dip of the boundary, about 17° to the east. Dampness was visible on both walls at the time of excavation (Oct. 1996), but by July, 1997, dampness was only apparent on the right wall.

At Sta. 70+58, a fault is present which juxtaposes the pre-Pah bedded tuffs (Tpbt2) against the Topopah Spring crystal-poor, middle nonlithophysal zone. At the time of excavation, and continuing to July 1997, the fault rubble and gouge zone remain damp. The fault is oriented

approximately 170°/60°. The fault is composed of clayey gouge and fault rubble varying from 20 cm thick on the right wall up to 80 cm thick on the left wall. The damp area is limited to the fault zone proper, and does not appear to extend into the surrounding rock on either side of the fault. For more information on this fault refer to the description on p. 67.

At Sta. 72+43, moisture was observed along a fracture oriented approximately 205°/85°. The fracture is in the Topopah Spring Tuff, crystal-poor middle nonlithophysal zone, continuous across the width of the tunnel, tight along most of the trace, and has no visible secondary mineralization.

At Sta. 74+95, a damp zone was observed along the right wall. This stratigraphic horizon is the same as the damp zone at Station 67+00, the contact between the pre-Yucca Mountain Tuff bedded tuffs (Tpbp3) and the pre-Tiva Canyon Tuff bedded tuffs (Tpbt4). On the left wall at this location (75+00) a damp zone is present at a slightly higher stratigraphic position, just below the contact between the pre-Tiva Canyon Tuff bedded tuffs (Tpbt4) and the base of the Tiva Canyon Tuff (Tpcpv1). On both walls the damp zone is 10-20 cm high and generally parallels and engulfs the dipping contact.

At Sta. 76+08, dampness was observed along a distinct breccia-filled fracture oriented 184°/81°. The breccia varies from <1cm near the right wall invert to 15 cm just above the right springline. The breccia is clast supported with maximum clast size approximately 20 cm; the clasts are derived from the wall rock -- the Tiva Canyon crystal-poor, middle nonlithophysal zone. The clasts are angular and slightly rotated. The matrix is composed mostly of calcite with minor amounts of opal/silica, and is generally white and non-crystalline. The matrix includes about 20 percent sand to gravel-size particles (less than 10 cm). The fracture is tight over most of the tunnel perimeter, but has apertures up to 4 cm in the upper right side of the crown. Moisture was observed during mapping near these open portions of the fracture.

A fault was encountered near Sta. 76+32 oriented 144°/71°. The fault has less than 1 m normal

offset, but contains a rather large breccia zone across much of the tunnel. The breccia is 30-80 cm thick, and primarily clast-supported. The clasts are angular and derived primarily from the Tiva Canyon Tuff, crystal-poor, middle nonlithophysal zone of the wall rock. Maximum clast size is about 30 cm. The matrix is primarily sand and silt-sized particles, and is uncemented. The feature was damp at the time of mapping (March 1997), but had dried out by July, 1997.

"Breathing" Fracture at Station 74+36

On April 24, 1997 a feature at Sta. 74+36 along the right wall was observed to be "exhaling" significant amounts of cool air. The ambient temperature in the tunnel (near the TBM) was in the upper 80°s F and the cool air was first observed by personnel working in the geologic mapping area of the TBM because of a dramatic temperature difference from the tunnel air. This observation was coincident with the passing of a low pressure system through southern Nevada. The feature with the air flow was a small fault, oriented 157/83. Approximately 1 m below the right springline, the fault has an aperture of 1 cm, but this opening is only present along 1 m of the fracture trace length where the fault passes through the densely welded vitrophyre of the Topopah Spring Tuff, crystal-rich, vitric zone (Tptrv1). Above and below the open portions of the fault, the aperture closes to 0 cm. These tighter portions of the fault are where the fault traverses through the nonwelded portions of Tptrv1 and Tptrv2. Detailed descriptions of these and surrounding lithostratigraphy are presented on p. 41. This feature is one of several short faults in this area of the tunnel which are present primarily in the densely welded vitrophyre of the Topopah Spring Tuff. These small faults die out as they penetrate the much softer nonwelded portions of the Topopah above and below the vitrophyre. A possible explanation for the relatively short trace lengths of these faults is that they formed during cooling and welding of the Topopah Spring ash-flow sheet. Since the vitrophyre cools and becomes brittle rather quickly during cooling of the sheet, and settling and adjustment of the upper surfaces of the ash-flow would fracture the brittle vitrophyre, but the offset would be accommodated by plastic deformation in the underlying (still hot) nonlithophysal zone, and would be accommodated by shearing in the overlying nonwelded units.

Exposures in the ESF fit this "settling fault" concept. Small faults, such as the one at Sta. 74+36, typically extend into the overlying nonwelded material (Tptrv2) as smooth, small offset faults, gradually dying out in the overlying bedded tuffs. In the brittle vitrophyre, these faults typically exhibit highly irregular walls, and frequently have significant apertures. Where the vitrophyre intersects the crown in this portion of the tunnel near Station 74+25, apertures are visible in the crown up to 10 cm. Below the vitrophyre, offset along the faults decreases rapidly with depth in the underlying 4 m, often becoming indistinguishable in the crystal-rich nonlithophysal of the Topopah Spring Tuff (Tptrn). These "settling faults" were also evident in the Topopah vitrophyre in the North Ramp of the ESF, especially between Sta. 10+50 and 11+00.

The presence of air flow from the fault at Sta. 74+36 suggests a somewhat interconnected set of fractures and faults, well developed in the relatively thin vitrophyre, with a somewhat direct connection with the surface.

SUMMARY

U.S. Bureau of Reclamation personnel have collected detailed information about the lithology, structure, and geotechnical properties of the rock units at Yucca Mountain from the South Ramp of the Exploratory Studies Facility, as well as Alcoves 5, 6, and 7. These data can be used in geologic and hydrologic site characterization studies, regional interpretations, and repository design.

The pre-construction cross section and the as-built cross section are comparable. The discrepancies occur at Sta. 71+00 to 72+00 and 78+00. On the pre-construction section a down dropped block or graben is shown at around Sta. 72+00. On the as-built section there is only the fault at Sta. 71+30 with the graben pinching out above the tunnel alignment. At Sta. 78+00, surface mapping indicated a low angle reverse fault based on the geometry of the surface trace. This fault is shown as a high angle reverse fault on the as-built section, therefore this structure must be steepening with depth. In general conditions were as predicted.

From Sta. 55+00 to 78+77 there are 716 faults and shears. Of these, 710 have an offset of less than 4.0 m. The distribution of these features along this portion of the ESF is variable with the highest concentration of faults and shears around Sta. 70+00. The azimuths range from 0° to 360° with the highest concentration around 140°. Of the six faults with over 4.0 m of offset, three are significant. The Dune Wash fault at Sta. 67+87.25 has about 52 m of down the west offset. The Ghost Dance fault at Sta. 57+30 has about 1.2 m of down-to-the west offset. The fault at Sta. 70+58 has about 50 m down-to-the west offset.

This portion of the ESF is characterized by frequent changes in lithology due to faulting. Some of the lithologic units are repeated two or three times. Analysis identified fracture sets with similarities to the fracture sets found in the Main Drift, but with a general clockwise rotation. The dominant set in the Main Drift centered around azimuth 120° is in contrast with peaks of 122°, 138°, and 146° found in the South Ramp. The secondary set in the Main Drift is also

rotated clockwise from 220° to 241°. Comparisons of stereonet contour plots between intervals of same lithology resulted in generally similar contours with some minor variations. Between Sta. 60+00 and 62+00 a set of fractures with azimuths ranging from185 to 220° is present, which is not found in the Main Drift. This set does not come into prominence again until after Sta. 65+00 where it dominates over the fractures in the 220°- 250° range.

The bias against sampling fractures in the DLS that have strike azimuths near to the bearing of the tunnel is well illustrated on the stereonet plots of the 100 meter FPGM's. A strike azimuth vs. station scatter plot illustrating the bearing of the tunnel in the Main Drift and the South Ramp as well as in the curved section portrays the "blind zone" as well.

Three primary fracture sets are identified in most of the South Ramp fracture data by using cluster analysis. These are similar to sets identified in the Main Drift fracture data (Albin and others, 1997), and consist of northwest and northeast trending sets, and a low-angle set of fractures. Fracture orientations do not change significantly across the Drill Hole Wash fault, suggesting that rigid block rotation is not a significant factor in fracture orientations in the South Ramp. The sets in the South Ramp differ from peak fracture orientations observed in the North Ramp, and preliminary comparisons suggest a change in fracture characteristics may occur across the Dune Wash area. South Ramp Tiva Canyon Tuff fracture characteristics differ from those of the Topopah Spring Tuff. The degree of welding, crystallization, and vapor-phase alteration is not significantly different between the two tuffs, and therefore is not likely to be the explanation for this difference in fracturing. This suggests that the fracturing in the two tuffs is probably related to different stress environments.

Thermal-mechanical unit TSw1 is the best quality rock mass in the South Ramp. Nearly one-third of the PTn is unrated. These unrated sections of PTn may have long term deformations which cannot be evaluated by visual observation. Based on Q ratings, the theoretical ground support is that 79 percent of the length of the South Ramp should be Class 2 or heavier support. Class 1 support was actually installed in 65 percent of the South Ramp. It is not the conclusion of this

report that ground support in the South Ramp is inadequate. Ground support generally appears to be adequate. The differences in installed and theoretical support may be almost entirely due to the beneficial effect of the tunnel boring machine excavation is evaluated.

During the excavation of the South Ramp, the tunnel walls were dry for most of the ramp. Some areas were damp at the time of excavation. No "free" water was observed, at any of these locations, i.e. no running or dripping water was present at the time of excavation. The concentrations of water were frequently observed near the base of the Tiva Canyon Tuff (Tpcpv1), or near the stratigraphic top of the Tiva Canyon, crystal-poor, vitric, just below the densely welded portion the ash-flow unit. At two locations, damp areas were also associated with individual discontinuities in the densely welded Tiva Canyon and Topopah Spring Tuffs.

On February 27, 1997 a feature at Sta. 74+36 along the right wall was observed to be "exhaling" significant amounts of cool air. The feature transmitting the air flow was a small fault, oriented 157°/83°. Approximately 1 m below the right springline, the fault had an aperture of 1 cm, but this opening was only present along 1 m of the fracture trace length where the fault passes through the densely welded vitrophyre of the Topopah Spring Tuff, crystal-rich, vitric zone (Tptrv1). Approximately 1 m below the right springline, where the air flow was emanating, the fault had an aperture of 1 cm, but this opening was only present along 1 m of the fracture trace length where the fault passes through the densely welded vitrophyre of the Topopah Spring Tuff, crystal-rich, vitric zone (Tptrv1). Above and below the open portions of the fault, the aperture becomes tight. The presence of air flow from the fault at Station 74+36 suggests a somewhat interconnected set of fractures and faults, well developed in the relatively thin vitrophyre, with a somewhat direct connection with the surface.

REFERENCES

Albin, A. L., Singleton, W. L., Moyer, T. C., Lee, A. C., Lung, R. C., Eatman, G. L. W., and Barr, D. L., 1997, Geology of the Main Drift - Station 28+00 to 55+00, Exploratory Studies Facility, Yucca Mountain Project, Yucca Mountain, Nevada, DOE Report, DTN GS970208314224.005.

Barr, D.L., Moyer, T.C., Singleton, W.L., Albin, A.L., Lung, R.C., Lee, A.C., Beason, S.C., and Eatman, G.L.W., 1996, Geology of the North Ramp - Station 4+00 to 28+00, Exploratory Studies Facility, Yucca Mountain Project, Yucca Mountain, Nevada, DOE Report, DTN GS960908314224.020.

Barton, N., Lien, R., Lunde. J., 1974, " Engineering Classification of Rock Masses for the Design of Tunnel Support", *Rock Mechanics* vol. 6 no. 4.

Bieniawski, Z.T., 1989, " *Engineering Rock Mass Classifications*", John Wiley and Sons, New York

Broxton, D.E., Chipera, S.J., Byers, F.M., Jr., and Rautman, C.A., 1993. Geologic evaluation of six nonwelded tuff sites in the vicinity of Yucca Mountain, Nevada, for a surface-based test facility for the Yucca Mountain Project: Los Alamos National Laboratory Report LA-12542-MS, 83 p.

Buesch, D.C., Spengler, R.W., Moyer, T.C., and Geslin, J.K., 1996, Proposed stratigraphic nomenclature and macroscopic identification of lithostratigraphic units of the Paintbrush Group exposed at Yucca Mountain, Nevada: U.S. Geological Survey Open-File Report 94-469, 47 p.

Byers, F.M, Jr., Carr, M.J., Orkild, P.P., Quinlivan, W.D., and Sargent, K.A., 1976, Volcanic suites and related cauldrons of the Timber Mountain-Oasis Valley caldera complex, southern Nevada: U.S. Geological Survey Professional Paper 919, 70 p.

Cheeney, R.F., 1983, Statistical Methods in Geology, George Allen & Unwin Ltd, London UK, 169 p.

Christiansen, R.L., Lipman, P.W., Carr, M.J., Byers, F.M., Jr., Orkild, P.P., and Sargent, K.A., 1977, The Timber Mountain-Oasis Valley caldera complex of southern Nevada: Geological Society of America Bulletin, v. 88, p.943-959.

Compton, R.R., 1962, Manual of Field Geology, John Wiley & Sons, New York, New York, 378 p.

Day, W.C., Potter, C.J., Sweetkind, D.S., Dickerson, R.P., and San Juan, C.A., in press, Bedrock geologic map of the central block area, Yucca Mountain, Nye County, Nevada: U.S. Geological Survey Miscellaneous Investigation Series I-2601, 1:6,000 scale, 2 plates with text.

Deere, D.U., 1989, Rock Quality Designation (RQD) After Twenty Years, US Army Corps of Engineers.

Fisher, R.V. and Schmincke, H.U., 1984, Pyroclastic Rocks: Springer-Verlag, New York, 409 p.

Flint, L.E. and Flint. A.L., 1997, Hydrologic properties of 23 cored neutron-access boreholes, U.S. Geological Survey Open-File Report 97-XXX (in preparation).

Geological Society of America, 1991, Rock-color chart: Boulder, Colorado, Geological Society of America

Gibson, J.D., Shephard, L.E., Swan, F.H., Wesling, J.R., and Kerl, F.A., 1990, Synthesis of studies for the potential of fault rupture at the proposed surface facilities, Yucca Mountain, Nevada: Proceedings of International Topical Meeting, High Level Radioactive Waste management, April 8-12, v. 1, p. 109-116.

Gillett, S.L., 1987, Online users manual: Extract clusters from axial data sets using the algorithm of Shanley and Mahtab.

Goodman, R.E., 1980, Introduction to Rock Mechanics, John Wiley & Sons, New York, New York, 478 p.

Keith, T.E.C., 1991, Fossil and active fumaroles in the 1912 eruptive deposits, Valley of Ten Thousand Smokes, Alaska, Journal of Volcanology and Geothermal Research, vol. 45, p. 227-254.

Kirkaldie, 1987, US Dept of Agriculture, Soil Conservation Service, Engineering Division, Technical Release #71, Feb 1987, 2nd edition, "Rock Material Field Classification Procedures".

Levy, S.S., Norman, D.I., and Chipera, S.J., 1996, Alteration history studies in the Exploratory Studies Facility, Yucca Mountain, Nevada, USA: Material Research Society Symposium Proceedings, vol. 412, p. 783-790.

Lipman, P.W., Christiansen, R.L., and O'Connor, J.T., 1966, A compositionally zoned ash-flow sheet in southern Nevada: U.S. Geological Survey Professional Paper 524-F, 47 p.

M&O ESF Design Team, 1991, TS North Ramp Ground Support Master Elevation and Sections, No. BABEAB0000-01717-2100-40151.

M&O ESF Design Team, 1996, 7.2 m Tunnel Ground Support Master Sections, No. BAABEE0000-01717-2100-40151-00.

Moyer, T.C., Geslin, J.K., and Flint, L.E., 1996, Stratigraphic relations and hydrologic properties of the Paintbrush Tuff nonwelded (PTn) hydrologic unit, Yucca Mountain, Nevada: U.S. Geological Survey Open-File Report 95-397, 84 p.

Peterman, Z.E., Spengler, R.W., Singer, F.R., and Beason, S.C., 1996, Localized alteration of the Paintbrush nonwelded hydrologic unit within the Exploratory Studies Facility: Proceedings of the 7th annual conference on high-level radioactive waste management, v. 1, p. 46-47.

Priest, S.D., 1993, Discontinuity Analysis for Rock Engineering, Chapman and Hall, London UK, 473 p.

Rock, N.M.S., 1988, Numerical Geology, Springer-Verlag, Berlin, Germany, 427 p.

Rowley, P.D., Kuntz, M.A., and Macleod, N.S., 1981, Pyroclastic-flow deposits, in Lipman, P.W. and Mullineaux, D.R., eds., The 1980 eruption of Mount St. Helens, Washington: U.S. Geological Survey Professional Paper 1250, p. 489-512.

Sawyer, D.A., Fleck, R.J., Lanphere, M.A., Warren, R.G., and Broxton, D.E., 1994, Episodic volcanism in the Miocene southwest Nevada volcanic field — Stratigraphic revision, 40Ar/39Ar geochronologic framework, and implications for magmatic evolution: Geological Society of America Bulletin, vol. 106, p. 1304-1314.

Scott, R.B., 1990, Tectonic setting of Yucca Mountain, southwest Nevada, in Wernicke, B.P., ed., Basin and Range extensional tectonics near the latitude of Las Vegas, Nevada: Boulder, Colorado, Geological Society of America Memoir 176, p. 251-282.

Scott, R.B., and Bonk, J., 1984, Preliminary geologic map of Yucca Mountain, Nye County, Nevada, with geologic sections: U.S. Geologic Survey Open-File Report 84-494, (map scale 1:12000)

Schuraytz, B.C., Vogel, T.A., and Younker, L.W., 1989, Evidence for dynamic withdrawal from a layered magma body: The Topopah Spring Tuff, southwestern Nevada: Journal of Geophysical Research, vol. 94, p. 5925-5942.

Sheridan, M.F., 1970, Fumarolic mounds and ridges of the Bishop Tuff, California: Geological Society of America Bulletin, vol. 81, p. 851-868.

U.S. Bureau of Reclamation, 1988, Engineering Geology Field Manual: Government Printing Office, p. 91-93.

U.S. Bureau of Reclamation and U.S. Geological Survey, 1997, Rock Mass Classification: Technical Procedure YMP-USGS-GP-54, R0.

U.S. Bureau of Reclamation and U.S. Geological Survey, 1997, Underground Geologic Mapping: Technical Procedure YMP-USGS-GP-32, R1, 47 p.

APPENDIX I: Tunnel Terminology

The following is a list of the tunnel terms commonly used in this report.

crown	the uppermost part of the tunnel
drift	a horizontal excavation with only one entrance
heading	the excavated face (end) of the tunnel
invert	the bottom (floor) of the tunnel. In the ESF, the precast invert sections are placed in the tunnel to provide a flat working surface
portal	the tunnel entrance
right and left	refers to the right or left when facing the heading
springline	the line at which the tunnel wall breaks from sloping outward to sloping inward toward the crown. In the case of a round tunnel like the ESF, the springline is midway up the wall
station	the distance from the portal measured in meters e.g. Sta. 28+44 = 2,844 meters from the portal Note: the location of discontinuities in the ESF is given as stationing on the right springline, unless stated otherwise.
wall	the side of the tunnel

APPENDIX II: Photogrammetric Negative Numbers and Camera Locations

06/04/96	Camera Body No.	Lens No.	Position 1	Position 2	Negative Nos.	ID	Comments
	210660004	7155685	55+00.00	55+01.80	17893/17902	Wehner	ESF Tunnel
	210660004	7155685	55+03.60	55+05.40	17903/17912	Wehner	ESF Tunnel
	210660004	7155685	55+07.20	55+09.00	17913/17922	Wehner	ESF Tunnel
	210660004	7155685	55+10.80		17923/17927	Wehner	ESF Tunnel
06/05/96	Camera Body No.	Lens No.	Position 1	Position 2	Negative Nos.	ID	Comments
	210660004	7155685	55+10.80	55+12.60	17928/17937	Wehner	ESF Tunnel
	210660004	7155685	55+14.40	55+16.20	17938/17947	Wehner	ESF Tunnel
	210660004	7155685	55+18.00	55+19.80	17948/17957	Wehner	ESF Tunnel
	210660004	7155685	55+21.60	55+23.40	17958/17967	Wehner	ESF Tunnel
06/06/96	Camera Body No.	Lens No.	Position 1	Position 2	Negative Nos.	ID	Comments
	210660004	7155685	55+23.40	55+25.20	17968/17977	Wehner	ESF Tunnel
	210660004	7155685	55+27.00	55+28.80	17978/17987	Wehner	ESF Tunnel
	210660004	7155685	55+30.60	55+32.40	17988/17997	Wehner	ESF Tunnel
	210660004	7155685	55+34.20	55+36.00	17998/18007	Wehner	ESF Tunnel
06/07/96	Camera Body No.	Lens No.	Position 1	Position 2	Negative Nos.	ID	Comments
	210660004	7155685	55+36.00	55+37.80	18008/18017	Wehner	ESF Tunnel
	210660004	7155685	55+39.60	55+41.40	18018/18027	Wehner	ESF Tunnel
	210660004	7155685	55+43.20	55+45.00	18028/18037	Wehner	ESF Tunnel
06/10/96	Camera Body No.	Lens No.	Position 1	Position 2	Negative Nos.	ID	Comments
	210660004	7155685	55+45.00	55+46.80	18038/18047	Wehner	ESF Tunnel
	210660004	7155685	55+48.60	55+50.40	18048/18057	Wehner	ESF Tunnel
	210660004	7155685	55+52.20	55+54.00	18058/18067	Wehner	ESF Tunnel
	210660004	7155685	55+55.80		18068/18072	Wehner	ESF Tunnel
06/11/96	Camera Body No.	Lens No.	Position 1	Position 2	Negative Nos.	ID	Comments
	210660004	7155685	55+55.80	55+57.60	18073/18082	Wehner	ESF Tunnel
	210660004	7155685	55+59.40	55+61.20	18083/18092	Wehner	ESF Tunnel
	210660004	7155685	55+63.00	55+64.80	18093/18102	Wehner	ESF Tunnel
	210660004	7155685	55+66.60		18103/18107	Wehner	ESF Tunnel
06/12/96	Camera Body No.	Lens No.	Position 1	Position 2	Negative Nos.	ID	Comments
	210660004	7155685	55+66.60	55+68.40	18108/18117	Wehner	ESF Tunnel
	210660004	7155685	55+70.20	55+72.00	18118/18127	Wehner	ESF Tunnel
	210660004	7155685	55+73.80	55+75.60	18128/18137	Wehner	ESF Tunnel
	210660004	7155685	55+77.40	55+79.20	18138/18147	Wehner	ESF Tunnel
	210660004	7155685	55+81.00	55+82.80	18148/18157	Wehner	ESF Tunnel
06/14/96	Camera Body No.	Lens No.	Position 1	Position 2	Negative Nos.	ID	Comments
	210660004	7155685	55+82.80	55+84.60	18158/18167	USBR	ESF Tunnel
	210660004	7155685	55+86.40	55+88.20	18168/18177	USBR	ESF Tunnel
	210660004	7155685	55+90.00	55+91.80	18178/18187	USBR	ESF Tunnel
	210660004	7155685	55+93.60	55+95.40	18188/18197	USBR	ESF Tunnel
	210660004	7155685	55+97.20	55+99.00	18198/18207	USBR	ESF Tunnel
	210660004	7155685	55+00.80	56+02.60	18208/18217	USBR	ESF Tunnel

APPENDIX II: Photogrammetric Negative Numbers and Camera Locations

06/17/96	Camera Body No.	Lens No.	Position 1	Position 2	Negative Nos.	ID	Comments
	210660004	7155685	56+02.60	56+04.40	18218/18227	Wehner	ESF Tunnel
	210660004	7155685	56+06.20	56+08.00	18228/18237	Wehner	ESF Tunnel
	210660004	7155685	56+09.80	56+11.60	18238/18247	Wehner	ESF Tunnel
	210660004	7155685	56+13.40	56+15.20	18248/18257	Wehner	ESF Tunnel
	210660004	7155685	56+17.00	56+18.80	18258/18267	Wehner	ESF Tunnel
06/19/96	Camera Body No.	Lens No.	Position 1	Position 2	Negative Nos.	ID	Comments
	210660004	7155685	56+18.80	56+20.60	18268/18277	Wehner	ESF Tunnel
	210660004	7155685	56+22.40	56+24.20	18278/18287	Wehner	ESF Tunnel
	210660004	7155685	56+26.00	56+27.80	18288/18297	Wehner	ESF Tunnel
	210660004	7155685	56+29.60	56+31.40	18298/18307	Wehner	ESF Tunnel
	210660004	7155685	56+33.20	56+35.00	18308/18317	Wehner	ESF Tunnel
	210660004	7155685	56+36.80	56+38.60	18318/18327	Wehner	ESF Tunnel
	210660004	7155685	56+40.40	56+42.20	18328/18337	Wehner	ESF Tunnel
06/20/96	Camera Body No.	Lens No.	Position 1	Position 2	Negative Nos.	ID	Comments
	210660004	7155685	56+42.20	56+44.00	18338/18347	Unglesbee	ESF Tunnel
	210660004	7155685	56+45.80	56+47.60	18348/18357	Unglesbee	ESF Tunnel
	210660004	7155685	56+49.40	56+51.20	18358/18367	Unglesbee	ESF Tunnel
	210660004	7155685	56+53.00	56+54.80	18368/18377	Unglesbee	ESF Tunnel
	210660004	7155685	56+56.60	56+58.40	18378/18387	Unglesbee	ESF Tunnel
	210660004	7155685	56+60.20	56+62.00	18388/18397	Unglesbee	ESF Tunnel
	210660004	7155685	56+63.80	56+65.60	18398/18407	Unglesbee	ESF Tunnel
06/21/96	Camera Body No.	Lens No.	Position 1	Position 2	Negative Nos.	ID	Comments
	210660004	7155685	56+65.60	56+67.40	18408/18417	USBR	ESF Tunnel
	210660004	7155685	56+69.20	56+71.00	18418/18427	USBR	ESF Tunnel
	210660004	7155685	56+72.80	56+74.60	18428/18437	USBR	ESF Tunnel
	210660004	7155685	56+76.40	56+78.20	18438/18447	USBR	ESF Tunnel
	210660004	7155685	56+80.00	56+81.80	18448/18457	USBR	ESF Tunnel
06/24/96	Camera Body No.	Lens No.	Position 1	Position 2	Negative Nos.	ID	Comments
	210660004	7155685	56+81.80	56+83.60	18458/18467	Wehner	ESF Tunnel
	210660004	7155685	56+85.40	56+87.20	18468/18477	Wehner	ESF Tunnel
	210660004	7155685	56+89.00	56+90.80	18478/18487	Wehner	ESF Tunnel
	210660004	7155685	56+92.60	56+94.40	18488/18497	Wehner	ESF Tunnel
	210660004	7155685	56+96.20	56+98.00	18498/18507	Wehner	ESF Tunnel
	210660004	7155685	56+99.80	57+01.60	18508/18517	Wehner	ESF Tunnel
	210660004	7155685	57+03.40	57+05.20	18518/18527	Wehner	ESF Tunnel
	210660004	7155685	57+07.00	57+08.80	18528/18537	Wehner	ESF Tunnel
06/25/96	Camera Body No.	Lens No.	Position 1	Position 2	Negative Nos.	ID	Comments
	210660004	7155685	57+08.80	57+10.60	18538/18547	Wehner	ESF Tunnel
	210660004	7155685	57+12.40	57+14.20	18548/18557	Wehner	ESF Tunnel
	210660004	7155685	57+16.00	57+17.80	18558/18567	Wehner	ESF Tunnel
	210660004	7155685	57+19.60	57+21.40	18568/18577	Wehner	ESF Tunnel
	210660004	7155685	57+23.20	57+25.00	18578/18587	Wehner	ESF Tunnel
	210660004	7155685	57+26.80	57+28.60	18588/18597	Wehner	ESF Tunnel
	210660004	7155685	57+30.40	57+32.20	18598/18607	Wehner	ESF Tunnel

	210660004	7155685	57+34.00	57+35.80	18608/18617	Wehner	ESF Tunnel
	210660004	7155685	57+37.60	57+39.40	18618/18627	Wehner	ESF Tunnel
06/26/96	Camera Body No.	Lens No.	Position 1	Position 2	Negative Nos.	ID	Comments
	210660004	7155685	57+39.40	57+41.20	18628/18637	Wehner	ESF Tunnel
	210660004	7155685	57+43.00	57+44.80	18638/18647	Wehner	ESF Tunnel
	210660004	7155685	57+46.60	57+48.40	18648/18657	Wehner	ESF Tunnel
	210660004	7155685	57+50.20	57+52.00	18658/18667	Wehner	ESF Tunnel
	210660004	7155685	57+53.80	57+55.60	18668/18677	Wehner	ESF Tunnel
	210660004	7155685	57+57.40	57+59.20	18678/18687	Wehner	ESF Tunnel
06/27/96	Camera Body No.	Lens No.	Position 1	Position 2	Negative Nos.	ID	Comments
	210660004	7155685	57+59.20	57+61.00	18688/18697	Wehner	ESF Tunnel
	210660004	7155685	57+62.80	57+64.60	18698/18707	Wehner	ESF Tunnel
	210660004	7155685	57+66.40	57+68.20	18708/18717	Wehner	ESF Tunnel
	210660004	7155685	57+70.00	57+71.80	18718/18727	Wehner	ESF Tunnel
	210660004	7155685	57+73.60	57+75.40	18728/18737	Wehner	ESF Tunnel
	210660004	7155685	57+77.20	57+79.00	18738/18747	Wehner	ESF Tunnel
06/28/96	Camera Body No.	Lens No.	Position 1	Position 2	Negative Nos.	ID	Comments
	210660004	7155685	57+79.00	57+80.80	18748/18757	Unglesbee	ESF Tunnel
	210660004	7155685	57+82.60	57+84.40	18758/18767	Unglesbee	ESF Tunnel
	210660004	7155685	57+86.20	57+88.00	18768/18777	Unglesbee	ESF Tunnel
	210660004	7155685	57+89.80	57+91.60	18778/18787	Unglesbee	ESF Tunnel
	210660004	7155685	57+93.40	57+95.20	18788/18797	Unglesbee	ESF Tunnjel
	210660004	7155685	57+97.00	57+98.80	18798/18807	Unglesbee	ESF Tunnel
	210660004	7155685	58+00.60		18808/18812	Unglesbee	ESF Tunnel
07/02/96	Camera Body No.	Lens No.	Position 1	Position 2	Negative Nos.	ID	Comments
	210660004	7155685	58+00.60	58+02.40	18813/18822	Wehner	ESF Tunnel
	210660004	7155685	58+04.20	58+06.00	18823/18832	Wehner	ESF Tunnel
	210660004	7155685	58+07.80	58+09.60	18833/18842	Wehner	ESF Tunnel
	210660004	7155685	58+11.40	58+13.20	18843/18852	Wehner	ESF Tunnel
	210660004	7155685	58+15.00	58+16.80	18853/18862	Wehner	ESF Tunnel
	210660004	7155685	58+18.60	58+20.40	18863/18872	Wehner	ESF Tunnel
	210660004	7155685	58+22.20	58+24.00	18873/18882	Wehner	ESF Tunnel
07/03/96	Camera Body No.	Lens No.	Position 1	Position 2	Negative Nos.	ID	Comments
	210660004	7155685	58+24.00	58+25.80	18883/18892	Wehner	ESF Tunnel
	210660004	7155685	58+27.60	58+29.40	18893/18902	Wehner	ESF Tunnel
	210660004	7155685	58+31.20	58+33.00	18903/18912	Wehner	ESF Tunnel
	210660004	7155685	58+34.80	58+36.60	18913/18922	Wehner	ESF Tunnel
	210660004	7155685	58+38.40	58+40.20	18923/18932	Wehner	ESF Tunnel
	210660004	7155685	58+42.00	58+43.80	18933/18942	Wehner	ESF Tunnel
	210660004	7155685	58+45.60		18943/18947	Wehner	ESF Tunnel
07/08/96	Camera Body No.	Lens No.	Position 1	Position 2	Negative Nos.	ID	Comments
	210660004	7155685	58+45.60	58+47.40	18948/18957	Unglesbee	ESF Tunnel
	210660004	7155685	58+49.20	58+51.00	18958/18967	Unglesbee	ESF Tunnel
	210660004	7155685	58+52.80	58+54.60	18968/18977	Unglesbee	ESF Tunnel
	210660004	7155685	58+56.40	58+58.20	18978/18987	Unglesbee	ESF Tunnel

	210660004	7155685	58+60.00	58+61.80	18988/18997	Unglesbee	ESF Tunnel
	210660004	7155685	58+63.60	58+65.40	18998/19007	Unglesbee	ESF Tunnel
	210660004	7155685	58+67.20	58+69.00	19008/19017	Unglesbee	ESF Tunnel
07/15/96	Camera Body No.	Lens No.	Position 1	Position 2	Negative Nos.	ID	Comments
	210660004	7155685	58+69.00	58+70.80	19018/19027	Wehner	ESF Tunnel
	210660004	7155685	58+72.60	58+74.40	19028/19037	Wehner	ESF Tunnel
	210660004	7155685	58+76.20	58+78.00	19038/19047	Wehner	ESF Tunnel
	210660004	7155685	58+79.80	58+81.60	19048/19057	Wehner	ESF Tunnel
	210660004	7155685	58+83.40	58+85.20	19058/19067	Wehner	ESF Tunnel
	210660004	7155685	58+87.00	58+88.80	19068/19077	Wehner	ESF Tunnel
	210660004	7155685	58+90.60	58+92.40	19078/19087	Wehner	ESF Tunnel
	210660004	7155685	58+94.20	58+96.00	19088/19097	Wehner	ESF Tunnel
	210660004	7155685	58+97.80	58+99.60	19088/19107	Wehner	ESF Tunnel
	210660004	7155685	59+01.40	59+03.20	19108/19117	Wehner	ESF Tunnel
07/16/96	Camera Body No.	Lens No.	Position 1	Position 2	Negative Nos.	ID	Comments
	210660004	7155685	59+03.20	59+05.00	19118/19127	Wehner	ESF Tunnel
	210660004	7155685	59+06.80	59+08.60	19128/19137	Wehner	ESF Tunnel
	210660004	7155685	59+10.40	59+12.20	19138/19147	Wehner	ESF Tunnel
	210660004	7155685	59+14.00	59+15.80	19148/19157	Wehner	ESF Tunnel
	210660004	7155685	59+17.60	59+19.40	19158/19167	Wehner	ESF Tunnel
	210660004	7155685	59+21.20	59+23.00	19168/19177	Wehner	ESF Tunnel
07/17/96	Camera Body No.	Lens No.	Position 1	Position 2	Negative Nos.	ID	Comments
	210660004	7155685	59+23.00	59+24.80	19178/19187	Wehner	ESF Tunnel
	210660004	7155685	59+26.60	59+28.40	19188/19197	Wehner	ESF Tunnel
	210660004	7155685	59+30.20	59+32.00	19198/19207	Wehner	ESF Tunnel
	210660004	7155685	59+33.80	59+35.60	19208/19217	Wehner	ESF Tunnel; Point of Curve at 59+35.46
	210660004	7155685	59+37.40	59+39.20	19218/19227	Wehner	ESF Tunnel
	210660004	7155685	59+41.00	59+42.80	19228/19237	Wehner	ESF Tunnel
	210660004	7155685	59+44.60	59+46.40	19238/19247	Wehner	ESF Tunnel
	210660004	7155685	59+48.20		19248/19252	Wehner	ESF Tunnel
07/18/96	Camera Body No.	Lens No.	Position 1	Position 2	Negative Nos.	ID	Comments
	210660004	7155685	00+37.	00+39.	19253/19262	Wehner	ESF Tunnel; Alcove No.5 (HTA); See Page Nos. 83 and 93
	210660004	7155685	00+41.	00+43.	19263/19272	Wehner	ESF Tunnel; Alcove No.5 (HTA); See Pages 83 and 93
	210660004	7155685	00+45.	00+47.	19273/19282	Wehner	ESF Tunnel; Alcove No.5 (HTA); see pages 83 and 93
	210660004	7155685	00+49.	00+51.	19283/19292	Wehner	ESF Tunnel; Alcove No.5 (HTA); See Pages 83 and 93
	210660004	7155685	00+53.	00+55.	19293/19302	Wehner	ESF Tunnel; Alcove No.5 (HTA); See Pages 83 and 93

	210660004	7155685	00+57.	00+59.	19303/19312	Wehner	ESF Tunnel; Alcove No.5 (HTA); See Pages 83 and 93
	210660004	7155685	00+61.	00+63.	19313/19322	Wehner	ESF Tunnel; Alcove No.5 (HTA); See Pages 83 and 93
	210660004	7155685	00+65.	00+67.	19323/19332	Wehner	ESF Tunnel; Alcove No.5 (HTA); See Pages 83 and 93
	210660004	7155685	00+69.	00+71.	19333/19342	Wehner	ESF Tunnel; Alcove No.5 (HTA); See Pages 83 and 93
	210660004	7155685	00+73.	00+75.	19343/19352	Wehner	ESF Tunnel; Alcove No.5 (HTA); See Pages 83 and 93
	210660004	7155685	00+77.	00+79.	19353/19362	Wehner	ESF Tunnel; Alcove No.5 (HTA); See Pages 83 and 93
	210660004	7155685	00+81.	00+83.	19363/19372	Wehner	ESF Tunnel; Alcove No.5 (HTA); See Pages 83 and 93
	210660004	7155685	00+85.	00+87.	19373/19382	Wehner	ESF Tunnel; Alcove No.5 (HTA); See Pages 83 and 93
	210660004	7155685	00+89.	00+91.	19383/19392	Wehner	ESF Tunnel; Alcove No.5 (HTA); See Pages 83 and 93
	210660004	7155685	00+93.	00+95.	19393/19402	Wehner	ESF Tunnel; Alcove No.5 (HTA); See Pages 83 and 93
	210660004	7155685	00+97.	00+99.	19403/19412	Wehner	ESF Tunnel; Alcove No.5 (HTA); See Pages 83 and 93
	210660004	7155685	01+01.	01+03.	19413/19422	Wehner	ESF Tunnel; Alcove No.5 (HTA); See Pages 83 and 93
	2106600094	7155685	01+05.	01+07.	19423/19432	Wehner	ESF Tunnel; Alcove No.5 (HTA); See Pages 83 and 93
	210660004	7155685	01+09.	01+11.	19433/19442	Wehner	ESF Tunnel; Alcove No.5 (HTA); See Pages 83 and 93
	210660004	7155685	01+13.	01+15.	19443/19452	Wehner	ESF Tunnel; Alcove No.5 (HTA); See Pages 83 and 93
	210660004	7155685	01+17.	10+19.	19453/19462	Wehner	ESF Tunnel; Alcove No.5 (HTA); See Pages 83 and 93
	210660004	7155685	01+21.	01+23.	19463/19472	Wehner	ESF Tunnel; Alcove No.5 (HTA); See Pages 83 and 93

07/23/96	Camera Body No.	Lens No.	Position 1	Position 2	Negative Nos.	ID	Comments
	210660004	7155685	59+48.20	59+50.00	19473/19482	Wehner	ESF Tunnel
	210660004	7155685	59+51.80	59+53.60	19483/19492	Wehner	ESF Tunnel
	210660004	7155685	59+55.40	59+57.20	19493/19502	Wehner	ESF Tunnel
	210660004	7155685	59+59.00	59+60.80	19503/19512	Wehner	ESF Tunnel
	210660004	7155685	59+62.60	59+64.40	19513/19522	Wehner	ESF Tunnel
07/30/96	Camera Body No.	Lens No.	Position 1	Position 2	Negative Nos.	ID	Comments
	210660004	7155685	59+93.20	59+95.00	19503/19612	Wehner	ESF Tunnel
	210660004	7155685	59+64.40	59+66.20	19523/19532	Wehner	ESF Tunnel
	210660004	7155685	59+68.00	59+69.80	19533/19542	Wehner	ESF Tunnel
	210660004	7155685	59+71.60	59+73.40	19543/19552	Wehner	ESF Tunnel
	210660004	7155685	59+75.20	59+77.00	19553/19562	Wehner	ESF Tunnel
	210660004	7155685	59+78.80	59+80.60	19563/19572	Wehner	ESF Tunnel
	210660004	7155685	59+82.40	59+84.20	19573/19582	Wehner	ESF Tunnel
	210660004	7155685	59+86.00	59+87.80	19583/19592	Wehner	ESF Tunnel
	210660004	7155685	59+89.60	59+91.40	19593/19602	Wehner	ESF Tunnel
07/31/96	Camera Body No.	Lens No.	Position 1	Position 2	Negative Nos.	ID	Comments
	210660004	7155685	59+95.00	59+96.80	19613/19622	Wehner	ESF Tunnel
	210660004	7155685	59+98.60	60+00.40	19623/19632	Wehner	ESF Tunnel
	210660004	7155685	60+02.20	60+04.00	19633/19642	Wehner	ESF Tunnel
	210660004	7155685	60+05.80	60+07.60	19643/19652	Wehner	ESF Tunnel
	210660004	7155685	60+09.40	60+11.20	19653/19662	Wehner	ESF Tunnel
	210660004	7155685	60+13.00	60+14.80	19663/19672	Wehner	ESF Tunnel
	210660004	7155685	60+16.60		19673/19677	Wehner	ESF Tunnel
08/01/96	Camera Body No.	Lens No.	Position 1	Position 2	Negative Nos.	ID	Comments
	210660004	7155685	60+16.60	60+18.40	19678/19687	Wehner	ESF Tunnel
	210660004	7155685	60+20.20	60+22.00	19688/19697	Wehner	ESF Tunnel
	210660004	7155685	60+23.80	60+25.60	19698/19707	Wehner	ESF Tunnel
	210660004	7155685	60+27.40	60+29.20	19708/19717	Wehner	ESF Tunnel
08/02/96	Camera Body No.	Lens No.	Position 1	Position 2	Negative Nos.	ID	Comments
	210660004	7155685	60+29.20	60+31.00	19718/19727	Unglesbee	ESF Tunnel
	210660004	7155685	60+32.80	60+34.60	19728/19737	Unglesbee	ESF Tunnel
	210660004	7155685	60+36.40	60+38.20	19738/19747	Unglesbee	ESF Tunnel
08/06/96	Camera Body No.	Lens No.	Position 1	Position 2	Negative Nos.	ID	Comments
	210660004	7155685	60+38.20	60+40.00	19748/19757	Wehner	ESF Tunnel
	210660004	71155685	60+41.80	60+43.60	19758/19767	Wehner	ESF Tunnel
	210660004	7155685	60+45.40	60+47.20	19768/19777	Wehner	ESF Tunnel
	210660004	7155685	60+49.00	60+50.80	19778/19787	Wehner	ESF Tunnel
	210660004	7155685	60+52.60	60+54.40	19788/19797	Wehner	ESF Tunnel
08/08/96	Camera Body No.	Lens No.	Position 1	Position 2	Negative Nos.	ID	Comments
	210660004	7155685	60+54.40	60+56.20	19798/19807	Wehner	ESF Tunnel
	210660004	7155685	60+58.00	60+59.80	19808/19817	Wehner	ESF Tunnel
	210660004	7155685	60+61.60	60+63.40	19818/19827	Wehner	ESF Tunnel
	210660004	71155685	60+65.20	60+67.00	19828/19837	Wehner	ESF Tunnel

	210660004	7155685	60+68.80	60+70.60	19838/19847	Wehner	ESF Tunnel
	210660004	7155685	60+72.40	60+74.20	19848/19857	Wehner	ESF Tunnel
	210660004	7155685	60+76.00	60+77.80	19858/19867	Wehner	ESF Tunnel
	210660004	7155685	60+79.60		19868/19872	Wehner	ESF Tunnel
08/09/96	Camera Body No.	Lens No.	Position 1	Position 2	Negative Nos.	ID	Comments
	210660004	7155685	60+77.80	60+79.60	19873/19882	Unglesbee	ESF Tunnel
	210660004	7155685	60+81.40	60+83.20	19883/19892	Unglesbee	ESF Tunnel
	210660004	7155685	60+85.00	60+86.80	19893/19902	Unglesbee	ESF Tunnel
	210660004	7155685	60+88.60	60+90.40	19903/19912	Unglesbee	ESF Tunnel
08/12/96	Camera Body No.	Lens No.	Position 1	Position 2	Negative Nos.	ID	Comments
	210660004	7155685	60+92.20	60+94.00	19913/19922	Wehner	ESF Tunnel
	210660004	7155685	60+95.80	60+97.60	19923/19932	Wehner	ESF Tunnel
	210660004	7155685	60+99.40	61+01.20	19933/19942	Wehner	ESF Tunnel
	210660004	7155685	61+03.00	61+04.80	19943/19952	Wehner	ESF Tunnel
	210660004	7155685	61+06.60	61+08.40	19953/19962	Wehner	ESF Tunnel
	210660004	7155685	61+10.20	61+12.00	19963/19972	Wehner	ESF Tunnel
08/15/96	Camera Body No.	Lens No.	Position 1	Position 2	Negative Nos.	ID	Comments
	210660004	7155685	61+12.00	61+13.80	19973/19982	Wehner	ESF Tunnel
	210660004	7155685	61+15.60	61+17.40	19983/19992	Wehner	ESF Tunnel
	210660004	7155685	61+19.20	61+21.00	19993/20002	Wehner	ESF Tunnel
	210660004	7155685	61+22.80	61+24.60	20003/20012	Wehner	ESF Tunnel
	210660004	7155685	61+26.40	61+28.20	20013/20022	Wehner	ESF Tunnel
	210660004	7155685	61+30.00	61+31.80	20023/20032	Wehner	ESF Tunnel
	210660004	7155685	61+33.60	61+35.40	20033/20042	Wehner	ESF Tunnel
	210660004	7155685	61+37.20	61+39.00	20043/20052	Wehner	ESF Tunnel
	210660004	7155685	61+40.80	61+42.60	20053/20062	Wehner	ESF Tunnel
08/20/96	Camera Body No.	Lens No.	Position 1	Position 2	Negative Nos.	ID	Comments
	210660004	7155685	61+42.60	61+44.40	20063/20072	Wehner	ESF Tunnel
	210660004	7155685	61+46.20	61+48.00	20073/20082	Wehner	ESF Tunnel
	210660004	7155685	61+49.80	61+51.60	20083/20092	Wehner	ESF Tunnel
	210660004	7155685	61+53.40	61+55.20	20093/20102	Wehner	ESF Tunnel
	210660004	7155685	61+57.00	61+58.80	20103/20112	Wehner	ESF Tunnel
08/23/96	Camera Body No.	Lens No.	Position 1	Position 2	Negative Nos.	ID	Comments
	210660004	7155685	61+58.80	61+60.60	20113/20122	Unglesbee	ESF Tunnel
	210660004	7155685	61+62.40	61+64.20	20123/20132	Unglesbee	ESF Tunnel
	210660004	7155685	61+66.00	61+67.80	20133/20142	Unglesbee	ESF Tunnel
	210660004	7155685	61+69.60	61+71.40	20143/20152	Unglesbee	ESF Tunnel
	210660004	7155685	61+73.20	61+75.00	20153/20162	Unglesbee	ESF Tunnel
	210660004	7155685	61+76.80	61+78.60	20163/20172	Unglesbee	ESF Tunnel
	210660004	7155685	61+80.40		20173/20177	Unglesbee	ESF Tunnel
08/26/96	Camera Body No.	Lens No.	Position 1	Position 2	Negative Nos.	ID	Comments
	210660004	7155685	61+80.40	61+83.20	20178/20187	Unglesbee	ESF Tunnel
	210660004	7155685	61+85.00	61+86.80	20188/20197	Unglesbee	ESF Tunnel; Survey Markers Off .8 Meters Beginning at 61+85.00

	210660004	7155685	61+88.60	61+90.40	20198/20207	Unglesbee	ESF Tunnel; Survey Markers Off .8 Meters Beginning at 61+85.00
	210660004	7155685	61+92.20	61+94.00	20208/20217	Unglesbee	ESF Tunnel; Survey Markes Off .8 Meters Beginning at 61+85.00
	210660004	7155685	61+95.80	61+97.60	20218/20227	Unglesbee	ESF Tunnel; Survey Markers Off .8 Meters Beginning at 61+85.00
	210660004	7155685	61+99.40	62+01.20	20228/20237	Unglesbee	ESF Tunnel; Survey Markers Off .8 Meters Beginning at 61+85.00
	210660004	7155685	62+03.00	62+04.80	20238/20247	Unglesbee	ESF Tunnel; Survey Markers Off .8 Meters Beginning at 61+85.00
	210660004	7155685	62+06.60	62+08.40	20248/20257	Unglesbee	ESF Tunnel; Survey Markers Off .8 Meters Beginning at 61+85.00
08/27/96	Camera Body No.	Lens No.	Position 1	Position 2	Negative Nos.	ID	Comments
	210660004	7155685	62+08.40	62+10.20	20258/20267	Wehner	ESF Tunnel; Survey Markers Off .8 Meters Beginning at 61+85.00
	210660004	7155685	62+12.00	62+13.80	20268/20277	Wehner	ESF Tunnel; Survey Markers Off .8 Meters Beginning at 61+85.00
	210660004	7155685	62+15.60	62+17.40	20278/20287	Wehner	ESF Tunnel; Survey Markers Off .8 Meters Beginning at 61+85.00
	210660004	7155685	62+19.20	62+21.00	20288/20297	Wehner	ESF Tunnel; Survey Markers Off .8 Meters Beginning at 61+85.00
08/28/96	Camera Body No.	Lens No.	Position 1	Position 2	Negative Nos.	ID	Comments
	210660004	7155685	62+18.20	62+22.00	20298/20307	Wehner	ESF Tunnel; Camera Repositioned on New Survey Locations
	210660004	7155685	62+21.80	62+23.60	20308/20317	Wehner	ESF Tunnel
	210660004	7155685	62+25.40	62+27.20	20318/20327	Wehner	ESF Tunnel
	210660004	7155685	62+29.00	62+30.80	20328/20337	Wehner	ESF Tunnel
08/29/96	Camera Body No.	Lens No.	Position 1	Position 2	Negative Nos.	ID	Comments
	210660004	7155685	62+30.80	62+32.60	20338/20347	Unglesbee	ESF Tunnel
	210660004	7155685	62+34.40	62+36.20	20348/20357	Wehner	ESF Tunnel
	210660004	7155685	62+38.00	62+39.80	20358/20367	Unglesbee	ESF Tunnel
	210660004	7155685	62+41.60	62+43.40	20368/20377	Unglesbee	ESF Tunnel
	210660004	7155685	62+45.20	62+47.00	20378/20387	Unglesbee	ESF Tunnel
08/30/96	Camera Body No.	Lens No.	Position 1	Position 2	Negative Nos.	ID	Comments
	210660004	7155685	62+45.20	62+47.00	20388/20397	Unglesbee	ESF Tunnel
	210660004	7155685	62+48.80	62+50.60	20398/20407	Unglesbee	ESF Tunnel

	210660004	7155685	62+52.40	62+54.20	20408/20417	Unglesbee	ESF Tunnel
	210660004	7155685	62+56.00	62+57.80	20418/20427	Unglesbee	ESF Tunnel
	210660004	7155685	62+59.60	62+61.40	20428/20437	Unglesbee	ESF Tunnel
	210660004	7155685	62+63.20	62+65.00	20438/20447	Unglesbee	ESF Tunnel
	210660004	7155685	62+66.80	62+68.60	20448/20457	Unglesbee	ESF Tunnel
	210660004	7155685	62+70.80		20458/20462	Unglesbee	ESF Tunnel
09/17/96	Camera Body No.	Lens No.	Position 1	Position 2	Negative Nos.	ID	Comments
	210660004	7155685	62+70.40	62+72.20	20463/20472	Wehner	ESF Tunnel; No mining progress since 8-30-96 (ventilation modifications).
	210660004	7155685	62+74.00	62+75.80	20473/20482	Wehner	ESF Tunnel
	210660004	7155685	62+77.60	62+79.40	20483/20492	Wehner	ESF Tunnel
	210660004	7155685	62+81.20	62+83.00	20493/20502	Wehner	ESF Tunnel
	210660004	7155685	62+84.80	62+86.60	20503/20512	Wehner	ESF Tunnel
09/18/96	Camera Body No.	Lens No.	Position 1	Position 2	Negative Nos.	ID	Comments
	210660004	7155685	62+86.60	62+88.40	20513/20522	Wehner	ESF Tunnel
	210660004	7155685	62+90.20	62+92.00	20523/20532	Wehner	ESF Tunnel
	210660004	7155685	62+93.80	62+95.60	20533/20542	Wehner	ESF Tunnel
	210660004	7155685	62+97.40		20543/20547	Wehner	ESF Tunnel
09/19/96	Camera Body No.	Lens No.	Position 1	Position 2	Negative Nos.	ID	Comments
	210660004	7155685	62+97.40	62+99.20	20548/20557	Wehner	ESF Tunnel
	210660004	7155685	63+01.00	63+02.80	20558/20567	Wehner	ESF Tunnel
	210660004	7155685	63+04.60	63+06.40	20568/20577	Wehner	ESF Tunnel
09/24/96	Camera Body No.	Lens No.	Position 1	Position 2	Negative Nos.	ID	Comments
	210660004	7155685	63+06.40	63+08.20	20578/20587	Wehner	ESF Tunnel
	210660004	7155685	63+10.00	63+11.80	20588/20597	Wehner	ESF Tunnel
	210660004	7155685	63+13.60	63+15.40	20598/20607	Wehner	ESF Tunnel
	210660004	7155685	63+17.20	63+19.00	20608/20617	Wehner	ESF Tunnel
	210660004	7155685	63+20.80	63+22.60	20618/20627	Wehner	ESF Tunnel
	210660004	7155685	63+24.40	63+26.20	20628/20637	Wehner	ESF Tunnel
	210660004	7155685	63+28.00	63+29.80	20638/20647	Wehner	ESF Tunnel
	210660004	7155685	63+31.60	63+33.40	20648/20657	Wehner	ESF Tunnel
	210660004	7155685	63+35.20	63+37.00	20658/20667	Wehner	ESF Tunnel
	210660004	7155685	63+28.80	63+40.60	20668/20677	Wehner	ESF Tunnel
	210660004	7155685	63+42.40	63+44.20	20678/20687	Wehner	ESF Tunnel
09/25/96	Camera Body No.	Lens No.	Position 1	Position 2	Negative Nos.	ID	Comments
	210660004	7155685	63+44.20	63+46.00	20688/20697	Wehner	ESF Tunnel
	210660004	7155685	63+47.80	63+49.60	20698/20707	Wehner	ESF Tunnel
	210660004	7155685	63+51.40	63+53.20	20708/20717	Wehner	ESF Tunnel
	107400029	7155685	63+55.00	63+56.80	20718/20727	Wehner	ESF Tunnel; Change of Camera Body
	400029	7155685	63+58.60	63+60.40	20728/20737	Wehner	ESF Tunnel
09/26/96	Camera Body No.	Lens No.	Position 1	Position 2	Negative Nos.	ID	Comments
	107400029	7155685	63+60.40	63+62.20	20738/20747	Unglesbee	ESF Tunnel

	107400029	7155685	63+64.00	63+65.80	20746/20757	Unglesbee	ESF Tunnel
	107400029	7155685	63+67.60	63+69.40	20758/20767	Unglesbee	ESF Tunnel
	107400029	7155685	63+71.20	63+73.00	20768/20777	Unglesbee	ESF Tunnel
09/30/96	Camera Body No.	Lens No.	Position 1	Position 2	Negative Nos.	ID	Comments
	107400029	7155685	63+73.00	63+74.80	20778/20787	Wehner	ESF Tunnel
	107400029	7155685	63+76.60	63+78.40	20788/20797	Wehner	ESF Tunnel
	107400029	7155685	63+80.20	63+82.00	20798/20807	Wehner	ESF Tunnel
	107400029	7155685	63+83.80	63+85.60	20808/20817	Wehner	ESF Tunnel
	107400029	7155685	63+87.40	63+89.20	20818/20827	Wehner	ESF Tunnel
	179400029	7155685	63+91.00	63+92.80	20828/20837	Wehner	ESF Tunnel
	179400029	7155685	63+94.60	63+96.40	20838/20847	Wehner	ESF Tunnel
	179400029	7155685	63+98.20	64+00.00	20848/20857	Wehner	ESF Tunnel
	179400029	7155685	64+01.80		20858/20862	Wehner	ESF Tunnel
10/08/96	Camera Body No.	Lens No.	Position 1	Position 2	Negative Nos.	ID	Comments
	311690019	7126302	64+01.80	64+03.60	20863/20872	Wehner	ESF Tunnel; Change of Camera Body and Lens
	311690019	7126302	64+05.40	64+07.20	20873/20882	Wehner	ESF Tunnel
	311690019	7126302	64+09.00	64+10.80	20883/20892	Wehner	ESF Tunnel
	311690019	7126302	64+12.60	64+14.40	20893/20902	Wehner	ESF Tunnel
	311690019	7126302	64+16.20	64+18.00	20903/20912	Wehner	ESF Tunnel
	311690019	7126302	64+19.80	64+21.60	20913/20922	Wehner	ESF Tunnel
	311690019	7126302	64+23.40	64+25.20	20923/20932	Wehner	ESF Tunnel; End of Curve at 64+25.20
	311690019	7126302	64+27.00		20933/20937	Wehner	ESF Tunnel
10/09/96	Camera Body No.	Lens No.	Position 1	Position 2	Negative Nos.	ID	Comments
	311690019	7126302	64+27.00	64+28.80	20938/230947	Wehner	ESF Tunnel
	311690019	7126302	64+30.60	64+32.40	20948/20957	Wehner	ESF Tunnel
	311690019	7126302	64+34.20	64+36.00	20958/20967	Wehner	ESF Tunnel
	311690019	7126302	64+37.80	64+39.60	20968/20977	Wehner	ESF Tunnel
	311690019	7126302	64+41.40	64+43.20	20978/20987	Wehner	ESF Tunnel
	311690019	7126302	64+45.00	64+46.80	20988/20997	Wehner	ESF Tunnel
	311690019	7126302	64+48.60	64+50.40	20998/21007	Wehner	ESF Tunnel
	311690019	7126302	64+52.20	64+54.00	21008/21017	Wehner	ESF Tunnel
	311690019	7126302	64+55.80	64+57.60	21018/21027	Wehner	ESF Tunnel
	311690019	7126302	64+59.40	64+61.20	21028/21037	Wehner	ESF Tunnel
10/10/96	Camera Body No.	Lens No.	Position 1	Position 2	Negative Nos.	ID	Comments
	311690019	7126302	64+61.20	64+63.00	21038/21047	Wehner	ESF Tunnel
	311690019	7126302	64+64.80	64+66.60	21048/21057	Wehner	ESF Tunnel
	311690019	7126302	64+68.40	64+70.20	21058/21067	Wehner	ESF Tunnel
	311690019	7126302	64+72.00	64+73.80	21068/21077	Wehner	ESF Tunnel
	311690019	7126302	64+75.60	64+77.40	21078/21087	Wehner	ESF Tunnel
	311690019	7126302	64+79.20	64+81.00	21088/21097	Wehner	ESF Tunnel
	311690019	7126302	64+82.90	64+84.60	21098/21107	Wehner	ESF Tunnel
	311690019	7126302	64+86.40	64+88.20	21108/21117	Wehner	ESF Tunnel
10/11/96	Camera Body No.	Lens No.	Position 1	Position 2	Negative Nos.	ID	Comments
	311690019	7126302	64+88.20	64+90.00	21118/21127	Unglesbee	ESF Tunnel

	311690019	7126302	64+91.80	64+93.60	21128/21137	Unglesbee	ESF Tunnel
	311690019	7126302	64+95.40	64+97.20	21138/21147	Unglesbee	ESF Tunnel
	311691109	7126302	64+99.00	65+00.80	21148/21157	Unglesbee	ESF Tunnel
	311690019	7126302	65+02.60	65+04.40	21158/21167	Unglesbee	ESF Tunnel
	311690019	7126302	65+06.20	65+08.00	21168/21177	Unglesbee	ESF Tunnel
	311690019	7126302	65+09.80	65+11.60	21178/21187	Unglesbee	ESF Tunnel
	311690019	7126302	65+13.40	65+15.20	21188/21197	Unglesbee	ESF Tunnel
10/14/96	Camera Body No.	Lens No.	Position 1	Position 2	Negative Nos.	ID	Comments
	311690019	7126302	65+15.20	65+17.00	21198/21207	Wehner	ESF Tunnel
	311690019	7126302	65+18.80	65+20.60	21208/21217	Wehner	ESF Tunnel
	311690019	7126302	65+22.40	65+24.20	21218/21227	Wehner	ESF Tunnel
	311690019	7126302	65+26.00	65+27.80	21228/21237	Wehner	ESF Tunnel
	311690019	7126302	65+29.60	65+31.40	21238/21247	Wehner	ESF Tunnel
	311690019	7126302	65+33.20	65+35.00	21248/21257	Wehner	ESF Tunnel
	311690019	7126302	65+36.80	65+38.60	21258/21267	Wehner	ESF Tunnel
10/15/96	Camera Body No.	Lens No.	Position 1	Position 2	Negative Nos.	ID	Comments
	311690019	7126302	65+38.60	65+40.40	21268/21277	Wehner	ESF Tunnel
	311690019	7126302	65+42.20	65+44.00	21278/21287	Wehner	ESF Tunnel
	311690019	7126302	65+45.80	65+47.60	21288/21297	Wehner	ESF Tunnel
	311690019	7126302	65+49.40	65+51.20	21298/21307	Wehner	ESF Tunnel
	311690019	7126302	65+53.00	65+54.80	21308/21317	Wehner	ESF Tunnel
	311690019	7126302	65+56.60	65+58.40	21318/21327	Wehner	ESF Tunnel
	311690019	7126302	65+60.20	65+62.00	21328/21337	Wehner	ESF Tunnel
	311690019	7126302	65+63.80	65+65.60	21338/21347	Wehner	ESF Tunnel
	311690019	7126302	65+67.40	65+69.20	21348/21357	Wehner	ESF Tunnel
	311690019	7126302	65+71.00	65+72.80	21358/21367	Wehner	ESF Tunnel
	311690019	7126302	65+74.60		21368/21372	Wehner	ESF Tunnel
10/16/96	Camera Body No.	Lens No.	Position 1	Position 2	Negative Nos.	ID	Comments
	311690019	7126302	65+74.60	65+76.40	21373/21382	Wehner	ESF Tunnel
	311690019	7126302	65+78.20	65+80.00	21383/21392	Wehner	ESF Tunnel
	311690019	7126302	65+81.80	65+83.60	21393/21402	Wehner	ESF Tunnel
	311690019	7126302	65+85.40	65+87.20	21403/21412	Wehner	ESF Tunnel
10/17/96	Camera Body No.	Lens No.	Position 1	Position 2	Negative Nos.	ID	Comments
	311690019	7126302	65+85.40	65+87.20	21413/21422	Wehner	ESF Tunnel
	311690019	7126302	65+89.00	65+90.80	21423/21432	Wehner	ESF Tunnel
	311690019	7126302	65+92.60	65+94.40	21433/21442	Wehner	ESF Tunnel
	311690019	7126302	65+96.20	65+98.00	21443/21452	Wehner	ESF Tunnel
	311690019	7126302	65+99.80	66+01.60	21453/21462	Wehner	ESF Tunnel
10/18/96	Camera Body No.	Lens No.	Position 1	Position 2	Negative Nos.	ID	Comments
	311690019	7126302	66+01.60	66+03.40	21463/21472	Unglesbee	ESF Tunnel
	311690019	7126302	66+05.20	66+07.00	21473/21482	Unglesbee	ESF Tunnel
	311690019	7126302	66+08.80	66+10.60	21483/21492	Unglesbee	ESF Tunnel
	311690019	7126302	66+12.40	66+14.20	21493/21502	Unglesbee	ESF Tunnel
	311690019	7126302	66+16.00	66+17.80	21503/21512	Unglesbee	ESF Tunnel
	311690019	7126302	66+19.60	66+21.40	21513/21522	Unglesbee	ESF Tunnel
	311690019	7126302	66+23.20	66+25.00	21523/21532	Unglesbee	ESF Tunnel

	311690019	7126302	66+26.80	66+28.60	21533/21542	Unglesbee	ESF Tunnel
	311690019	7126302	66+30.40	66+32.20	21543/21552	Unglesbee	ESF Tunnel
	311690019	7126302	66+34.00	66+35.80	21553/21562	Unglesbee	ESF Tunnel
	311690019	7126302	66+37.60	66+39.40	21563/21572	Unglesbee	ESF Tunnel
10/24/96	Camera Body No.	Lens No.	Position 1	Position 2	Negative Nos.	ID	Comments
	311690019	7126302	66+39.40	66+41.20	21573/21582	Wehner	ESF Tunnel
	311690019	7126302	66+43.00	66+44.80	21583/21592	Wehner	ESF Tunnel
	311690019	7126302	66+46.60	66+48.40	21593/21602	Wehner	ESF Tunnel
	311690019	7126302	66+50.20	66+52.00	21603/21612	Wehner	ESF Tunnel
	311690019	7126302	66+53.80	66+55.60	21613/21622	Wehner	ESF Tunnel
	311690019	7126302	66+57.40	66+59.20	21623/21632	Wehner	ESF Tunnel
	311690019	7126302	66+61.00	66+62.80	21633/21642	Wehner	ESF Tunnel
	311690019	7126302	66+64.60	66+66.40	21643/21652	Wehner	ESF Tunnel
10/25/96	Camera Body No.	Lens No.	Position 1	Position 2	Negative Nos.	ID	Comments
	311690019	7126302	66+66.40	66+68.20	21653/21662	Unglesbee	ESF Tunnel
	311690019	7126302	66+70.00	66+71.80	21663/21672	Unglesbee	ESF Tunnel
	311690019	7126302	66+73.60	66+75.40	21673/21682	Unglesbee	ESF Tunnel
	311690019	7126302	66+77.20	66+79.00	21683/21692	Unglesbee	ESF Tunnel
	311690019	7126302	66+80.80	66+82.60	21693/21702	Unglesbee	ESF Tunnel
	311690019	7126302	66+84.40	66+86.20	21703/21712	Unglesbee	ESF Tunnel
	311690019	7126302	66+88.00		21713/21717	Unglesbee	ESF Tunnel
10/31/96	Camera Body No.	Lens No.	Position 1	Position 2	Negative Nos.	ID	Comments
	210660004	7126302	66+88.00	66+89.80	21718/21727	Wehner	ESF Tunnel; Change of Camera Body
	210660004	7126302	66+91.60	66+93.40	21728/21737	Wehner	ESF Tunnel
	210660004	7126302	66+95.20	66+97.00	21738/21747	Wehner	ESF Tunnel
	210660004	7126302	66+98.80	67+00.60	21748/21757	Wehner	ESF Tunnel
	210660004	7126302	67+02.40	67+04.20	21758/21767	Wehner	ESF Tunnel
	210660004	7126302	67+06.00	67+07.80	21768/21777	Wehner	ESF Tunnel
	210660004	7126302	67+09.60	67+11.40	21778/21787	Wehner	ESF Tunnel
	210660004	7126302	67+13.20		21788/21792	Wehner	ESF Tunnel
11/01/96	Camera Body No.	Lens No.	Position 1	Position 2	Negative Nos.	ID	Comments
	210660004	7126302	67+13.20	67+15.00	21793/21802	Unglesbee	ESF Tunnel
	210660004	7126302	67+16.80	67+18.60	21803/21812	Unglesbee	ESF Tunnel
	210660004	7126302	67+20.40	67+22.20	21813/21822	Unglesbee	ESF Tunnel
	210660004	7126302	67+24.00	67+25.80	21823/21832	Unglesbee	ESF Tunnel
	210660004	7126302	67+27.60	67+29.40	21833/21842	Unglesbee	ESF Tunnel
	210660004	7126302	67+31.20	67+33.00	21843/21852	Unglesbee	ESF Tunnel
11/04/96	Camera Body No.	Lens No.	Position 1	Position 2	Negative Nos.	ID	Comments
	210660004	7126302	67+33.00	67+34.80	21853/21862	Wehner	ESF Tunnel
	210660004	7126302	67+36.60	67+38.40	21863/21872	Wehner	ESF Tunnel
	210660004	7126302	67+40.20	67+42.00	21873/21882	Wehner	ESF Tunnel
	210660004	7126302	67+43.80	67+45.60	21883/21892	Wehner	ESF Tunnel
	210660004	7126302	67+47.40	67+49.20	21893/21902	Wehner	ESF Tunnel
	210660004	7126302	67+51.00	67+52.80	21903/21912	Wehner	ESF Tunnel
	210660004	7126302	67+54.60	67+56.40	21913/21922	Wehner	ESF Tunnel

	210660004	7126302	67+58.20	67+60.00	21923/21932	Wehner	ESF Tunnel
	210660004	7126302	67+61.80	67+63.60	21933/21942	Wehner	ESF Tunnel
	210660004	7126302	67+65.40	67+67.20	21943/21952	Wehner	ESF Tunnel
11/05/96	Camera Body No.	Lens No.	Position 1	Position 2	Negative Nos.	ID	Comments
	210660004	7126302	67+67.20	67+69.00	21953/21962	Wehner	ESF Tunnel
	210660004	7126302	67+70.80	67+72.60	21963/21972	Wehner	ESF Tunnel
	210660004	7126302	67+74.40	67+76.20	21973/21982	Wehner	ESF Tunnel
	210660004	7126302	67+78.00	67+79.80	21983/21992	Wehner	ESF Tunnel
	210660004	7126302	67+81.60	67+83.40	21993/22002	Wehner	ESF Tunnel
	210660004	7126302	67+85.20	67+87.00	22003/22012	Wehner	ESF Tunnel
	210660004	7126302	67+88.80	67+90.60	22013/22022	Wehner	ESF Tunnel; Dune Wash Fault Zone
11/06/96	Camera Body No.	Lens No.	Position 1	Position 2	Negative Nos.	ID	Comments
	210660004	7126302	67+90.60	67+92.40	22023/22032	Wehner	ESF Tunnel; Dune Wash Fault Zone
	210660004	7126302	67+94.20	67+96.00	22033/22042	Wehner	ESF Tunnel
	210660004	7126302	67+97.80	67+99.60	22043/22052	Wehner	ESF Tunnel
	210660004	7126302	68+01.40	68+03.20	22053/22062	Wehner	ESF Tunnel
	210660004	7126302	68+05.00	68+06.80	22063/22072	Wehner	ESF Tunnel
	210660004	7126302	68+08.60	68+10.40	22073/22082	Wehner	ESF Tunnel
	210660004	7126302	68+12.20	68+14.00	22083/22092	Wehner	ESF Tunnel
	210660004	7126302	68+15.80	68+17.60	22093/22102	Wehner	ESF Tunnel
11/13/96	Camera Body No.	Lens No.	Position 1	Position 2	Negative Nos.	ID	Comments
	210660004	7126302	68+17.60	68+19.40	22103/22112	Wehner	ESF Tunnel
	210660004	7126302	68+21.20	68+23.00	22113/22122	Wehner	ESF Tunnel
	210660004	7126302	68+24.80	68+26.60	22123/22132	Wehner	ESF Tunnel
	210660004	7126302	68+28.40	68+30.20	22133/22142	Wehner	ESF Tunnel
11/14/96	Camera Body No.	Lens No.	Position 1	Position 2	Negative Nos.	ID	Comments
	210660004	7126302	68+30.20	68+32.00	22143/22152	Unglesbee	ESF Tunnel
	210660004	7126302	68+33.80	68+35.60	22153/22162	Unglesbee	ESF Tunnel
	210660004	7126302	68+37.40	68+39.20	22163/22172	Unglesbee	ESF Tunnel
11/15/96	Camera Body No.	Lens No.	Position 1	Position 2	Negative Nos.	ID	Comments
	210660004	7126302	68+39.20	68+41.00	22173/22182	Unglesbee	ESF Tunnel
	210660004	7126302	68+42.80	68+44.60	22183/22192	Unglesbee	ESF Tunnel
	210660004	7126302	68+46.40	68+48.20	22193/22202	Unglesbee	ESF Tunnel
	210660004	7126302	68+50.00	68+51.80	22203/22212	Unglesbee	ESF Tunnel
	210660004	7126302	68+53.60	68+55.40	22213/22222	Unglesbee	ESF Tunnel
	210660004	7126302	68+57.20	68+59.00	22223/22232	Unglesbee	ESF Tunnel
11/18/96	Camera Body No.	Lens No.	Position 1	Position 2	Negative Nos.	ID	Comments
	210660004	7126302	68+59.00	68+60.80	22233/22242	Wehner	ESF Tunnel
	210660004	7126302	68+62.60	68+64.40	22243/22252	Wehner	ESF Tunnel
	210660004	7126302	68+66.20	68+68.00	22253/22262	Wehner	ESF Tunnel
	210660004	7126302	68+69.80	68+71.60	22263/22272	Wehner	ESF Tunnel
	210660004	7126302	68+73.40	68+75.20	22273/22282	Wehner	ESF Tunnel
	210660004	7126302	68+77.00	68+78.80	22283/22292	Wehner	ESF Tunnel

	210660004	7126302	68+84.20	68+82.40	22293/22302	Wehner	ESF Tunnel
	210660004	7126302	68+84.20	68+86.00	22303/22312	Wehner	ESF Tunnel
11/19/96	Camera Body No.	Lens No.	Position 1	Position 2	Negative Nos.	ID	Comments
	210660004	7126302	68+86.00	68+87.80	22313/22322	Wehner	ESF Tunnel
	210660004	7126302	68+89.60	68+91.40	22323/22332	Wehner	ESF Tunnel
	210660004	7126302	68+93.20	68+95.00	22333/22342	Wehner	ESF Tunnel
11/20/96	Camera Body No.	Lens No.	Position 1	Position 2	Negative Nos.	ID	Comments
	210660004	7126302	68+95.00	68+96.80	22343/22352	Unglesbee	ESF Tunnel
	210660004	7126302	68+98.60	69+00.40	22353/22362	Unglesbee	ESF Tunnel
	210660004	7126302	69+02.20	69+04.00	22363/22372	Unglesbee	ESF Tunnel
11/21/96	Camera Body No.	Lens No.	Position 1	Position 2	Negative Nos.	ID	Comments
	210660004	7126302	69+04.00	69+05.80	22373/22382	Wehner	ESF Tunnel
	210660004	7126302	69+07.60	69+09.40	22383/22392	Wehner	ESF Tunnel
	210660004	7126302	69+11.20	69+13.00	22393/22402	Wehner	ESF Tunnel
	210660004	7126302	69+14.80	69+16.60	22403/22412	Wehner	ESF Tunnel
	210660004	7126302	69+18.40	69+20.20	22413/22422	Wehner	ESF Tunnel
	210660004	7126302	69+25.60	69+27.40	22433/22442	Wehner	ESF Tunnel
	210660004	7126302	69+22.00	69+23.80	232423/22432	Wehner	ESF Tunnel
11/22/96	Camera Body No.	Lens No.	Position 1	Position 2	Negative Nos.	ID	Comments
	210660004	7126302	69+27.40	69+29.20	22443/22452	Unglesbee	ESF Tunnel
	210660004	7126302	69+31.00	69+32.80	22453/22462	Unglesbee	ESF Tunnel
	210660004	7126302	69+34.60	69+36.40	22463/22472	Unglesbee	ESF Tunnel
	210660004	7126302	69+38.20	69+40.00	22473/22482	Unglesbee	ESF Tunnel
11/25/96	Camera Body No.	Lens No.	Position 1	Position 2	Negative Nos.	ID	Comments
	210660004	7126302	69+40.00	69+41.80	22483/22492	Wehner	ESF Tunnel
	210660004	7126302	69+43.60	69+45.40	22493/22502	Wehner	ESF Tunnel
	210660004	7126302	69+47.20	69+49.00	22503/22512	Wehner	ESF Tunnel
	210660004	7126302	69+50.80	69+52.60	22513/22522	Wehner	ESF Tunnel
	210660004	7126302	69+54.40	69+56.20	22523/22532	Wehner	ESF Tunnel
	210660004	7126302	69+58.00	69+59.80	22533/22542	Wehner	ESF Tunnel
	210660004	7126302	69+61.60	69+63.40	22543/22552	Wehner	ESF Tunnel
11/26/96	Camera Body No.	Lens No.	Position 1	Position 2	Negative Nos.	ID	Comments
	210660004	7126302	69+63.40	69+65.20	22553/22562	Wehner	ESF Tunnel
	210660004	7126302	69+67.00	69+68.80	22563/22572	Wehner	ESF Tunnel
	210660004	7126302	69+70.60	69+72.40	22573/22582	Wehner	ESF Tunnel
	210660004	7126302	69+74.20	69+76.00	22583/22592	Wehner	ESF Tunnel
	210660004	7126302	69+77.80	69+79.60	22593/22602	Wehner	ESF Tunnel
	210660004	7126302	69+81.40	69+83.20	22603/22612	Wehner	ESF Tunnel
	210660004	7126302	69+85.00	69+86.80	22613/22622	Wehner	ESF Tunnel
12/02/96	Camera Body No.	Lens No.	Position 1	Position 2	Negative Nos.	ID	Comments
	210660004	7126302	69+85.00	69+86.80	22623/22632	Wehner	ESF Tunnel
	210660004	7126302	69+88.60	69+90.40	22633/22642	Wehner	ESF Tunnel
	210660004	7126302	69+92.20	69+94.00	22643/22652	Wehner	ESF Tunnel
	210660004	7126302	69+95.80	69+97.60	22653/22662	Wehner	ESF Tunnel

	210660004	7126302	69+99.40	70+01.20	22663/22672	Wehner	ESF Tunnel
12/04/96	Camera Body No.	Lens No.	Position 1	Position 2	Negative Nos.	ID	Comments
	210660004	7126302	70+01.20	70+03.00	22673/22682	Wehner	ESF Tunnel
	210660004	7126302	70+04.80	70+06.60	22683/22692	Wehner	ESF Tunnel
	210660004	7126302	70+08.40	70+10.20	22693/22702	Wehner	ESF Tunnel
	210660004	7126302	70+12.00	70+13.80	22703/22712	Wehner	ESF Tunnel
	210660004	7126302	70+15.60	70+17.40	22713/22722	Wehner	ESF Tunnel
12/06/96	Camera Body No.	Lens No.	Position 1	Position 2	Negative Nos.	ID	Comments
	210660004	7126302	70+17.40	70+19.20	22723/22732	Unglesbee	ESF Tunnel
	210660004	7126302	70+21.00	70+22.80	22733/22742	Unglesbee	ESF Tunnel
	210660004	7126302	70+24.60	70+26.40	22743/22752	Unglesbee	ESF Tunnel
	210660004	7126302	70+28.20	70+30.00	22753/22762	Unglesbee	ESF Tunnel
	210660004	7126302	70+31.80	70+33.60	22763/22772	Unglesbee	ESF Tunnel
12/17/96	Camera Body No.	Lens No.	Position 1	Position 2	Negative Nos.	ID	Comments
	210660004	7126302	00+04.00	00+06.00	22773/22782	Wehner	ESF Tunnel, Alcove 6. Setup on page 136 of log book
	210660004	7126302	00+08.00	00+10.00	22783/22792	Wehner	ESF Tunnel, Alcove 6
	210660004	7126302	00+12.00	00+14.00	22793/22802	Wehner	ESF Tunnel, Alcove 6
	210660004	7126302	00+16.00	00+18.00	22803/22812	Wehner	ESF Tunnel, Alcove 6
	210660004	7126302	00+20.00	00+22.00	22813/22822	Wehner	ESF Tunnel, Alcove 6
	210660004	7126302	00+24.00	00+26.00	22823/22832	Wehner	ESF Tunnel, Alcove 6
	210660004	7126302	00+28.00	00+30.00	22833/22842	Wehner	ESF Tunnel, Alcove 6. 00+30 targets reversed.
	210660004	7126302	00+32.00	00+34.00	22843/22852	Wehner	ESF Tunnel, Alcove 6
	210660004	7126302	00+36.00	00+38.00	22853/22862	Wehner	ESF Tunnel, Alcove 6
	210660004	7126302	00+40.00	00+42.00	22863/22872	Wehner	ESF Tunnel, Alcove 6
	210660004	7126302	00+44.00	00+46.00	22873/22882	Wehner	ESF Tunnel, Alcove 6
	210660004	7126302	00+48.00	00+50.00	22883/22892	Wehner	ESF Tunnel, Alcove 6
	210660004	7126302	00+52.00	00+54.00	22893/22902	Wehner	ESF Tunnel, Alcove 6
	210660004	7126302	00+56.00	00+58.00	22903/22912	Wehner	ESF Tunnel, Alcove 6
	210660004	7126302	00+60.00	00+62.00	22913/22922	Wehner	ESF Tunnel, Alcove 6
	210660004	7126302	00+64.00	00+66.00	22923/22932	Wehner	ESF Tunnel, Alcove 6
	210660004	7126302	00+68.00	00+70.00	22933/22942	Wehner	ESF Tunnel, Alcove 6
	210660004	7126302	00+72.00	00+74.00	22943/22952	Wehner	ESF Tunnel, Alcove 6
	210660004	7126302	00+76.00	00+78.00	22953/22962	Wehner	ESF Tunnel, Alcove 6
	210660004	7126302	00+80.00	00+82.00	22963/22972	Wehner	ESF Tunnel, Alcove 6
	210660004	7126302	00+84.00	00+86.00	22973/22982	Wehner	ESF Tunnel, Alcove 6
	210660004	7126302	00+88.00		22983/22987	Wehner	ESF Tunnel, Alcove 6
12/18/96	Camera Body No.	Lens No.	Position 1	Position 2	Negative Nos.	ID	Comments
	210660004	7126302	70+33.60	70+35.40	22988/22997	Wehner	ESF Tunnel
	210660004	7126302	70+37.20	70+39.00	22998/23007	Wehner	ESF Tunnel
	210660004	7126302	70+40.80	70+42.60	23008/23017	Wehner	ESF Tunnel
	210660004	7126302	70+44.40	70+46.20	23018/23027	Wehner	ESF Tunnel
	210660004	7126302	70+48.00	70+49.80	23028/23037	Wehner	ESF Tunnel
01/23/97	Camera Body No.	Lens No.	Position 1	Position 2	Negative Nos.	ID	Comments

	210660004	7126302	70+49.80	70+51.60	23038/23047	Wehner	ESF Tunnel
	210660004	7126302	70+53.40	70+55.20	23048/23057	Wehner	ESF Tunnel
	210660004	7126302	70+57.00	70+58.80	23058/23067	Wehner	ESF Tunnel
	210660004	7126302	70+60.60	70+62.40	23068/23077	Wehner	ESF Tunnel
	210660004	7126302	70+64.20	70+66.00	23078/23087	Wehner	ESF Tunnel
02/04/97	Camera Body No.	Lens No.	Position 1	Position 2	Negative Nos.	ID	Comments
	210660004	7126302	70+66.00	70+67.80	23088/23097	Wehner	ESF Tunnel
	210660004	7126302	70+69.60	70+71.40	23098/23107	Wehner	ESF Tunnel
	210660004	7126302	70+73.20	70+75.00	23108/23117	Wehner	ESF Tunnel
	210660004	7126302	70+76.80	70+78.60	23118/23127	Wehner	ESF Tunnel
	210660004	7126302	70+80.40	70+82.20	23128/23137	Wehner	ESF Tunnel
02/06/97	Camera Body No.	Lens No.	Position 1	Position 2	Negative Nos.	ID	Comments
	210660004	7126302	70+85.80	70+87.60	23138/23147	Wehner	ESF Tunnel; -1.8 meters due to mining progress
	210660004	7126302	70+89.40	70+91.20	23148/23157	Wehner	ESF Tunnel
	210660004	7126302	70+93.00	70+94.80	23158/23167	Wehner	ESF Tunnel
	210660004	7126302	70+96.60	70+98.40	23168/23177	Wehner	ESF Tunnel
	210660004	7126302	71+00.20	71+02.00	23178/23187	Wehner	ESF Tunnel
	210660004	7126302	71+03.80	71+05.60	23188/23197	Wehner	ESF Tunnel
	210660004	7126302	71+07.40	71+09.20	23198/23207	Wehner	ESF Tunnel
	210660004	7126302	71+11.00	71+12.80	23208/23217	Wehner	ESF Tunnel
	210660004	7126302	71+14.60	71+16.40	23218/23227	Wehner	ESF Tunnel
	210660004	7126302	71+18.20	71+20.00	23228/23237	Wehner	ESF Tunnel
	210660004	7126302	71+21.80	71+23.60	23238/23247	Wehner	ESF Tunnel
	210660004	7126302	71+25.40		23248/23252	Wehner	ESF Tunnel
02/07/97	Camera Body No.	Lens No.	Position 1	Position 2	Negative Nos.	ID	Comments
	210660004	7126302	71+27.20	71+29.00	23253/23262	USBR	ESF Tunnel
	210660004	7126302	71+30.80	71+32.60	23263/23272	USBR	ESF Tunnel
	210660004	7126302	71+34.40	71+36.20	23273/23282	USBR	ESF Tunnel
	210660004	7126302	71+38.00	71+39.80	23283/23292	USBR	ESF Tunnel
	210660004	7126302	71+41.60	71+43.40	23293/23302	USBR	ESF Tunnel
	210660004	7126302	71+45.20	71+47.00	23303/23312	USBR	ESF Tunnel
	210660004	7126302	71+48.80	71+50.60	23313/23322	USBR	ESF Tunnel
	210660004	7126302	71+52.40		23323/23327	USBR	ESF Tunnel
02/10/97	Camera Body No.	Lens No.	Position 1	Position 2	Negative Nos.	ID	Comments
	210660004	7126302	71+48.80	71+50.60	23328/23337	Wehner	ESF Tunnel
	210660004	7126302	71+52.40	71+54.20	23338/23347	Wehner	ESF Tunnel
	210660004	7126302	71+56.00	71+57.80	23348/23357	Wehner	ESF Tunnel
	210660004	7126302	71+59.60	71+61.40	23358/23367	Wehner	ESF Tunnel
	210660004	7126302	71+63.20	71+65.00	23368/23377	Wehner	ESF Tunnel
	210660004	7126302	71+66.80	71+68.60	23378/23387	Wehner	ESF Tunnel
	210660004	7126302	71+70.40	71+72.20	23388/23397	Wehner	ESF Tunnel
	210660004	7126302	71+74.00	71+75.80	23398/23407	Wehner	ESF Tunnel
	210660004	7126302	71+77.60	71+79.40	23408/23417	Wehner	ESF Tunnel
02/11/97	Camera Body No.	Lens No.	Position 1	Position 2	Negative Nos.	ID	Comments

	210660004	7126302	71+79.40	71+81.20	23418/23427	Wehner	ESF Tunnel
	210660004	7126302	71+83.00	71+84.80	23428/23437	Wehner	ESF Tunnel
	210660004	7126302	71+86.60	71+88.40	23438/23447	Wehner	ESF Tunnel
	210660004	7126302	71+90.20	71+92.00	23448/23457	Wehner	ESF Tunnel
	210660004	7126302	71+93.80	71+95.60	23458/23467	Wehner	ESF Tunnel
02/12/97	Camera Body No.	Lens No.	Position 1	Position 2	Negative Nos.	ID	Comments
	210660004	7126302	00+12.00	00+13.50	23468/23477	Wehner	ESF Tunnel, Alcove 5 (Heat Drift); Set-up on Negative 140
	210660004	7126302	00+15.00	00+16.50	23478/23487	Wehner	ESF Tunnel, Alcove 5 (Heat Drift); Set-up on Negative 140
	210660004	7126302	00+18.00	00+19.50	23488/23497	Wehner	ESF Tunnel, Alcove 5 (Heat Drift); Set-up on Negative 140
	210660004	7126302	00+21.00	00+22.50	23498/23507	Wehner	ESF Tunnel, Alcove 5 (Heat Drift); Set-up on Negative 140
	210660004	7126302	00+24.00	00+25.50	23508/23517	Wehner	ESF Tunnel, Alcove 5 (Heat Drift), Set-up on Negative 140
	210660004	7126302	00+27.00	00+28.50	23518/23527	Wehner	ESF Tunnel, Alcove 5 (Heat Drift); Set-up on Negative 140
	210660004	7126302	00+30.00	00+31.50	23528/23537	Wehner	ESF Tunnel, Alcove 5 (Heat Drift); Set-up on Negative 140
	210660004	7126302	00+33.00	00+34.50	23538/23547	Wehner	ESF Tunnel, Alcove 5 (Heat Drift); Set-up on Negative 140
	210660004	7126302	00+36.00	00+37.50	23548/23557	Wehner	ESF Tunnel, Alcove 5 (Heat Drift); Set-up on Negative 140
	210660004	7126302	00+39.00	00+40.50	23558/23567	Wehner	ESF Tunnel, Alcove 5 (Heat Drift); Set-up on Negative 140
	210660004	7126302	00+42.00	00+43.50	23568/23577	Wehner	ESF Tunnel, Alcove 5 (Heat Drift); Set-up on Negative 140
	210660004	7126302	00+45.00	00+46.50	23578/23587	Wehner	ESF Tunnel, Alcove 5 (Heat Drift); Set-up on Negative 140
	210660004	7126302	00+48.00	00+49.50	23588/23597	Wehner	ESF Tunnel, Alcove 5 (Heat Drift); Set-up on Negative 140
	210660004	7126302	00+51.00	00+52.50	23598/23607	Wehner	ESF Tunnel, Alcove 5 (Heat Drift); Set-up on Negative 140

	210660004	7126302	00+54.00	00+55.50	23608/23617	Wehner	ESF Tunnel, Alcove 5 (Heat Drift); Set-up on Negative 140
	210660004	7126302	00+57.00	00+58.50	23618/23627	Wehner	ESF Tunnel, Alcove 5 (Heat Drift); Set-up on Negative 140
	210660004	7126302	00+60.00		23628/23632	Wehner	ESF Tunnel, Alcove 5 (Heat Drift); Set-up on Negative 140
02/13/97	Camera Body No.	Lens No.	Position 1	Position 2	Negative Nos.	ID	Comments
	210660004	7126302	71+95.60	71+97.40	23633/23642	Wehner	ESF Tunnel
	210660004	7126302	71+99.20	72+01.00	23643/23652	Wehner	ESF Tunnel
	210660004	7126302	72+02.80	72+04.60	23653/23662	Wehner	ESF Tunnel
	210660004	7126302	72+06.40	72+08.20	23663/23672	Wehner	ESF Tunnel
02/18/97	Camera Body No.	Lens No.	Position 1	Position 2	Negative Nos.	ID	Comments
	210660004	7126302	72+06.40	72+08.20	23673/23682	Wehner	ESF Tunnel, Walls Cleaned
	210660004	7126302	72+10.00	72+11.80	23683/23692	Wehner	ESF Tunnel
	210660004	7126302	72+13.60	72+15.40	23693/23702	Wehner	ESF Tunnel
	210660004	7126302	72+17.20	72+19.00	23703/23712	Wehner	ESF Tunnel
	210660004	7126302	72+20.80	72+22.60	23713/23722	Wehner	ESF Tunnel
	210660004	7126302	72+24.40	72+26.20	23723/23732	Wehner	ESF Tunnel
	210660004	7126302	72+28.00	72+29.80	23733/23742	Wehner	ESF Tunnel
	210660004	7126302	72+31.60	72+33.40	23743/23752	Wehner	ESF Tunnel
02/19/97	Camera Body No.	Lens No.	Position 1	Position 2	Negative Nos.	ID	Comments
	210660004	7126302	72+28.00	72+29.80	23753/23762	Wehner	ESF Tunnel; Walls Cleaned
	210660004	7126302	72+31.60	72+33.40	23763/23772	Wehner	ESF Tunnel, Walls Cleaned
	210660004	7126302	72+35.20	72+37.00	23773/23782	Wehner	ESF Tunnel
	210660004	7126302	72+38.80	72+40.60	23783/23792	Wehner	ESF Tunnel
	210660004	7126302	72+42.40	72+44.20	23793/23802	Wehner	ESF Tunnel
	210660004	7126302	72+46.00	72+47.80	23802/23812	Wehner	ESF Tunnel
	210660004	7126302	72+49.60	72+51.40	23813/23822	Wehner	ESF Tunnel
	210660004	7126302	72+53.20		23823/23827	Wehner	ESF Tunnel
02/20/97	Camera Body No.	Lens No.	Position 1	Position 2	Negative Nos.	ID	Comments
	210660004	7126302	72+53.20	72+55.00	23828/23837	Wehner	ESF Tunnel
	210660004	7126302	72+56.80	72+58.60	23838/23847	Wehner	ESF Tunnel
	210660004	7126302	72+60.40	72+62.20	23848/23857	Wehner	ESF Tunnel
	210660004	7126302	72+64.00	72+65.80	23858/23867	Wehner	ESF Tunnel
	210660004	7126302	72+67.60	72+69.40	23868/23877	Wehner	ESF Tunnel
	210660004	7126302	72+71.20	72+73.00	23878/23887	Wehner	ESF Tunnel
	210660004	7126302	72+74.80	72+76.60	23888/23897	Wehner	ESF Tunnel
	210660004	7126302	72+78.40	72+80.20	23898/23907	Wehner	ESF Tunnel
02/21/97	Camera Body No.	Lens No.	Position 1	Position 2	Negative Nos.	ID	Comments

	210660004	7126302	72+71.20	72+73.00	23908/23917	Wehner	ESF Tunnel, Walls Cleaned
	210660004	7126302	72+74.80	72+76.60	23918/23927	Wehner	ESF Tunnel, Walls Cleaned
	210660004	7126302	72+78.40	72+80.20	23928/23937	Wehner	ESF Tunnel, Walls Cleaned
	210660004	7126302	72+82.00	72+83.80	23938/23947	Wehner	ESF Tunnel
	210660004	7126302	72+85.60	72+87.40	23948/23957	Wehner	ESF Tunnel
	210660004	7126302	72+89.20	72+91.00	23958/23967	Wehner	ESF Tunnel
	210660004	7126302	72+92.80	72+94.60	23968/23977	Wehner	ESF Tunnel
	210660004	7126302	72+96.40	72+98.20	23978/23987	Wehner	ESF Tunnel
	210660004	7126302	73+00.00	73+01.80	23988/23997	Wehner	ESF Tunnel
	210660004	7126302	73+03.60	73+05.40	23998/24007	Wehner	ESF Tunnel
	210660004	7126302	73+07.20	73+09.00	24008/24017	Wehner	ESF Tunnel
	210660004	7126302	73+10.80	73+12.60	24018/24027	Wehner	ESF Tunnel
02/24/97	Camera Body No.	Lens No.	Position 1	Position 2	Negative Nos.	ID	Comments
	210660004	7126302	73+12.60	73+14.40	24028/24037	Wehner	ESF Tunnel
	210660004	7126302	73+16.20	73+18.00	24038/24047	Wehner	ESF Tunnel
	210660004	7126302	73+19.80	73+21.60	24048/24057	Wehner	ESF Tunnel
	210660004	7126302	73+23.40	73+25.20	24058/24067	Wehner	ESF Tunnel
	210660004	7126302	73+27.00	73+28.80	24068/24077	Wehner	ESF Tunnel
	210660004	7126302	73+30.60	73+32.40	24078/24087	Wehner	ESF Tunnel
	210660004	7126302	73+34.20	73+36.00	24088/24097	Wehner	ESF Tunnel
02/25/97	Camera Body No.	Lens No.	Position 1	Position 2	Negative Nos.	ID	Comments
	1007400029	7126302	73+79.20	73+81.00	13`98/24207	Wehner	ESF Tunnel
	1007400029	7126302	73+43.20	73+45.00	24098/24107	Wehner	ESF Tunnel; Meterage loss due to mining progress
	1007400029	7126302	73+46.80	73+48.60	24108/24117	Wehner	ESF Tunnel
	1007400029	7126302	73+50.40	73+52.20	24118/24127	Wehner	ESF Tunnel
	1007400029	7126302	73+54.00	73+55.80	24128/24137	Wehner	ESF Tunnel
	1007400029	7126302	73+57.60	73+59.40	24138/24147	Wehner	ESF Tunnel
	1007400029	7126302	73+64.80	73+66.60	24158/24167	Wehner	ESF Tunnel
	1007400029	7126302	73+68.40	73+70.20	24168/24177	Wehner	ESF Tunnel
	1007400029	7126302	73+72.00	73+73.80	24178/24187	Wehner	ESF Tunnel
	1007400079	7126302	73+75.60	73+77.40	24188/24197	Wehner	ESF Tunnel
	1007400029	7126302	73+82.80	73+84.60	24208/24217	Wehner	ESF Tunnel
02/26/97	Camera Body No.	Lens No.	Position 1	Position 2	Negative Nos.	ID	Comments
	311690019	7126302	73+84.60	73+86.40	24218/24227	Wehner	ESF Tunnel
	311690019	7126302	73+88.20	73+90.00	24228/24237	Wehner	ESF Tunnel
	311690019	7126302	73+91.80	73+93.60	24238/24247	Wehner	ESF Tunnel
	311690019	7126302	73+95.40	73+97.20	24248/24257	Wehner	ESF Tunnel
	311690019	7126302	73+99.00	74+00.80	24258/24267	Wehner	ESF Tunnel
	311690019	7126302	74+02.60	74+04.40	24268/24277	Wehner	ESF Tunnel
	311690019	7126302	74+06.20	74+08.00	24278/24287	Wehner	ESF Tunnel
	311690019	7126302	74+09.80	74+11.60	24288/24297	Wehner	ESF Tunnel
	311690019	7126302	74+13.40	74+15.20	24298/24307	Wehner	ESF Tunnel

02/27/97	Camera Body No.	Lens No.	Position 1	Position 2	Negative Nos.	ID	Comments
	311690019	7126302	74+15.20	74+17.00	24308/24317	Wehner	ESF Tunnel
	311690019	7126302	74+18.80	74+20.60	24318/24327	Wehner	ESF Tunnel
	311690019	7126302	74+22.40	72+24.20	24328/24337	Wehner	ESF Tunnel
	311690019	7126302	74+26.00	74+27.80	24338/24347	Wehner	ESF Tunnel
	311690019	7126302	74+29.60	74+31.40	24348/24357	Wehner	ESF Tunnel
	311690019	7126302	74+33.20	74+35.00	24358/24367	Wehner	ESF Tunnel
	311690019	7126302	74+36.80	74+38.60	24368/24377	Wehner	ESF Tunnel
02/28/97	Camera Body No.	Lens No.	Position 1	Position 2	Negative Nos.	ID	Comments
	311690019	7126302	74+38.60	74+40.40	24378/24387	Unglesbee	ESF Tunnel
	311690019	7126302	74+42.20	74+44.00	24388/24397	Unglesbee	ESF Tunnel
	311690019	7126302	74+45.80	74+47.60	24398/24407	Unglesbee	ESF Tunnel
	311690019	7126302	74+49.40	47+51.20	24408/24417	Unglesbee	ESF Tunnel
	311690019	7126302	74+53.00	74+54.80	24418/24427	Unglesbee	ESF Tunnel
03/05/97	Camera Body No.	Lens No.	Position 1	Position 2	Negative Nos.	ID	Comments
	311690019	7126302	74+56.60	74+58.40	24428/24437	Wehner	ESF Tunnel
	311690019	7126302	74+60.20	74+62.00	24438/24447	Wehner	ESF Tunnel
	311690019	7126302	74+63.80	74+65.60	24448/24457	Wehner	ESF Tunnel
	311690019	7126302	74+67.40	74+69.20	24458/24467	Wehner	ESF Tunnel
	311690019	7126302	74+71.00	74+72.80	24468/24477	Wehner	ESF Tunnel
	311690019	7126302	74+74.60	74+76.40	24478/24487	Wehner	ESF Tunnel
	311690019	7126302	74+78.20	74+80.00	24488/24497	Wehner	ESF Tunnel
	311690019	7126302	74+81.80	74+83.60	24498/24507	Wehner	ESF Tunnel
	311690019	7126302	74+85.40	74+87.20	24508/24517	Wehner	ESF Tunnel
	311690019	7126302	74+89.00	74+90.80	24518/24527	Wehner	ESF Tunnel
	311690019	7126302	74+92.60	74+94.40	24528/24537	Wehner	ESF Tunnel
	311690019	7126302	74+96.20	74+98.00	24538/24547	Wehner	ESF Tunnel
03/06/97	Camera Body No.	Lens No.	Position 1	Position 2	Negative Nos.	ID	Comments
	311690019	7126302	74+81.80	74+83.60	24548/24557	Wehner	ESF Tunnel; Walls Cleaned
	311690019	7126302	74+85.40	74+87.20	24558/24567	Wehner	ESF Tunnel; Walls Cleaned
	311690019	7126302	74+89.00	74+90.80	24568/24577	Wehner	ESF Tunnel; Walls Cleaned
	311690019	7126302	74+92.60	74+94.40	24578/24587	Wehner	ESF Tunnel; Walls Cleaned
	311690019	7126302	74+96.20	74+98.00	24588/24597	Wehner	ESF Tunnel; Walls Cleaned
	311690019	7126302	74+99.80	75+01.60	24598/24607	Wehner	ESF Tunnel
	311690019	7126302	74+03.40	75+05.20	24608/24617	Wehner	ESF Tunnel
	311690019	7126302	75+07.00	75+08.80	24618/24627	Wehner	ESF Tunnel
	311690019	7126302	75+10.60	75+12.40	24628/24637	Wehner	ESF Tunnel
03/07/97	Camera Body No.	Lens No.	Position 1	Position 2	Negative Nos.	ID	Comments
	311690019	7126302	75+12.40	75+14.20	24638/24647	USBR	ESF Tunnel
	311690019	7126302	75+16.00	75+17.80	24648/24657	USBR	ESF Tunnel
	311690019	7126302	75+19.60	75+21.40	24658/24667	USBR	ESF Tunnel

	311690019	7126302	75+23.20	75+25.00	24668/24677	USBR	ESF Tunnel
	311690019	7126302	75+26.80	75+28.60	24678/24687	USBR	ESF Tunnel
	311690019	7126302	75+30.40	75+32.20	24688/24697	USBR	ESF Tunnel
	311690019	7126302	75+34.00	75+35.80	24698/24707	USBR	ESF Tunnel
	311690019	7126302	75+37.60	75+39.40	24708/24717	USBR	ESF Tunnel
	311690019	7126302	75+41.20	75+43.00	24718/24727	USBR	ESF Tunnel
	311690019	7126302	75+44.80	75+46.60	24728/24737	USBR	ESF Tunnel
03/10/97	Camera Body No.	Lens No.	Position 1	Position 2	Negative Nos.	ID	Comments
	311690019	7126302	75+46.60	75+48.40	24738/24747	Wehner	ESF Tunnel
	311690019	7126302	75+50.20	75+52.00	24748/24757	Wehner	ESF Tunnel
	311690019	7126302	75+53.80	75+55.60	24758/24767	Wehner	ESF Tunnel
	311690019	7126302	75+57.40	75+59.20	24768/24777	Wehner	ESF Tunnel
	311690019	7126302	75+61.00	75+62.80	24778/24787	Wehner	ESF Tunnel
	311690019	7126302	75+64.60	75+66.40	24788/24797	Wehner	ESF Tunnel
	311690019	7126302	75+68.20	75+70.00	24798/24807	Wehner	ESF Tunnel
03/11/97	Camera Body No.	Lens No.	Position 1	Position 2	Negative Nos.	ID	Comments
	311690019	7126302	75+70.00	75+71.80	24808/24817	Unglesbee	ESF Tunnel
	311690019	7126302	75+73.60	75+75.40	24818/24827	Unglesbee	ESF Tunnel
	311690019	7126302	75+77.20	75+79.00	24828/24837	Unglesbee	ESF Tunnel
	311690019	7126302	75+80.80	75+82.60	24838/24847	Unglesbee	ESF Tunnel
03/12/97	Camera Body No.	Lens No.	Position 1	Position 2	Negative Nos.	ID	Comments
	311690019	7126302	75+82.60	75+84.40	24848/24857	Wehner	ESF Tunnel
	311690019	7126302	75+86.20	75+88.00	24858/24867	Wehner	ESF Tunnel
	311690019	7126302	75+89.80	75+91.60	24868/24877	Wehner	ESF Tunnel
	311690019	7126302	75+93.40	75+95.20	24878/24887	Wehner	ESF Tunnel
	311690019	7126302	75+97.00	75+98.80	24888/24897	Wehner	ESF Tunnel
	311690019	7126302	76+00.60	76+02.40	24898/24907	Wehner	ESF Tunnel
03/18/97	Camera Body No.	Lens No.	Position 1	Position 2	Negative Nos.	ID	Comments
	311690019	7126302	76+02.40	76+04.20	24908/24917	Wehner	ESF Tunnel
	311690019	7126302	76+06.00	76+07.80	24918/24927	Wehner	ESF Tunnel
	311690019	7126302	76+09.60	76+11.40	24928/24937	Wehner	ESF Tunnel
	311690019	7126302	76+13.20	76+15.00	24938/24947	Wehner	ESF Tunnel
	311690019	7126302	76+16.80	76+18.60	24948/24957	Wehner	ESF Tunnel
	311690019	7126302	76+20.40	76+22.20	24958/24967	Wehner	ESF Tunnel
	311690019	7126302	76+24.60	76+25.80	24968/24977	Wehner	ESF Tunnel
	311690019	7126302	76+27.60	76+29.40	24978/24987	Wehner	ESF Tunnel
	311690019	7126302	76+31.20	76+33.00	24988/24997	Wehner	ESF Tunnel
	311690019	7126302	76+34.80	76+36.6-	24998/25007	Wehner	ESF Tunnel
	311690019	7126302	76+38.40	76+40.20	25008/25017	Wehner	ESF Tunnel
03/25/97	Camera Body No.	Lens No.	Position 1	Position 2	Negative Nos.	ID	Comments
	100700029	7126302	73+61.20	73+63.00	24148/24157	Wehner	ESF Tunnel
03/27/97	Camera Body No.	Lens No.	Position 1	Position 2	Negative Nos.	ID	Comments
	311690019	7126302	76+40.20	76+42.00	25018/25027	Wehner	ESF Tunnel
	311690019	7126302	76+43.80	76+45.60	25028/25037	Wehner	ESF Tunnel
	311690019	7126302	76+47.40	76+49.20	25038/25047	Wehner	ESF Tunnel

	311690019	7126302	76+51.00	76+52.80	25048/25057	Wehner	ESF Tunnel
	311690019	7126302	76+54.60	76+56.40	25058/25067	Wehner	ESF Tunnel
	311690019	7126302	76+58.20	76+60.00	25068/25077	Wehner	ESF Tunnel
04/04/97	Camera Body No.	Lens No.	Position 1	Position 2	Negative Nos.	ID	Comments
	311690019	7126302	76+60.00	76+61.80	25078/25087	USBR	ESF Tunnel
	311690019	7126302	76+63.60	76+65.40	25088/25097	USBR	ESF Tunnel
	311690019	7126302	76+67.20	76+69.00	25098/25107	USBR	ESF Tunnel
	311690019	7126302	76+70.80	76+72.60	25108/25117	USBR	ESF Tunnel
	311690019	7126302	76+74.40	76+76.20	25118/25127	USBR	ESF Tunnel
	311690019	7126302	76+78.00	76+79.80	25128/25137	USBR	ESF Tunnel
	311690019	7126302	76+81.60	76+83.40	25138/25147	USBR	ESF Tunnel
	311690019	7126302	76+85.20	76+87.00	25148/25157	USBR	ESF Tunnel
04/07/97	Camera Body No.	Lens No.	Position 1	Position 2	Negative Nos.	ID	Comments
	311690019	7126302	76+81.60	76+83.40	25158/25167	Wehner	ESF Tunnel; Walls Cleaned
	311690019	7126302	76+85.20	76+87.00	25168/25177	Wehner	ESF Tunnel; Walls Cleaned
	311690019	7126302	76+88.80	76+90.60	25178/25187	Wehner	ESF Tunnel
	311690019	7126302	76+92.40	76+94.20	25188/25197	Wehner	ESF Tunnel
	311690019	7126302	76+96.00	76+97.80	25198/25207	Wehner	ESF Tunnel
	311690019	7126302	76+99.60	77+01.40	25208/25217	Wehner	ESF Tunnel
	311690019	7126302	77+03.20	77+05.00	25218/25227	Wehner	ESF Tunnel
	311690019	7126302	77+06.80	77+08.60	25228/25237	Wehner	ESF Tunnel
	311690019	7126302	77+10.40	77+12.20	25238/25247	Wehner	ESF Tunnel
04/08/97	Camera Body No.	Lens No.	Position 1	Position 2	Negative Nos.	ID	Comments
	311690019	7126302	77+08.60	77+10.40	25248/25257	Wehner	ESF Tunnel; Walls Cleaned
	311690019	7126302	77+12.20	77+14.00	25258/25267	Wehner	ESF Tunnel
	311690019	7126302	77+15.80	77+17.60	25268/25277	Wehner	ESF Tunnel
	311690019	7126302	77+19.40	77+21.20	25278/25287	Wehner	ESF Tunnel
	311690019	7126302	77+23.00	77+24.80	25288/25297	Wehner	ESF Tunnel
	311690019	7126302	77+26.60	77+28.40	25298/25307	Wehner	ESF Tunnel
04/09/97	Camera Body No.	Lens No.	Position 1	Position 2	Negative Nos.	ID	Comments
	311690019	7126302	77+28.40	77+30.20	25308/25317	Wehner	ESF Tunnel
	311690019	7126302	77+32.00	77+33.80	25318/25327	Wehner	ESF Tunnel
	311690019	7126302	77+35.60	77+37.40	25328/25337	Wehner	ESF Tunnel
	311690019	7126302	77+39.20	77+41.00	25338/25347	Wehner	ESF Tunnel
	311690019	7126302	77+42.80	77+44.60	25348/25357	Wehner	ESF Tunnel
	311690019	7126302	77+46.40		25358/25362	Wehner	ESF Tunnel
04/15/97	Camera Body No.	Lens No.	Position 1	Position 2	Negative Nos.	ID	Comments
	311690019	7126302	77+46.40	77+48.20	25363/25372	Wehner	ESF Tunnel
	311690019	7126302	77+50.00	77+51.80	25373/25382	Wehner	ESF Tunnel
	311690019	7126302	77+53.60	77+55.40	25383/25392	Wehner	ESF Tunnel
	311690019	7126302	77+57.20	77+59.00	25393/25402	Wehner	ESF Tunnel
	311690019	7126302	77+60.80	77+62.60	25402/25412	Wehner	ESF Tunnel
	311690019	7126302	77+64.40	77+66.20	25413/25422	Wehner	ESF Tunnel

	311690019	7126302	77+68.00	77+69.80	25423/25432	Wehner	ESF Tunnel
	311690019	7126302	77+71.60	77+73.40	25433/25442	Wehner	ESF Tunnel
04/16/97	Camera Body No.	Lens No.	Position 1	Position 2	Negative Nos.	ID	Comments
	311690019	7126302	77+75.20	77+77.00	25443/25452	Wehner	ESF Tunnel
	311690019	7126302	77+78.80	77+80.60	25453/25462	Wehner	ESF Tunnel
	311690019	7126302	77+82.40	77+84.20	25463/25472	Wehner	ESF Tunnel
	311690019	7126302	77+86.00	77+87.80	25473/25482	Wehner	ESF Tunnel
	311690019	7126302	77+89.60	77+91.40	25483/25492	Wehner	ESF Tunnel
	311690019	7126302	77+93.20	77+95.00	25493/25502	Wehner	ESF Tunnel
	311690019	7126302	77+96.80	77+98.60	25503/25512	Wehner	ESF Tunnel; TBM at 78+73.60 (4 meters from daylight).
05/20/97	Camera Body No.	Lens No.	Position 1	Position 2	Negative Nos.	ID	Comments
	311690019	7123602	00+36.00	00+37.50	25513/25522	Wehner	Alcove 7, ESF Tunnel
	311690019	7123602	00+39.00	00+40.50	25523/25532	Wehner	Alcove 7, ESF Tunnel
	311690019	7123602	00+42.00	00+43.50	25533/25542	Wehner	Alcove 7, ESF Tunnel
	311690019	7123602	00+45.00	00+46.50	25543/25552	Wehner	Alcove 7, ESF Tunnel
	311690019	7123602	00+48.00	00+49.50	25553/25562	Wehner	Alcove 7, ESF Tunnel
	311690019	7123602	00+51.00	00+52.50	25563/25572	Wehner	Alcove 7, ESF Tunnel
	311690019	7123602	00+54.00	00+55.50	25573/25582	Wehner	Alcove 7, ESF Tunnel
	311690019	7123602	00+57.00	00+58.50	25583/25592	Wehner	Alcove 7, ESF Tunnel
	311690019	7123602	00+60.00	00+61.50	25593/25602	Wehner	Alcove 7, ESF Tunnel
	311690019	7123602	00+63.00	00+64.50	25603/25612	Wehner	Alcove 7, ESF Tunnel
	311690019	7123602	00+66.00	00+67.50	25613/25622	Wehner	Alcove 7, ESF Tunnel
	311690019	7123602	00+69.00	00+70.50	25623/25632	Wehner	Alcove 7, ESF Tunnel
	311690019	7123602	00+72.00	00+73.50	25633/25642	Wehner	Alcove 7, ESF Tunnel
	311690019	7123602	00+75.00	00+76.50	25643/25652	Wehner	Alcove 7, ESF Tunnel
	311690019	7123602	00+78.00	00+79.50	25653/25662	Wehner	Alcove 7, ESF Tunnel
	311690019	7123602	00+81.00	00+82.50	25663/25672	Wehner	Alcove 7, ESF Tunnel
	311690019	7123602	00+84.00	00+85.50	25673/25682	Wehner	Alcove 7, ESF Tunnel
	311690019	7123602	00+87.00	00+88.50	25683/25692	Wehner	Alcove 7, ESF Tunnel
	311690019	7123602	00+90.00	00+91.50	25693/25702	Wehner	Alcove 7, ESF Tunnel
	311690019	7123602	00+93.00	00+94.50	25703/25712	Wehner	Alcove 7, ESF Tunnel
	311690019	7123602	00+96.00	00+97.50	25713/25722	Wehner	Alcove 7, ESF Tunnel
	311690019	7123602	00+99.00	01+00.50	25723/25732	Wehner	Alcove 7, ESF Tunnel
	311690019	7123602	01+02.00	01+03.50	25733/25742	Wehner	Alcove 7, ESF Tunnel
	311690019	7123602	01+05.00	01+06.50	25743/25752	Wehner	Alcove 7, ESF Tunnel
	311690019	7123602	01+08.00	01+09.50	25753/25762	Wehner	Alcove 7, ESF Tunnel
	311690019	7123602	01+11.00	01+12.50	25763/25772	Wehner	Alcove 7, ESF Tunnel
	311690019	7123602	01+14.00	01+15.50	25773/25782	Wehner	Alcove 7, ESF Tunnel
	311690019	7123602	01+17.00	01+18.50	25783/25792	Wehner	Alcove 7, ESF Tunnel
	311690019	7123602	01+20.00	01+21.50	25793/25802	Wehner	Alcove 7, ESF Tunnel
	311690019	7123602	01+23.00	01+24.50	25803/25812	Wehner	Alcove 7, ESF Tunnel
	311690019	7123602	01+26.00	01+27.50	25813/25822	Wehner	Alcove 7, ESF Tunnel
	311690019	7123602	01+29.00	01+30.50	25823/25832	Wehner	Alcove 7, ESF Tunnel
	311690019	7123602	01+32.00	01+33.50	25833/25842	Wehner	Alcove 7, ESF Tunnel
	311690019	7123602	01+35.00	01+36.50	25843/25852	Wehner	Alcove 7, ESF Tunnel
	311690019	7123602	01+38.00	01+39.50	25853/25862	Wehner	Alcove 7, ESF Tunnel
	311690019	7123602	01+41.00	01+42.50	25863/25872	Wehner	Alcove 7, ESF Tunnel

	311690019	7123602	01+44.00		25873/25877	Wehner	Alcove 7, ESF Tunnel
05/21/97	Camera Body No.	Lens No.	Position 1	Position 2	Negative Nos.	ID	Comments
	311690019	7123602	77+84.20	77+86.00	25878/25887	Wehner	ESF Tunnel; Wall Cleaned
	311690019	7123602	77+87.80	77+89.60	25888/25897	Wehner	ESF Tunnel
	311690019	7123602	77+91.40	77+93.20	25898/25907	Wehner	ESF Tunnel
	311690019	7123602	77+95.00	77+96.80	25908/25917	Wehner	ESF Tunnel
	311690019	7123602	77+98.60	78+00.40	25918/25927	Wehner	ESF Tunnel
	311690019	7123602	78+02.20	78+04.00	25928/25937	Wehner	ESF Tunnel
	311690019	7123602	78+05.80	78+07.60	25938/25947	Wehner	ESF Tunnel
06/09/97	Camera Body No.	Lens No.	Position 1	Position 2	Negative Nos.	ID	Comments
	311690019	7123602	78+07.60	78+09.40	25948/25957	Wehner	ESF Tunnel
	311690019	7123602	78+11.20	78+13.00	25958/25967	Wehner	ESF Tunnel
	311690019	7123602	78+14.80	78+16.60	25968/25977	Wehner	ESF Tunnel
	311690019	7123602	78+18.40	78+20.20	25978/25987	Wehner	ESF Tunnel
	311690019	7123602	78+22.00	78+23.80	25988/25997	Wehner	ESF Tunnel
	311690019	7123602	78+25.60	78+27.40	25998/26007	Wehner	ESF Tunnel
	311690019	7123602	78+29.20	78+31.00	26008/26017	Wehner	ESF Tunnel
	311690019	7123602	78+32.80	78+34.60	26018/26027	Wehner	ESF Tunnel
06/10/97	Camera Body No.	Lens No.	Position 1	Position 2	Negative Nos.	ID	Comments
	311690019	7123602	78+34.60	78+36.40	26028/26037	Wehner	ESF Tunnel
	311690019	7123602	78+38.20	78+40.00	26038/26047	Wehner	ESF Tunnel
	311690019	7123602	78+41.80	78+43.60	26048/26057	Wehner	ESF Tunnel
	311690019	7123602	78+45.40	78+47.20	26058/26067	Wehner	ESF Tunnel
	311690019	7123602	78+49.00	78+50.80	26068/26077	Wehner	ESF Tunnel
	311690019	7123602	78+52.60	78+54.40	26078/26087	Wehner	ESF Tunnel
	311690019	7123602	78+56.20	78+58.00	26088/26097	Wehner	ESF Tunnel
06/11/97	Camera Body No.	Lens No.	Position 1	Position 2	Negative Nos.	ID	Comments
	311690019	7123602	78+58.00	78+59.80	26098/26107	Wehner	ESF Tunnel
	311690019	7123602	78+61.60	78+63.40	26108/26117	Wehner	ESF Tunnel
	311690019	7123602	78+65.20	78+67.00	26118/26127	Wehner	ESF Tunnel
	311690019	7123602	78+68.80	78+70.60	26128/26137	Wehner	ESF Tunnel
	311690019	7123602	78+72.40	78+74.20	26138/26147	Wehner	ESF Tunnel
	311690019	7123602	78+76.00		26148/26152	Wehner	Tunnel Hole-Out; End of ESF Main

APPENDIX III: Sample Locations and Descriptions

APPENDIX III: Sample Locations and Descriptions

Constr. Station	Bar Code	Date	PI Name	Partici-pant	Location Detail	Location Description
55+00	SPC00510748	6/26/96	June Fabryka-Martin	LANL	Right Rib	0.5 meters above invert
55+00	SPC00521405	12/10/96	Alan Flint	USGS	Right Rib	Approx. 0.5 to 1.0 meters above invert
55+20	SPC00521604	4/15/97	Alan Flint	USGS	Right Rib	sample collected approx. 0.5 to 1.5 m above the invert
55+21	SPC00510759	6/28/96	Zell Peterman	USGS	Right Rib	1.5 meters above invert
55+40	SPC00521404	12/10/96	Alan Flint	USGS	Right Rib	Approx. 0.5 to 1.0 meters above the invert
55+60	SPC00521603	4/15/97	Alan Flint	USGS	Right Rib	Sample collected approx. 0.5 to 1.5 m above the invert
55+80	SPC00521403	12/10/96	Alan Flint	USGS	Right rib	Approx. 0.5 to 1.0 meters above the invert
55+92	SPC00510758	6/28/96	Zell Peterman	USGS	Right Rib	1 meter below springline
55+97	SPC00510785	8/27/96	Steve Castor	UNR	Right Rib	2 meters above invert
56+00	SPC00521602	4/15/97	Alan Flint	USGS	Right rib	Sample collected approx. 0.5 to 1.5 m above invert
56+20	SPC00521402	12/10/96	Alan Flint	USGS	Right Rib	Approx. 0.5 to 1.0 meters above the invert
56+40	SPC00521601	4/15/97	Alan Flint	USGS	Right Rib	Sample collected approx. 0.5 to 1.5 m above invert
56+46	SPC00510757	6/28/96	Zell Peterman	USGS	Right rib	1 meter below springline
56+60	SPC00521401	12/10/96	Alan Flint	USGS	Right Rib	Approx. 0.5 to 1.0 meters above the invert
56+63	SPC00510756	6/26/96	June Fabryka-Martin	LANL	Right rib	.5 meters below springline
56+63	SPC00510755	6/28/96	Zell Peterman	USGS	Right Rib	1 meter below springline
56+68	SPC00510753	6/28/96	Zell Peterman	USGS	Right Rib	2 meters above invert
56+80	SPC00521600	4/15/97	Alan Flint	USGS	Right Rib	Sample collected approx. 0.5 to 1.5 m above invert
56+85	SPC00510754	6/28/96	June Fabryka-Martin	LANL	Right Rib	2 meters above invert
56+85	SPC00510752	6/28/96	Zell Peterman	USGS	Right rib	2 meters above invert
56+93	SPC00510750	6/28/96	June Fabryka-Martin	LANL	Right Rib	1.5 meters above invert
56+93	SPC00510751	6/28/96	Zell Peterman	USGS	Right Rib	1.5 meters above invert
57+00	SPC00515143	10/9/96	June Fabryka-Martin	LANL	Right Rib	1 meter above invert
57+00	SPC00521400	12/10/96	Alan Flint	USGS	Right rib	Approx. 0.5 to 1.0 meters above the invert
57+26.80	SPC00515144	10/9/96	June Fabryka-Martin	LANL	Right Rib	1 meter above invert
57+28	SPC00510770	8/27/96	Steve Castor	UNR	Right Rib	2 meters above invert
57+71.70	SPC00515131	10/9/96	Zell Peterman	USGS	Right Rib	2 meters above invert
58+11.50	SPC00515130	10/9/96	Zell Peterman	USGS	Right Rib	1 meter above invert
58+66	SPC00515145	10/9/96	June Fabryka-Martin	LANL	Right Rib	1 meter above invert
58+77	SPC00515146	10/9/96	June Fabryka-Martin	LANL	Right Rib	1 meter above invert
59+00	SPC00515147	10/9/96	June Fabryka-Martin	LANL	Right Rib	1 meter above invert
59+98	SPC00521128	12/17/96	June Fabryka-Martin	LANL	Right Rib	0.2m aboave invert
60+07.40	SPC00515129	10/9/96	Zell Peterman	USGS	Right rib	1 meter above invert
60+18.80	SPC00515128	10/9/96	Zell Peterman	USGS	Right Rib	1.5 meters above invert
60+65.60	SPC00515127	10/9/96	Zell Peterman	USGS	Right rib	1.5 - 2.0 m above invert.
61+00	SPC00515148	10/9/96	June Fabryka-Martin	LANL	Right Rib	
61+82.80	SPC00515126	10/9/96	Zell Peterman	USGS	Right rib	2.5 meters above invert

61+92	SPC00515149	10/9/96	June Fabryka-Martin	LANL	Right rib	1 meter above invert
62+00	SPC00515150	10/9/96	June Fabryka-Martin	LANL	Right Rib	1 meter above invert
62+05	SPC00515151	10/9/96	June Fabryka-Martin	LANL	Right Rib	1 meter above invert
62+18.20	SPC00515152	10/9/96	June Fabryka-Martin	LANL	Right Rib	1 meter above invert
62+30.00	SPC00515125	10/9/96	Zell Peterman	USGS	Right Rib	2 meters above invert.
62+43.30	SPC00515124	10/9/96	Zell Peterman	USGS	Right Rib	1.5 meters above invert
62+55.80	SPC00515123	10/9/96	Zell Peterman	USGS	Right Rib	1.5 meter above invert. Cavity is adjacent to steeply dipping fracture
62+71	SPC00515153	10/9/96	June Fabryka-Martin	LANL	Right Rib	1 meter above invert
62+71.06	SPC00515122	10/9/96	Zell Peterman	USGS	Right Rib	1 meter below spring line
63+00	SPC00515154	10/9/96	June Fabryka-Martin	LANL	Right Rib	1 meeter above invert
63+20.2	SPC00510774	10/9/96	Zell Peterman	USGS	Right Rib	2 meters above invert
63+21	SPC00515156	10/9/96	June Fabryka-Martin	LANL	Right Rib	1 meter above invert
63+26	SPC00515157	10/9/96	June Fabryka-Martin	LANL	Right Rib	1 meter above invert
63+30	SPC00515158	10/9/96	June Fabryka-Martin	LANL	Right Rib	1 meter above invert
63+38.1	SPC00510773	10/9/96	Zell Peterman	USGS	Right Rib	2 meters above invert
63+6+60	SPC00515155	10/9/96	June Fabryka-Martin	LANL	Right rib	1 meter above invert
63+64.52	SPC00510775	10/9/96	Zell Peterman	USGS	Right Rib	2 meters above invert
63+7.75	SPC00515121	10/9/96	Zell Peterman	USGS	right Rib	1.5 meters above invert - brecciate zone at 7 cm wide
63+73	SPC00515188	11/19/96	June Fabryka-Martin	LANL	Right Rib	1 meter above invert
63+81	SPC00515187	11/19/96	June Fabryka-Martin	LANL	Right Rib	1 meter above invert
64+00	SPC00515186	11/20/96	June Fabryka-Martin	LANL	Right Rib	1 meter above invert
64+12.4	SPC00521215	12/17/96	Zell Peterman	USGS	Right rib	In upper lithophysal zone of Tpt, Tptpn, lithophysal cavity opal
64+34.5	SPC00515185	11/20/96	June Fabryka-Martin	LANL	Right Rib	1 meter above invert
64+50	SPC00515184	11/20/96	June Fabryka-Martin	LANL	Right Rib	1 meter above invert
64+93	SPC00515182	11/19/96	June Fabryka-Martin	LANL	Right Rib	cc in fract. below lythophysal cavity - 1.5 m above invert
64+96.1	SPC00521285	4/2/97	Zell Peterman	LANL	Right Rib	approx. 2 m above invert
65+00	SPC00515181	11/19/96	June Fabryka-Martin	LANL	Right Rib	Systematic - 1 meter above invert
65+20	SPC00515180	11/19/96	June Fabryka-Martin	LANL	Right Rib	Frx zone 1 meter above invert
65+56	SPC00515179	11/19/96	June Fabryka-Martin	LANL	Right rib	large fracture zone 1.5 m wide, 1 meter above invert
65+80	SPC00515178	11/19/96	June Fabryka-Martin	LANL	Right Rib	large 2 m wide fracture zone - 1 meter above invert
66+00	SPC00515177	11/19/96	June Fabryka-Martin	LANL	Right Rib	Systematic w/2 intersecting fractures - 1 meter above invert
66+00	SPC00521284	4/2/97	Zell Peterman	LANL	Right rib	approx.20-40 cm above invert
66+15	SPC00515176	11/19/96	June Fabryka-Martin	LANL	Right Rib	cc cemented fault breccia - 2.5 meters above invert
66+15	SPC00521283	4/2/97	Zell Peterman	LANL	Right Rib	approx. 2 meters above invert
66+40	SPC00515175	11/19/96	June Fabryka-Martin	LANL	Right Rib	Fault Zone in TSw w/2 meter offset - I meter above invert

66+88.6	SPC00521214	12/17/96	Zell Peterman	USGS	Right Rib	Three samples across calcite-rich horizon at contact in Tpbt4 between upper pyroclastic fill and reworked tuff
67+00	SPC00515174	11/19/96	June Fabryka-Martin	LANL	Right Rib	Systematic in non-faulted/non-welded
67+20.4	SPC00515183	11/20/96	June Fabryka-Martin	LANL	Right Rib	.5 meters below string line
67+27	SPC00515172	11/19/96	June Fabryka-Martin	LANL	Right Rib	Fault in high porosity zone of non-welded wetted appearance - 1 meter above invert
67+35	SPC00515173	11/19/96	June Fabryka-Martin	LANL	Right Rib	Contact welded/Non-welded - 1 meter above invert
67+61.5	SPC00515170	11/19/96	June Fabryka-Martin	LANL	Right Rib	1 meter above invert
67+73	SPC00515171	11/19/96	June Fabryka-Martin	LANL	Right Rib	Sandy Zone (subhorizontal) in Ptn that appears damp - 1 meter above invert
67+81.0	SPC00521212	12/17/96	Zell Peterman	USGS	Right Rib	3 m from Dual Wash Fault in monderately welded Tiva Canyon
67+84	SPC00521213	12/17/96	Zell Peterman	USGS	Right Rib	Fracture filling of only calcite in moderately welded Tiva Canyon - breciated crystalline
67+87	SPC00515133	11/19/96	June Fabryka-Martin	LANL	Right Rib	1 meter above invert
67+87.2	SPC00515134	11/19/96	June Fabryka-Martin	LANL	Right Rib	1 meter above invert
67+90.5	SPC00515132	11/19/96	June Fabryka-Martin	LANL	Right Rib	1 meter above invert
68+00	SPC00521127	12/17/96	June Fabryka-Martin	LANL		0.5 meter above invert
68+18	SPC00521211	12/17/96	Zell Peterman	USGS	Right Rib	Upper lithophysal zone in lithophysal cavity
68+38.1	SPC00521210	12/17/96	Zell Peterman	USGS	Right Rib	lithophysal cavity filling
68+63	SPC00521126	12/17/96	June Fabryka-Martin	LANL	right rib	2.5 meter above invert
68+76	SPC00521209	12/17/96	Zell Peterman	USGS	Right Rib	Uppedr lithophysal zone of Topopah Spring
68+88.28	SPC00521208	12/17/96	Zell Peterman	USGS		Topopah spring
69+00	SPC00521123	12/17/96	June Fabryka-Martin	LANL		0.5 m from invert
69+14.5	SPC00521122	12/17/96	June Fabryka-Martin	LANL	Right Rib	1 meter from invert
69+32.5	SPC00521121	12/17/96	June Fabryka-Martin	LANL	Right Rib	10 cm fracture w/gouge
69+41.7	SPC00521207	12/17/96	Zell Peterman	USGS		Lower part of crystal rich topopah spring TpTRN1 (Nonwelding) Fracture filling along gouge zone (1 foot)
69+41.7	SPC00521120	12/17/96	June Fabryka-Martin	LANL	Right Rib	1.5 meter above invert
69+47	SPC00522221	4/29/97	June Fabryka-Martin	LANL	Right Rib	.25 meter above invert
69+47	SPC00522222	4/29/97	June Fabryka-Martin	LANL	Right Rib	
69+68	SPC00522220	4/29/97	June Fabryka-Martin	LANL	Right Rib	1 meter above invert
69+79	SPC00521282	4/2/97	Zell Peterman	LANL	Right Rib	30-80 cm above invert
69+95.8	SPC00522219	4/29/97	June Fabryka-Martin	LANL	Right Rib	1 meter above invert
69+96	sPC00521281	4/2/97	Zell Peterman	LANL	right rib	approx. 150 cm above invert
70+00	SPC00521280	4/2/97	Zell Peterman	LANL	Right Rib	about 180 cm above invert

70+19	SPC00522218	4/29/97	June Fabryka-Martin	LANL	Right Rib	.5 meter above invert
70+36	SPC00522217	4/29/97	June Fabryka-Martin	LANL	Right Rib	.75 meter above invert
70+50	SPC00522216	4/29/97	June Fabryka-Martin	LANL	Right Rib	same level as invert
70+55.5	SPC00521279	4/2/97	Zell Peterman	LANL	Right Rib	approx. 1 m above invert
70+55.5	SPC00522215	4/29/97	June Fabryka-Martin	LANL	Right Rib	.75 meters above invert
70+62	SPC00521278	4/2/97	Zell Peterman	LANL	Right Rib	approx. 100-130 cm above invert
70+66	SPC00522214	4/29/97	June Fabryka-Martin	LANL	Right Rib	1 meter above invert
70+90.3	sPC00521277	4/2/97	Zell Peterman	LANL	Right Rib	100-130 cm above invert
71+03	SPC00521276	4/2/97	Zell Peterman	LANL	Right Rib	right rib over a distance of approx. 1 to 3 meters below springline
71+34	SPC00522212	4/29/97	June Fabryka-Martin	LANL	Right Rib	.75 meters above invert
71+39	SPC00522213	4/29/97	June Fabryka-Martin	LANL	Right Rib	.5 meters above invert
71+41	SPC00522211	4/29/97	June Fabryka-Martin	LANL	Right Rib	.5 meters above invert
71+50	SPC00522210	4/29/97	June Fabryka-Martin	LANL	Right Rib	.25 meters above invert
71+65.8	SPC00521275		Zell Peterman	LANL	Right rib	approx. 120 cm above invert
71+83.3	SPC00521274	4/1/97	Zell Peterman	LANL	Right Rib	170 cm above invert
72+31.3	SPc00521273	4/1/97	Zell Peterman	LANL	Right Rib	approx. 140 cm above invert.
72+50	SPC00522209	4/29/97	June Fabryka-Martin	LANL	Right Rib	1 meter above invert
72+69	SPC00522208	4/29/97	June Fabryka-Martin	LANL	Right Rib	1 meter above invert
72+94.5	SPC00521272	4/1/97	Zell Peterman	LANL	right rib	approx. 1 meter below springline
73+48	SPC00522207	4/28/97	June Fabryka-Martin	LANL	Right Rib	.5 meters above invert
73+66	SPc00521270	4/1/97	Zell Peterman	LANL	Right Rib	aapprox.120 cm below springline
73+66	SPC00521271	4/1/97	Zell Peterman	LANL	Right Rib	approx. 2 meters above invert
74+33.2	SPC00521269	4/1/97	Zell Peterman	LANL	Right Rib	1-1.5m below spring line
74+38	SPC00521267	4/1/97	Zell Peterman	LANL	Right Rib	approx. 2-2.5 m above invert
74+42.5	SPC00521268	4/1/97	Schon Levy/Dave Vani	LANL	right rib	1 m above the invert at right rib
74+43	SPC00521266	4/1/97	Zell Peterman	LANL	Right Rib	approx. 130 cm above invert
74+43	SPC00522206	4/28/97	June Fabryka-Martin	LANL	Right Rib	.5 meters above invert
74+50	SPC00522205	4/28/97	June Fabryka-Martin	LANL	Right Rib	.25 meters above invert
74+89	SPC00522202	4/28/97	June Fabryka-Martin	LANL	Right Rib	.5 meters above invert
74+98	SPC00521265	4/1/97	Zell Peterman	LANL	Right Rib	approx. 150 cm above invert
75+06.8	SPC00521264	4/1/97	Zell Peterman	LANL	Right Rib	approx. 20 m above invert.
75+09	SPC00522201	4/28/97	June Fabryka-Martin	LANL	Right Rib	.5 meters above invert
75+10	SPC00522204	4/28/97	June Fabryka-Martin	LANL	Right Rib	.5 meters above invert
75+15.5	SPC00521263	4/1/97	Zell Peterman	LANL	Right Rib	150 cm below springline
75+20	SPC00522200	4/28/97	June Fabryka-Martin	LANL	Right Rib	1 meter above invert
75+34	SPC00521287	4/28/97	June Fabryka-Martin	LANL	Right Rib	1.5 meters above invert
75+47	SPC00521288	4/28/97	June Fabryka-Martin	LANL	Right Rib	.5 meters above invert
75+53	SPC0052189	4/28/97	June Fabryka-Martin	LANL	Right Rib	.75 meters above invert
75+53.1	SPC00521262	4/1/97	Zell Peterman	LANL	Right rib	approx. 150 cm above invert
75+7.7	SPC00521261	4/1/97	Zell Peterman	LANL	Right Rib	150 cm above invert
75+70	SPC00521260	4/2/97	Zell Peterman	LANL	Right Rib	150 cm above invert
75+78	SPC00521290	4/28/97	June Fabryka-Martin	LANL	Right Rib	1 meter above invert
75+78	SPC0052190	4/28/97	June Fabryka-Martin	LANL	Right Rib	.75 meters above invert
76+30	SPC0052191	4/28/97	June Fabryka-Martin	LANL	Right Rib	1 meter above invert

76+31	SPC0052192	4/28/97	June Fabryka-Martin	LANL	Right Rib	1 meter above invert
76+50	SPC0052195	4/28/97	June Fabryka-Martin	LANL	Right Rib	.25 meters above invert
76+76	SPC00521294	4/28/97	June Fabryka-Martin	LANL	Right Rib	1 meter above invert
77+00	SPC00521293	4/28/97	June Fabryka-Martin	LANL	Right Rib	.25 meters above invert
77+19.4	SPC00524901	7/15/97	June Fabryka-Martin	LANL	Right Rib	bulk rock
77+28	SPC00524903	7/16/97	Zell Peterman	USGS	Right Rib	2 m above invert
77+38	SPC00524904	7/16/97	Zell Peterman	USGS	Right Rib	2 m above invert
78+06.4	SPC00524905	7/16/97	Zell Peterman	USGS	Right Rib	2 m above invert
78+56	SPC00524906	7/16/97	Zell Peterman	USGS	Right Rib	1.5 m above invert
0+95	SPC00521129	12/17/96	June Fabryka-Martin	LANL		Alcove 6, Tptmn - East Side of Sundance Fault
0+98	SPC00521130	12/17/96	June Fabryka-Martin	LANL		Alcove 6 approx. at Sundance Flt.
	SPC00521216	12/17/96	Zell Peterman	USGS	Left Rib	Alcove 6, Tptmn - East Side of Sundance Fault
	SPC00521296	4/18/97	Ann Marie Meike	LLNL	Right Rib	Turnaround niche in alcove #7, taken from the muck pile

APPENDIX IV: Descriptive Statistics for Fractures, Shears, and Faults

APPENDIX IV: Descriptive Statistics for Fractures, Shears, and Faults

General

Each of the lithologic units mapped in the South Ramp area is analyzed for general statistics. The data were obtained from DLS measurements of strike, dip, trace length, aperture, and roughness. The stratigraphic units analyzed include: Tptpll, Tptpmn, Tptpul, Tptrl, Tptrn, Tptrv, Tiva Canyon, and bedded tuff units. The objective is to provide summary statistics for each of the units.

The mechanical response of any rock unit controls the detailed fracture distribution and the univariate properties of fracture sets. The statistics are based on a lumping of the fracture properties for all occurrences of any unit. Plots of some of these properties against stationing reveal the appropriateness of this concept.

For trace length, spacing, aperture, and roughness, univariate statistics are used. This assumes that there is no correlation between these properties. The statistics include three measures of central tendency: the mean, the median, and the mode. The mean is the sum of the data values divided by the number of data. The median is the middle ranked value. In a data set with an odd number of values, the median is the value with rank (n+1)/2; with an even number of values, the median is a value halfway between the two middle values with ranks n/2 and n/2+1. The mode is the most frequently occurring value. The range equals the maximum value minus the minimum value. Kurtosis measures the degree of peakedness in symmetric distributions. If a symmetric distribution is flatter than the normal distribution, that is, if there are more values in the tails than a corresponding normal distribution, the kurtosis is positive. If the distribution is more peaked (if there are fewer values in the tails) then the kurtosis is negative. Skewness refers to the lack of symmetry in a distribution. If there are few extreme values in the positive direction, we say that the distribution is positively skewed, or skewed to the right. If there are few extreme values in the negative direction, then the distribution is skewed to the left. If the mode is less than the

mean then the distribution is skewed to the left. If the mode is greater than the mean, the distribution is skewed to the right. Otherwise, the distribution is symmetric or approximately symmetric. The spreadsheet program Excel v5.0 is used to estimate the univariate statistical measures.

The distribution of fracture length is seldom normal and usually is skewed. Measurement of fracture length is a problem when only the apparent, rather than the true length can be measured. The mean fracture length estimate can be low if only the visible lengths are used due to truncation of the exposure or lack of visibility of both ends of the fracture. This is called censoring. This is avoided in two ways. First, the length statistics are computed for only those fractures with two ends exposed. Second, correction for censoring is done by summing the lengths observed regardless of the number of ends exposed and then dividing by the number of 2-ended fractures (Baecher, 1980). This method is valid for a set of fractures.

Roughness as measured is not a continuous numeric parameter. There are six roughness measures: R1 is stepped; R2 is rough; R3 is moderately rough; R4 is slightly rough; R5 is smooth; and R6 is polished. Further details for roughness parameter assignment are given in Technical Procedure GP-32. Because roughness is a categorical parameter, categorical statistics are used to characterize the range of values observed. A cumulative percentage curve (plot of percentage of population less than or equal to the value) is given to represent the distribution of roughness values for the fractures. If the curve is vertical then roughness has a single value equal to the roughness value of the vertical line. As the curve flattens, a more uniform distribution of values is measured. Averages of this type of parameter may not be meaningful, but the range and median are.

Aperture, as measured in an excavation, is influenced by the removal of overburden stresses. The univariate statistics of maximum aperture are presented for all orientations in the hope that some of the stress relief effects will be negated.

Lithologic Units

Tptpll: crystal-poor lower lithophysal

The univariate statistics description of properties is appropriate for each set of fractures identified. Only Set 1, the dominant set, is characterized. Set 1 has azimuths ranging from 140° to 170° and complementary azimuths of 320° to 350°. A frequency-of-occurrence histogram shows the extent of Set 1 azimuths (fig. A4.1).

Within Set 1, there are fractures with two ends visible, one end visible, and no ends visible. Only for the two-ends-visible class is an unbiased estimate of length. For the other classes, the lengths are minimum values. Mixing these classes with the two-ends-visible class is technically incorrect without adjusting the minimum values. For simplicity and clarity, only the two-ends-visible class is analyzed. There are 9 fractures out of the 11 measured fractures in this class. The mean length is 2.11 meters. The median length is 1.73 meters. The range is denoted by square brackets [min, max], [1.03, 5.67], and is 4.64 meters. Kurtosis is positive, so the crystal-poor lower lithophysal, Set-1, two-ends-visible lengths are flatter than a normal distribution. The corrected mean length is 3.10 meters (Baecher, 1980).

Spacing is an interpreted parameter. First, sets are identified and then spacing can be estimated from the interfracture distance along the traceline. For this parameter, all fractures regardless of their truncation style (one-ended, two-ended, or no-ended) are used in the estimate. The values of the mean, median, and mode are dependent on the angle of intersection between the set orientation and the orientation of the traceline but the distribution is not (Priest, 1993). For sets that are not perpendicular to the traceline, the mean, median, and mode values are larger than the "true" values. For the purpose of this report the description of the distribution is of significance, not the true values. The mean interfracture distance is 3.56 meters. The median distance is 2.77 meters. The range, [0.3, 10.48], is 10.18 meters. Kurtosis is negative, so the crystal-poor lower

lithophysal, Set-1, interfracture distances are more peaked than a normal distribution.

Roughness ranges from 1 to 5 with most of the values less than 4. The median roughness is between 2 and 3 (fig A4.1.1), rough to moderately rough.

The maximum aperture ranges from 0 mm to 5 mm. Approximately 61 percent of the 23 apertures measured are 0 mm, approximately 96 percent of the maximum apertures are less than or equal to 4 mm. The kurtosis is slightly positive and the mode is less than the mean, so the maximum apertures are approximately normally distributed but are skewed to the left.

Tptpmn: crystal-poor middle nonlithophysal

The univariate statistics description of properties is appropriate for each set of fractures identified. Only Set 1, the dominant set, is characterized. Set 1 has azimuths ranging from 130° to 180° and complementary azimuths of 310° to 360°. A frequency-of-occurrence histogram shows the extent of Set 1 azimuths (fig. A4.2).

Within Set 1, there are fractures with two ends visible, one end visible, and no ends visible. Only for the two-ends-visible class is there an unbiased estimate of length. For the other classes, the lengths are minimum values. Mixing these classes with the two-ends-visible class is technically incorrect without adjusting the minimum values. For simplicity and clarity, only the two-ends-visible class is analyzed. There are 299 fractures out of the 543 measured fractures in this class. The mean length is 2.53 meters. The median length is 1.86 meters. The mode length is 1.1 meters. The range is denoted by square brackets [min, max], [1, 14.21], and is 13.21 meters. Kurtosis is positive and the mode is less than the mean, so the crystal-poor non-lithophysal, Set-1, two-ends-visible lengths are flatter than a normal distribution and are skewed to the left. The corrected mean length is 4.97 meters (Baecher, 1980).

The mean interfracture distance is 1.19 meters. The median distance is 0.7 meters. The mode

distance is 0.3 meters. The range, [0.01, 10.49], is 10.48 meters. Kurtosis is positive and the mode is less than the mean, so the crystal-poor non-lithophysal, Set-1, interfracture distances are flatter than a normal distribution and are skewed to the left. Because there are segments of the non-lithophysal lithology, separated by other lithologies, the distances between end fractures (for example, the last fracture station in one segment and the first in the next segment) are not used in the distribution statistics.

Roughness ranges from 1 to 5 with most of the values between 2 and 4. The median roughness is close to 3 (fig A4.2.1), moderately rough.

The maximum aperture ranges from 0 mm to 300 mm. Approximately 79 percent of the 1188 apertures measured are 0 mm; approximately 96 percent of the maximum apertures are less than or equal to 8 mm. The kurtosis is positive and the mode is less than the mean, so the maximum apertures are flatter than a normal distribution and are skewed to the left.

Tptpul: crystal-poor upper lithophysal

The univariate statistics description of properties is appropriate for each set of fractures identified. Only Set 1, the dominant set, is characterized. Set 1 has azimuths ranging from 130° to 180° and complementary azimuths of 310° to 360°. A frequency-of-occurrence histogram shows the extent of Set 1 azimuths (fig. A4.3).

Within Set 1, there are fractures with two ends visible, one end visible, and no ends visible. Only for the two-ends-visible class is there an unbiased estimate of length. For the other classes, the lengths are minimum values. Mixing these classes with the two-ends-visible class is technically incorrect without adjusting the minimum values. For simplicity and clarity, only the two-ends-visible class is analyzed. There are 59 fractures out of the 102 measured fractures in this class. The mean length is 1.81 meters. The median length is 1.6 meters. The mode length is 1.5 meters. The range is denoted by square brackets [min, max], [1, 4.67], and is 3.67 meters. Kurtosis is

positive and the mode is less than the mean, so the crystal-poor upper lithophysal, Set-1, two-ends-visible-lengths are flatter than a normal distribution and are skewed to the left. The corrected mean length is 3.86 meters (Baecher, 1980).

The mean interfracture distance is 3.18 meters. The median distance is 1.93 meters. The mode distance is 0.22 meters. The range, [0.01, 20.72], is 20.71 meters. Kurtosis is positive and the mode is less than the mean, so the crystal-poor upper lithophysal, Set-1, interfracture distances are flatter than a normal distribution and are skewed to the left. Because there are segments of the lithophysal lithology, separated by other lithologies, the distances between end fractures (for example, the last fracture station in one segment and the first in the next segment) are not used in the distribution statistics.

Roughness ranges from 1 to 5 with most of the values between 2 and 4. The median roughness is between 2 and 3 (fig A4.3.1), rough to moderately rough.

The maximum aperture ranges from 0 mm to 20 mm. Approximately 80 percent of the 174 apertures measured are 0 mm; approximately 96 percent of the maximum apertures are less than or equal to 8 mm. The kurtosis is positive and the mode is less than the mean, so the maximum apertures are flatter than a normal distribution and are skewed to the left.

Tptrl: crystal-rich lithophysal

The univariate statistics description of properties is appropriate for each set of fractures identified. Only Set 1, the dominant set, is characterized. Set 1 has azimuths ranging from 130° to 170° and complementary azimuths of 310° to 350°. A frequency-of-occurrence histogram shows the extent of Set 1 azimuths (fig. A4.4).

Within Set 1, there are fractures with two ends visible, one end visible, and no ends visible. Only for the two-ends-visible class is there an unbiased estimate of length. For the other classes, the

lengths are minimum values. Mixing these classes with the two-ends-visible class is technically incorrect without adjusting the minimum values. For simplicity and clarity, only the two-ends-visible class is analyzed. There are 16 fractures out of the 31 measured fractures in this class. The mean length is 2.11 meters. The median length is 1.93 meters. The range is denoted by square brackets [min, max], [1.15, 3.8], and is 2.65 meters. Kurtosis is positive, so the crystal-rich lithophysal, Set-1, two-ends-visible lengths are flatter than a normal distribution. The corrected mean length is 4.78 meters (Baecher, 1980).

The mean interfracture distance is 4.19 meters. The median distance is 1.93 meters. The range, [0.1, 32.85], is 32.75 meters. Kurtosis is positive, so the crystal-rich lithophysal, Set-1, interfracture distances are flatter than a normal distribution. Because there are segments of the lithophysal lithology, separated by other lithologies, the distances between end fractures (for example, the last fracture station in one segment and the first in the next segment) are not used in the distribution statistics.

Roughness ranges from 1 to 5 with most of the values between 1 and 4. The median roughness is close to 2 (fig A4.4.1), rough.

The maximum aperture ranges from 0 mm to 110 mm. Approximately 69 percent of the 61 apertures measured are 0 mm; approximately 92 percent of the maximum apertures are less than or equal to 6 mm. The kurtosis is positive and the mode is less than the mean, so the maximum apertures are flatter than a normal distribution and are skewed to the left.

Tptprn: crystal-rich nonlithophysal

The univariate statistics description of properties is appropriate for each set of fractures identified. Only Set 2, the dominant set, is characterized. Set 2 has azimuths ranging from 190° to 210° and complementary azimuths of 010° to 040°. A frequency-of-occurrence histogram shows the extent of Set 2 azimuths (fig. A4.5).

Within Set 2, there are fractures with two ends visible, one end visible, and no ends visible. Only for the two-ends-visible class is there an unbiased estimate of length. For the other classes, the lengths are minimum values. Mixing these classes with the two-ends-visible class is technically incorrect without adjusting the minimum values. For simplicity and clarity, only the two-ends-visible class is analyzed. There are 45 fractures out of the 65 measured fractures in this class. The mean length is 2.22 meters. The median length is 1.8 meters. The mode length is 1.8 meters. The range is denoted by square brackets [min, max], [1, 8.86], and is 7.86 meters. Kurtosis is positive and the mode is equal to the mean, so the crystal-rich nonlithophysal, Set-2, two-ends-visible lengths are flatter than a normal distribution and are not skewed. The corrected mean length is 4.7 meters (Baecher, 1980).

The mean interfracture distance is 3.78 meters. The median distance is 2.33 meters. The mode distance is 1.71 meters. The range, [0.09, 21.93], is 21.84 meters. Kurtosis is positive and the mode is less than the mean, so the crystal-rich nonlithophysal, Set-2, interfracture distances are flatter than a normal distribution and are skewed to the left. Because there are segments of the non-lithophysal lithology, separated by other lithologies, the distances between end fractures (for example, the last fracture station in one segment and the first in the next segment) are not used in the distribution statistics.

Roughness ranges from 1 to 5 with most of the values between 1 and 3. The median roughness is 2 (fig A4.5.1), rough.

The maximum aperture ranges from 0 mm to 250 mm. Approximately 64 percent of the 207 apertures measured are 0 mm; approximately 98 percent of the maximum apertures are less than or equal to 40 mm. The kurtosis is positive and the mode is less than the mean, so the maximum apertures are flatter than a normal distribution and are skewed to the left.

Tptrv: crystal-rich vitric

The univariate statistics description of properties is appropriate for each set of fractures identified. Only Set 1, the dominant set, is characterized. Set 1 has azimuths ranging from 170° to 210° and complementary azimuths of 350° to 030°. A frequency-of-occurrence histogram shows the extent of Set 1 azimuths (fig. A4.6).

Within Set 1, there are fractures with two ends visible, one end visible, and no ends visible. Only for the two-ends-visible class is there an unbiased estimate of length. For the other classes, the lengths are minimum values. Mixing these classes with the two-ends-visible class is technically incorrect without adjusting the minimum values. For simplicity and clarity, only the two-ends-visible class is analyzed. There are 9 fractures out of the 21 measured fractures in this class. The mean length is 1.67 meters. The median length is 1.22 meters. The mode length is 1.15 meters. The range is denoted by square brackets [min, max], [1, 3.8], and is 2.8 meters. Kurtosis is positive and the mode is less than the mean, so the crystal-rich vitric, Set-1, two-ends-visible lengths are flatter than a normal distribution and are skewed to the left. The corrected mean length is 4.11 meters (Baecher, 1980).

The mean interfracture distance is 1.73 meters. The median distance is 1.25 meters. The mode distance is 1.25 meters. The range, [0.17, 4.12], is 3.95 meters. Kurtosis is negative and the mode is less than the mean, so the crystal-rich vitric, Set-1, interfracture distances are more peaked than a normal distribution and are skewed to the left. Because there are segments of the crystal-rich vitric lithology, separated by other lithologies, the distances between end fractures (for example, the last fracture station in one segment and the first in the next segment) are not used in the distribution statistics.

Roughness ranges from 1 to 4 with most of the values between 1 and 3. The median roughness is 2 (fig A4.6.1), rough.

The maximum aperture ranges from 0 mm to 30 mm. Approximately 68 percent of the 34 apertures measured are 0 mm; approximately 82 percent of the maximum apertures are less than or equal to 3 mm. The kurtosis is positive and the mode is less than the mean, so the maximum apertures are flatter than a normal distribution and are skewed to the left.

Bedded tuffs

The univariate statistics description of properties is appropriate for each set of fractures identified. All of the bedded tuff fractures are characterized.

Within the bedded tuff, there are fractures with two ends visible, one end visible, and no ends visible. Only for the two-ends-visible class is there an unbiased estimate of length. For the other classes, the lengths are minimum values. Mixing these classes with the two-ends-visible class is technically incorrect without adjusting the minimum values. For simplicity and clarity, only the two-ends-visible class is analyzed. There are 11 fractures out of the 22 measured fractures in this class. The mean length is 1.42 meters. The median length is 1.35 meters. The range is denoted by square brackets [min, max], [1, 1.9], and is 0.9 meters. Kurtosis is negative, so that the bedded tuff two-ends-visible lengths are more peaked than normal distribution. The corrected mean length is 11.4 meters (Baecher, 1980).

The mean interfracture distance is 3.20 meters. The median distance is 1.66 meters. The range, [0.05, 22.69], is 22.64 meters. Kurtosis is positive, so the bedded tuff, interfracture distances are flatter than a normal distribution. Because there are segments of the bedded tuff lithology, separated by other lithologies, the distances between end fractures (for example, the last fracture station in one segment and the first in the next segment) are not used in the distribution statistics.

Tiva Canyon: undivided

The univariate statistics description of properties is appropriate for each set of fractures

identified. Only Set 1, the dominant set, is characterized. Set 1 has azimuths ranging from 120° to 210° and complementary azimuths of 300° to 30°. A frequency-of-occurrence histogram shows the extent of Set 1 azimuths (fig. A4.7).

Within Set 1, there are fractures with two ends visible, one end visible, and no ends visible. Only for the two-ends-visible class is there an unbiased estimate of length. For the other classes, the lengths are minimum values. Mixing these classes with the two-ends-visible class is technically incorrect without adjusting the minimum values. For simplicity and clarity, only the two-ends-visible class is analyzed. There are 351 fractures out of the 449 measured fractures in this class. The mean length is 2.09 meters. The median length is 1.71 meters. The mode length is 1.08 meters. The range is denoted by square brackets [min, max], [1, 9.8], and is 8.8 meters. Kurtosis is positive and the mode is less than the mean, so the Tiva Canyon, Set-1, two-ends-visible lengths are flatter than a normal distribution and are skewed to the left. The corrected mean length is 2.8 meters (Baecher, 1980).

The mean interfracture distance is 1.47 meters. The median distance is 0.84 meters. The mode distance is 0.47 meters. The range, [0, 15.64], is 15.64 meters. Kurtosis is positive and the mode is less than the mean, so the Tiva Canyon, Set-1, interfracture distances are flatter than a normal distribution and are skewed to the left. Because there are segments of the Tiva Canyon lithology, separated by other lithologies, the distances between end fractures (for example, the last fracture station in one segment and the first in the next segment) are not used in the distribution statistics.

Roughness ranges from 1 to 5 with most of the values between 2 and 4. The median roughness is close to 3 (fig A4.7.1), moderately rough.

The maximum aperture ranges from 0 mm to 100 mm. Approximately 61 percent of the 449 apertures measured are 0 mm; approximately 99 percent of the maximum apertures are less than or equal to 40 mm. The kurtosis is positive and the mode is less than the mean, so the maximum

apertures are flatter than a normal distribution and are skewed to the left.

Faults and Shears:

Faults and shears are discontinuities with offset. The difference between a fault and a shear is that a shear has less than 0.1 meter offset. For this reason, orientations are examined for the composite class faults and shears and compared to results of separate orientation analyses for faults and for shears. Faults and shears occur in all lithologies mapped. (fig. A4.8).

There are at least two distinct sets of shears. Set 1 has azimuths of 120° to 170° and complements of 300° to 350°. Set 2 has azimuths of 120° to 170° and complements of 010° to 030° (fig. A4.9). Set 1 faults have azimuths 190° to 210° and complements of 320° to 020° (fig. A4.10). For this report, the sense of offset is not directly used in the analysis. Recurrent movement occurs at Yucca Mountain so that the current sense of movement may not be as significant as the orientation of the discontinuity. There appears to be a relationship between the orientation of faults and shear sets. The fault trend bisects the shear set orientations as if the shears are complementary to the fault planes, much as secondary shears would be to a major throughgoing fault system.

In addition to the occurrence of sets which are subparallel to the fractures sets, the dip magnitude of the faults and shears changes across the approximate location of the Dune Wash Fault at Sta. 67+87 to 67+91. East of this fault, the range of dips increases, ranging as shallow as 45°; west of the fault, the dip magnitude predominantly is steeper than 70°. Across the Ghost Dance intersection at Sta. 57+30 no change in dip is observed (fig. A4.11).

Intensity of shears is asymmetric with respect to both the Ghost Dance Fault and the Dune Wash Fault but for different reasons. The Ghost Dance Fault has the Topopah Spring middle nonlithophysal unit on each side. The asymmetry may be a function of which side is actually moving with respect to the other. The moving block is disrupted more because it rides over

large-scale roughness. The Dune Wash fault asymmetry is attributed to the change of lithology across the fault; bedded units on the less intensely sheared west side and Topopah Spring units on more intensely sheared east side of the fault. The contrast in mechanical properties may be significant and adequate for explanation.

APPENDIX IV FIGURES

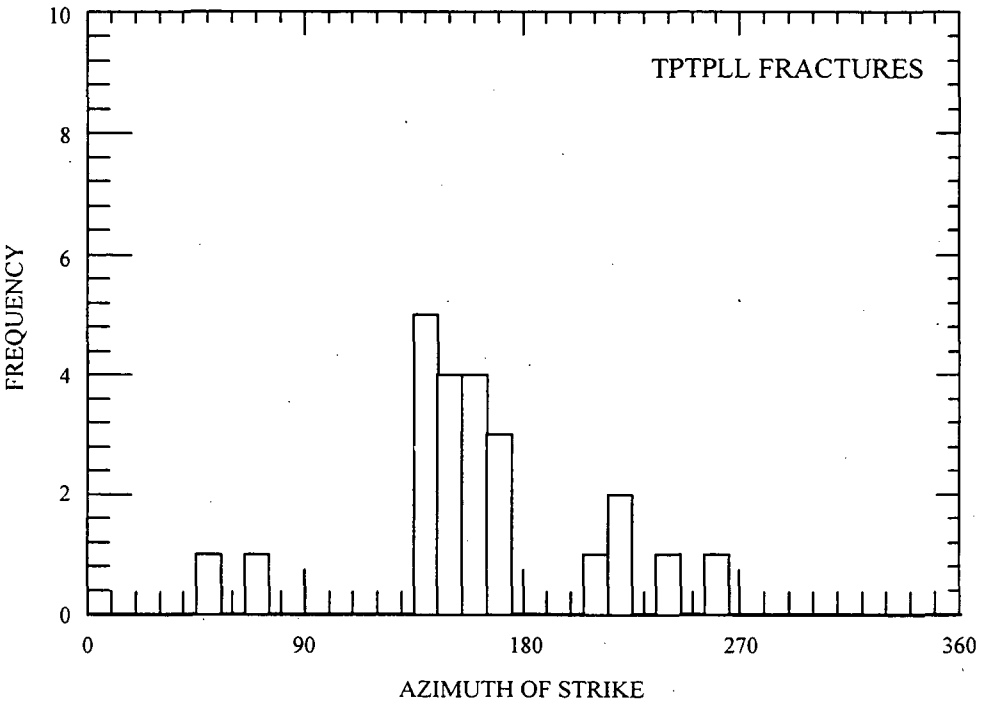

FIGURE A4.1: HISTOGRAM OF FRACTURE STRIKE: Tptpll

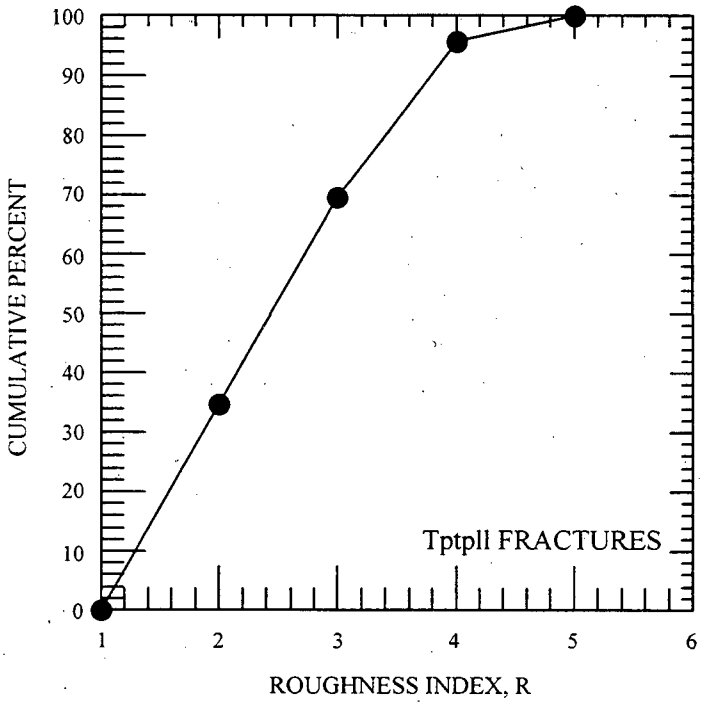

FIGURE A4.1.1: CUMULATIVE PERCENT OF ROUGHNESS: Tptpll

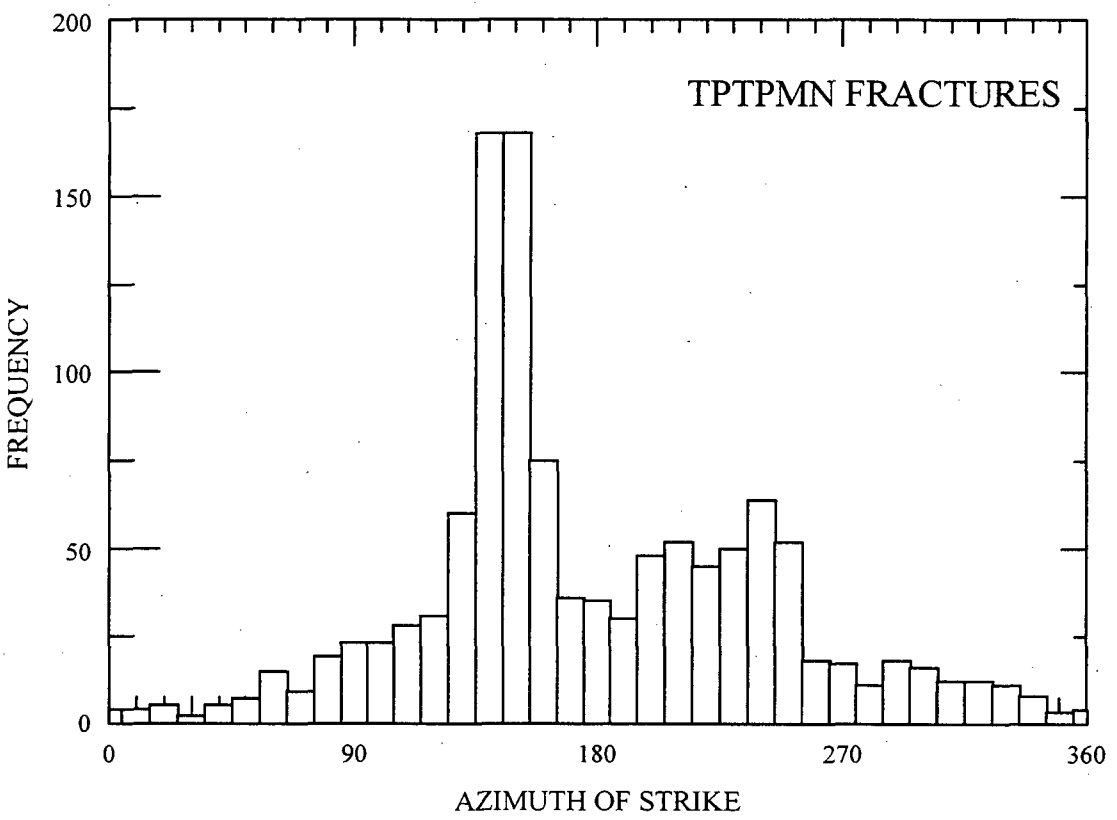

FIGURE A4.2: HISTOGRAM OF FRACTURE STRIKE: Tptpmn

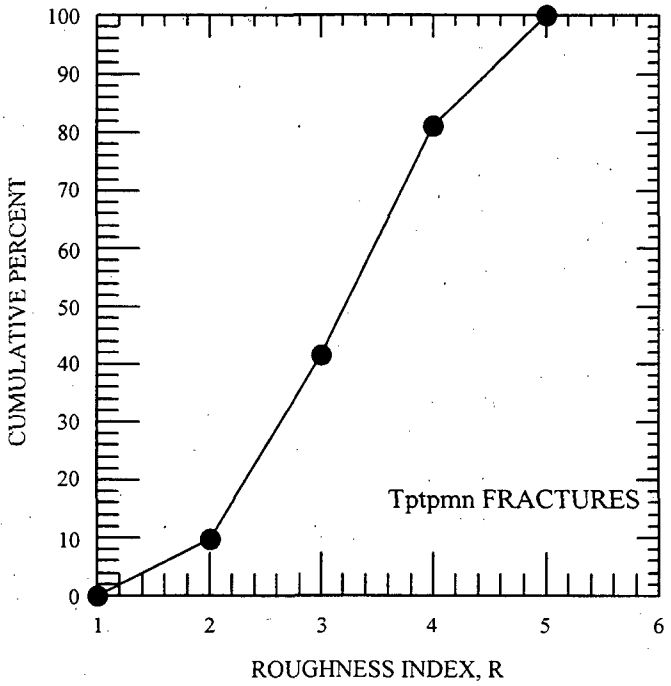

FIGURE A4.2.1: CUMULATIVE PERCENT OF ROUGHNESS: Tptpmn

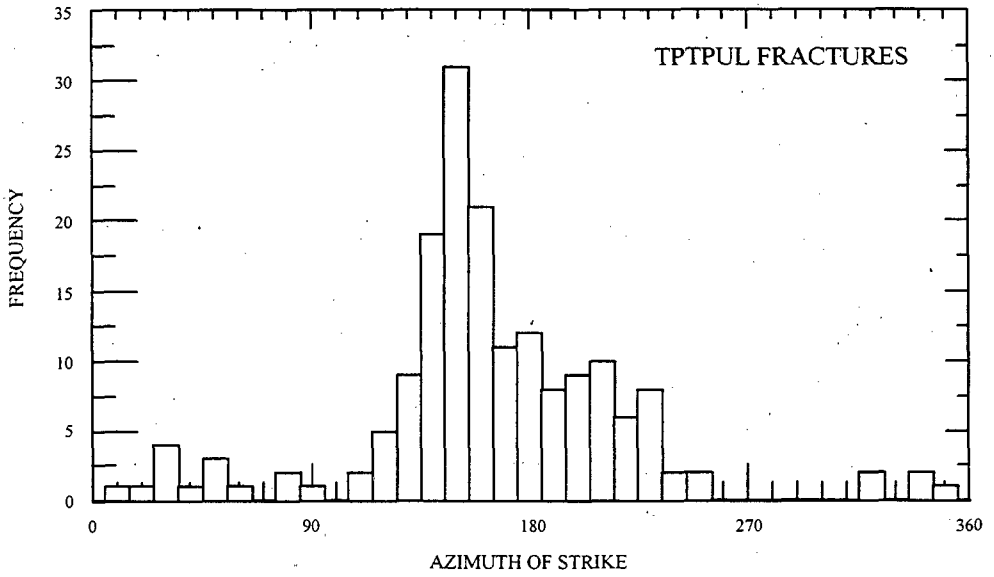

FIGURE A4.3: HISTOGRAM OF FRACTURE STRIKE: Tptpul

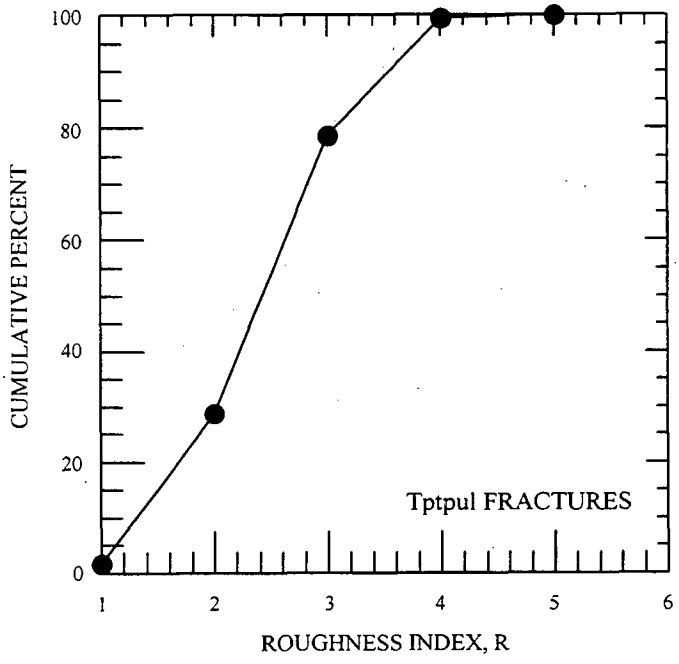

FIGURE A4.3.1: CUMULATIVE PERCENT OF ROUGHNESS: Tptpul

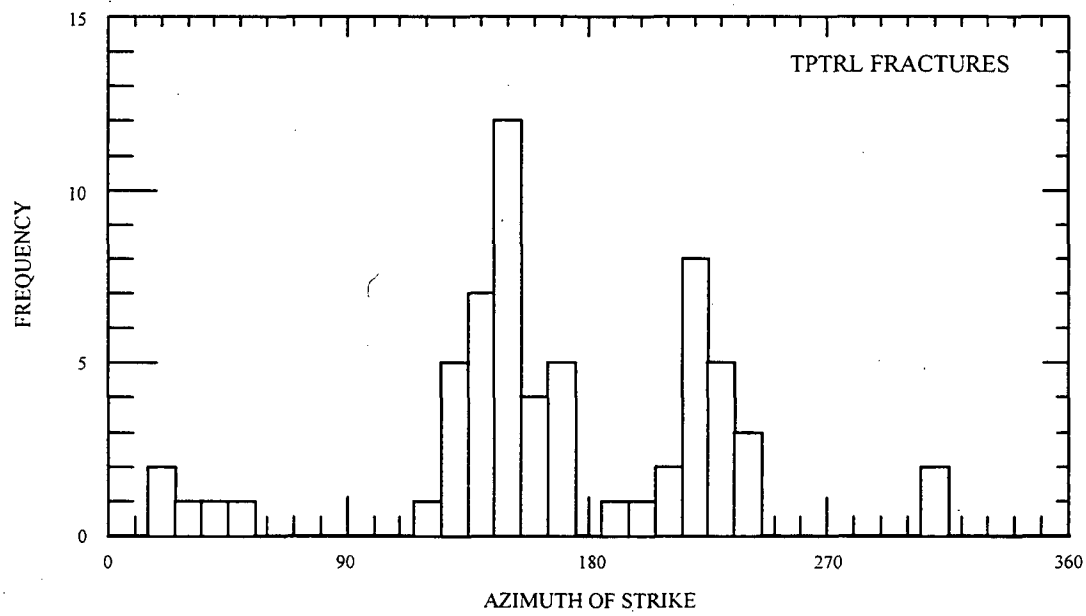

FIGURE A4.4: HISTOGRAM OF FRACTURE STRIKE: Tptrl

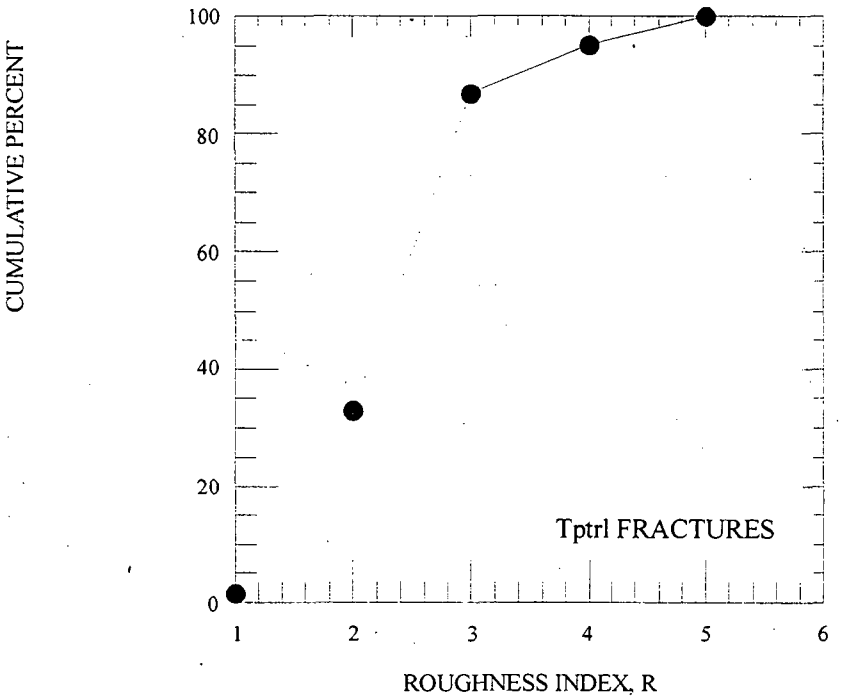

FIGURE A4.4.1: CUMULATIVE PERCENT OF ROUGHNESS: Tptrl

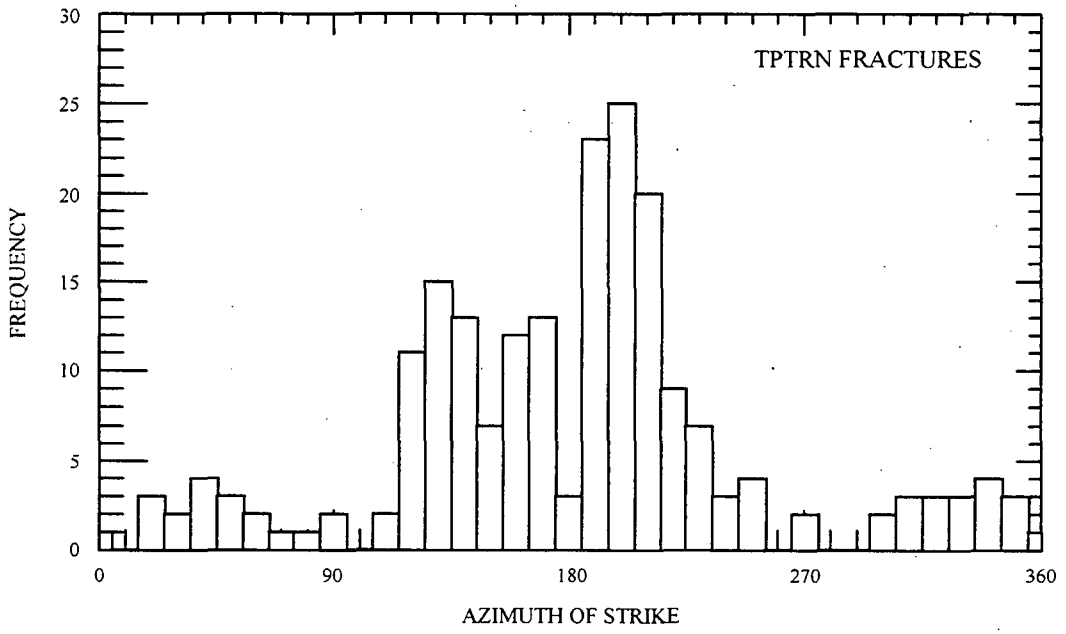

FIGURE A4.5: HISTOGRAM OF FRACTURE STRIKE: Tptrn

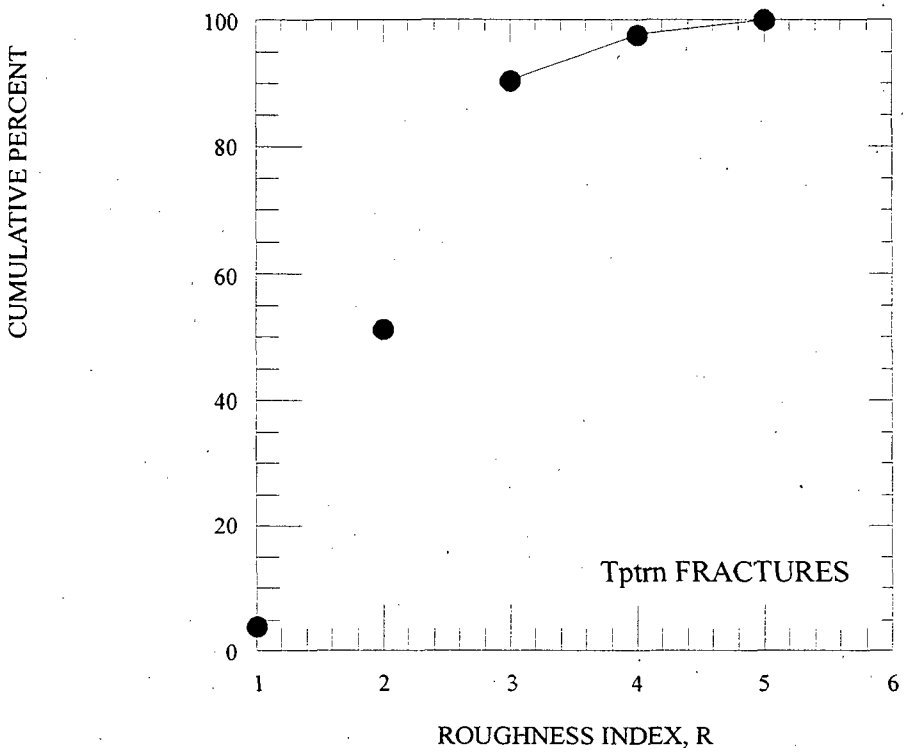

FIGURE A4.5.1: CUMULATIVE PERCENT OF ROUGHNESS: Tptrn

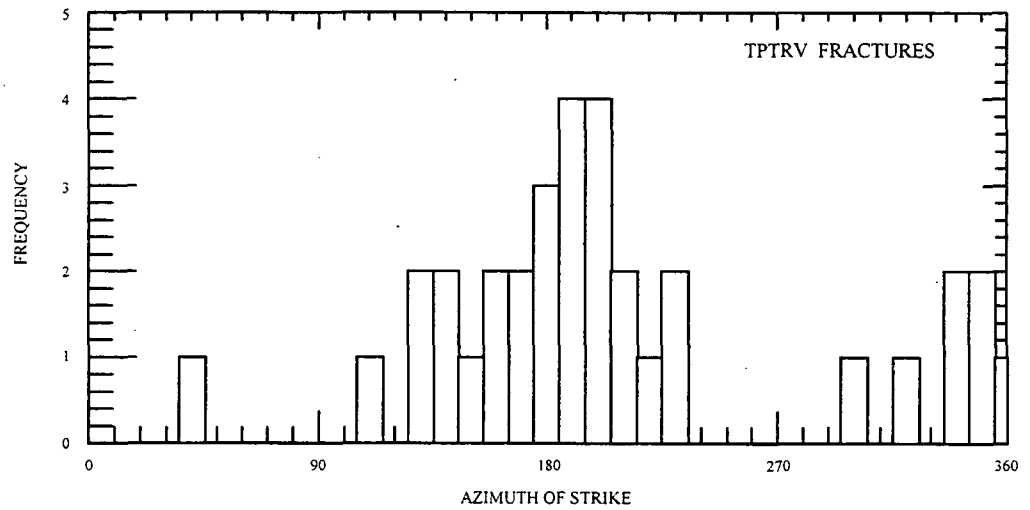

FIGURE A4.6: HISTOGRAM OF FRACTURE STRIKE: Tptrv

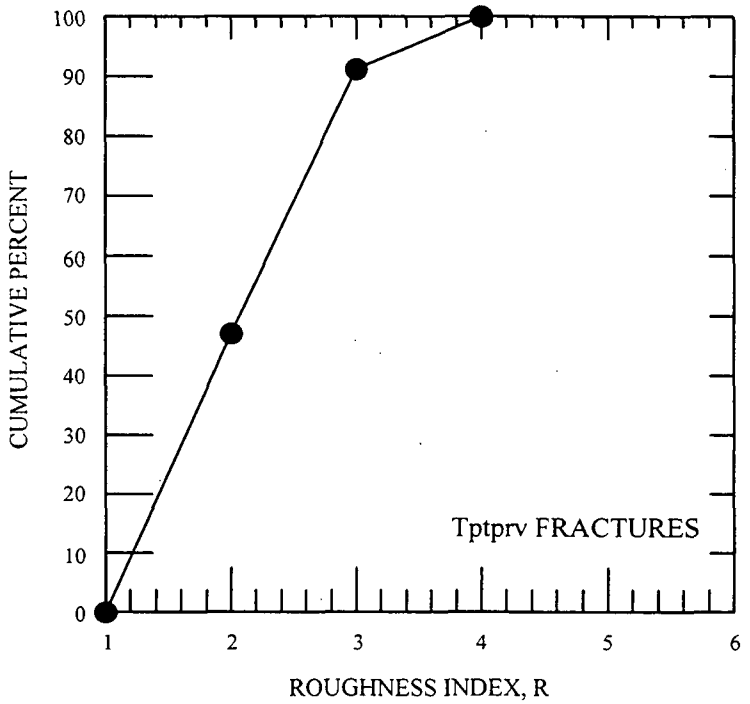

FIGURE A4.6.1: CUMULATIVE PERCENT OF ROUGHNESS: Tptrv

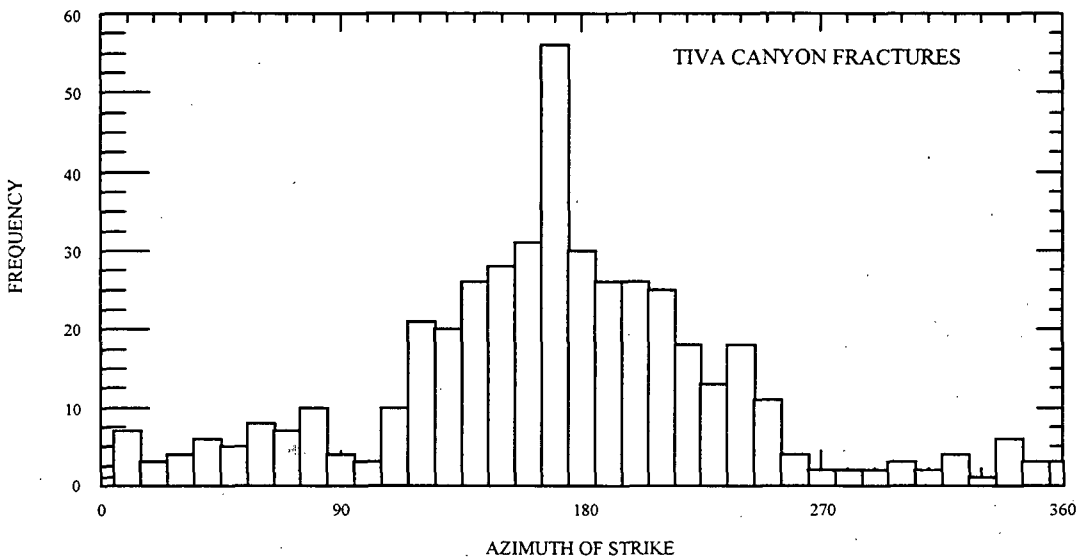

FIGURE A4.7: HISTOGRAM OF FRACTURE STRIKE: TIVA CANYON

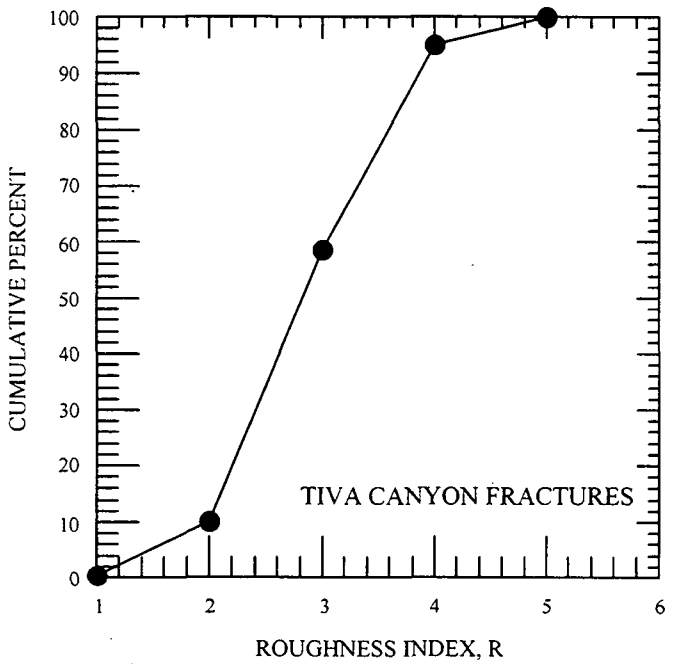

FIGURE A4.7.1: CUMULATIVE PERCENT ROUGHNESS: TIVA CANYON

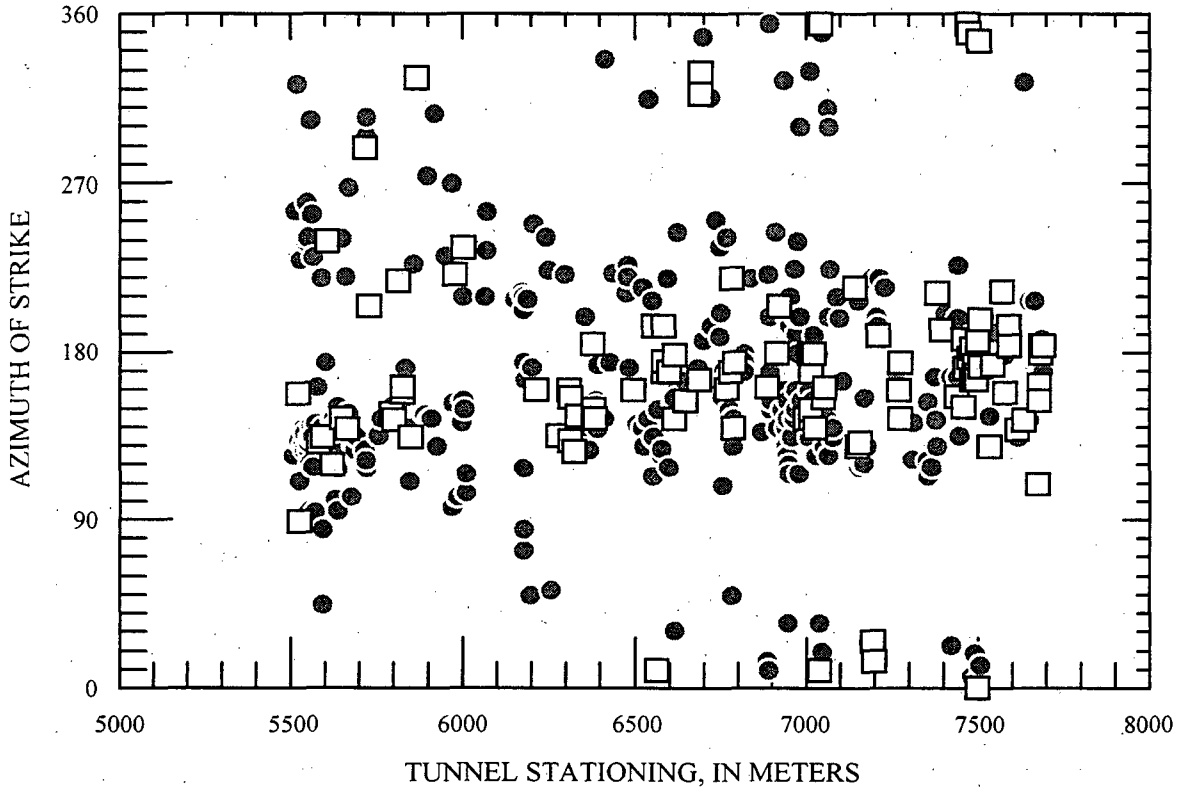

FIGURE A4.8: FAULTS AND SHEARS: AZIMUTH OF STRIKE AND STATIONING
FILLED CIRCLES:SHEARS
OPEN SQUARES:FAULTS

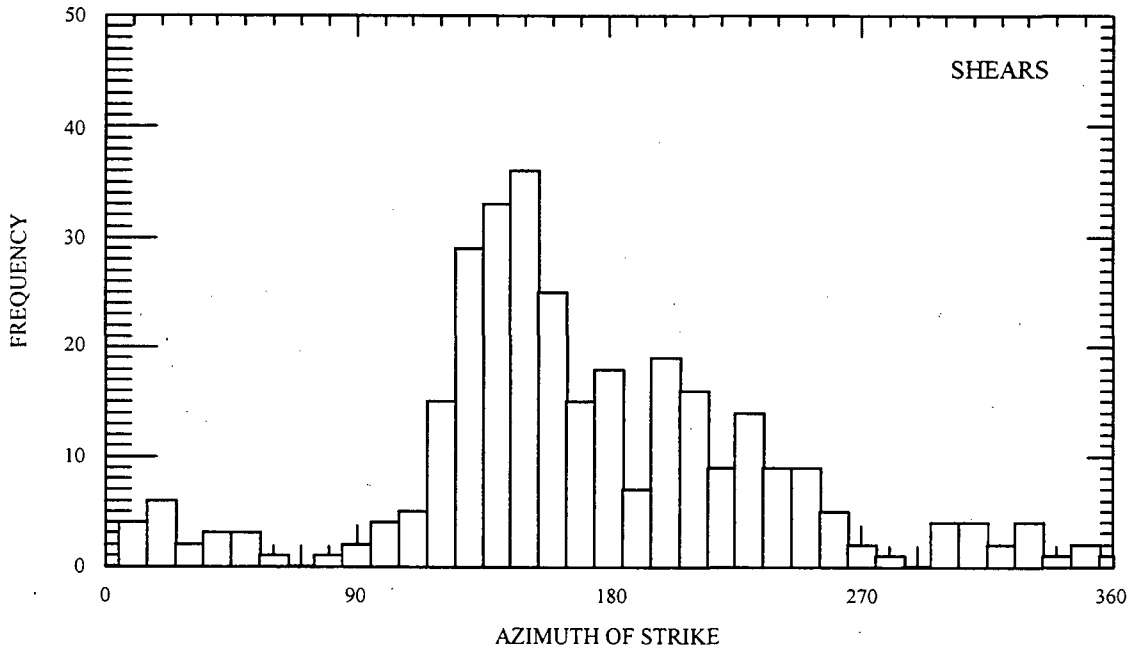

FIGUE A4.9: HISTOGRAM OF SHEAR STRIKE

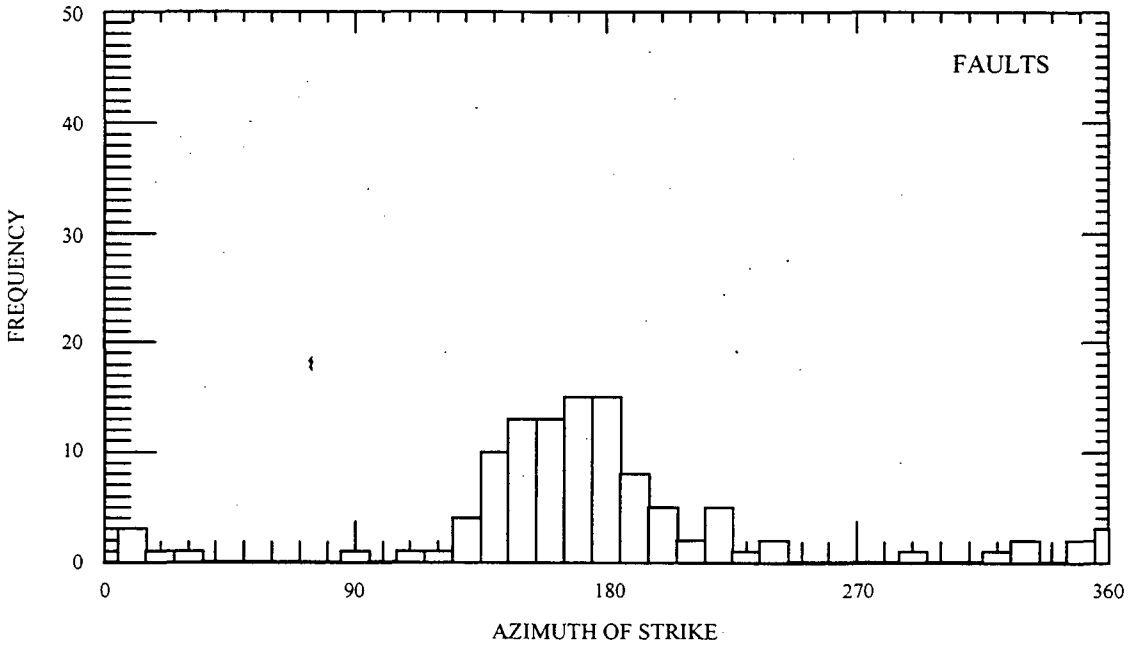

FIGURE A4.10: HISTOGRAM OF FAULT STRIKE

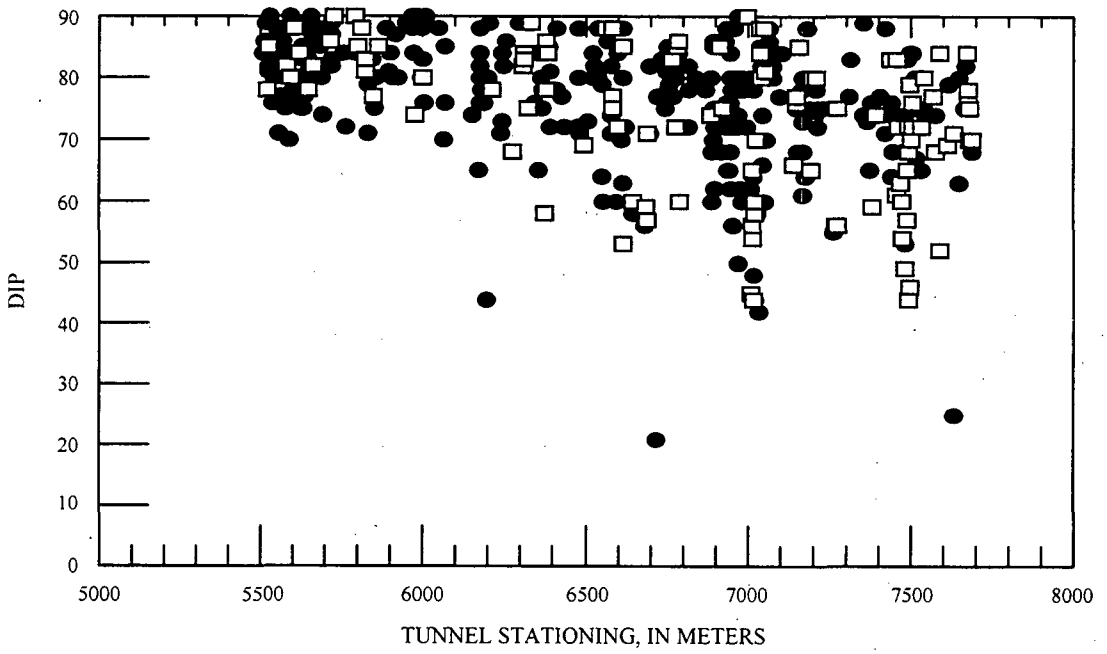

FIGURE A4.11: FAULTS AND SHEARS:DIP MAGNITUDE AND STATIONING
FILLED CIRCLES:SHEARS
OPEN SQUARES:FAULTS

APPENDIX V: Data Tracking Numbers for Review Packages

APPENDIX V: Data Tracking Numbers for Review Packages

Stations 55+00 to 60+00

DLS GS961108314224.023
FPGM GS970108314224.002 (Drawings OA-46-257 through -262)

Stations 60+00 to 65+00

DLS GS970208314224.003
FPGM GS970208314224.004 (Drawings OA-46-263 through -268)

Stations 65+00 to 70+00 GS970808314224.xxx

DLS GS970808314224.008
FPGM GS970808314224.009 (Drawings OA-46-269 through -274)

Stations 70+00 to 75+00

DLS GS970808314224.010
FPGM GS970808314224.011 (Drawings OA-46-275 through -280)

Stations 75+00 to 78+77

DLS GS970808314224.012
FPGM GS970808314224.013 (Drawings OA-46-281, -282, -293, -294, -302)

Alcove 5

FPGM GS9706-08314224.007 (Drawings OA-46-222 and -300) (Heated Drift)
FPGM GS9609-08314224.021 (Drawings OA-46-290 and -292) (5 and 5a)

DLS GS960908314224.018
DLS GS970608314224.006 (Heated Drift)

Alcove 6

DLS GS970808314224.014
FPGM GS970808314224.015 (Drawings OA-46-303 through -305)

South Ramp Report

GS970808314224.016

APPENDIX VI: Photographs and Plates

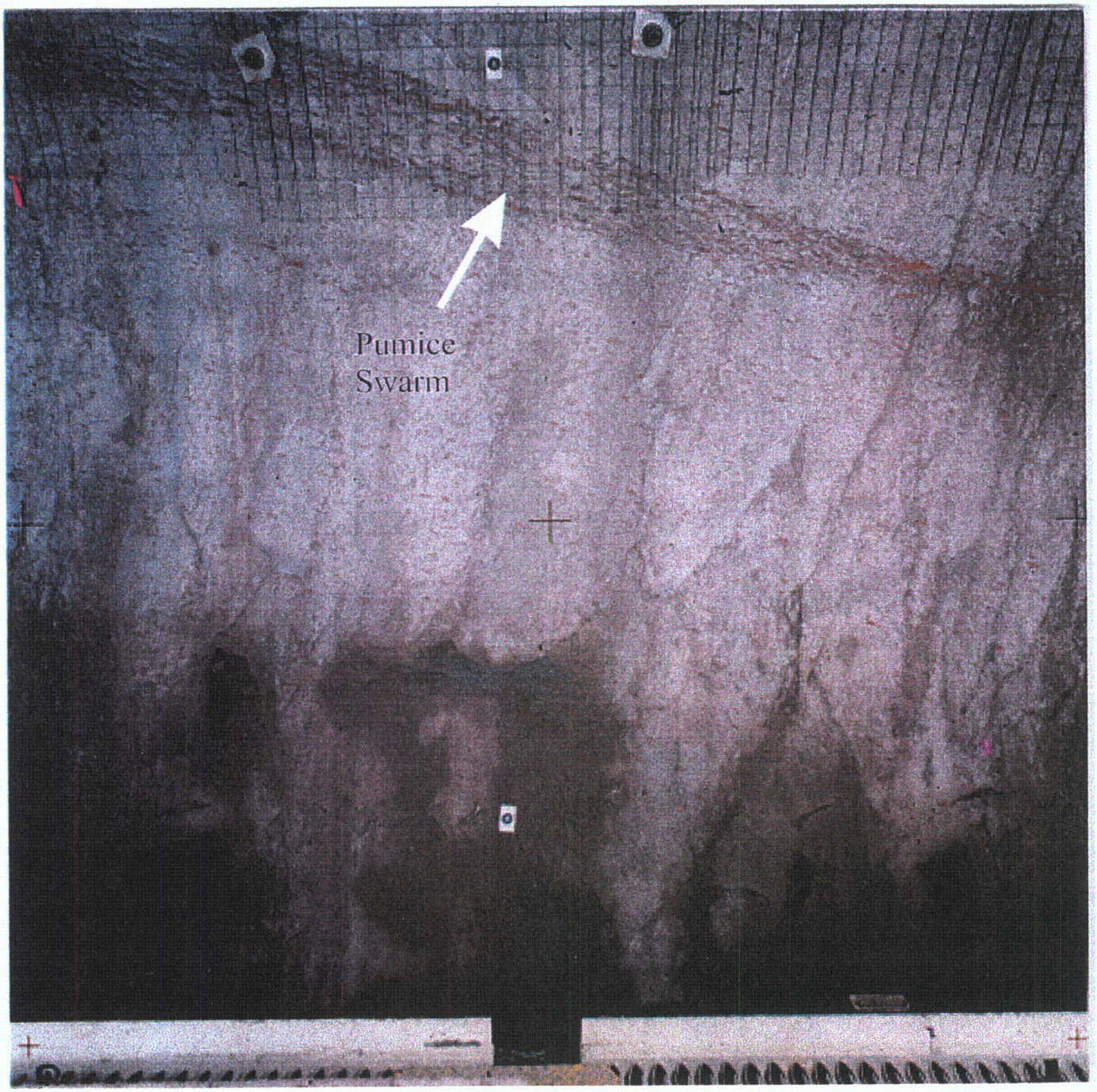

Photo 1. View of the crystal-poor lower nonlithophysal zone of the Tiva Canyon Tuff near Sta. 67+42, left rib, showing the higher of two pumice swarms observed in this location. Pumice clasts are argillically altered. Field of view is approximately 4.5 m; rock bolt bearing plates are 15 cm across. Photo PG021882.

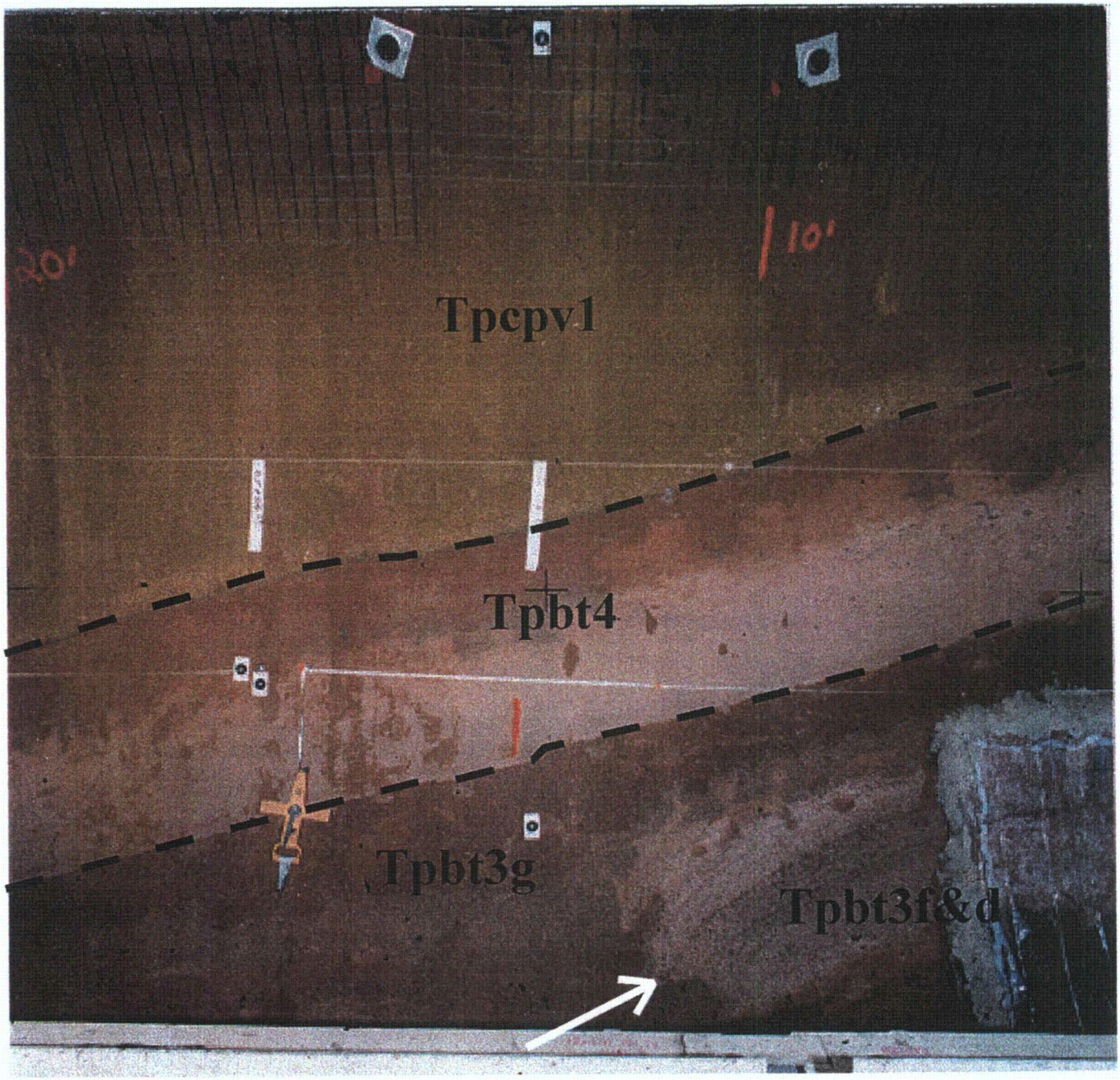

Photo 2. The contact between the Tiva Canyon Tuff and underlying pre-Tiva Canyon Tuff bedded tuffs (Tpbt4) at Sta. 67+00, right rib. Units d and f of the underlying pre-Yucca Mountain Tuff bedded tuffs (Tpbt3) are eroded and incorporated into unit g near the base of the photo (arrow). Field of view is approximately 4.5 m; rock bolt bearing plates are 15 cm across. Photo PG021748.

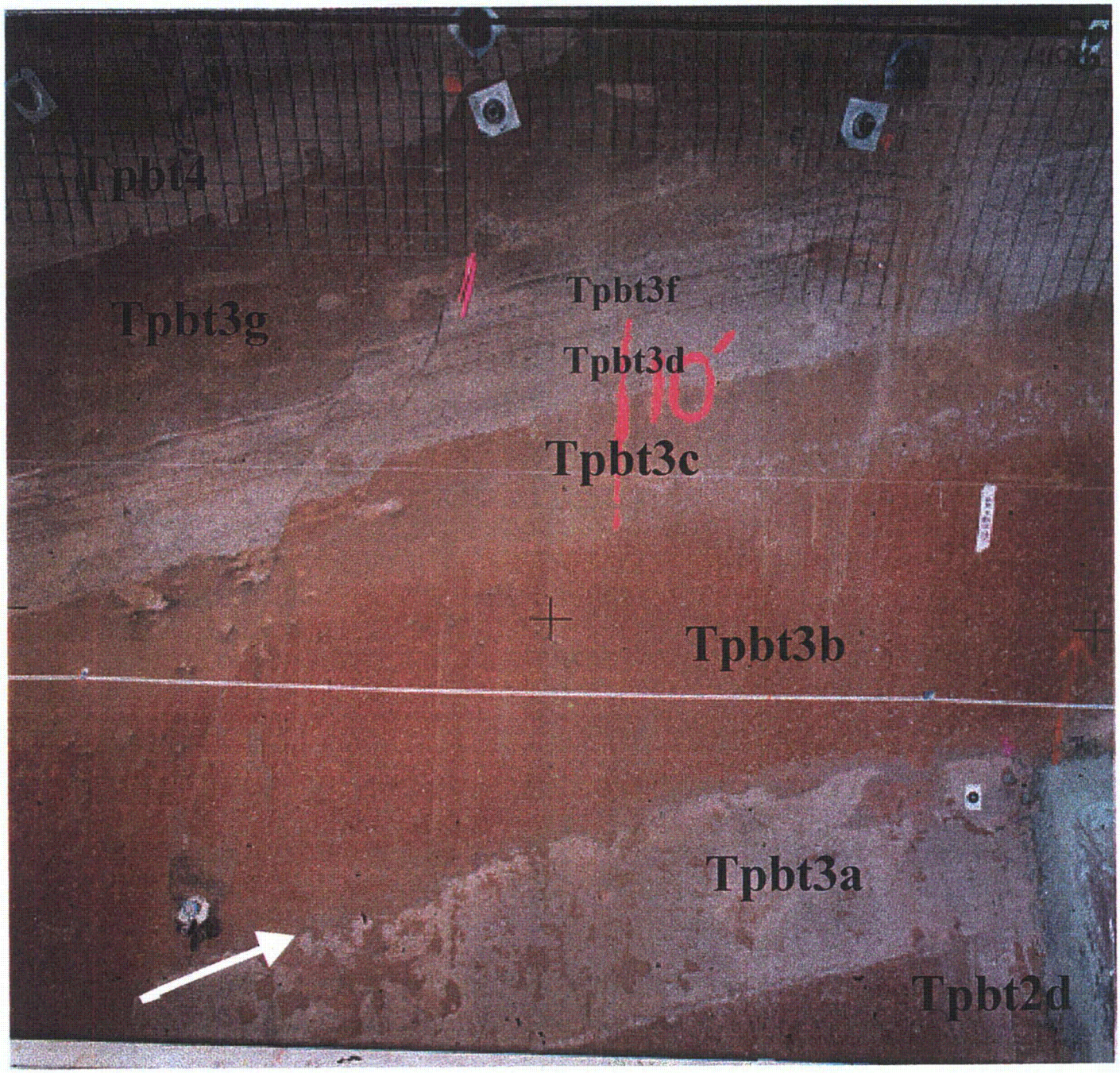

Photo 3. The pre-Yucca Mountain Tuff bedded tuffs (Tpbt3) exposed near Sta. 66+88, right rib. Arrow points to disturbed upper surface of unit a. Infilled burrow structures can be found in Tpbt3g and 3c. Field of view is approximately 4.5 m; rock bolt bearing plates are 15 cm across. Photo PG021723.

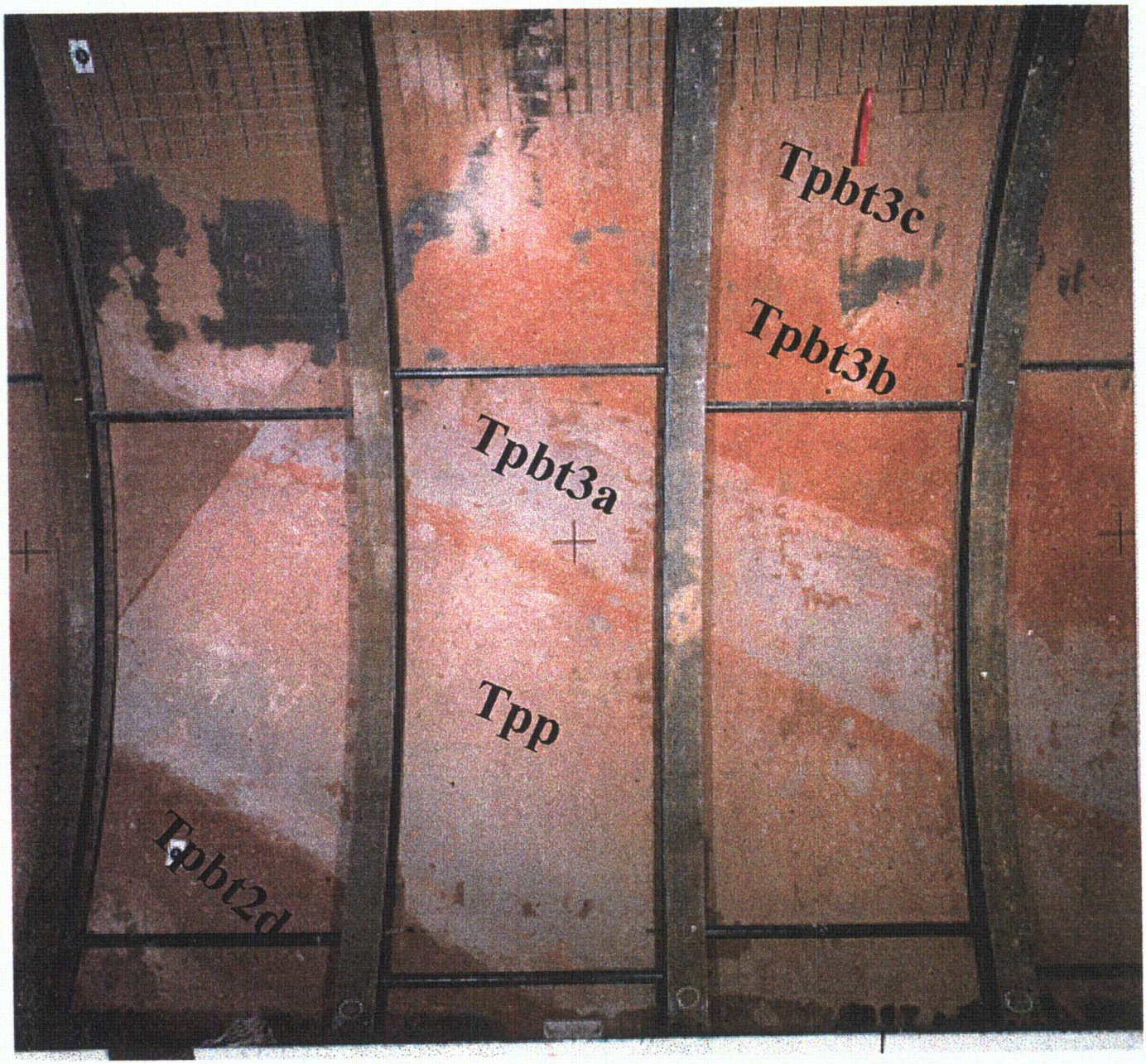

Photo 4. Pah Canyon Tuff showing reverse grading of pumice fragments along the left rib near Sta. 74+91. A small fault truncates the unit on the left side of the photo. Field of view is approximately 4.5 m. Photo PG024572.

Photo 5. The upper part of the post-Topopah Spring Tuff pumice-fall deposits, showing crude stratification near the top of the deposit, the "red clay layer", and the base of the overlying reworked tephra deposit, Tpbt2D (arrow). Field of view is approximately 4.5 m; rock bolt bearing plates are 15 cm across. Photo PG021682.

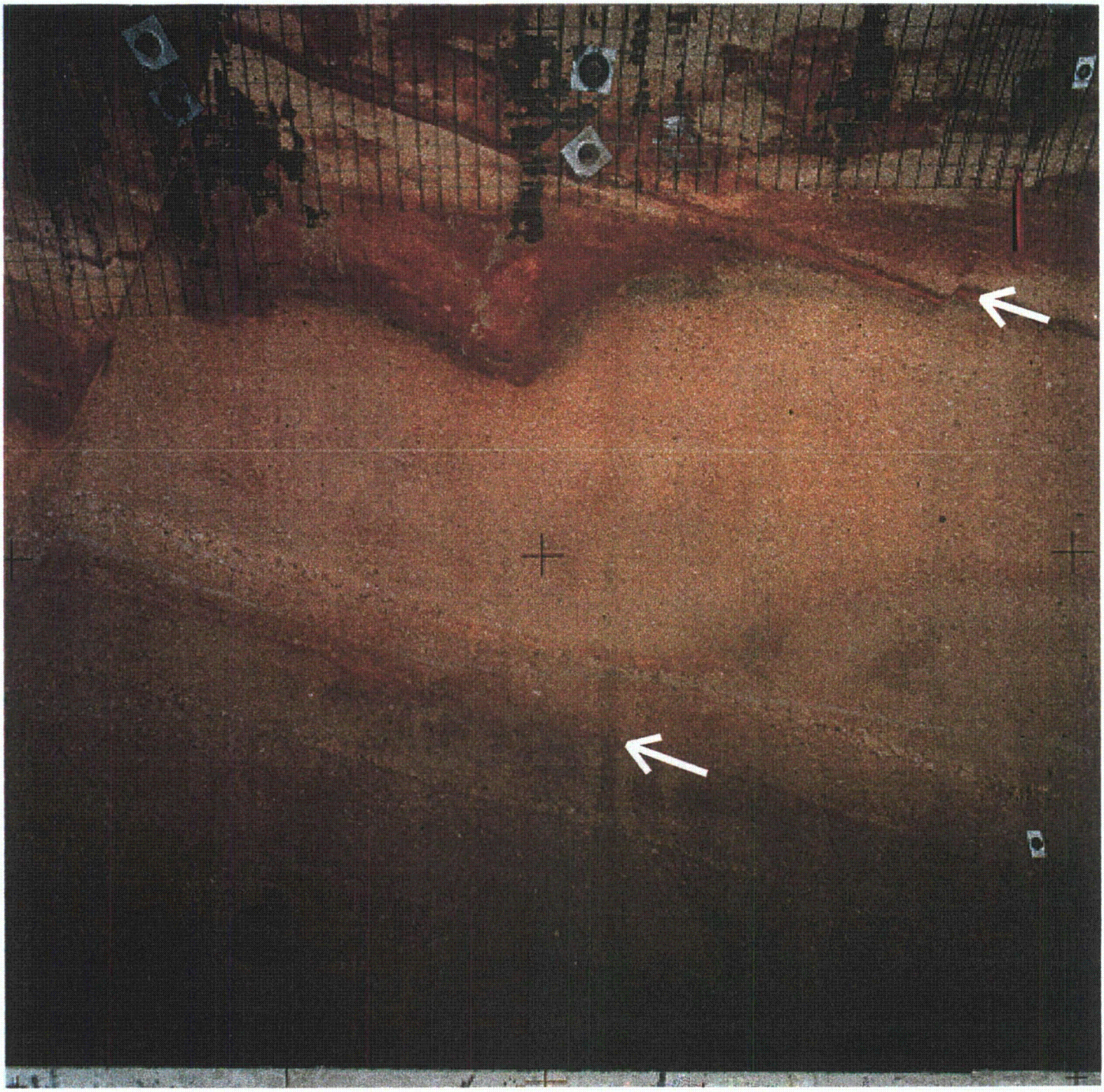

Photo 6. View of the post-Topopah Spring Tuff pumice-fall deposits near Sta. 74+00, left rib, showing ash layer 2 and ash layer 1 (arrows) truncated by a small fault on the right side of the image. Argillic alteration associated with fumarolic degassing of the underlying pyroclastic-flow deposits creates discoloration of the pumice-fall material in the upper part of the photo. Field of view is approximately 4.5 m; rock bolt bearing plates are 15 cm across. Photo PG024437.

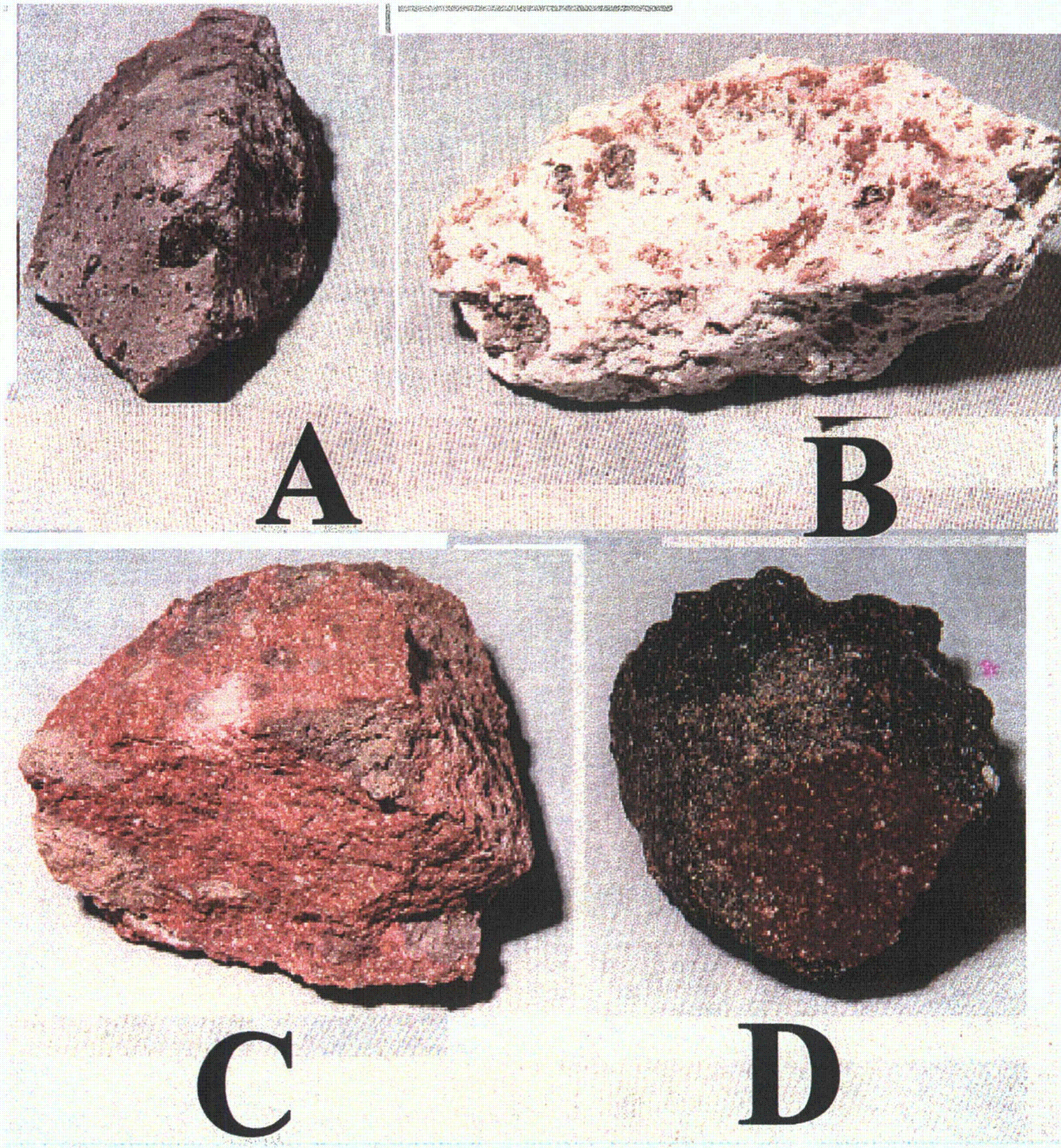

Photo 7. A series of hand samples collected from the South Ramp showing variations in the character of the upper part of the Topopah Spring Tuff pyroclastic-flow deposits. A. Moderately welded, vapor-phase altered tuff from Sta. 70+00. B. Moderately welded, bleached and vapor-phase altered tuff from Sta. 74+48. C. Moderately welded, devitrified and vapor-phase altered tuff of the crystal-rich nonlithophysal zone (Tptrn2) from Sta. 69+68. D. Densely welded, crystal-rich vitrophyre (Tptrv1) from Sta. 69+96. All samples collected from approximately 1 m above the right invert. Photo YM15609

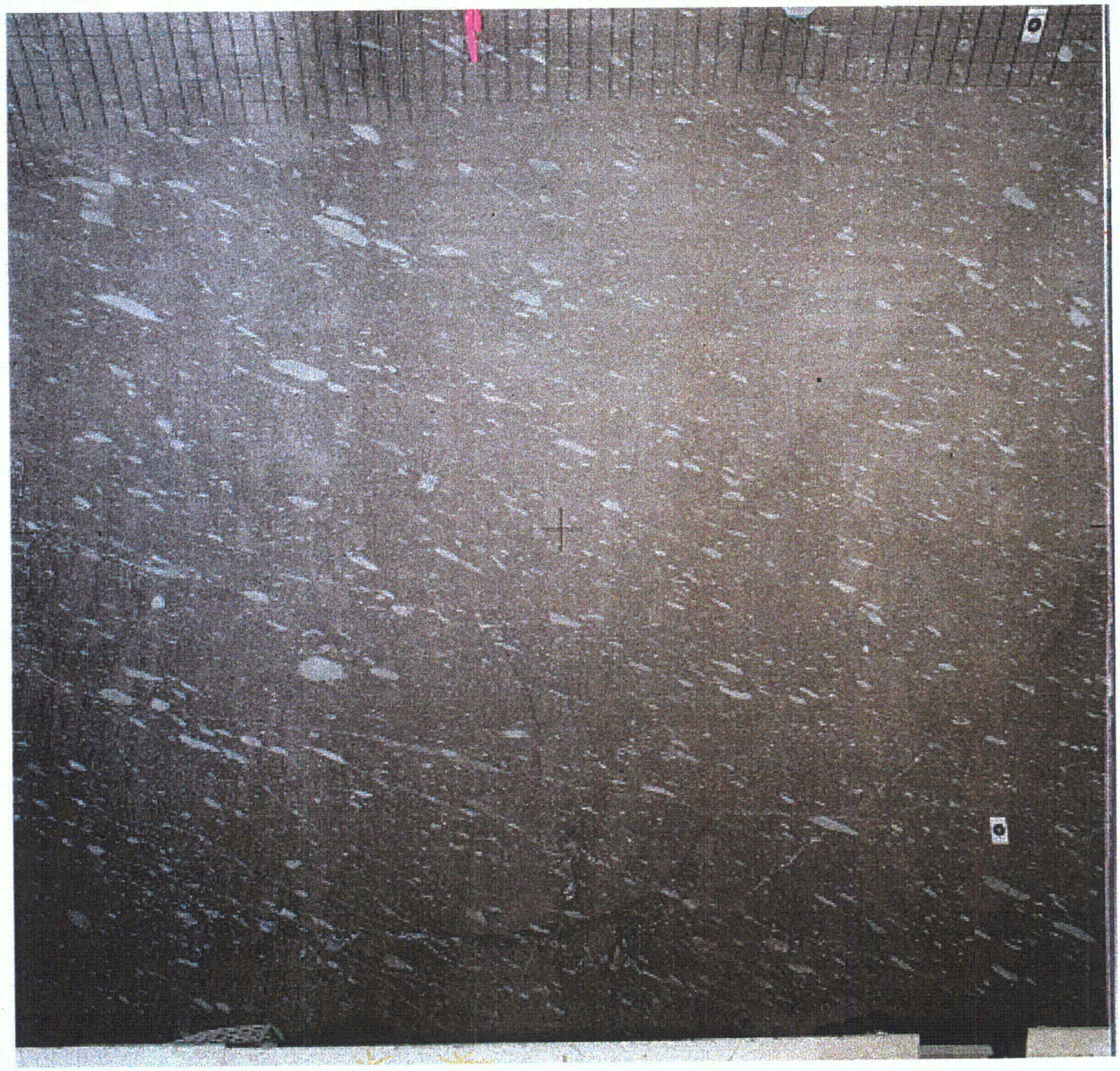

Photo 8. View of the crystal-rich nonlithophysal zone of the Topopah Spring Tuff at Sta. 66+07, left rib. Field of view is approximately 4.5 m. Photo PG021477.

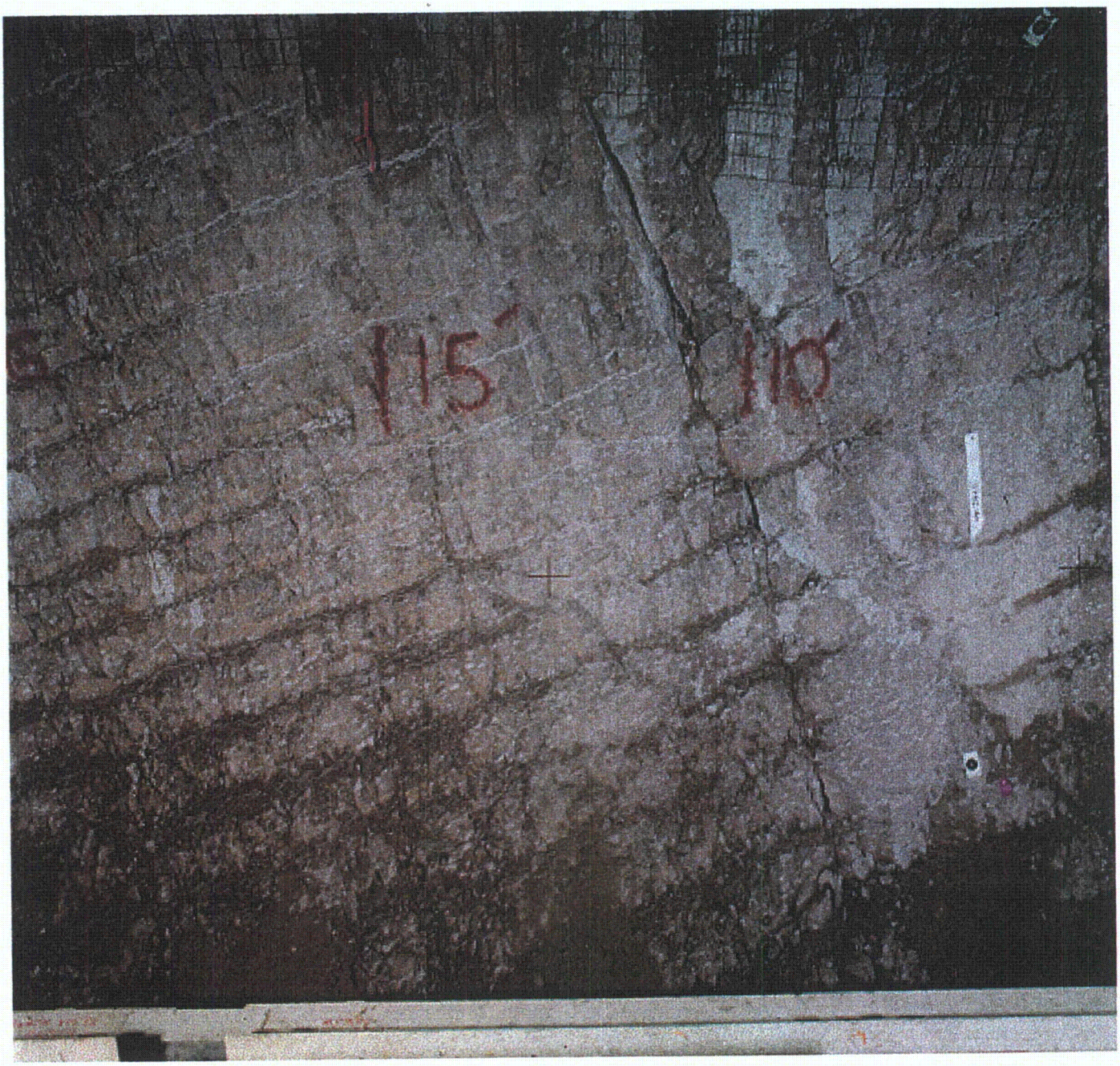

Photo 9. View of the upper portion of the crystal-poor middle nonlithophysal zone of the Topopah Spring Tuff along the right rib near Sta. 71+52. This interval is characterized by a series of laterally continuous vapor-phase partings spaced on vertical intervals of 25 to 40 cm. Field of view is approximately 4.5 m; rock bolt bearing plates are 15 cm across. Photo PG023343.

Photo 10. View of the contact between the pyroclastic-flow deposits of the Topopah Spring Tuff and the overlying pumice-fall deposits exposed along the left rib near Sta. 66+45. Alteration of the pumice-fall material is along a small fault that offsets the flow-fall contact. The fault can be traced downward through the pyroclastic-flow deposits which were not altered. Field of view is approximately 4.5 m; rock bolt bearing plates are 15 cm across. Photo PG021582.

Photo 11. Photograph of tunnel boring machine after breaking through at the South Portal. Photo YM1434

Photo 12. Photograph of South Ramp showing fault zone at Sta. 71+31. Photo shows heavy ground support with steel sets and lagging, and the loss of grade of more than 1 meter where the TBM dropped while excavating through this zone. Photo YM13876.

The 9 Drawings specifically referenced in the table of contents have been processed into ADAMS.

These drawings can be accessed within the ADAMS package or by performing a search on the Document/Report Number.

D-01 thru D-09